

Stony Brook University



OFFICIAL COPY

The official electronic file of this thesis or dissertation is maintained by the University Libraries on behalf of The Graduate School at Stony Brook University.

© All Rights Reserved by Author.

Fertilin β and Cyritestin Mimic Polymers
Interrogate the Mechanism of Mammalian Fertilization

A Dissertation Presented

by

Younjoo Lee

to

The Graduate School
in Partial Fulfillment of the
Requirements
for the Degree of

Doctor of Philosophy

in

Chemistry

Stony Brook University

December 2008

Stony Brook University

The Graduate School

Younjoo Lee

We, the dissertation committee for the above candidate for the

Doctor of Philosophy degree, hereby recommend

acceptance of this dissertation.

Nicole S. Sampson – Dissertation Advisor

Professor of Chemistry

Kathlyn A. Parker – Chairperson of Defense

Professor of Chemistry

Daniel P. Raleigh – Third member of Defense

Professor of Chemistry

Kent Kirshenbaum – Outside Member of Defense

Associate Professor of Chemistry at New York University

This dissertation is accepted by the Graduate School

Lawrence Martin

Dean of the Graduate School

Abstract of the Dissertation

Fertilin β and Cyritestin Mimic Polymers
Interrogate the Mechanism of Mammalian Fertilization

by

Younjoo Lee

Doctor of Philosophy

in

Chemistry

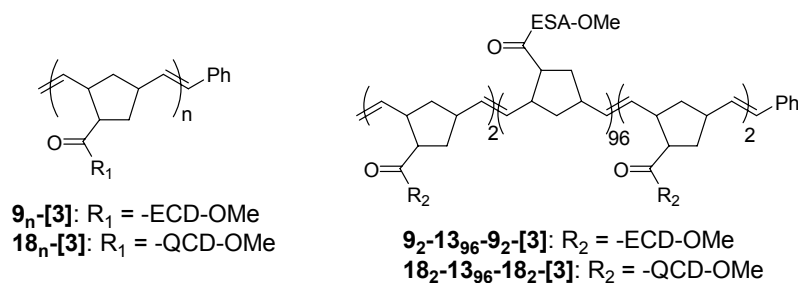
Stony Brook University

2008

The sperm proteins fertilin β and cyritestin, members of the ADAM family of proteins, are critical for mammalian sperm-oocyte binding. Multivalent probes containing the three-amino acid binding sequence of fertilin β , ECD, and cyritestin, QCD have been designed, synthesized, and tested to investigate gamete interactions.

To improve the binding affinity of monomeric peptide ligands for the oocyte surface, we developed synthetic multivalent polymers to mimic the multivalent display of fertilin β on the sperm surface. We employed ruthenium-catalyzed ring opening metathesis polymerization (ROMP) to prepare these mimics. Tricyclohexylphosphine substituted ruthenium catalyst **2**, [(H₂IMes)(PCy₃)(Cl)₂Ru=CHPh] did not initiate

efficiently with norbornenyl monomers, and the resulting polymers had uncontrolled and broadly distributed molecular weights. However, 3-bromo-pyridine substituted ruthenium catalyst **3**, [(H₂IMes)(3-Br-pyr)(Cl)₂Ru=CHPh] initiates more rapidly than propagation. Therefore, the controlled living ROMP of norbornenyl polymers was achieved.



Fertilin β mimic polymers $\mathbf{9}_{100}\text{-[3]}$ synthesized with catalyst **3** were compared to previously synthesized fertilin β mimic polymers. In addition, the inhibition potencies of multivalent cyritestin mimic polymers $\mathbf{18}_n\text{-[3]}$ were tested. Tri-block copolymers $\mathbf{9}_2\text{-13}_{96}\text{-9}_2\text{-[3]}$ and $\mathbf{18}_2\text{-13}_{96}\text{-18}_2\text{-[3]}$ containing both ECD and QCD ligands were assayed to explore the relationship and degree of identity between fertilin β and cyritestin receptors. These block copolymers were the same length as their corresponding homopolymers, but they had a lower density of fertilin β and cyritestin peptides. The homo and block polymers had the same potencies, and there was no synergy of inhibition between fertilin β and cyritestin mimics. Both polymers require the oocyte β_1 integrin for inhibition. We conclude that QCD and ECD mimics bind in the same complex of proteins and may bind to the same receptors.

The structural requirements defined were incorporated into new linear polymer systems that include tagging elements for probing the identity of oocyte surface receptors for fertilin β and cyritestin. Bivalent homopolymers were used to minimize non-specific interactions. Fluorescent fertilin β and cyritestin mimic polymers labeled the oolemma of the wild-type mouse oocytes, but not the oolemma of β_1 integrin knockout mouse oocytes. Thus, β_1 integrins are required for binding of fertilin β and cyritestin mimic polymers. The polymer synthesis was further developed to enable photo cross-linking and identification of additional members of the integrin receptor complex.

Table of Contents

List of Figures	ix
List of Schemes	xii
List of Tables	xiv
List of Appendix Contents	xvi
List of Abbreviations	xviii

Chapter 1

Introduction

I.	Mammalian Fertilization	2
II.	Gamete Membrane Interactions	8
III.	Multivalent Interactions and Linear Scaffold Polymerization	19
IV.	Specific Aims	34

Chapter 2

Analysis of Oligopeptide-Polymers Synthesized by Ruthenium Catalysts: Tricyclohexylphosphine versus 3-Bromo-Pyridine Substitution

I.	Introduction	38
II.	Results	42
III.	Discussion	59
IV.	Summary	67

Chapter 3

Mixed Fertilin β and Cyritestin Mimic Polymers Interrogate Sperm-Oocyte Binding Mechanisms

I.	Introduction	70
II.	Results	74
III.	Discussion	87
IV.	Summary	91

Chapter 4

Identification of Fertilin β and Cyritestin Receptors on the Oocyte Surface Membrane with “Clickable” Polymers

I.	Introduction	94
II.	Results	97
III.	Discussion	110
IV.	Summary	118

Chapter 5

Experimental Methods

I.	Synthesis and Preparation of Compounds	120
II.	<i>In vitro</i> Fertilization Assay	147
III.	Fluorescence Staining Protocol	152
IV.	Photoaffinity Labeling Protocol	154

Bibliography	160
Appendix	185

List of Figures

Figure		Page
Chapter 1		
1-1	Overview of early events in mammalian fertilization	3
1-2	Sperm acrosome reaction	5
1-3	Domain structures of ADAMs and SVMPs	9
1-4	Reassociation of monovalent versus multivalent ligand binding	20
1-5	Commonly used scaffolds for multivalent systems and their approximate size	21
1-6	Schematic representation of the concept of the flexibility of spacer of a block copolymer system	23
1-7	Molybdenum-based imido alkylidene catalysts	29
Chapter 2		
2-1	Comparison of GPC eluted peaks of $9'_2$ -[3], $9'_2$ -13' ₇ -[3], $9'_2$ -13' ₉ -[3], $9'_2$ -13' ₇ -9' ₂ -[3] and $9'_{10}$ -[3]	55
2-2	Comparison of GPC eluted peaks of $18'_3$ -[3], $18'_6$ -[3], $18'_{10}$ -[3] and $18'_{100}$ -[3]	57
2-3	Examples of secondary metathesis reactions in ROMP	63

Chapter 3

3-1	Schematic representation of competition between sperm and mimics for binding to the oocyte plasma membrane	71
3-2	Ru catalysts 1 , 2 and 3 , and fertilin β mimic polymers, 9_n-[catalyst]	74
3-3	<i>In vitro</i> fertilization assay	76
3-4	Inhibition of fertilization by fertilin β mimic polymers at 0.05 μ M and 0.5 μ M in polymer concentration	80
3-5	Cyritestin mimic polymers, 18_n-[3] , and mutant polymers, 13_n-[3] and 21_n-[3]	80
3-6	Inhibition of fertilization by a mixture of 9₁₀₀-[3] at 0.5 μ M and 18₁₀₀-[3] at 0.5 μ M in polymer concentration	82
3-7	Inhibition of fertilization by homopolymers and bivalent block copolymers at 0.5 μ M in polymer concentration	83
3-8	Inhibition of fertilization by PEGylated ECD polymers	84
3-9	Inhibition of β_1 integrin knockout oocyte fertilization by homopolymers at 1 μ M in polymer concentration.	86
3-10	Proposed model for bivalent fertilin β and cyritestin receptors on polymer binding	90

Chapter 4

4-1	Autoradiograms of photoaffinity-labeled oocyte proteins	95
4-2	Photoaffinity labeling of zona pellucida-free oocytes performed by Jaechul Lee in the Sampson group	96

4-3	Binding of polymers with zona pellucida-free oocytes	104
4-4	Labeling of polymers with zona pellucida-free oocytes	105
4-5	Labeling of polymers with zona pellucida-free β_1 integrin knockout oocytes	107
4-6	Photoaffinity cross-linking of benzophenone with a hydrogen donor compound	111
4-7	Schematic representation of enzyme-substrate (NB-GKG-Bpa-ECD-OMe) complex	112
4-8	Representation of biotin-tagged polymer-protein receptor complex extraction strategy	113
4-9	Schematic representation of the photoaffinity labeling and identification of the receptors	116

List of Schemes

Scheme		Page
Chapter 1		
1-1	Atom transfer radical polymerization	25
1-2	Overview of a typical ROMP reaction	26
1-3	Ruthenium-based catalysts 1 , 2 and 3	30
Chapter 2		
2-1	Ruthenium-based olefin metathesis catalysts	38
2-2	Ruthenium-catalyzed ROMP with tricyclohexylphosphine-substituted catalyst 2 or 3-bromo-pyridine-substituted catalyst 3	39
2-3	Synthesis of oligopeptide substituted norbornenyl polymers, ECDVT ₁₀ and CTEVD ₁₀	41
2-4	Synthesis of ECD monomers	43
2-5	Purification of 5-norbornen-exo-carboxylic acid, 10	44
2-6	Synthesis of ESA monomers	45
2-7	Synthesis of QCD monomers	46
2-8	Alternative synthesis of Ac-QCD-OMe, 17	47
2-9	Synthesis of norbornenyl ASD monomer, 21	48
2-10	Synthesis of norbornene carboxylic acid <i>N</i> -hydroxysuccinimide ester, NB-NHS, 22	48
2-11	Norbornenyl bio-functional polymers synthesized by ROMP	50

2-12	Metallacarbene-norbornenyl oligopeptide complexes	66
------	---	----

Chapter 4

4-1	Synthesis of fertilin β and cyritestin mimic, and mutant oligopeptides containing Bpa	97
4-2	A series of norbornenyl monomers containing trypsin cleavable oligopeptides	98
4-3	Synthesis of norbornenyl fertilin β and cyritestin mimic, and mutant monomers containing enzymatic cleavable peptide, Lys	100
4-4	Synthesis of Alexa ₄₈₈ -conjugated azido compound, 41	100
4-5	Synthesis of biotin-tagged azido compound, 43	101
4-6	Synthesis of alkyne-tagged bivalent polymer, 47 , 48 and 49 synthesized by ROMP	102
4-7	Synthesis of fluorophore-labeled bivalent polymers, 50 , 51 and 52 synthesized by Huisgen 1, 3-dipolar cycloaddition	103

List of Tables

Table		Page
Chapter 1		
1-1	Sequence alignment of SVMP-II, SVMP-III and ADAM disintegrins	10
1-2	Functional group tolerance of early and late transition metal-based ROMP catalysts	30
Chapter 2		
2-1	Analytical data for homo fertilin β mimic polymers synthesized with catalyst 2 , [2]	52
2-2	Analytical data for homopolymers of the fertilin β mimic oligopeptide or <i>N</i> -hydroxysuccinimide (NHS) ester norbornenyl monomers	53
2-3	Analytical data for fertilin β mimic polymers	54
2-4	Analytical data for cyritestin mimic polymers	56
2-5	Analytical data for fertilin β and cyritestin mimic bivalent block copolymers	58
2-6	Analytical data for mutant polymers	58

Chapter 3

3-1	Inhibition of fertilization by fertilin β mimics	72
3-2	Inhibition of fertilization by fertilin β mimic and mutant polymers synthesized with catalyst 2	78
3-3	Inhibition of fertilization by fertilin β mimic and mutant polymers synthesized with catalyst 3	79
3-4	Inhibition of fertilization by cyritestin mimic and mutant polymers	81

Chapter 4

4-1	Results of trypsin digestion	99
4-2	List of proteins analyzed by LTQ Orbitrap XL ETD mass spectrometry	109

Chapter 5

5-1	Composition of M16 buffer	148
-----	---------------------------	-----

List of Appendix Contents

Appendix		Page
A-1	Checklist for compounds	186
A-2	MALDI-TOF mass spectrum of photo-affinity labeling mouse oocyte with fertilin β mimic polymer after immunoprecipitation and trypsin digestion	188
A-3	$^1\text{H-NMR}$ spectrum of NB-Glu(OtBu)Cys(Trt)Asp(OtBu)-OMe, 9	189
A-4	$^{13}\text{C-NMR}$ spectrum of NB-Glu(OtBu)Cys(Trt)Asp(OtBu)-OMe, 9	190
A-5	$^1\text{H-NMR}$ spectrum of NB-Glu(OtBu)Ser(tBu)Ala-OMe, 13	191
A-6	$^{13}\text{C-NMR}$ spectrum of NB-Glu(OtBu)Ser(tBu)Ala-OMe, 13	192
A-7	$^1\text{H-NMR}$ spectrum of NB-Gln(Trt)Cys(Trt)Asp(OtBu)-OMe, 18	193
A-8	$^{13}\text{C-NMR}$ spectrum of NB-Gln(Trt)Cys(Trt)Asp(OtBu)-OMe, 18	194
A-9	$^1\text{H-NMR}$ spectrum of NB-AlaSer(tBu)Asp(OtBu)-OMe, 21	195
A-10	$^1\text{H-NMR}$ spectrum of polymer 9 ' ₃ -[2]	196
A-11	$^1\text{H-NMR}$ spectrum of polymer 9 ₃ -[3]	197
A-12	$^1\text{H-NMR}$ spectrum of polymer 9 ₆ -[3]	198
A-13	$^1\text{H-NMR}$ spectrum of polymer 9 ' ₁₀ -[2]	199
A-14	$^1\text{H-NMR}$ spectrum of polymer 9 ₁₀ -[2]	200
A-15	$^1\text{H-NMR}$ spectrum of polymer 9 ' ₁₀ -[2]-a	201
A-16	$^1\text{H-NMR}$ spectrum of polymer 9 ' ₁₀ -[3]	202
A-17	$^1\text{H-NMR}$ spectrum of polymer 9 ₁₀ -[3]	203
A-18	$^1\text{H-NMR}$ spectrum of polymer 9 ' ₁₀₀ -[2]	204

A-19	¹ H-NMR spectrum of polymer 9' ₁₀₀ -[3]	205
A-20	¹ H-NMR spectrum of polymer 9 ₁₀₀ -[3]	206
A-21	¹ H-NMR spectrum of polymer 13 ₁₀ -[3]	207
A-22	¹ H-NMR spectrum of polymer 13 ₁₀₀ -[3]	208
A-23	¹ H-NMR spectrum of polymer 18 ₃ -[3]	209
A-24	¹ H-NMR spectrum of polymer 18 ₆ -[3]	210
A-25	¹ H-NMR spectrum of polymer 18 ₁₀ -[3]	211
A-26	¹ H-NMR spectrum of polymer 18 ₁₀₀ -[3]	212
A-27	¹ H-NMR spectrum of polymer 21 ₁₀ -[3]	213
A-28	¹ H-NMR spectrum of polymer 22 ₁₀ -[2]-a	214
A-29	¹ H-NMR spectrum of polymer 22 ₁₀ -[2]-b	215
A-30	¹ H-NMR spectrum of polymer 22 ₁₀ -[3]-c	216
A-31	¹ H-NMR spectrum of polymer 9 ₂ - 13 ₉₆ - 9 ₂ -[3]	217
A-32	¹ H-NMR spectrum of polymer 9 ₂ - 13 ₉₆ - 18 ₂ -[3]	218
A-33	¹ H-NMR spectrum of polymer 18 ₂ - 13 ₉₆ - 18 ₂ -[3]	219
A-34	¹ H-NMR spectrum of polymer 47	220
A-35	¹ H-NMR spectrum of polymer 48	221
A-36	¹ H-NMR spectrum of polymer 49	222

List of Abbreviations

Ac	acetyl
ADAM	A disintegrin and a metalloprotease
Ala, A	alanine
AEG	acidic epididymal glycoprotein
AMP	adenosine monophosphate
Arg, R	arginine
Asn, N	asparagine
Asp, D	aspartic acid
Ar	argon
ATRP	atom transfer radical polymerization
Bpa	4-benzoyl-L-phenylalanine
Boc	<i>t</i> -butyloxycarbonyl
BSA	bovin serum albumin
CCA	α -cyano-4-hydroxy cinnamic acid
CRISP	cysteine rich secretory protein
CRP	cationic radical polymerization
Cys, C	cysteine
DBU	1, 8-diazabicyclo[5.4.0]undec-7-ene
ddI H ₂ O	distilled and deionized water
DIC	differential interference contrast

DIEA	<i>N,N</i> -diisopropylethylamine
DMAP	4-dimethylaminopyridine
DMF	<i>N,N</i> -dimethylformamide
DMSO	dimethyl sulfoxide
DTT	dithiothreitol
EC	extracellular
ECD	glutamic acid-cysteine-aspartic acid
EGF	epidermal growth factor
ESA	glutamic acid-serine-alanine
ESI-MS	electrospray ionization mass spectrometry
Et ₂ O	diethyl ether
EtOAc	ethyl acetate
Fmoc	fluorenylmethoxycarbonyl
F.I.	fertilization index
F.R.	fertilization rate
GalTase	galactosyl transferase
Gln, Q	glutamine
Glu, E	glutamic acid
Gly, G	glycine
GPC	gel permeation chromatography
GPI	glycosylphosphatidylinositol
h	hour
H ₂	hydrogen

HBTU	<i>O</i> -benzotriazole- <i>N,N,N',N'</i> -tetramethyluronium hexafluorophosphate
Ig	immunoglobulin
IgSF	immunoglobulin super-family
InsP ₃ , IP ₃	inositol 1,4,5-trisphosphate
IP	immunoprecipitation
IPI	international protein index
IVF	<i>in vitro</i> fertilization
KO	knockout
Leu, L	leucine
Lys, K	lysine
MALDI-TOF	matrix assisted laser desorption ionization-time of flight
MDC	metalloprotease disintegrin cysteine rich
Mes	2,4,6-trimethylphenyl
M_n	number-average molecular weight
Mo	molybdenum
M_w	weight-average molecular weight
N ₂	nitrogen gas
NB	norbornene
NHC	<i>N</i> -heterocyclic carbene
NHS	<i>N</i> -hydroxysuccinimide
NMR	nuclear magnetic resonance
PBS	phosphate-buffered saline

Pd/C	palladium on carbon
PDI	polydispersity index
PEG	polyethylene glycol
Phe, F	phenylalanine
PLC	phospholipase C
PMA	phosphomolybdic acid
PMSG	pregnant mare's serum gonadotropin
ppm	parts per million
PVP	polyvinylpyrrolidone
QCD	glutamine-cysteine-aspartic acid
RGD	arginine-glycine-aspartic acid
ROMP	ring opening metathesis polymerization
RP-HPLC	reversed phase-high performance liquid chromatography
RPM	rotation per minute
rt	room temperature
Ru	ruthenium
SDS-PAGE	sodium dodecyl sulfate-polyacrylamide gel electrophoresis
SFQ	serine-phenylalanine-glutamine
SRN	serine-arginine-asparagine
SVMP	snake venom metalloprotease
TCEP-HCl	tris(2-carboxyethyl) phosphine hydrochloride
TFA	trifluoroacetic acid
TIPS	triisopropylsilane

THF	tetrahydrofuran
Thr, T	threonine
TLC	thin layer chromatography
TM	transmembrane
TRPC	transient receptor potential channel
Trt	trityl
Tyr, Y	tyrosine
UV	ultraviolet
Val, V	valine
WT	wild-type
Z, Cbz	benzyloxycarbonyl
ZP	zona pellucida

Chapter 1

Introduction

- I. Mammalian Fertilization
- II. Gamete Membrane Interactions
- III. Multivalent Interactions and Linear Scaffold Polymerization
- IV. Specific Aims

I. Mammalian Fertilization and Gamete Membrane Interactions

Mammalian fertilization is a multi-step process whereby two gametes (oocyte and sperm) bind and fuse together to form a zygote. The oocyte activates the sperm metabolism that is necessary for fertilization, and the sperm reciprocates by activation of the oocyte metabolism to initiate the onset of development.¹ The ovulated oocyte is surrounded by the cumulus layer and the zona pellucida. A capacitated and acrosome-intact sperm can pass through the cumulus complex, and bind in a species-specific manner to the thick extracellular coat of the zona pellucida consisting of three glycoproteins, ZP1, ZP2, and ZP3. The acrosome reaction results in the release of the contents of the acrosomal vesicle including proteolytic enzymes, and allows the sperm to penetrate the zona pellucida. Once the sperm reaches the perivitelline space between the zona pellucida and the oocyte plasma membrane, the sperm adhere to and fuse with the oocyte plasma membrane where oocyte activation is triggered. The cortical granules from the oocyte cortex are released into the perivitelline space and the content of the cortical granules alters the zona pellucida to prevent fertilization by further sperm.^{2,3} However, the precise mechanisms of sperm binding and fusion are not yet understood. The fertilization mechanism is a model in which to study cellular and developmental events.⁴ Moreover, an understanding of the molecular interaction between sperm and oocyte proteins is essential for the study of infertility and the development of new contraception strategies.

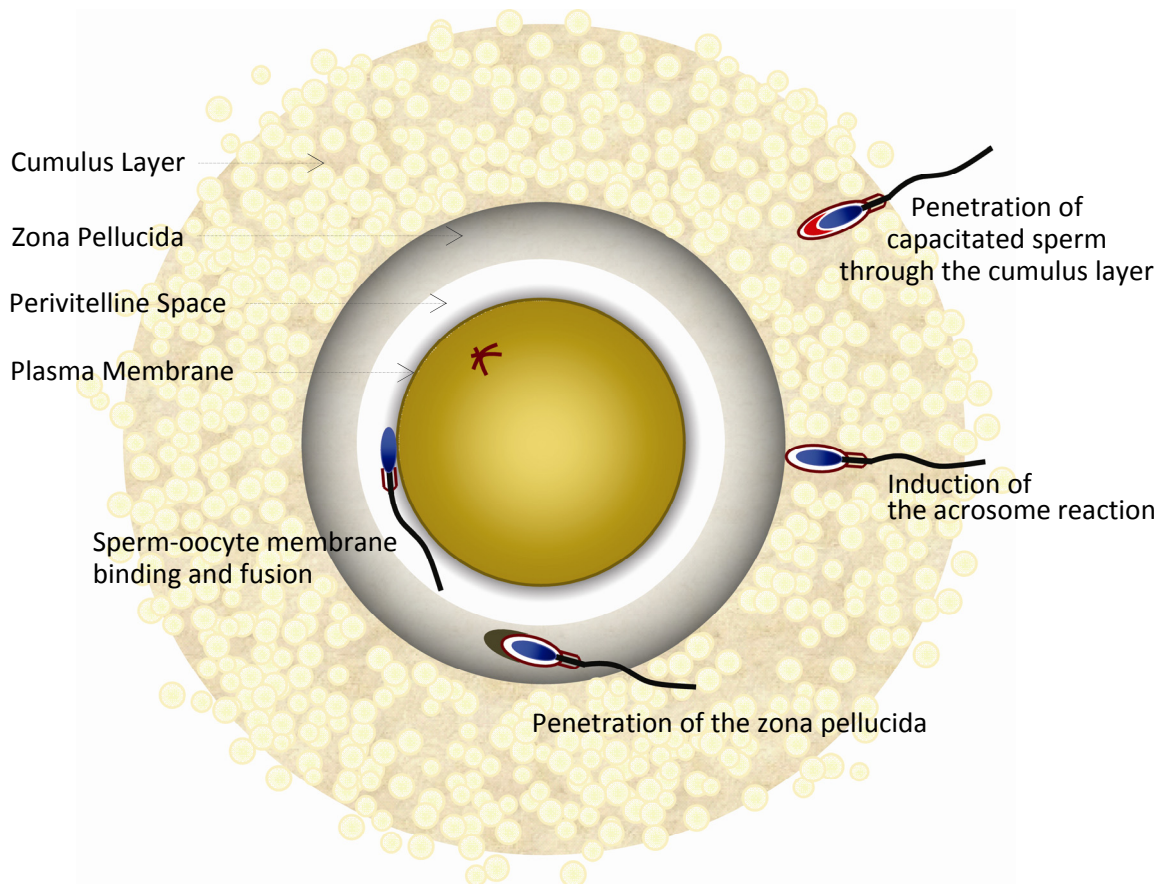


Figure 1-1. Overview of early events in mammalian fertilization

1.1. Sperm capacitation

Sperm are able to fertilize oocytes through a maturation process of capacitation in the female reproductive tract. The process is accompanied by modifications of membrane biophysical characteristics, changes in protein phosphorylation state, elevations of intracellular pH and calcium levels, and hyperpolarization of membrane potential.^{3, 5-7} Cholesterol efflux from the sperm membranes induces the sperm membranes to be reorganized. Cholesterol removal leads to the elevation of calcium and bicarbonate concentrations in the cytosol, which activates adenylyl cyclase⁸ to produce cyclic-AMP.

c-AMP activates a protein kinase A that increases phosphorylation of sperm proteins on tyrosine residues. Also c-AMP leads to increments in intracellular pH and bicarbonate levels which may operate the cyclic nucleotide-gated channels related to the control of flagellar motility.⁹ Hyperpolarization also is a part of capacitation. When T-type calcium channels are released, membrane hyperpolarization proceeds, which makes the sperm respond to the zona pellucida for further processing.¹⁰ Through a set of multiple reactions during the capacitation process, the sperm becomes more competent to fertilize an oocyte.

1.2. Sperm binding to the zona pellucida

The zona pellucida is an extracellular glycoprotein matrix surrounding the oocyte plasma membrane. After capacitation, sperm are capable of binding to the zona pellucida consisting of glycoproteins ZP1, ZP2, and ZP3 with molecular weights of 200, 120, and 83 kDa respectively.¹¹ Although it is not applicable to all species, sperm bind to the zona pellucida in a species specific manner.^{12, 13} The glycoprotein ZP3 is responsible for sperm binding, and binds to receptors on the plasma membrane of the acrosome-intact sperm head. Isolated ZP3 directly adheres to sperm,¹⁴ and so blocks binding of sperm to oocytes.¹⁵ However, the other glycoproteins, ZP1 and ZP2 do not function as inhibitors of adhesion.¹⁶ Sperm binding to the zona pellucida is a carbohydrate mediated process. All three glycoproteins have oligosaccharides on both asparagine (N-linked) and serine/threonine (O-linked) residues.¹⁷ Although it is reported that N-linked oligosaccharides have binding affinity in other species,¹⁸ O-linked oligosaccharides of ZP3 are responsible for binding to the receptors on mouse sperm.¹⁷ Sperm binding to ZP3 occurs at oligosaccharides linked to serine-332 and serine-334 found at the carboxy

terminus of ZP3.^{19, 20} Several sperm proteins binding to ZP3 have been reported.²¹⁻²³ Moreover, a plasma membrane molecule, β 1,4-galactosyl-transferase (GalTase) has been proposed as an adhesion receptor of ZP3.^{24, 25} However, the identification of the receptors on ZP3 has not yet been clearly established.

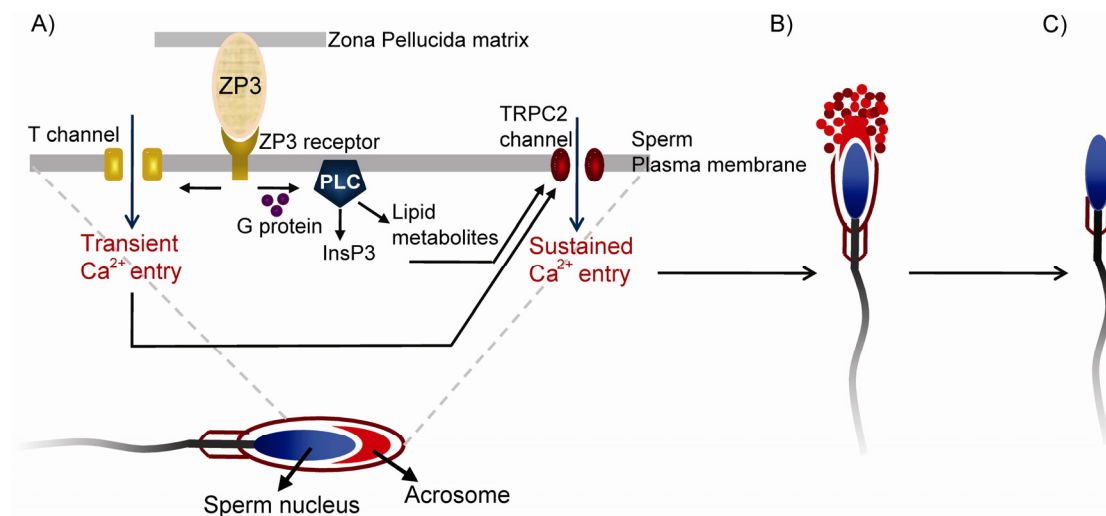


Figure 1-2. Sperm acrosome reaction. A) A model of the events involved in ZP3 signal transduction.⁴ B) Acrosomal contents are released. C) Acrosomal reacted sperm.

1.3. Sperm acrosome reaction

Once bound to the zona pellucida, sperm undergo a specialized type of cellular exocytosis known as the acrosome reaction. Sperm release of the contents of the acrosomal vesicle including digestive enzymes allows sperm to penetrate the zona pellucida.³ ZP3 on the zona pellucida is involved in the induction of the sperm acrosome reaction, and it may bind to the sperm receptors in a multivalent fashion.¹⁹ In sperm, ZP3 signal transduction is initiated by binding ZP3 into receptors on the sperm head (Figure

1-2). The ZP3 binding triggers the opening of T-type, low voltage-activated calcium channels²⁶ to cause calcium influx via T-type channels, and the activation of the heterotrimeric G proteins, G_{i1} and G_{i2}.²⁷ The G proteins activate the phospholipase C (PLC),²⁸⁻³⁰ and the intracellular pH is increased,^{31, 32} resulting in a sustained calcium influx that directly drives exocytosis.^{31, 33} An alternative model suggested that the receptors of inositol-1,4,5-trisphosphate (InsP₃) are present in the sperm acrosome³⁴ and may participate in the activation of the classical mammalian *Drosophila melanogaster* transient receptor potential (TRPC2) channels by ZP3.⁴ Through a series of ZP3 signal transduction events, sperm induce the acrosome reaction, which is a required step before the sperm fuse with the oocyte plasma membrane.^{3, 7}

1.4. Sperm-oocyte adhesion and fusion

Acrosome-reacted sperm which pass through the zona pellucida into the perivitelline space adhere to and fuse with the oocyte plasma membrane. The sperm protein fertilin was found to be a member of a family of sperm proteins, ADAMs- A Disintegrin and A Metalloprotease^{35, 36} or MDCs- Metalloprotease Disintegrin Cysteine-rich.^{37, 38} At least two testis-specific ADAM family members, fertilin β (ADAM2) and cyritestin (ADAM3) have roles in sperm-oocyte adhesion leading to sperm-oocyte fusion.³⁹ CRISPs- cysteine-rich secretory proteins⁴⁰ known as Acidic Epididymal Glycoprotein (AEG) related proteins and Izumo⁴¹ a member of immunoglobulin superfamily (IgSF) proteins on sperm are involved in sperm adhesion to the oocyte plasma membrane.

Integrins are a well-characterized family of cell adhesion molecules on the oocyte. The identification of an integrin ligand-like (disintegrin) domain in fertilin β suggested that sperm ADAMs adhere to integrins on the oocyte membrane.⁴² Cysteine-rich Secretory Protein, CRISPs and tetraspanins are also known to adhere to proteins on the oocyte. The sperm-oocyte adhesion leads to sperm-oocyte membrane fusion to form a new single cell called a zygote. However, the molecular basis of the intercellular fusion process is still not understood.⁴

1.5. Oocyte activation

The sperm-oocyte binding and fusion process induces a series of signaling events called oocyte activation that prepares the oocyte for embryonic development.^{43, 44} In the early stage of oocyte activation, the cytosolic calcium concentration is elevated up to approximately 1 μ M. The increased calcium concentration occurs in waves or oscillations across the oocyte from the point of sperm fusion.^{43, 44} The elevation of the cytosolic calcium concentration induces release from the meiotic arrest (metaphase II), progression into mitosis, and the exocytosis of the cortical granules.³ The contents of the cortical granules consist of proteases, mucopolysaccharides, hyalin, and peroxidases.⁴⁵ ZP3 is modified and ZP2 is cleaved by unidentified proteases released at oocyte activation.⁴⁶ The cortical granules are released from the oocyte cortex via the perivitelline space and the contents of the cortical granules alter the zona pellucida to prevent fertilization by additional sperm.^{2, 3} However, the precise mechanism of oocyte activation is still under debate.

II. Gamete Membrane Interactions

Acrosome reacted sperm are able to penetrate the zona pellucida, reach the perivitelline space, and then adhere to and fuse with the oocyte plasma membrane, at which point oocyte activation is triggered to prepare the oocyte for embryonic development. There are known sperm proteins involved in sperm-oocyte interaction, and their binding partners on oocyte plasma membrane.

II.1. Proteins on sperm

II.1.1. A disintegrin and a metalloprotease (ADAM)

Nearly 40 members of the ADAM- A Disintegrin and A Metalloprotease^{35, 36} family have been identified in various tissues and cell types. About half of the ADAMs are expressed in the mammalian male reproductive tissues, such as testis and epididymis.⁴⁷ Based on a phylogenetic tree of the ADAM genes, mammalian ADAMs with gene expression are divided into three major groups: ADAMs 1, 4, 6, 20, 21, 24, 25, 26, 29, 30, and 34 (the first group); ADAMs 2, 3, 5, 27, and 32 (the second group); and ADAMs 7 and 28 (the third group).⁴⁸ In the first group of ADAMs, all the genes are expressed specifically or predominantly in the testis, and many of genes are found as multiple copies in the mouse genome.⁴⁹ The genes of the second group of ADAMs are also expressed exclusively or predominantly in the wide regions of the genomes in the testis.^{50, 51} The third group of ADAM genes are abundantly expressed in the epididymis.⁵² ADAMs 1, 2, 3, 7, 24, and 28 in mouse have been studied at the protein level: ADAMs 1,

2, 3, and 24 are present in spermatogenic cells, and ADAMs 1b, 2, 3, 7, 24 are present in sperm.^{39, 52-64}

ADAM 2, fertilin β , was identified as the antigen of an antibody, PH-30 which inhibited fertilization of guinea pig oocytes.⁶⁵ ADAM 1, fertilin α , was found as a sperm surface heterodimer with fertilin β .^{56, 65, 66} ADAM 3, cyritestin, was identified by cloning strategies in mouse and monkey.^{36, 67, 68} The ADAM sperm proteins have been found in all mammals studied to date. ADAM proteins contain a distinct highly conserved domain structure that includes an N-terminal signal sequence, a pro-domain, a metalloprotease-like domain, a disintegrin domain, a cysteine-rich domain, an epidermal growth factor (EGF)-like repeat, a transmembrane domain, and a cytoplasmic domain (Figure 1-3). These proteins are related to the snake venom metalloproteases (SVMPs).⁶⁹⁻⁷¹ The soluble disintegrin domain has been of great interest, due to its role in blocking cell adhesion to integrins.

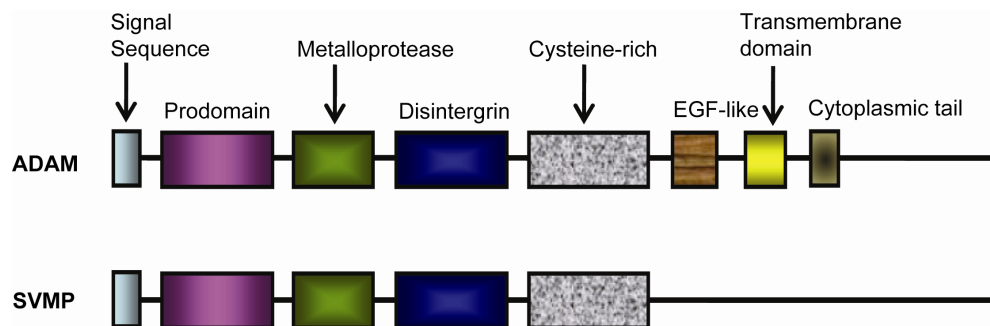


Figure 1-3. Domain structures of ADAMs and SVMPs.

The disintegrin domains of SVMPs-II have an arginine-glycine-aspartic acid (RGD) consensus sequence within a 13 amino acid stretch at the tip of hairpin loop called

the disintegrin loop. The disintegrin loops containing the RGD sequence are antagonists of $\alpha_{11b}\beta_3$ and $\alpha_v\beta_3$ integrins. Although the disintegrin domains of many ADAMs are ligands for integrin receptors, most ADAMs do not have an RGD sequence in their disintegrin loop except human ADAM 15 (Table 1-1).^{72, 73}

Table 1-1. Sequence alignment of SVMP-II, SVMP-III and ADAM disintegrins.^{71, 74-76}

		SVMP-II disintegrins		
	Kistrin		CKFSRAGKIC <u>RIP</u> RGD -MPDDRCTGQSADC	
	Echistatin		CKFLKEGTIC <u>KRAR</u> RGD -DMDDY CNGKTCDC	
	Barbourin		CRFMKKGTVCR <u>VAK</u> GD -WNDDTCTGQSADC	
		SVMP-III disintegrins		
	HR1B		CRFRTAGTEC <u>RAAES</u> ECD IPESCTGQSADC	
	Jararhagin		CKFKSAGTEC <u>RASMS</u> ECD PAEHCTGQSSEC	
	Atrolysin E		CKFTSAGNVCR <u>PARS</u> ECD IAESCTGQSADC	
		ADAM disintegrins		
	Other names	Species	Disintegrin Loop	Integrin-binding
1	PH-30 α ; Fertilina	Mouse	CTFKKKGSLCR <u>PAEDV</u> CDL PEYCDGSTQEC	$\alpha_6\beta_1$ ⁷³ $\alpha_9\beta_1$ ⁷⁷
2	PH-30 β ; Fertilin β	Mouse	CKLKRKGEVCR <u>LAQD</u> ECD VTEY CNGTSEVC	$\alpha_4\beta_1$
		Monkey	CLFMSQERVCR <u>PSFD</u> ECD LPEY CNGTSASC	$\alpha_6\beta_1$ ^{57, 78, 79}
		Guinea pig	CEFKTKGEVCR <u>RESTD</u> ECD LPEY CNGSSGAC	$\alpha_9\beta_1$ ⁷³
		Human	CLFMSKERMCR <u>PSFE</u> ECD LPEY CNGSSASC	
		Cow	CAFIPKGHIC <u>RGSTD</u> ECD LHEY CNGSSASC	
		Rat	CNLKAKGELCR <u>PANO</u> ECD VTEY CNGTSEVC	
		Rabbit	CTFKERGQSCR <u>PPVG</u> ECD LFEY CNGTSALC	

Table 1-1. (continued)

	Other names	Species	Disintegrin Loop	Integrin-binding
3	Cyritlestin; tMDC I	Mouse	CTIAERGRLCRKSKD QCDF FPEFCNGETEGC	$\alpha_6\beta_1$
		Rat	CRKSTD QCDF FPEFC	$\alpha_9\beta_1$ ⁷³
		Human	CTIHERGHVCRKSVDM CDF FPEYCNGTSEFC	
		Monkey	CTIYARGHVCRKSIDM CDF FPEYCNGTSEFC	
4	TMDCV	Mouse	CKFAPTGTICRDKNGI CDL PEYCSGASEHC	ND
5	tMDC II	Mouse	CTVKMNDVWCRKSVDE CDL LLEYCNGKDPYC	ND
6	tMDC IV	Rat	CTYSPSGTLCRPIQNI CDL PEYCSGNNIGC	ND
7	EAP I	Monkey	CQIKKAGSICRPAED ECDF PEMCTGHSPAC	$\alpha_4\beta_1$, $\alpha_4\beta_7$ ⁸⁰
8	MS2, CD156	Mouse	CKVKPAGEVCRLSKDK CDL EEFC DGRKPTC	ND
9	MDC9, meltrin γ	Mouse	CQFLPGGSMCRGKTS ECDV PEYCN GSSQFC	$\alpha_2\beta_1$
				$\alpha_3\beta_1$ ⁷⁹
				$\alpha_6\beta_1$ ⁸¹
				$\alpha_9\beta_1$ ⁸¹
				$\alpha_6\beta_4$ ⁸²
				$\alpha_v\beta_5$
10	MADM; kuzbanian	Rat	<u>RDDSDCAKEGIC</u>	ND
		Human	<u>RDDSDCAREGIC</u>	
11	MDC	Human	<u>REAVNECDIAFTC</u>	ND
12	Meltrina	Human	CQFLPGGSMCRDSSNS CDL PEFCNGSSQFC	$\alpha_4\beta_1$ ⁸³
				$\alpha_7\beta_1$ ⁸⁴
				$\alpha_9\beta_1$ ^{84, 85} β_3 ⁸⁶
13	(<i>Xenopus laevis</i>)			ND
14	adm-1, UNC-71	<i>C.elegans</i>	CELRKAGDTCRSSKSP CDV AEQCDGKSGDC	ND
15	Metargidin; MDC 15	Mouse	CKLHPAGWLCRPPTDD CDL PEFCPGDSSQC	$\alpha_4\beta_1$ ⁸⁷
		Human	CQLRPSGWQCRPTRGD CDL PEFCPGDSSQC	$\alpha_5\beta_1$ ⁷² $\alpha_9\beta_1$ ⁸⁴ $\alpha_v\beta_3$ ⁷²
16	MDC 16	<i>X.laevis</i>	CKLLPKGTLCRMPKT ECDL AEYCDGASNHC	ND
17	TACE			$\alpha_5\beta_1$ ⁸⁸
18	TMDCIII	Rat	CELSAAGTPCRKVDP ECDF TEYCNGTSSDC	ND

Table 1-1. (continued)

	Other names	Species	Disintegrin Loop	Integrin-binding
19	Meltrin β			$\alpha_4\beta_1$ ⁸⁸ $\alpha_5\beta_1$
20		Human	CFKPSGTLCRQQVGECDLPEWCNGTSHQC	ND
21	ADAM-31	Mouse	CKFMLLGELCRPKINECDLPEWCNGTSHQC	ND
22	MDC 2	Mouse	CKFQPLGTVCREAVNDCDIREICSGNSSQC	ND
23	MDC 3	Human	CLFQPRGYECRDAVNECDITEYCTGDSGQC	$\alpha_v\beta_3$ ⁸⁹
24	Testase-1	Mouse	CQIQPSGTLCRARENECDLPEWCNGTSHEC	ND
25	Testase-2	Mouse	CQIMPAGTVCRQEVNECDLPEWCNGHSHKC	ND
26	Testase-3	Mouse	CQFLKTGTVCREEKNECDLPEWCNGTSAEC	ND
27	ADAM-18	Mouse	CELSASGTVCRKVDPECD E TEYCDGSSSHC	ND
28	eMDCII, MD-Lm, MDC-Ls, TECADAM	Mouse	CQLKPGWVCRAAKDECDLPEYCDGKSSHC	$\alpha_4\beta_1$ ⁸⁰ $\alpha_4\beta_7$
29		Human	CKFLPSGKVC R KEVNECDLPEWCNGTSHKC	ND
30				ND
31	ADAM-21			ND
32		Mouse	CQFLPEKHQCRPEKLYCDIPEVCNGSSGNC	ND
33		Mouse	CLLKSAGTPCRPAATDCDLPEFCTGTSPYC	$\alpha_4\beta_7$ ⁸⁰ $\alpha_5\beta_1$ ⁸⁸ $\alpha_9\beta_1$
34	Testase 4	Mouse	CQFLKTGTVCREEKNECDLPEWCNGTSAEC	ND
35	Meltrin epsilon	<i>G.gallus</i>	CHFHPSGHKCRSEVDECDLPEYCNGTSEWC	ND
36	Testase 6	Mouse	CQFLQTGTVC R QEKNECDLPEWCNGTSGEC	ND
37	Testase 7	Mouse	CQFLKAGTVCRQEKNECDLPEWCNGTSGEC	ND
38	Testase 8	Mouse	CQIMPAGTVCREEVNECDLPEWCNGHSHKC	ND
39	Testase 9	Mouse	CQIMEAGTVCRKRDNECDLPEWCNGHSHKC	ND
40	Testase 10	Mouse	CQIMPAGTVCREEVNECDLPEWCNGHSHKC	ND

Fertilin β and cyritestin have roles in sperm-oocyte binding and fusion.^{90, 91}

Antibodies against fertilin β and cyritestin,^{39, 65, 92} and recombinant forms of two ADAM

proteins^{73, 78, 93-98} inhibit oocyte fertilization. Synthetic fertilin β and cyritestin oligopeptides from the disintegrin loops^{39, 53, 95, 96, 99-102} also inhibit fertilization. These experiments support that fertilin β and cyritestin disintegrin domains are the primary binding domains.

The short peptide sequence glutamic acid-cysteine-aspartic acid (ECD) and glutamine-cysteine-aspartic acid (QCD) are highly conserved in the fertilin β and cyritestin disintegrin loops, respectively.¹⁰³ Fertilin β and cyritestin are located in the equatorial region of the sperm head, and during sperm maturation, their disintegrin domains are exposed on the sperm head.^{3, 39, 92-94, 103, 104} It has been reported that these tripeptides, ECD^{78, 95, 101, 105} and QCD^{96, 101} are the minimal recognition element necessary for the binding to the oocyte.

Knockout of the fertilin β or cyritestin gene in mice reduces binding of sperm to the oocyte plasma membrane.^{55, 106} Male fertilin β knockout mice are infertile, and fertilin β $-/-$ sperm are defective in binding to and fusing with wild-type oocytes in vitro.⁵⁵ Fertilin β knockout sperm show impaired migration from the uterus to the oviduct. However, interpretation of the genetic studies is complicated by the unexpected interdependence of protein expression amongst ADAM proteins in the testis. Knockout of the fertilin β gene results in a significant reduction of other ADAM protein levels on the sperm surface, including ADAM1a, ADAM1b, ADAM3 (cyritestin), ADAM5 and ADAM7, whereas others are unchanged, e.g., ADAM27 and ADAM32.^{48, 60, 61, 107, 108} Nishimura and co-workers produced mice lacking the sperm surface protein, cyritestin, and found those mutant males are infertile as well.¹⁰⁶ Cyritestin knockout sperm have normal movement to oviduct,^{58, 106} however, cyritestin knockout sperm binding to the

oocyte plasma membrane is greatly reduced.^{55, 106} Knockout of the cyritestin gene shows a similar, but not identical codependence of protein expression and maturation. The dependence of non-ADAM protein expression levels on the presence of ADAM genes is unknown. In addition, at least 9 testis-expressed ADAM proteins contain the ECD motif.^{39, 71, 73, 109} The array of ADAM proteins expressed in sperm with potentially overlapping functions makes a genetic approach problematic.

II.1.2. Sperm-associated cysteine-rich secretory protein 1 (CRISP1)

The protein known as DE (protein bands D and E) was first identified in rat epididymal protein lysates in 1976.¹¹⁰ Additional related proteins were characterized, and the CRISP family was identified. CRISP2 is found primarily in the testis,^{40, 111} and the tissue distribution of CRISP1 is variable.^{112, 113} CRISP1 has been studied mostly in the rat. The protein is secreted on the dorsal region of the acrosome of cauda epididymal rat and mouse sperm,¹¹⁴ and relocates to the equatorial segment during capacitation.¹¹⁵ There are data regarding how this protein is implicated in gamete interactions. Anti-DE antibodies inhibit rat oocytes in vitro fertilization.¹¹⁶ CRISP1 protein purified from rat epididymal extracts adheres to the oocyte plasma membrane, and so inhibits fertilization.^{114, 115} However, binding partners of sperm-associated CRISP1 on the oocyte membrane are not identified. The molecular mechanism of gamete interaction involved in CRISP1 is also not yet understood.

II.1.3. Izumo

The sperm protein Izumo was identified by screening studies of anti-sperm monoclonal antibodies. The monoclonal antibody OBF13 adheres to the head of the capacitated sperm, and inhibits sperm-oocyte binding on zona pellucida-free oocytes in vitro.^{41, 117} The Izumo gene for the OBF13 antigen was identified, and is a member of the immunoglobulin super-family of proteins. This protein is exposed on the sperm surface membrane after the acrosome reaction. Izumo *-/-* sperm are able to adhere to zona pellucida-free oocytes. However, they cannot fuse with the oocyte plasma membrane. These results suggest that Izumo plays a critical role for fusion. However, the fusion mechanism is not yet clear.

II.2. Oocyte proteins

II.2.1. Integrins

Integrins are a family of cell adhesion molecules, and so may mediate sperm-oocyte adhesion. Since the disintegrin domains in fertilin β and cyritestin were identified, studies were launched to determine whether oocyte integrins mediate gamete interaction, and if sperm ADAMs interact with oocyte integrins.

Integrins are $\alpha\beta$ heterodimers. The combination of 18 α units and 8 β units generates 24 unique integrins. The α and β subunits form a quaternary structure with a length of about 23 nm, and the final 5 nm N-termini of each subunit serves as a ligand-binding region for extracellular matrix proteins. The X-ray crystal structure was

published for the complete extracellular domain of an integrin $\alpha_V\beta_3$ in 2001.¹¹⁸ This structure is not the active form. The structure of the integrin $\alpha_V\beta_3$ consists of a globular head part supported by two rod-like leg parts.¹¹⁹ In mammalian oocytes, the following integrin subunits have been identified: α_2 , α_3 , α_4 , α_5 , α_6 , α_V , α_9 , α_M , β_1 , β_2 , β_3 and β_5 (Table 1-1).

ADAM proteins are known to interact with integrins. A monoclonal antibody to integrin α_6 (GoH3) inhibited sperm binding to mouse oocyte surface membrane,¹²⁰ but inhibition was dependent on the type of IVF assay used.^{90, 93, 121} Chen and Sampson showed that a photoaffinity tagged fertilin β oligopeptide binds to and labels the integrin $\alpha_6\beta_1$ on the mouse oocyte surface.¹²² Peptide competition and direct adhesion experiments have suggested that fertilin β as well as cyritestin bind to integrin $\alpha_9\beta_1$ on epithelial cells.^{73, 84, 98} And $\alpha_4\beta_1/\alpha_9\beta_1$ specific inhibition does not inhibit fertilization in the mouse.¹²³ Although α_9 cDNA is detected in mouse oocyte cDNA libraries, $\alpha_9\beta_1$ integrin has not been detected on oocytes.¹²⁴ However, female mice with a conditional knockout of integrin β_1 in their oocytes are still fertile in vivo and in vitro.¹²⁵ Thus, none of the known integrins present on the oocyte plasma membrane are essential in sperm-oocyte binding and fusion,^{121, 123, 125} which suggests that there might be receptors other than integrin $\alpha_6\beta_1$ or $\alpha_9\beta_1$ for fertilin β and cyritestin on oocyte surface membrane.

II.2.2. Tetraspanins

Tetraspanins are a family of cell membrane proteins expressed in all multicellular eukaryotes. The proteins have four transmembrane domains, a short extracellular loop (EC1), a very short intracellular loop (typically 4 amino acids), and a longer extracellular

loop (EC2).¹²⁶ The EC2 is divided into a constant region containing three α helices and a variable region containing various protein-protein interaction sites.^{127, 128}

Tetraspanins do not function as receptors for extracellular ligands, but have functional roles in biological processes, such as cellular adhesion, motility, proliferation and tumor cell metastasis.¹²⁹⁻¹³¹ They form intramembrane associations with other tetraspanins, integrins, immunoglobulin super-family members, proteoglycans, complement regulatory proteins, and growth factor receptors.^{129, 130, 132-134}

There are 34 tetraspanins in mammals reported, and one of the family members, CD9 is related to gamete interaction. It has been reported that CD9 knockout female mice are defective in sperm-oocyte fusion.¹³⁵⁻¹³⁷ Sperm observed in the perivitelline space of zona pellucida-intact oocytes are not capable of fusing with the oocyte plasma membrane. Moreover, anti-CD9 antibodies inhibit mouse oocyte fertilization in vitro.¹³⁸ A tripeptide sequence, SFQ in positions 173-175 was characterized as a key sequence for sperm-oocyte fusion.¹³⁹ Besides CD9's function for sperm-oocyte fusion, CD9 is implicated in sperm-oocyte binding. CD9 or a CD9-associated complex may be involved in the oocyte supporting sperm binding.¹⁴⁰ When anti-CD9 antibodies or the recombinant large extracellular loop are preincubated with oocytes, sperm binding to the oocyte plasma membrane is decreased.^{138, 141} Anti-CD9 antibodies prevent binding of recombinant forms of the sperm proteins, fertilin β and cyritestin, when the two proteins are immobilized on beads.^{96, 98} These results suggest that CD9 functions in strengthening adhesion of the sperm to the oocyte membrane. Another protein member of tetraspanins, CD151 also has a function in strengthening adhesion to laminin.¹⁴²

CD81 expressed in mouse oocytes is also involved in gamete interactions. CD81 knockout female mice have decreased fertility because the protein is utilized in sperm-oocyte fusion as well.¹⁴³ CD81 knockout oocytes are rarely fertilized in vitro. Anti-CD81 antibodies or recombinant large extracellular loop inhibit sperm-oocyte binding and fusion moderately.^{96, 141}

Notably, CD9 and CD81 double knockout female mice are completely infertile, which suggests that these two proteins serve as a complement to each other.¹⁴³ In CD9 knockout oocytes, CD81 is over-expressed, thus oocytes are partially rescued from infertility.¹⁴⁴ However, the molecular mechanisms involved in either of CD9 or CD81 are not yet understood.

II.2.3. GPI-anchored proteins

GPI-anchored proteins on the oocyte plasma membrane are involved in gamete interactions. Glycosylphosphatidylinositol (GPI-anchor) is a glycolipid on the cell surface which can be attached to the GPI moiety of a protein. PIG-A is a subunit of an N-acetyl glucosaminyl transferase, which takes part in GPI synthesis.¹⁴⁵ Female mice with an oocyte-specific knockout of PIG-A are infertile.¹⁴⁶ In PIG-A deficient oocytes, sperm are observed in the perivitelline space of oocytes, and sperm binding and fusion to the oocyte plasma membrane is decreased.¹⁴⁶ Upon addition of GPI-anchor cleavage enzyme, PI-PLC, to the mouse oocyte, sperm-oocyte binding and fusion are reduced as well.¹⁴⁷ However, the identity of specific oocyte GPI-anchored proteins and the characterization of their functions are unknown. Because GPI-anchored proteins participate in various

cellular processes, such as signal transduction, membrane trafficking and cell adhesion,¹⁴⁸
¹⁴⁹ further investigations are needed to identify the role of GPI-anchored proteins.

III. Multivalent Interactions and Linear Scaffold Polymerization

III.1. Multivalent interactions

Why is engineering cell surface and substrate interactions of interest? Cell surface membranes contain various proteins such as receptor proteins, cell adhesion proteins, as well as other functional proteins. Especially understanding the pathway of receptor proteins is crucial to grasp a cell's activity in its entirety. Although cell surface receptors vary the ways to carry the information into the cellular interior, universally the binding of substrate to receptor initiates a series of responsive incidents. These binding events on the cell surface trigger molecular interactions, and then alter the cellular state. Through the elucidation of cell surface and substrate interactions, the receptor topology on a cell surface required to initiate and antagonize cellular signaling may be characterized. These types of investigations further lead to the practical application of biosensing pathogens and toxins, drug delivery to specific cell types, and tissue engineering.

Among the diverse approaches to engineer cell surface receptor and substrate interactions, multivalent molecules have been specially adopted for use in the field. Molecules with multiple copies of a ligand can lead to stronger overall cell surface adhesion¹⁵⁰ and biosensing.¹⁵¹

Multivalency is defined as the interaction between multiple copies of receptors and ligands. A multivalent ligand contains multiple binding domains tethered together through a backbone scaffold. Because the numerous individual binding sites in a single multivalent ligand interact sequentially, the binding efficiency of multivalent ligand is greatly enhanced compared to that of sequential monomeric interactions. The probability of the ligands specifically binding to the cell surface receptors or active sites is increased, and simultaneous high-affinity interactions occur. The valency of a single multiple ligand is defined by the number of binding elements present. In most cases, there is a strong link between valency and binding affinity. The binding affinity in multimeric interactions is also described by the binding avidity.¹⁵²

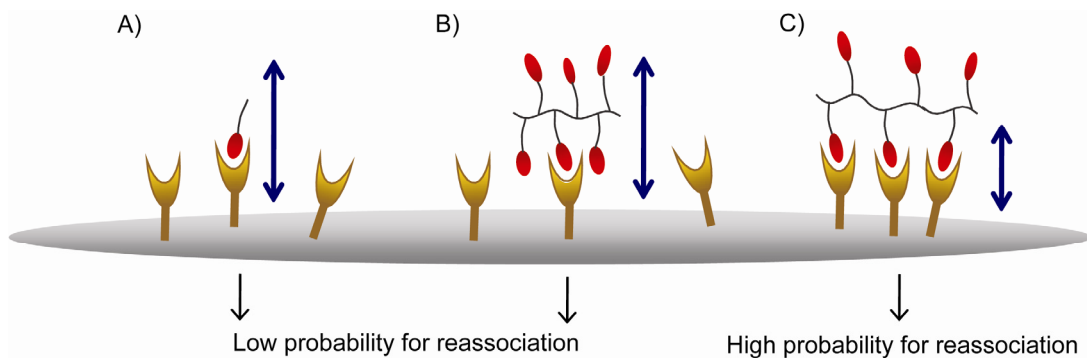


Figure 1-4. Reassociation of monovalent versus multivalent ligand binding. A) Monomer binds to a receptor, and the reassociation probability is low. B) A multimeric ligand binds to a receptor monovalently, and its reassociation probability is low. C) A multimeric ligand binds to receptors multivalently, and there is high probability for reassociation.

The binding of molecules with multivalent ligands compared with a monovalent ligand to the cell has increased avidity, such as dendrimers, liposomes,¹⁵³ monolayers,

and grafted bulk polymers. Dendrimers built from branched monomeric units have numerous biologically potential applications. Unlike linear polymers, dendritic polymers have their own distinct biodistribution and pharmacokinetic properties. They have high structural and chemical homogeneity, and their degradation is controlled.¹⁵⁴

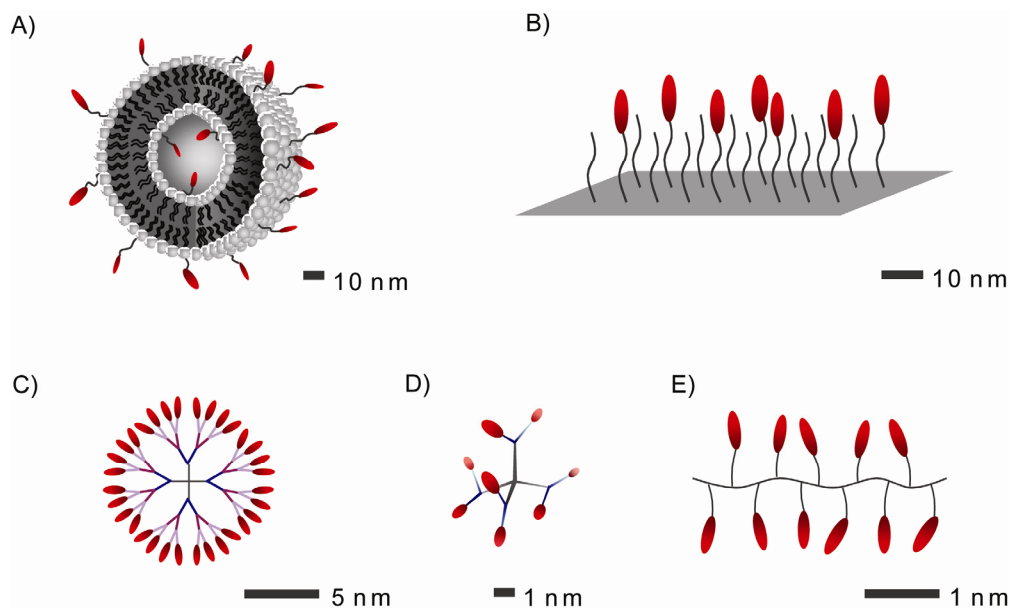


Figure 1-5. Commonly used scaffolds for multivalent systems and their approximate size.¹⁵⁵ A) Liposome. B) Monolayer. C) Fourth generation dendrimer. D) Second generation dendrimer. E) Linear polymer.

Spherical, self-closed structures, liposomes are able to display proteins, peptides, polymers and other molecules to their surface. Due to their biocompatibility and huge capacities as specific molecule carriers, liposomes are widely used in the biomedical area. However, it is still challenging to formulate with quality control.¹⁵⁶ End-grafted polymer brush layers have polymer dangling chains attached by one end to a surface, and the

polymer chains stretch out from the surface in order to decrease their interaction. Due to their molecular order and high density, polymer brushes are also useful in molecular recognition, biosensing and scaffolding for tissue engineering.¹⁵⁷

The advantages of synthetic multivalent molecules are improved avidity as well as specificity. Although heterogeneously mixed compounds with recognition ligands could increase their affinity to the cell, it is difficult to determine the precise length between receptors on the cell surface. Therefore, linear polymers with engineered density and spacing are of high interest currently. For example, a wide range of polymers varying density and length has been published such as proteins bearing polymers^{158, 159} by atom transfer radical polymerization (ATRP), and neoglycopolymers¹⁶⁰⁻¹⁶² and oligopeptide-substituted polymers¹⁶³⁻¹⁶⁵ by ring opening metathesis polymerization (ROMP). For more precise studies of multivalent molecular interactions, it can be beneficial to use a block copolymer system. However, a choice of the density of ligands, and the flexibility and length of backbones or spacers are critical to optimize the design of multimeric ligands. A spacer should be decided with care to its architecture, rigidity, length and biological compatibility.¹⁶⁶ The distance between two adjacent receptors should be considered for designing block copolymers.¹⁶⁷ Two binding sites corresponding to the distance between their targets result in increased avidity.^{168, 169} Ligands at each terminus of a short spacer are not capable of binding bivalently, therefore affinity is not increased as well. In the case of ligands with a longer spacer than the distance between their binding sites, the conformational entropy is enhanced making the system less favorable for effective binding.

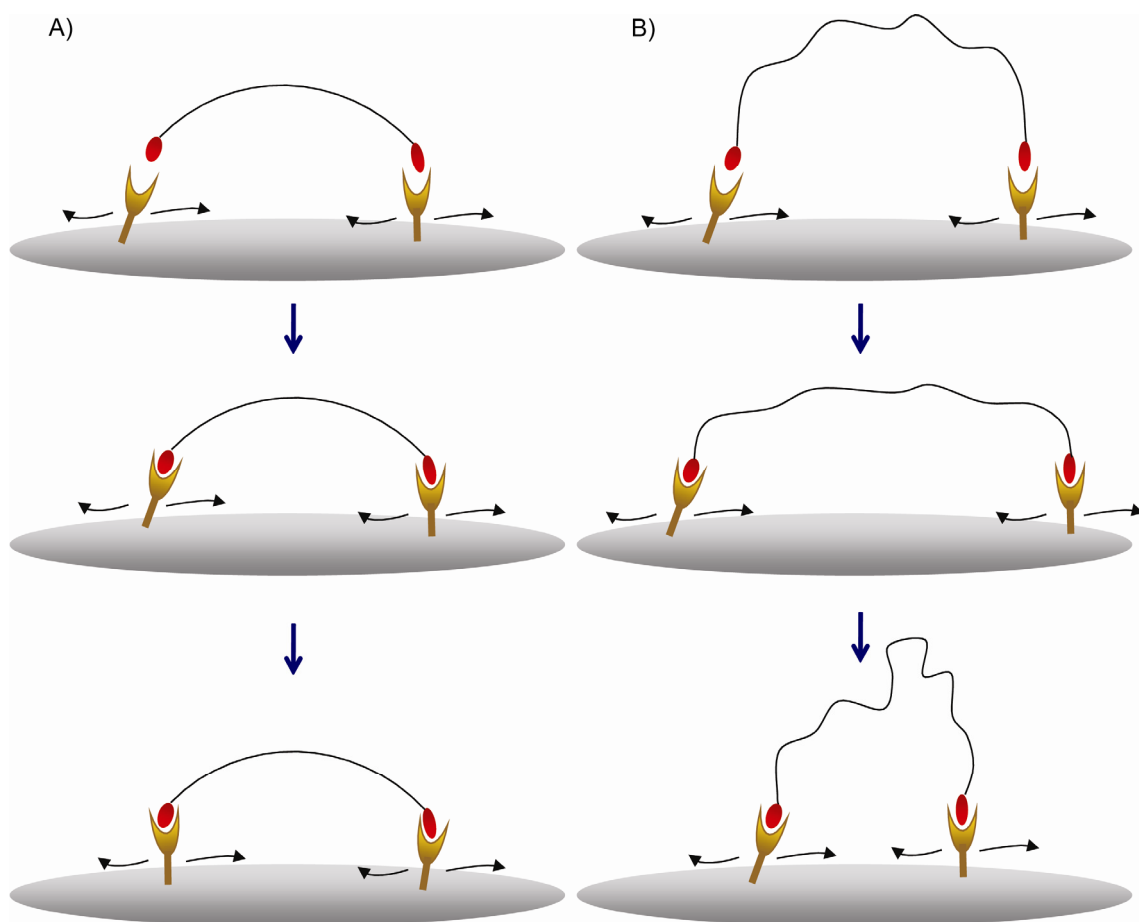


Figure 1-6. Schematic representation of the concept of the flexibility of spacer of a block copolymer system. A) A rigid spacer polymer bound to receptors. B) A more flexible spacer polymer bound to receptors.

Another aspect would require the flexibility of the spacer when designing a bivalent system. Various examples of spacers have been reported such as the highly hydrophilic and flexible polyethylene glycol (PEG),^{169, 170} more rigid aromatic moieties,¹⁷¹ and substituted oligosaccharides.¹⁷² If a spacer is extremely rigid, the additional ligand would not be free for reaching between the binding sites. Although ligands in a rigid spacer bind the ligand-receptor pair, the entropy loss of the rigid spacer may be increased due to constraining receptor movement (Figure 1-6A). On the other

hand, if a spacer is too flexible, first ligand-receptor interaction occurs readily (Figure 1-6B), and the spacer allows for movement of the receptor within the membrane. However, owing to more entropy from the flexible spacer, the degree of subsequent binding events may be reduced. Therefore, it is recommended that spacers should be relatively rigid.¹⁵²

173

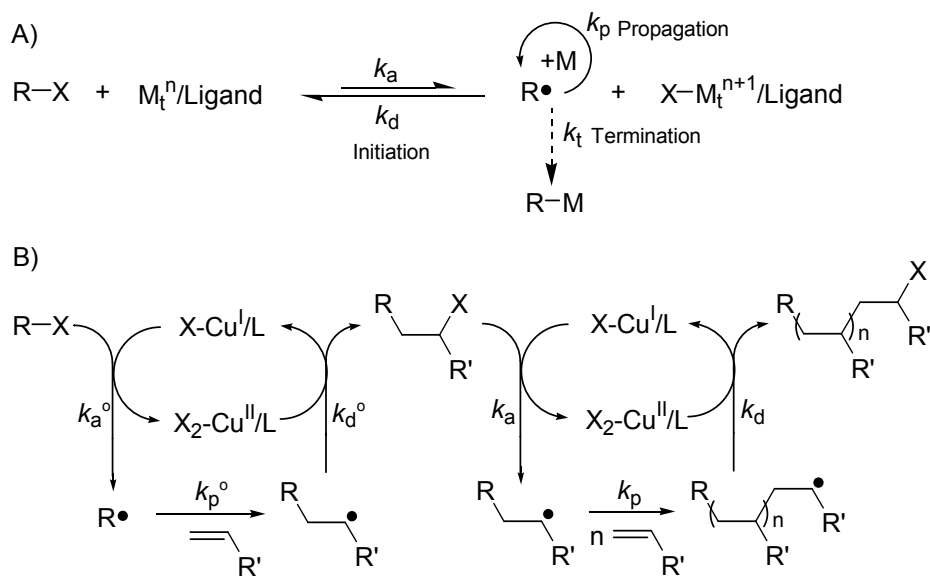
III.2. Linear scaffold polymerization

More advanced techniques to prepare controlled polymers which have various architectures, solubility, flexibility and functionality have become available. The flexibility of polymers depends on their backbone structure as well as the functional groups. Control of density, location and length of functional group is crucial to investigate receptors on the cell surface. The different synthetic routes to polymers are comprised in living anionic (ROMP), living cationic, and living radical (ATRP) polymerization. By living polymerization techniques, polymers with exact predetermined length and density and narrow polydispersities can be prepared.

III.2.1. Atom transfer radical polymerization (ATRP)

Cationic radical polymerization (CRP) was developed and extended to atom transfer radical polymerization (ATRP) involving free radical reactions in 1995. Matyjaszewski and coworkers reported a controlled “living” polymerization that used simple, readily accessible, and inexpensive catalysts and initiators.¹⁷⁴ The polymerization

is tolerant of water and oxygen, and can be performed with a wide variety of monomers including various styrenes, acrylates and methacrylates as well as other monomers such as acrylonitrile, vinyl pyridine, and dienes. Simple alkyl halides initiate the polymerization, and transition metal-based catalysts (iron, copper) allow the reactions to be controlled. The radical species, before and after addition of the unsaturated monomer possess comparable reactivity, and then the activation-addition-deactivation cycle repeats to form chain transferred polymers.



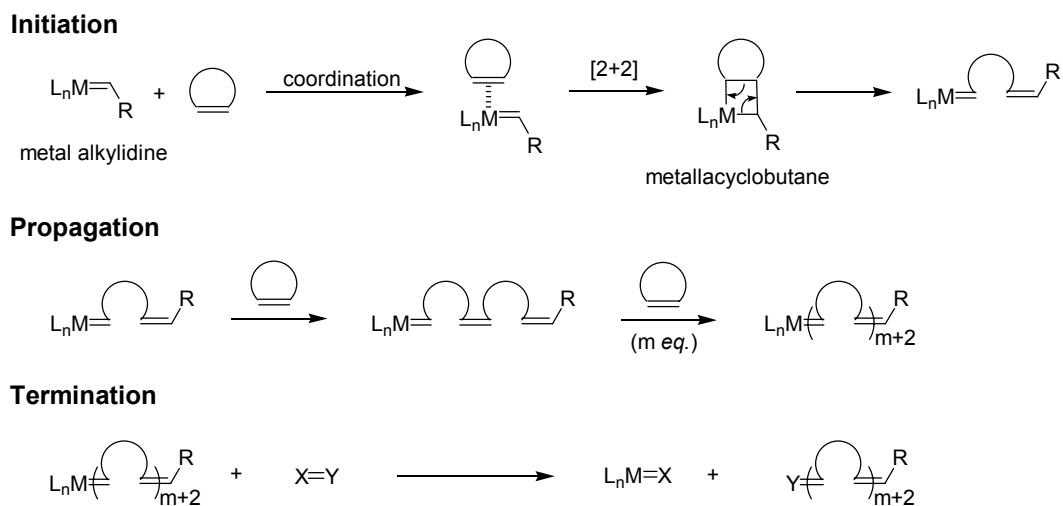
Scheme 1-1. Atom transfer radical polymerization. A) Overview of ATRP. B) Chain growth polymerization.

Synthesis of block copolymers is also accessible by a macro-initiator route or by sequential monomer addition. Biologically active ATRP polymers containing carbohydrates have been reported recently.^{175, 176} Moreover, protected alkyne

monomers¹⁷⁷ and azido monomers^{178, 179} are polymerized via ATRP in a controlled manner. These polymers are elaborated by Cu(I)-catalyzed Huisgen 1,3 dipolar cycloaddition (click chemistry) with azido- and alkyne-functionalized ligands, respectively.

III.2.2. Ring opening metathesis polymerization (ROMP)

ROMP is a chain growth polymerization in which cyclic olefins are elongated to a polymeric material.^{180, 181} A metal-mediated carbon double bond is converted to polymer. Chauvin *et al.* proposed a general mechanism for ROMP in 1971.¹⁸² The cyclic olefin monomer forms a metal alkylidene complex with a transition metal catalyst, so the reaction is initiated (Scheme 1-2).



Scheme 1-2. Overview of a typical ROMP reaction.

After formation of the metal-carbene complex, subsequent [2+2] cycloaddition forms a highly strained metallacyclobutane intermediate. The ring in the intermediate opens to give a new metal alkylidene. The chain growth process proceeds during the propagation stage until all monomer is consumed. Then the reaction is terminated by adding specialized reagent.

There are three noteworthy aspects for metal-mediated ROMP reaction reported by Bielawski and Grubbs.¹⁸³ First, the metal centers in the propagating polymer chains may exist in either the metallacyclobutane or metal alkylidene form. According to the transition metal and its ligands, and the reaction condition, the population of the intermediate species differs. Second, ROMP reactions are equilibrium-controlled, that is, the reactions are reversible. The equilibrium between monomer and polymer can be predicted, so the desired polymers can be obtained. The driving force of the reaction is the release of ring strain of the cyclic olefin. The most common cyclic olefin monomers possess greater than 5 kcal/mol of ring strain, such as cyclobutene, cyclopentene, cis-cyclooctene, and norbornene.¹⁸⁴ Last, a successful ROMP reaction may be performed with the highest monomer concentration at the lowest temperature possible, due to enthalpic contribution from the relief of ring strain.

A “living polymerization” was defined by Swarzc as a reaction proceeding without chain transfer or termination.^{185, 186} Besides Swarzc’s original concept of the living polymerization, a ROMP reaction requires three more features for its living and controlled reaction.^{187, 188} First, the initiation should be fast and complete. Second, there should be a linear relationship between polymer formation and monomer consumption. Third, polymers should be narrowly polydispersed with PDIs < 1.5.

III.3. Metal-mediated ROMP catalysts

Early catalytic systems were extremely air and moisture sensitive heterogeneous mixtures. Because a catalyst plays a pivotal role to provide a well-defined polymer, enormous studies have been pursued to develop well-defined and functional group tolerant catalysts. Homogenous catalytic systems mediating living ROMP reactions have been reported, such as titanium-based Tebbe reagents,¹⁸⁹⁻¹⁹¹ tantalum complexes by Schrock and coworkers,¹⁹²⁻¹⁹⁴ tungsten-based catalysts by Schrock and Osborn,¹⁹⁵⁻¹⁹⁸ molybdenum-based alkylidenes,¹⁹⁹ and ruthenium-based complexes.²⁰⁰

III.3.1. Molybdenum-based catalysts

When Schrock and coworkers developed metal-based catalytic systems, well-defined molybdenum catalysts were introduced for ROMP reactions (Figure 1-7). The catalysts show functional group tolerances with a broader range than other metal-based catalysts: ester, amide, imide, ketal, ether, cyano, trifluoromethyl, and primary halogen-containing monomers. The catalysts display increased tolerance to oxygen and water, and more stability to decomposition and side reactions. Norbornenyl monomers undergo polymerization with the Mo-based catalysts to provide living ROMP polymers with narrow polydispersities and controlled molecular weights.

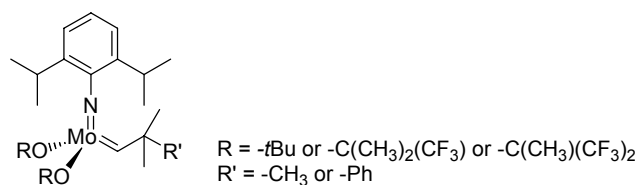


Figure 1-7. Molybdenum-based imido alkylidene catalysts.

Owing to the high functional group tolerances, the catalysts were able to provide synthetically homogeneous and linear biological polymers,^{201, 202} and star shape polymers.²⁰³ One of the remarkable benefits is their ability to produce stereoregular polymers.²⁰⁴⁻²⁰⁶ ROMP reactions of 2,3-bis(trifluoromethyl)bicyclo[2.2.1]hepta-2,5-diene with *tert*-butyl substituted catalyst provide over 98% trans olefin geometry on the polymer backbone. However, fluoride-derived (-C(CH₃)(CF₃)₂) catalyst provides over 98% cis polymers. Based on the results, a new class of Mo-based catalysts with C₂-symmetric diolate ligands was introduced, which allowed the synthesis of highly isotactic polymers.²⁰⁷

III.3.2. Ruthenium-based catalysts

Since the transition metal, ruthenium complexes were introduced for polymerization,²⁰⁸⁻²¹⁵ well-defined Ru-based catalytic systems have been developed for ROMP.^{216, 217} The Ru-based catalysts have exceptional functional group tolerances compared to other transition metal-based catalysts, especially toward polar functionalities (Table 1-2).


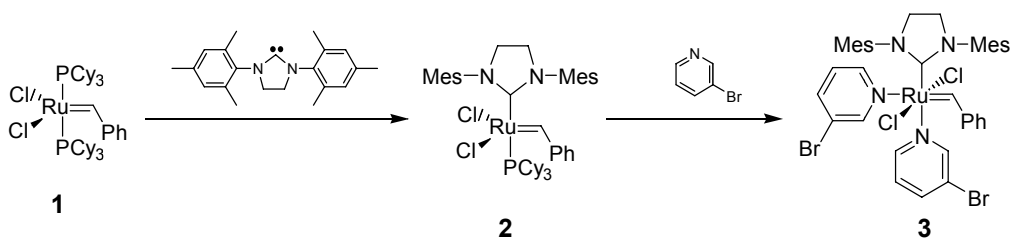
Reactivity	Ti/Ta	W	Mo	Ru
	acids	acids	acids	olefins
	alcohols	alcohols	alcohols	acids
	aldehydes	aldehydes	aldehydes	alcohols
	ketones	ketones	olefins	aldehydes
	esters/amides	olefins	ketones	ketones
	olefins	esters/amides	esters/amides	esters/amides

Table 1-2. Functional group tolerance of early and late transition metal-based ROMP catalysts.

The first homogeneous well-defined Ru complex for ROMP was $(PPh_3)_2Cl_2Ru=CH-CH=CPh_2$.²⁰⁰ Although this catalyst has a broad range of functional group tolerance and mediates living ROMP reaction with norbornene and cyclobutene monomers, the catalytic activities for other olefins are reduced. To increase the catalytic activities, the bulky and electron-rich phosphine ligands were substituted. The catalysts containing phosphine are tolerant to a broader range of functional groups, such as water and alcohols. However, ROMP reactions of norbornene with the catalyst containing phosphine are not controlled. Because of the different reaction rates between initiation and propagation, the catalyst is not able to provide the desired polymers. Besides, chain transfer reactions occur to yield broadly polydispersed polymers ($PDI > 2$).²¹⁸



Scheme 1-3. Ruthenium-based catalysts **1**, **2** and **3**.

The treatment of $(\text{PPh}_3)_3\text{RuCl}_2$ with diazobenzylidene provides a catalyst that has more enhanced activity. Complex **1** catalyzes norbornene and cyclobutene monomer metathesis in the presence of various functionalities.²¹⁹⁻²²² However, ROMP reactions with complex **1** are still not highly controlled polymerizations, because of the slow initiation rates. A phosphine ligand must dissociate from the catalyst from olefin-ruthenium coordination to occur. However, the intermediate is not coordinately saturated. Because *N*-heterocyclic carbenes (NHCs) are strong σ -donors with less lability than phosphines, they provide enhanced electrons to stabilize intermediates.²²³⁻²²⁷ Catalyst **2** containing NHCs has exceptional activities in an enormous number of ROMP reactions.²²⁸ However, ROMP reactions with catalyst **2** produce polymers with uncontrolled molecular weights and broad polydispersities due to relatively slow initiation rates and secondary chain transfer reactions. A new class of Ru-based catalysts was developed including catalyst **3**.²²⁹⁻²³³ This class has NHCs with weakly coordinating pyridines, and so exhibits extremely improved initiation rates. In addition, ROMP reaction with catalyst **3** provides polymers with highly controlled molecular weights and PDIs as low as 1.06. However, complete living ROMP remains to be achieved. Therefore, the development of a new class of catalysts and monomers should be considered.

III.4. Analysis of polymers

Synthetic multivalent ligands which mimic binding elements of natural proteins have been used to identify their receptors as well as their mechanism of action on living cells.²³⁴ Various polymer systems containing biologically active ligands have been

synthesized and their biological activities tested. The identity and purity of these biological polymer systems should be assessed for precise results. Numerous analytic methods have been developed to determine physical parameters including molecular mass (M_w and M_n), particle size and degree of aggregation. In particular, characterizing molecular weights and their distributions is one of the powerful ways to define the macromolecules.

Mass spectrometry is a core technique for characterizing polymers due to its high sensitivity and accuracy. Matrix-assisted laser desorption ionization (MALDI) and electrospray ionization (ESI) mass spectrometry enable the analysis of large biomolecules without thermal decompositions. However, there are technical limits for studying their behaviors in solution or their polymeric state.²³⁵

Another common technique for measuring molecular mass is gel permeation chromatography (GPC). In this case, a differential refractive index detector and a multi-angle light scattering detector allow the molecular mass to be measured.

Laser light scattering is a direct method for determining absolute molecular mass and the size of macromolecules in solution. When light hits a small particle, light scatters in all directions, which is called Rayleigh scattering. If polarized monochromatic light passes through a solution containing macromolecules, the excess light scatters. The amount of light scattered by molecules is directly proportional to the molecular mass and concentration. Static light scattering measurements on dilute polymer solutions provide the weight-average molecular weight (M_w), the z-average radius of gyration (R_g), and the second virial coefficient, A_2 . The following is the Rayleigh-Debye-Zimm approximation for dilute polymer solutions.²³⁶⁻²³⁸

$$\frac{K^*c}{R(\theta)} = \frac{1}{M_w P(\theta)} + 2A_2c$$

Where c is the sample concentration, $R(\theta)$ is the excess intensity of scattered light at angle θ , M_w is the weight-average molecular weight, and A_2 is a second virial coefficient. Form factor, $P(\theta)$ describes the angular dependence of scattered light, and can be expressed as $P(\theta) = 1 - (16\pi^2/3\lambda_0^2)R_g^2\sin^2(\theta/2)$: R_g^2 is the mean square radius of the molecules. The physical constant K^* is an optical parameter equal to $4\pi^2n^2(dn/dc)^2/(\lambda_0^4N_A)$: n is the solvent refractive index, dn/dc is the refractive index increment, λ_0 is the wavelength of the scattered light in vacuum, and N_A is Avogadro's number. So, only M_w and A_2 determinations depend on the value of dn/dc .

The number-average molecular weight (M_n) is the ordinary arithmetic mean of the molecular weights of the individual macromolecules, and is determined by GPC utilizing the differential refractive index detector. This is calculated by the molecular weight of n polymer molecules, summing the weights, and dividing by n . ($M_n = \frac{\sum_i N_i M_i}{\sum_i N_i}$) The weight-average molecular weight is determined by light scattering. ($M_w = \frac{\sum_i N_i M_i^2}{\sum_i N_i M_i}$) The polydispersity of a sample is determined by M_w divided by M_n , which indicates how narrow the molecular weight distribution is. The polydispersity index (PDI) is an indicator of molecular mass distribution, and is always greater than 1 unless the polymer is homogenous.

IV. Specific Aims

IV.1. Analysis of oligopeptide-polymers synthesized by ruthenium catalysts: tricyclohexylphosphine versus 3-bromo-pyridine substitution

Because the concept of multivalent molecules is regarded as an effective strategy for designing inhibitors, Roberts in the Sampson group in 2003 used ROMP to prepare norbornenyl polymers, and synthesized multivalent polymers containing oligopeptides (glutamic acid-cysteine-aspartic acid-valine-threonine), **ECDVT₁₀** with catalyst **1** to investigate the role of surface concentration.¹⁶⁴ The norbornenyl polymer, **ECDVT₁₀** was a significantly better inhibitor of sperm-oocyte adhesion than its monomeric peptide counterpart.²³⁹ This result ascertained the importance of multivalent interactions with the fertilin β mimic polymer for inhibition of fertilization.

Based on the biological results from fertilin β mimic, **ECDVT₁₀**, we extended our investigation of various ROMP polymers as inhibitors of fertilization. Using norbornene carboxylic acids containing bio-functional groups has led to easy access to well-defined multivalent systems for biological and medicinal applications. However, the bio-functional polymers were not very well characterized. Thus, we reinvestigate the polymerization conditions to obtain the desired polymers and the characterization of these linear oligopeptide polymers synthesized by ruthenium-catalyzed ROMP with catalyst **2** or catalyst **3**.

IV.2. Mixed fertilin β and cyritestin mimic polymers interrogate sperm-oocyte binding mechanisms

To improve the binding affinity of monomeric peptide ligands on the oocyte surface, we developed synthetic multivalent probes to mimic the active site of fertilin β protein. To define the optimal ECD presentation system for inhibition of fertilization, a simplified multivalent system was needed for further ligand-receptor binding studies. We synthesized a series of linear ECD polymers which were designed to have various copies of ECD ligand by ROMP. Also, a series of cyritestin mimics, linear QCD polymers was tested for inhibition of fertilization to compare their inhibition affinities and patterns with fertilin β mimics. From the assay, we developed a more optimal mimic system for investigating ligand-receptor interactions.

IV.3. Identification of fertilin β and cyritestin receptors on the oocyte surface membrane with “clickable” polymers

ADAM proteins are known to interact with integrins, combinations of α and β integrins in mammals. Especially, integrin $\alpha_6\beta_1$ and $\alpha_9\beta_1$ are known as the binding partners of sperm protein fertilin β and cyritestin. Chen and Sampson showed that a photoaffinity tagged fertilin β peptide binds and labels the integrin $\alpha_6\beta_1$ on the mouse oocyte surface.¹²² Peptide competition and direct adhesion experiments have suggested that integrin $\alpha_9\beta_1$ binds fertilin β as well as cyritestin on epithelial cells.^{73, 84, 98} However, female mice with a conditional knockout of integrin β_1 in their oocytes are fertile in vivo and in vitro,¹²⁵ suggesting that none of the known integrins present on the oocyte plasma

membrane are essential in sperm-oocyte binding and fusion.^{121, 125} Therefore, there might be receptors other than integrin $\alpha_6\beta_1$ or $\alpha_9\beta_1$ for fertilin β and cyritestin on the oocyte surface membrane.

Previously, Jaechul Lee in the Sampson group prepared fluorophore-linked fertilin β mimic block copolymers, and applied them for photoaffinity labeling to identify binding partners on the oocyte plasma membrane. Although zona pellucida-free oocytes were labeled with the polymers, the identification of the labeled oocyte receptors was not achieved. Hence, we developed a more optimal bivalent mimic system, which may serve as a strategy of identifying fertilin β and cyritestin receptors.

Chapter 2

Analysis of Oligopeptide-Polymers Synthesized by Ruthenium Catalysts:
Tricyclohexylphosphine versus 3-Bromo-Pyridine Substitution

V. Introduction

VI. Results

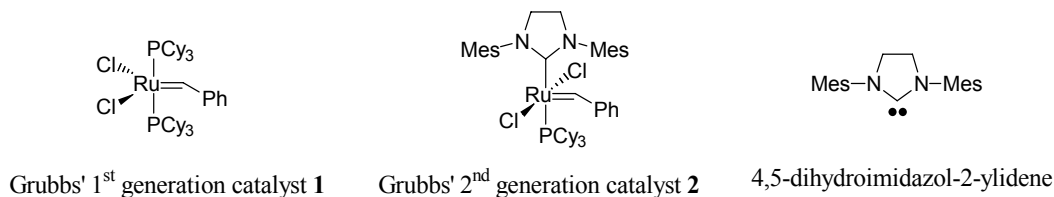
VII. Discussion

VIII. Summary

I. Introduction

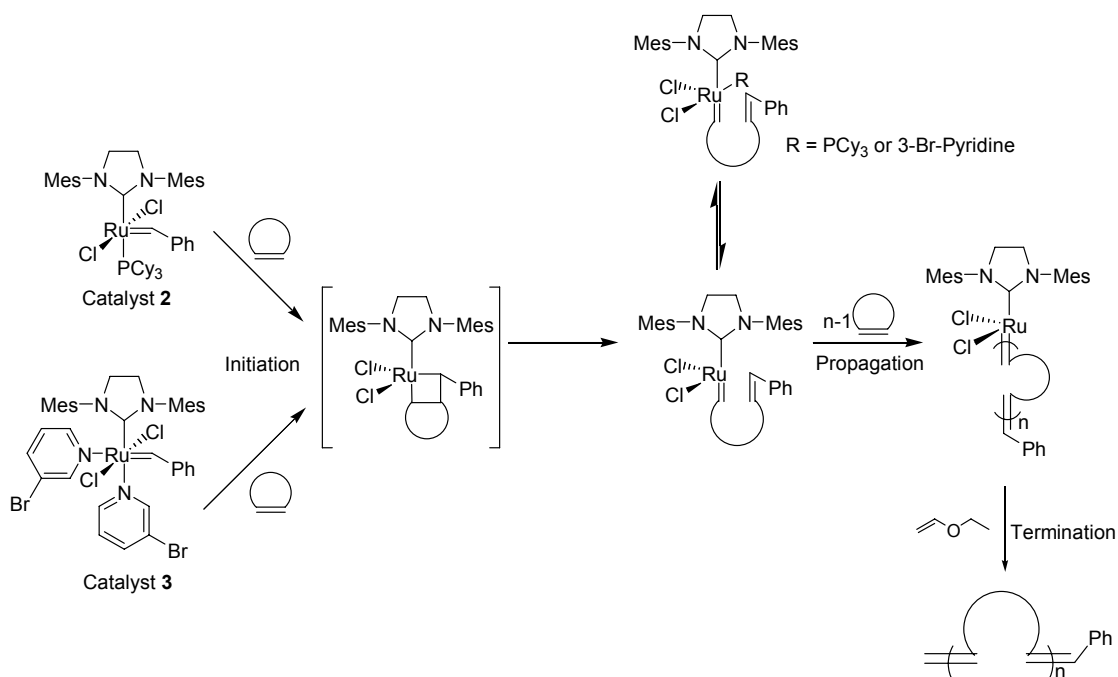
In nature, multiple copies of both ligands and their receptors are available for binding. Multivalent interactions to cell surfaces can promote superior binding affinities in complex biological system, and these interactions are also highly specific. Therefore, they serve as inhibitors^{152, 240} or activators.^{241, 242} Multiple copies of binding ligands enhance binding probabilities- intercellular adhesion to the receptors in numbers. Synthetic multivalent ligands which mimic binding elements of natural proteins have been used to identify their receptors as well as their mechanism of action on living cells.²³⁴

For designing inhibitors, the concept of multivalent molecules is regarded as an effective strategy as well. Various multivalent scaffolds have been reported such as liposomes, dendrimers, end-grafted monolayers, and linear polymers. However, due to more optimal methods being required for precise characterization, the linear polymer systems have had more attention. Owing to their synthetic facilities and narrow molecular weight distributions, the linear polymer systems have been of benefit to characterize the topology of molecules on cell surface and further investigation.



Scheme 2-1. Ruthenium-based olefin metathesis catalysts: Grubbs' 1st generation catalyst **1** and Grubbs' 2nd generation catalyst **2**. Mes=2,4,6-trimethylphenyl.

The reactivity of ring opening metathesis polymerization (ROMP) is increased with well-defined transition metal catalysts, molybdenum and ruthenium-based complexes. Even though the molybdenum-based complexes have higher reactivity with various substrates, their air and moisture sensitivities hamper wide application in olefin metathesis reactions. In contrast, ruthenium-based ROMP has gained wide popularity for making functional polymers, because the ruthenium catalysts are very functional group tolerant, and are more air and moisture stable (Scheme 2-1). The stabilities and reactivities of the ruthenium catalysts give us access to well-defined living polymerizations.



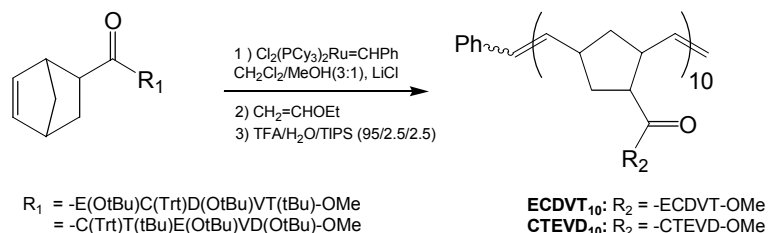
Scheme 2-2. Ruthenium-catalyzed ROMP with tricyclohexylphosphine-substituted catalyst **2** or 3-bromo-pyridine-substituted catalyst **3**.

Since the benzyldiene ruthenium complex, $\text{RuCl}_2(=\text{CHPh})(\text{PCy}_3)_2$, catalyst **1** was first reported, various new generations of ruthenium-based catalysts have been developed. In particular, an enormous number of metathesis reactions with commercially available catalyst **2**, $[(\text{H}_2\text{IMes})(\text{PCy}_3)(\text{Cl})_2\text{Ru}=\text{CHPh}]$, also known as Grubbs' 2nd generation catalyst, have been published. The 4,5-dihydroimidazol-2-ylidene coordinated catalyst **2** elevated the olefin metathesis activities, and the air and moisture stability of catalyst **1** was still retained.²⁴³ In 2002, a much less air sensitive, 3-bromo-pyridine substituted, $[(\text{H}_2\text{IMes})(3\text{-Br-pyr})_2(\text{Cl})_2\text{Ru}=\text{CHPh}]$, catalyst **3** was reported.²³¹ Catalyst **3** has increased initiation rates at least six orders of magnitude faster than catalyst **2**,²³¹ enabling the preparation of narrowly distributed polymers (Scheme 2-2).

Synthetic norbornenyl polymers with oligopeptides containing RGD (Agr-Gly-Asp) or SRN (Ser-Arg-Asn) by ROMP have been successfully prepared and their bioactivities tested.^{163, 244} Polymerizations were performed in dichloromethane/methanol with catalyst **2** at 55 °C, and the polymers had relatively low PDIs. The remarkable applicability of ROMP for the synthesis of multivalent systems led us to adopt the ruthenium-based polymerization for our biologically active, oligopeptide substituted multivalent inhibitors. Oligopeptides from disintegrin binding loops of fertilin β and cyritestin inhibited sperm binding and fusion to the oocyte plasma membrane in vitro. Various kinds of sperm protein mimics have been used to probe biological function, such as identification of the corresponding receptors and the role of specific proteins. However, because of the weak ligand-receptor interactions of these protein mimics, the studies had difficulty probing the mechanism of sperm-oocyte adhesion. A mimic system with highly

increased affinity for target receptors was necessary to elucidate those biological functions.

Previously, Kenny Roberts in the Sampson group in 2003 used ROMP to prepare norbornenyl polymers, and synthesized multivalent oligopeptide polymers, **ECDVT**₁₀ and **CTEVD**₁₀ with catalyst **1** to investigate the role of surface concentration (Scheme 2-3).¹⁶⁴ The norbornenyl polymer, **ECDVT**₁₀ designed to bear 10 monomer units with fertilin β peptide Glu-Cys-Asp-Val-Thr (ECDVT) was a significantly better inhibitor of sperm-oocyte adhesion than its monomeric peptide counterpart.²³⁹ In contrast to fertilin β peptide polymer, **ECDVT**₁₀, the scrambled sequence (Cys-Thr-Glu-Val-Asp) polymer, **CTEVD**₁₀ showed no inhibition at 400 μ M in peptide. This result ascertained the importance of multivalent interactions with the fertilin β mimic polymer for inhibition of fertilization.



Scheme 2-3. Synthesis of oligopeptide substituted norbornenyl polymers, **ECDVT**₁₀ and **CTEVD**₁₀. Catalyst **1** was initiated with norbornenyl monomers to yield linear multivalent inhibitors.

Based on the biological results with the fertilin β mimic, **ECDVT**₁₀, we extended our investigation of various ROMP polymers as inhibitors of fertilization. The ECDVT sequence was shortened to ECD (Glu-Cys-Asp) in the fertilin β disintegrin domain, which

is the minimum sequence required for inhibition of sperm-oocyte binding. In order to study the length and density dependence, polymers with a short peptide sequence were required to improve solubility. In addition, polymers with QCD (Gln-Cys-Asp) from the cyritestin disintegrin were prepared to test their biological activities.

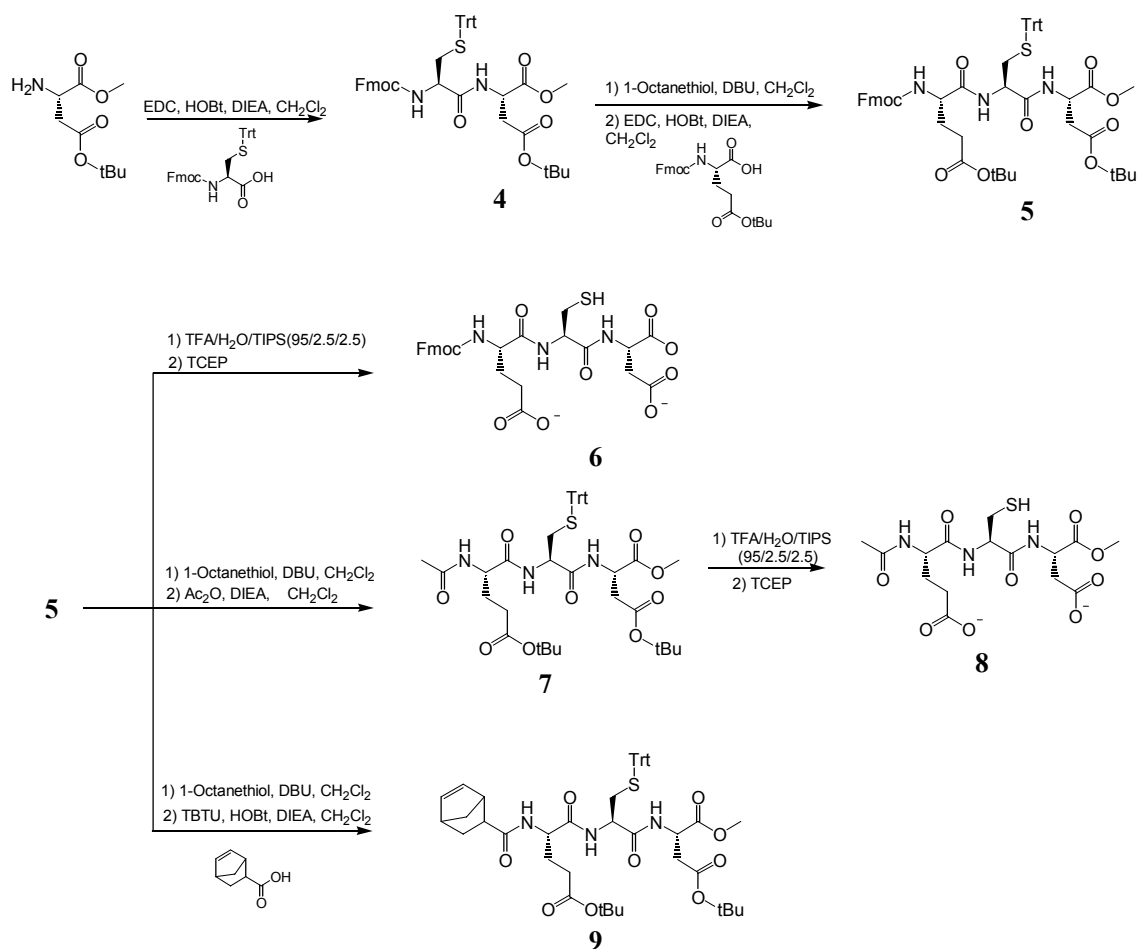
As mentioned previously, using norbornene carboxylic acids containing bio-functional groups has led to easy access of well-defined multivalent systems for biological and medicinal applications. Mostly, the norbornenyl bio-functional polymerizations were performed at 55 °C, a relatively high temperature, for efficient and narrowly distributed polymerizations.^{163, 244} However, the increased reaction temperature allows the reaction solvent to easily evaporate. Especially in small scale polymerization reactions for biological assays, reaction concentrations were hard to control. Moreover, the bio-functional polymers were not very well characterized. In this chapter, we report the polymerization conditions to obtain the desired polymers and the characterization of these linear oligopeptide polymers synthesized by ruthenium-catalyzed ROMP with catalyst **2** or catalyst **3**.

II. Results

II.1. Synthesis of fertilin β mimic, cyritestin mimic, and mutant oligopeptides; H-Glu-Cys-Asp-OMe (ECD), H-Gln-Cys-Asp-OMe (QCD), H-Glu-Ser-Ala-OMe (ESA), and H-Ala-Ser-Asp-OMe (ASD).

Typically amino acid couplings were performed in dichloromethane with 1-(3-dimethylampropyl)-3-ethylcarbodiimide hydrochloride (EDC), 1-hydroxy-benzo-

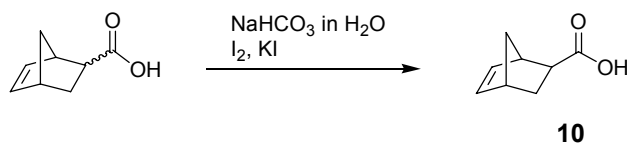
triazole (HOBT), and *N,N*-diisopropylethylamine (DIPEA) at room temperature. The Fmoc group was removed with 1-octanethiol and a catalytic amount of 1,8-diazabicyclo[5.4.0]undec-7-ene (DBU) at room temperature, and the Cbz group was removed by hydrogenation with 10% Pd/C in dichloromethane/methanol at room temperature. Coupling and deprotection reactions were monitored by thin layer chromatography (TLC). Synthesized compounds were purified by silica flash column chromatography and characterized by ^1H and ^{13}C NMR spectroscopy and ESI mass spectroscopy.



Scheme 2-4. Synthesis of ECD monomers.

The full synthesis of fertilin β mimics, ECD monomers is shown in Scheme 2-4. The syntheses of Fmoc-C(Trt)D(OtBu)-OMe **4**, monomer moiety followed standard procedures for Fmoc protected amino acid coupling with EDC, HOBt and DIEA.

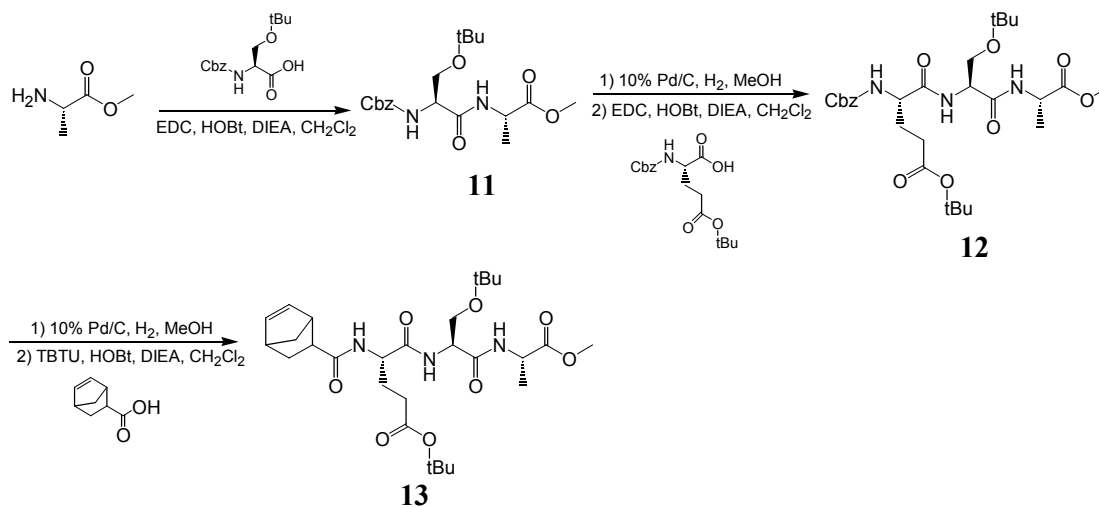
After deprotection of Fmoc groups with 1-octanethiol and DBU, H-C(Trt)D(OtBu)-OMe was coupled with Fmoc-E(OtBu)-OH to obtain Fmoc-E(OtBu)C(Trt)D(OtBu)-OMe **5**. Side chain *tert*-butyl and trityl groups on monomer **5** were removed with a TFA/H₂O/TIPS cocktail mixture, and the reaction was purified by reversed phase C₁₈ HPLC. According to HPLC and ESI mass spectral analyses, we attained the synthesis of side chain deprotected Fmoc-ECD-OMe, monomer **6**. However, the deprotected monomer **6** had solubility problems in IVF assays because of the bulky Fmoc group. So, we decided to introduce an acetyl group at the N terminus instead of the big hydrophobic Fmoc group. We prepared Ac-E(OtBu)C(Trt)D(OtBu)-OMe, monomer **7** with acetic anhydride and DIEA from H-E(OtBu)C(Trt)D(OtBu)-OMe. After deprotection of the trityl and the *tert*-butyl side chain protecting groups with a TFA/H₂O/TIPS cocktail mixture, Ac-ECD-OMe, monomer **8** was obtained for IVF assays, and analyzed by RP-HPLC and ESI mass spectroscopy.



Scheme 2-5. Purification of 5-norbornene-exo-carboxylic acid, **10**.

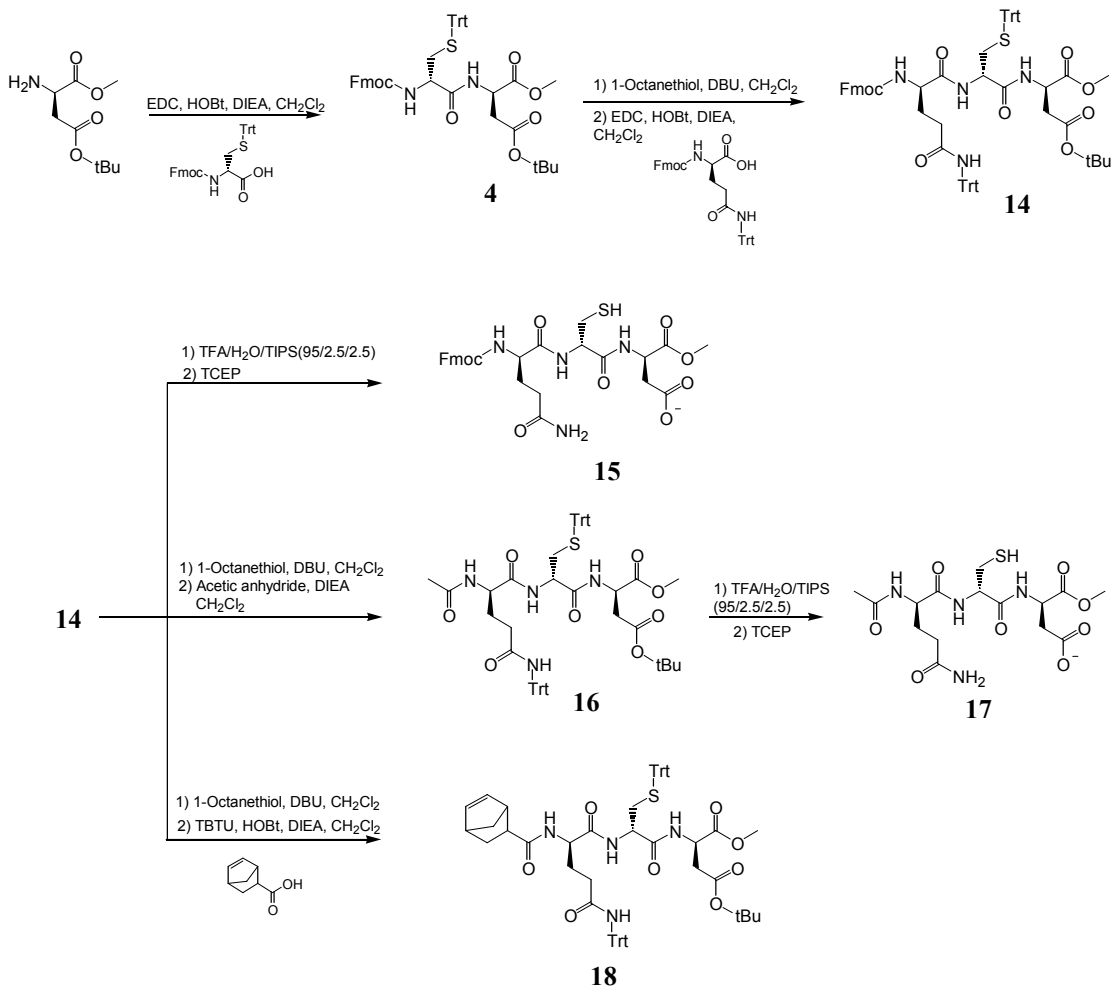
The highly strained cyclic norbornene-*exo* carboxylic acid, **10** was purified from the *endo*, *exo* mixture according to the literature (Scheme 2-5).²⁴⁵ The *exo*-bicyclic compound, **10** was coupled to cap the N-terminus of the fertilin β and cyritestin mimic oligopeptides, and their mutated oligopeptides. After coupling of Fmoc deprotected H-E(OtBu)C(Trt)D(OtBu)-OMe with norbornene-*exo* carboxylic acid, fully side chain protected NB-E(OtBu)C(Trt)D(OtBu)-OMe, monomer **9** was prepared and ready for the polymerization.

The Cbz-S(*t*Bu)A-OMe, monomer **11** was prepared by standard procedures for Cbz protected amino acid coupling with EDC, HOBT and DIEA from H-A-OMe. H₂ and 10% Pd/C were used to remove Cbz groups in the solution phase without further purification. H-S(*t*Bu)A-OMe was coupled with Cbz-E(OtBu)-OH to yield Cbz-E(OtBu)S(*t*Bu)A-OMe **12**. NB-E(OtBu)S(*t*Bu)A-OMe **13** was synthesized from **12** as a mutated control monomer (Scheme 2-6).



Scheme 2-6. Synthesis of ESA monomers.

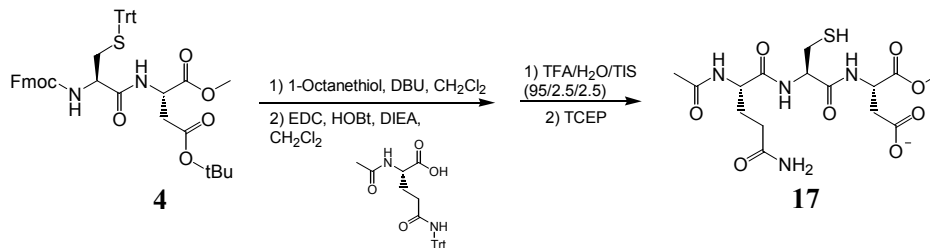
The synthesis of the Fmoc-Q(Trt)C(Trt)D(OtBu)-OMe, monomer **14** followed standard procedures for Fmoc protected amino acid couplings with EDC, HOBT and DIEA, and 1-octanethiol and DBU were used to remove Fmoc groups in the solution phase (Scheme 2-7).



Scheme 2-7. Synthesis of QCD monomers.

As a monomeric control, we prepared side-chain deprotected Fmoc-QCD-OMe **15**. But monomer **15**, like the deprotected Fmoc-ECD-OMe **6**, had solubility problems in the

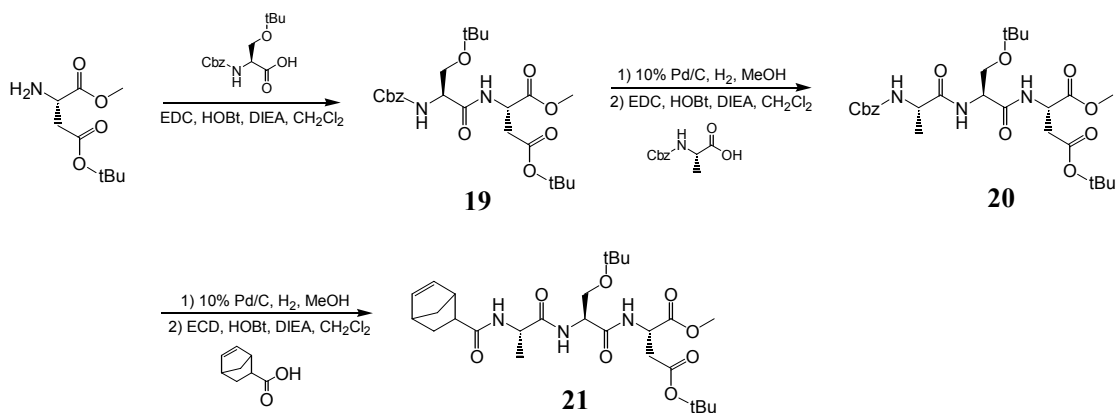
aqueous IVF assays because of the bulky Fmoc group. So, we prepared acetylated Ac-Q(Trt)C(Trt)D(OtBu)-OMe **16** as a monomeric control. We removed the Fmoc group in **14** and acetylated the product with acetic anhydride and DIEA to obtain **16**. After silica column chromatography purification of Fmoc deprotected H-Q(Trt)C(Trt)D(OtBu)-OMe, byproducts still remained and the yield was low. Moreover, after the reaction with acetic anhydride, the R_f values of the byproduct of H-Q(Trt)C(Trt)D(OtBu) and **16** were very close making the separation more difficult.



Scheme 2-8. Alternative synthesis of Ac-QCD-OMe, **17**.

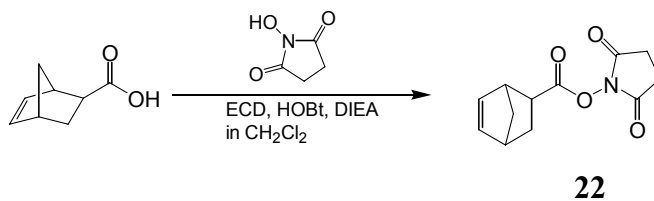
As the second-best solution, we removed the Fmoc group from monomer **4** first. With H-C(Trt)D(OtBu)-OMe and commercially available acetylated glutamine, Ac-Q(Trt)-OH, we successfully obtained **17** (Scheme 2-8). The NB-Q(Trt)C(Trt)D(OtBu)-OMe monomer **18** was prepared by coupling H-Q(Trt)C(Trt)D(OtBu)-OMe and norbornene-exo carboxylic acid, **10** (Scheme 2-7).

The synthesis of NB-AS(tBu)D(OtBu)-OMe **21** followed standard procedures for Cbz protected amino acid couplings with EDC, HOBT and DIEA, and Cbz deprotection with H₂ and 10% Pd/C in the solution phase. Mutated monomer, **21** was prepared for polymerization as a mutant control (Scheme 2-9).



Scheme 2-9. Synthesis of norbornenyl ASD monomer, **21**.

Norbornene-*exo* carboxylic acid was coupled with *N*-hydroxysuccinimide ester to obtain preactivated NB-NHS, monomer **22** (Scheme 2-10).



Scheme 2-10. Synthesis of norbornene carboxylic acid *N*-hydroxysuccinimide ester, NB-NHS, **22**.

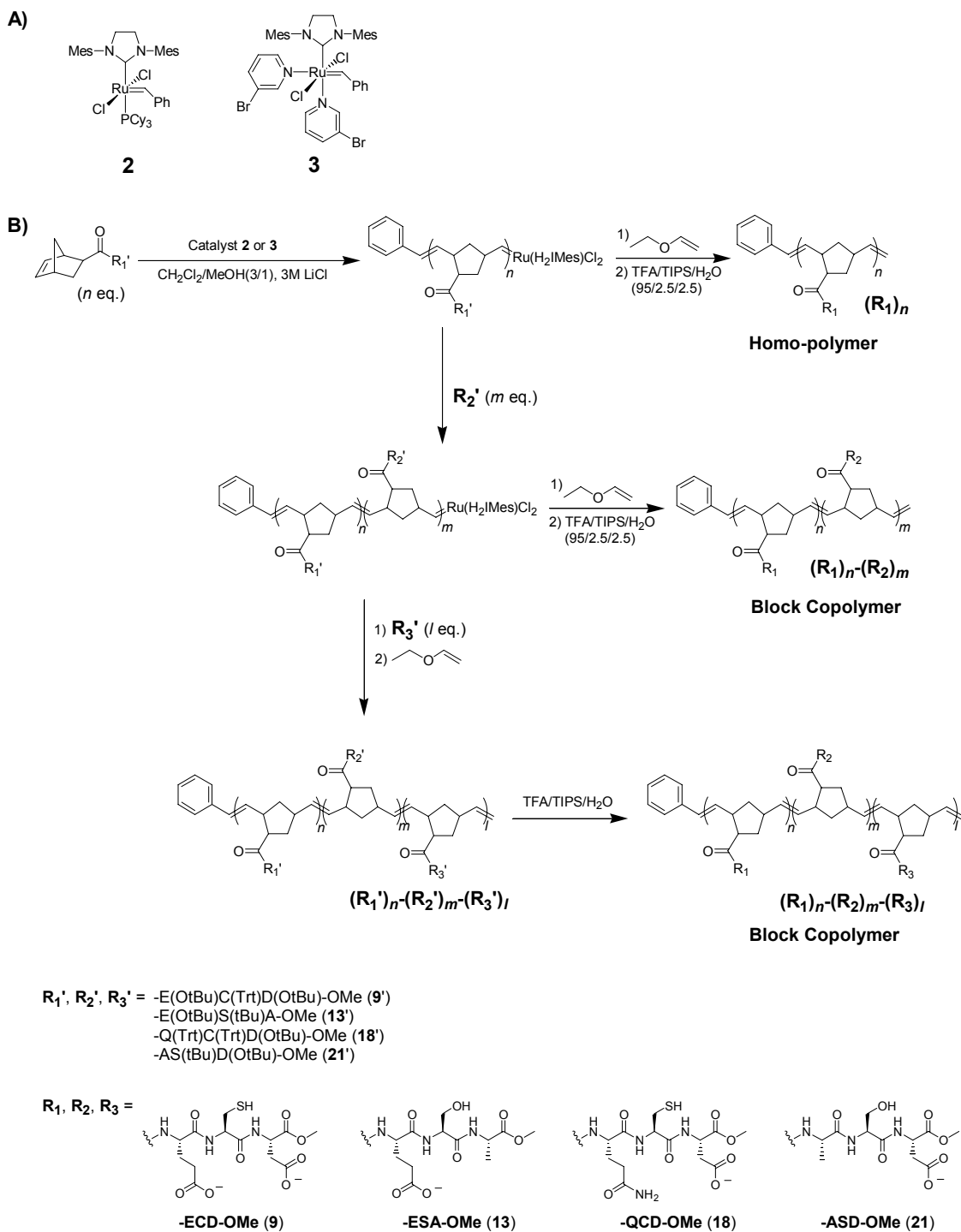
II. 2. Synthesis of fertilin β mimic, cyritestin mimic, and mutant polymers

Various lengths of ECD polymers were synthesized by ROMP using fully protected peptide **9** using (H₂IMes)(PCy₃)Cl₂Ru=CHPh, catalyst **2**, or (H₂IMes)(3-Br-pyr)₂Cl₂Ru=CHPh, catalyst **3** in dichloromethane/methanol (3/1) with 3M LiCl to solubilize the polymers during the polymerization (Scheme 2-11).¹⁶⁴

After quenching the polymerization with ethylvinyl ether, side chain intact ECD polymers, **9_n'-[catalyst]** were prepared: Apostrophe (') represents side chain intact polymer, _n stands for the length of the polymer, and square bracket ([]) denotes the catalyst used. The side chain protecting groups were deprotected with a TFA/H₂O/TIPS cocktail mixture for 5 h to obtain **9₃-[2]**, **9₁₀-[2]**, **9₅₀-[2]**, **9₁₀₀-[2]**, **9₃-[3]**, **9₆-[3]**, **9₁₀-[3]**, and **9₁₀₀-[3]**.

Mutant ESA polymers were synthesized by ROMP using fully protected peptide **13** and catalyst **3** in dichloromethane/methanol (3/1) with 3M LiCl. The polymerization was terminated by adding ethylvinyl ether, and the side chain intact ESA polymers, **13_n'-[3]** were prepared. After quenching the polymerization, the protecting groups on side-chains of polymers were deprotected to obtain **13₁₀-[3]** and **13₁₀₀-[3]**. After removing solvent with N₂, the deprotected polymers were precipitated with diethyl ether.

QCD polymers and a mutant ASD polymer were prepared by ROMP using fully protected peptides **18** and **21** respectively. Catalyst **3** was initiated for polymerization in dichloromethane/methanol with 3M LiCl to prepare QCD polymer, **18_n'-[3]** and ASD polymer, **21₁₀'-[3]**.



Scheme 2-11. Norbornenyl bio-functional polymers synthesized by ROMP. A) Ruthenium catalysts **2** and **3**. B) Polymerization of homopolymer and block copolymer with norbornenyl monomers containing oligopeptide peptides **9**, **13**, **18**, and **21**.

After quenching the polymerization with ethylvinyl ether, the protecting groups on the polymer side chains were deprotected with a TFA/H₂O/TIPS cocktail mixture to obtain **18₁-[3]**, **18₃-[3]**, **18₆-[3]**, **18₁₀-[3]**, **18₁₀₀-[3]**, and **21₁₀-[3]**. After removing solvent with N₂, the deprotected polymers were precipitated with diethyl ether. Various block copolymers were synthesized by ROMP using catalyst **3** as well. The synthetic precursors were analyzed with side-chain protection intact. For each reaction, TLC was used to monitor the disappearance of monomer before addition of the subsequent monomer, and ethylvinyl ether was added to quench each polymerization reaction. After treating with a TFA/H₂O/TIPS cocktail mixture, side-chain deprotected 11-mer block copolymers, **9₂-13₉-[3]**, **9₂-13₇-9₂-[3]**, **18₂-13₇-18₂-[3]**, **9₂-13₇-18₂-[3]**, **9₂-18₇-9₂-[3]**, and **18₂-9₇-18₂-[3]**, and 100-mer block copolymers, **9₂-13₉₆-9₂-[3]**, **18₂-13₉₆-18₂-[3]**, and **9₂-13₉₆-18₂-[3]** were prepared.

II. 3. Analysis of fertilin β mimic, cyritestin mimic, and mutant polymers

Fertilin β and cyritestin mimic homopolymers and block copolymers were characterized by NMR spectroscopy, gel permeation chromatography (GPC), and laser light scattering. The number-average molecular weights (M_n) and the weight-average molecular weights (M_w) were determined for side-chain protection-intact polymers containing oligopeptides by GPC utilizing a UV visible detector, or a differential refractometer and a multiangle light scattering detector.

Polymer	R ₁ ' ^a	[M] ₀ /[C] ₀	Reaction temp. (°C)	Theo. M _n ^b (×10 ³)	M _n ^c (×10 ³)	M _w ^c (×10 ³)	PDI ^c
9 ₃ '-[2]	ECD	3	25	2.7	6.0	9.0	1.50
9 ₁₀ '-[2]	ECD	10	25	8.6	82.1	119.4	1.46
9 ₅₀ '-[2]	ECD	50	25	42.8	120.3	165.4	1.38
9 ₁₀₀ '-[2]	ECD	100	25	85.5	130.7	201.7	1.54

Table 2-1. Analytical data for fertilinβ mimic homopolymers synthesized with catalyst **2**, [**2**]. Polymerization were performed in 3M LiCl, CH₂Cl₂:CH₃OH (3:1) at 25 °C under Ar. ^aSide-chains of ECD were fully protected: E(OtBu)C(Trt)D(OtBu)-OMe. ^bTheoretical molecular weights were calculated based on the catalyst-to-monomer ratio assuming full conversion. ^cDetermined from GPC in THF utilizing a differential refractometer and a multiangle light scattering detector. R₁' and subscripts correspond to the polymer structures in Scheme 2-11.

Fertilinβ mimic polymers of various lengths were synthesized with catalyst **2** and the side-chain intact polymers were characterized (Table 2-1). Catalyst **2** was initiated with norbornenyl fertilinβ monomer **9** at 25 °C for less than 1 h under Ar. The molecular weight distributions were monomodal for all of the polymers, **9**₃'-[**2**], **9**₁₀'-[**2**], **9**₅₀'-[**2**], and **9**₁₀₀'-[**2**]. The 3 monomer unit short polymer, **9**₃'-[**2**] had an M_n and an M_w of 6 000 and 9 000 respectively, and its PDI value was relatively high at 1.50. Although the ratio of the catalyst to monomer was increased, the molecular weights of **9**₁₀'-[**2**], **9**₅₀'-[**2**], and **9**₁₀₀'-[**2**] were similar (M_ns of 82 100, 120 300 and 130 700, and M_ws of 119 400, 165 400 and 201 700 respectively). The actual M_ns of polymers were at least 2-fold to 10-fold greater than expected. Moreover, polymers were broadly distributed in molecular weight with PDIs of 1.46, 1.38, and 1.54 respectively.

Fertilinβ mimic polymers, **9**₁₀'-[**2**] and **9**₁₀'-[**2**]-**a** were synthesized with catalyst **2** at 25 °C or 55 °C under Ar, while catalyst **3** was initiated with monomer **9** to prepare

9₁₀'-[3] at 25 °C under Ar. The M_n s of **9₁₀'-[2]-a** (14 900) and **9₁₀'-[3]** (14 000) were similar to the desired polymer with a theoretical value of 8 600. However, **9₁₀'-[2]-a** had small shoulders in the GPC trace which resulted in a higher PDI than that of **9₁₀'-[3]**. On the other hand, **9₁₀'-[2]** by catalyst **2** at 25 °C had an M_n of 82 100, which was 10-fold greater than the theoretical value and 6-fold greater than that of **9₁₀'-[3]**. Moreover, the PDI was 1.46, which means that the polymer lengths were broadly distributed.

Polymer	Cat. ^a	R ₁ '	[M] ₀ /[C] ₀	Reaction temp. ^c (°C)	Theo. M_n^d ($\times 10^3$)	M_n^e ($\times 10^3$)	M_w^e ($\times 10^3$)	PDI ^e
9₁₀'-[2]	2	ECD ^b	10	25	8.6	82.1	119.4	1.46
9₁₀'-[2]-a	2	ECD ^b	10	55	8.6	12.8	17.5	1.37
9₁₀'-[3]	3	ECD ^b	10	25	8.6	14.9	17.0	1.15
22₁₀-[2]-a	2	NHS	10	25	2.5	169.8	248.4	1.48
22₁₀-[2]-b	2	NHS	10	55	2.5	4.6	7.2	1.58
22₁₀-[3]-c	3	NHS	10	25	2.5	2.4	2.5	1.04

Table 2-2. Analytical data for homopolymers of the fertilin β mimic oligopeptide or *N*-hydroxysuccinimide (NHS) ester norbornenyl monomers. Polymerizations were performed in 3M LiCl, CH₂Cl₂:CH₃OH (3:1) under Ar. ^aRuthenium catalyst used: catalyst **2**, [**2**] and catalyst **3**, [**3**]. ^bSide-chains of ECD were fully protected: E(OtBu)C(Trt)D(OtBu)-OMe. ^cReaction at 25 °C or 55 °C. ^dTheoretical molecular weights were calculated based on the catalyst-to-monomer ratio assuming full conversion. ^eDetermined from GPC in THF utilizing a differential refractometer and a multiangle light scattering detector. R₁' and subscripts correspond to the polymer structures in Scheme 2-11.

Polymers containing NHS ester, **22₁₀-[2]-a**, **22₁₀-[2]-b**, and **22₁₀-[3]-c** were synthesized and characterized to compare the polymer quality with fertilin β mimic oligopeptide polymers. **22₁₀-[3]-c** with catalyst **3** at 25 °C had an M_n of 24 000 with a relatively low PDI of 1.04, while an M_n of **22₁₀-[2]-a** with catalyst **2** at 25 °C had an M_n

of 169 800, which was about 70-fold greater than that of the expected polymer. **22**₁₀-[**2**]-**a** also had a broad molecular weight distribution with a PDI of 1.48. **22**₁₀-[**2**]-**b** was synthesized with catalyst **2** at 55 °C, and its M_n was 4 600. However, its PDI was equally high at 1.58.

Polymer	R ₁ '	R ₂ '	R ₃ '	<i>n</i>	<i>m</i>	<i>l</i>	Theo. M_n^c ($\times 10^3$)	M_n^d ($\times 10^3$)	PDI ^d
9 ₃ '-[3]	ECD ^a	-	-	3	-	-	2.7	3.6	1.10
9 ₆ '-[3]	ECD ^a	-	-	6	-	-	5.2	7.0	1.08
9 ₁₀ '-[3]	ECD ^a	-	-	10	-	-	8.6	14.9	1.15
9 ₁₀₀ '-[3]	ECD ^a	-	-	100	-	-	85.5	133.0	1.21
9 ₂ '- 13 ₉ '-[3]	ECD ^a	ESA ^b	-	2	9	-	6.8	11.2	1.16
9 ₂ '- 13 ₇ '- 9 ₂ '-[3]	ECD ^a	ESA ^b	ECD ^a	2	7	2	7.4	14.5	1.21
9 ₂ '- 13 ₉₆ '- 9 ₂ '-[3]	ECD ^b	ESA ^b	ECD ^a	2	96	2	56.5	-	-

Table 2-3. Analytical data for fertilin β mimic polymers. Polymerizations were performed in 3M LiCl, CH₂Cl₂:CH₃OH (3:1) under Ar with catalyst **3**, [**3**]. ^aSide-chains of ECD were fully protected: E(OtBu)C(Trt)D(OtBu)-OMe. ^bSide-chains of ESA were fully protected: E(OtBu)S(tBu)A-OMe. ^cTheoretical molecular weights were calculated based on the catalyst-to-monomer ratio assuming full conversion. ^dDetermined from GPC in THF utilizing a differential refractometer and a multiangle light scattering detector. R₁', R₂', R₃' and subscripts correspond to the polymer structures in Scheme 2-11.

Fertilin β mimic homopolymers of various lengths, **9**₃'-[**3**], **9**₆'-[**3**], **9**₁₀'-[**3**], and **9**₁₀₀'-[**3**], and a series of block copolymers, **9**₂'-**13**₉'-[**3**], **9**₂'-**13**₇'-**9**₂'-[**3**], and **9**₂'-**13**₉₆'-**9**₂'-[**3**] were prepared by ROMP using fully protected monomers, **9** and **13**, and catalyst **3** (Table 2-3). The molecular weight distributions of the fertilin β mimic homopolymers were monomodal. The M_n s of homopolymers, **9**₃'-[**3**], **9**₆'-[**3**], **9**₁₀'-[**3**] and **9**₁₀₀'-[**3**] were 3 600, 7 000, 14 900, and 133 000 with PDIs of 1.10, 1.08, 1.15, and 1.21 respectively.

The molecular weight distributions of the polymer block intermediates in the synthesis of block copolymers, $9_2'-13_7'-9_2'-[3]$ and $9_2'-13_9'-[3]$ were monitored by GPC as shown in Figure 2-1. The synthetic precursors $9_2'-[3]$, $9_2'-13_7'-[3]$, $9_2'-13_7'-9_2'-[3]$, and $9_2'-13_9'-[3]$ were analyzed with side-chain protection intact. For each reaction, TLC was used to monitor the disappearance of monomer before addition of the subsequent monomer, and ethylvinyl ether was added to quench each polymerization reaction.

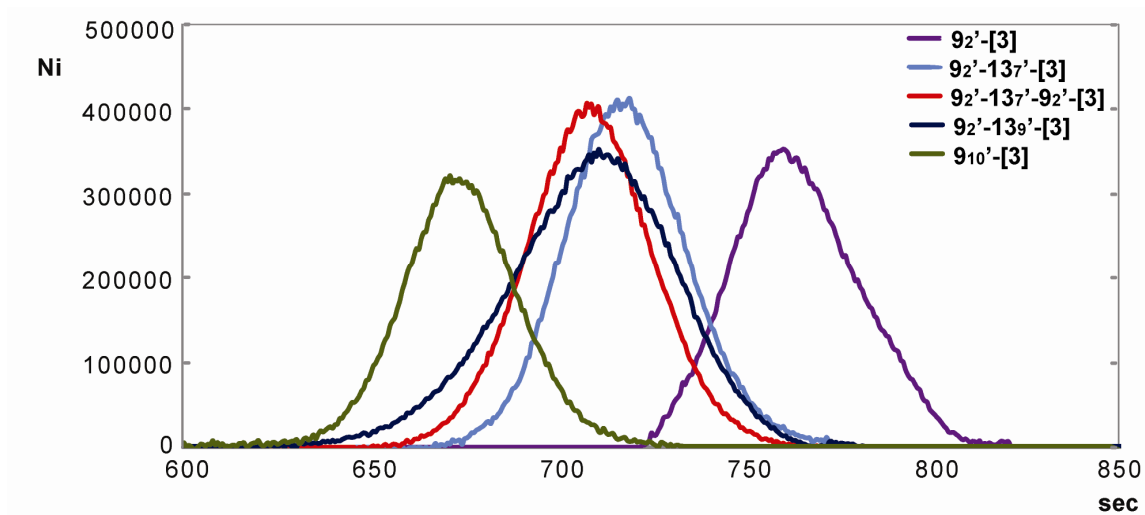


Figure 2-1. Comparison of GPC eluted peaks of $9_2'-[3]$, $9_2'-13_7'-[3]$, $9_2'-13_9'-[3]$, $9_2'-13_7'-9_2'-[3]$ and $9_{10}'-[3]$. Phenogel 5μ linear (2) column was used in 10% CH_3OH in CH_2Cl_2 .

The peak of block copolymer $9_2'-13_7'-9_2'-[3]$ (M_n of 14 500) eluted earlier than the peaks of $9_2'-[3]$, $9_2'-13_7'-[3]$, and $9_2'-13_9'-[3]$ which had smaller M_n and M_w than that of $9_2'-13_7'-9_2'-[3]$. The block copolymers, $9_2'-13_7'-9_2'-[3]$ and $9_2'-13_9'-[3]$ were narrowly distributed, and their PDIs were as low as that of $9_{10}'-[3]$. The 100-mer block copolymer, $9_2'-13_{96}'-9_2'-[3]$ was not characterizable by GPC, because no peaks were detected.

Polymer	R ₁ '	R ₂ '	R ₃ '	<i>n</i>	<i>m</i>	<i>l</i>	Theo. <i>M_n</i> ^{<i>d</i>} (×10 ³)	<i>M_n</i> (×10 ³)	PDI
18₁'-[3] [*]	QCD ^{<i>a</i>}	-	-	1	-	-	0.6	0.6 ^{<i>e</i>}	1.00 ^{<i>e</i>}
18₂'-[3] [*]	QCD ^{<i>a</i>}	-	-	2	-	-	1.1	1.1 ^{<i>e</i>}	1.00 ^{<i>e</i>}
18₃'-[3]	QCD ^{<i>b</i>}	-	-	3	-	-	3.2	3.6 ^{<i>f</i>}	1.15 ^{<i>f</i>}
18₆'-[3]	QCD ^{<i>b</i>}	-	-	6	-	-	6.3	4.9 ^{<i>f</i>}	1.21 ^{<i>f</i>}
18₁₀'-[3]	QCD ^{<i>b</i>}	-	-	10	-	-	10.5	20.8 ^{<i>f</i>}	1.06 ^{<i>f</i>}
18₁₀₀'-[3]	QCD ^{<i>b</i>}	-	-	100	-	-	104.0	149.9 ^{<i>f</i>}	1.45 ^{<i>f</i>}
18₂'-13₇'-18₂'-[3]	QCD ^{<i>b</i>}	ESA ^{<i>c</i>}	QCD ^{<i>b</i>}	2	7	2	8.1	11.3 ^{<i>f</i>}	1.19 ^{<i>f</i>}
18₂'-13₉₆'-18₂'-[3]	QCD ^{<i>b</i>}	ESA ^{<i>c</i>}	QCD ^{<i>b</i>}	2	96	2	57.2	-	-

Table 2-4. Analytical data for cyritestin mimic polymers. Polymerizations were performed in 3M LiCl, CH₂Cl₂:CH₃OH (3:1) under Ar with catalyst **3**, [**3**]. *After polymerization, side-chain protecting groups were deprotected with a cocktail mixture of TFA, TIPS, and H₂O, and purified by RP-HPLC; C₁₈ column. ^{*a*}Side-chains of QCD were deprotected: QCD-OMe. ^{*b*}Side-chains of QCD were fully protected: Q(Trt)C(Trt)-D(OtBu)-OMe. ^{*c*}Side-chains of ESA were fully protected: E(OtBu)S(tBu)A-OMe. ^{*d*}Theoretical molecular weights were calculated based on the catalyst-to-monomer ratio assuming full conversion. ^{*e*}Determined from ESI mass spectroscopy after deprotection. ^{*f*}Determined from GPC in THF utilizing a differential refractometer and a multiangle light scattering detector. R₁', R₂', R₃' and subscripts correspond to the polymer structures in Scheme 2-11.

Cyritestin mimic homopolymers of various lengths, **18₁'-[3]**, **18₃'-[3]**, **18₆'-[3]**, **18₁₀'-[3]**, and **18₁₀₀'-[3]**, and bivalent block copolymers, **18₂'-13₇'-18₂'-[3]** and **18₂'-13₉₆'-18₂'-[3]** were prepared by ROMP using catalyst **3**, and characterized (Table 2-4). The molecular weight distribution of the protected homo and block cyritestin mimic polymers were monomodal. After polymerization of **18₁'-[3]**, side-chain protecting *tert*-butyl and trityl groups were deprotected with a cocktail mixture of TFA/H₂O/TIPS. **18₁'-[3]** along with **18₂'-[3]** were separated by reversed phase C₁₈ HPLC for further biological assay.

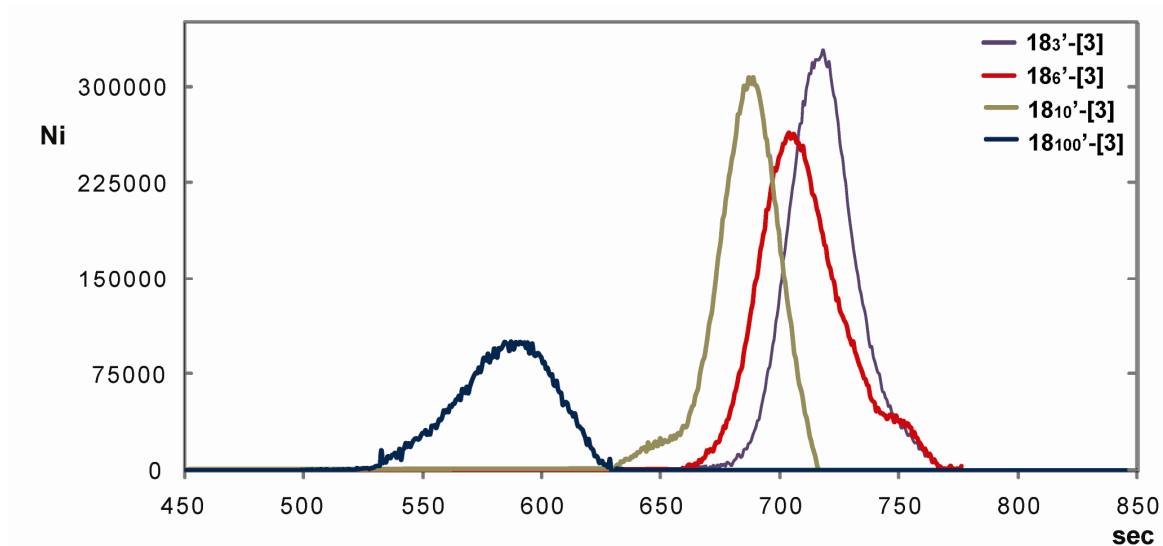


Figure 2-2. Comparison of GPC eluted peaks of **18₃'-[3]**, **18₆'-[3]**, **18₁₀'-[3]**, and **18₁₀₀'-[3]**. Phenogel 5 μ linear (2) column was used in 10% CH₃OH in CH₂Cl₂.

GPC was used to monitor the molecular weight distribution of the polymers, **18₃'-[3]**, **18₆'-[3]**, **18₁₀'-[3]**, and **18₁₀₀'-[3]** which were analyzed with side-chain protection-intact (Figure 2-2). The longest homopolymer **18₁₀₀'-[3]** (M_n of 149 900) eluted first, and the other polymers eluted in order **18₁₀'-[3]** (M_n of 20 800), **18₆'-[3]** (M_n of 4 900), and **18₃'-[3]** (M_n of 3 600). The block copolymer, **18₂'-13₇'-18₂'-[3]** had an M_n of 11 300, and a PDI of 1.19.

A series of fertilin β and cyritestin mixture block copolymers, **9₂'-18₇'-9₂'-[3]**, **18₂'-9₇'-18₂'-[3]**, **9₂'-13₇'-18₂'-[3]**, and **9₂'-13₉₆'-18₂'-[3]** were synthesized with catalyst **3**, and analyzed as well (Table 2-5). The 11-mer monomer unit block copolymers, **9₂'-18₇'-9₂'-[3]**, **18₂'-9₇'-18₂'-[3]**, and **9₂'-13₇'-18₂'-[3]** had narrow monomodal size distributions (PDIs of 1.21, 1.19 and 1.19), and had M_n s of 11 200, 12 300, and 14 200 respectively.

Polymer	R ₁ '	R ₂ '	R ₃ '	n	m	l	Theo. M _n ^d (×10 ³)	M _n ^e (×10 ³)	PDI ^e
9₂'-18₇'-9₂'-[3]	ECD ^a	QCD ^b	ECD ^a	2	7	2	10.8	11.2	1.21
18₂'-9₇'-18₂'-[3]	QCD ^b	ECD ^a	QCD ^b	2	7	2	10.2	12.3	1.19
9₂'-13₇'-18₂'-[3]	ECD ^a	ESA ^c	QCD ^b	2	7	2	7.8	14.2	1.19
9₂'-13₉₆'-18₂'-[3]	ECD ^a	ESA ^c	QCD ^b	2	96	2	-	-	-

Table 2-5. Analytical data for fertilinβ and cyritestin mixture bivalent block copolymers. Polymerizations were performed in 3M LiCl, CH₂Cl₂:CH₃OH (3:1) under Ar with catalyst **3**, [**3**]. ^aSide-chains of ECD were fully protected: E(OtBu)C(Trt)D(OtBu)-OMe. ^bSide-chains of QCD were fully protected: Q(Trt)C(Trt)D(OtBu)-OMe. ^cSide-chains of ESA were fully protected: E(OtBu)S(tBu)A-OMe. ^dTheoretical molecular weights were calculated based on the catalyst-to-monomer ratio assuming full conversion. ^eDetermined from GPC in THF utilizing a differential refractometer and a multiangle light scattering detector. R₁', R₂', R₃' and subscripts correspond to the polymer structures in Scheme 2-11.

The control mutant polymers, **13₁₀'-[3]** and **13₁₀₀'-[3]** were prepared with catalyst **3** (Table 2-6). The narrowly distributed **13₁₀'-[3]** had an M_n of 10 100, and a PDI of 1.07.

Polymer	R ₁ ' ^a	R ₂ '	R ₃ '	n	m	l	Theo. M _n ^b (×10 ³)	M _n ^c (×10 ³)	PDI ^c
13₁₀'-[3]	ESA	-	-	10	-	-	5.6	10.1	1.07
13₁₀₀'-[3]	ESA	-	-	100	-	-	55.3	-	-

Table 2-6. Analytical data for mutant polymers. Polymerizations were performed in 3M LiCl, CH₂Cl₂:CH₃OH (3:1) under Ar with catalyst **3**, [**3**]. ^aSide-chains of ESA were fully protected: E(OtBu)S(tBu)A-OMe. ^bTheoretical molecular weights were calculated based on the catalyst-to-monomer ratio assuming full conversion. ^cDetermined from GPC in THF utilizing a differential refractometer and a multiangle light scattering detector. R₁' and subscripts correspond to the polymer structures in Scheme 2-11.

III. Discussion

Fertilization is the complicated multistep process whereby two gametes bind and fuse together. The binding properties and mechanisms of gametes from different individuals are still unknown. To elucidate the molecular mechanism, synthetic models of receptor-ligand complexes between oocyte and sperm have been developed. Because monomeric oligopeptides derived from ADAM disintegrin loops were poor inhibitors of fertilization, synthetic mimicry of multivalent interactions was attempted. Hence, we have employed chemical synthesis, ROMP, to prepare multivalent mimics of fertilin β and cyritestin to imitate sperm-oocyte binding complexes. Although ROMP can be living and has provided well-defined polymers, we needed to ascertain the best polymerization conditions for our polymer system bearing bioactive oligopeptides. In this chapter, we describe the synthesis of norbornenyl monomers and their polymers, and their characterization to produce well-defined, our desired polymers.

III.1. Synthesis of fertilin β mimic, cyritestin mimic, and mutant oligopeptides; H-Glu-Cys-Asp-OMe (ECD), H-Gln-Cys-Asp-OMe (QCD), H-Glu-Ser-Ala-OMe (ESA), and H-Ala-Ser-Asp-OMe (ASD)

A series of monomers with the fertilin β and cyritestin mimic oligopeptides, and their mutated oligopeptides was synthesized for use in polymerizations. The ECD^{78, 95, 101, 105} sequence from the fertilin β disintegrin domain and QCD^{96, 101} from the cyritestin disintegrin domain, that are the minimum sequences required for inhibition of sperm-oocyte binding, were chosen as the recognition ligands. The ESA and ASD mutated sequences were chosen rather than scrambled peptides. Because at least one pair of the

two adjacent charges remained constantly, we did not able to scramble the tripeptide sequence. We mutated the cysteine, because it is critical for binding.^{95, 105} Either of glutamic acid or aspartic acid residues was replaced with alanine. In order to prepare large quantities of oligopeptides for ROMP polymerizations, solution phase peptide synthesis methods were used. For ROMP, the highly ring strained norbornene-exo carboxylic acid was coupled to the *N*-terminus of synthetic oligopeptides to yield NB-E(OtBu)C(Trt)D(OtBu)-OMe **9**, NB-Q(Trt)C(Trt)D(OtBu)-OMe **18**, NB-E(OtBu)-S(tBu)A-OMe **13**, and NB-AS(tBu)-D(OtBu)-OMe **21**. Norbornene is a widely used monomer in ROMP with the ruthenium catalyst.^{163, 165, 244, 246-248} The bridged cyclic compound carries a double bond. Because of the bridge and the double bond, the cyclohexene ring contains a significant ring strain. The driving force of ROMP is relief of ring strain. Hence, the highly strained cyclic structure of norbornene induces a significant reaction activity. However, norbornene monomers provide stereochemically heterogeneous products.^{244, 249} The Sampson group developed cyclobutene derivatives as ROMP monomers, which yielded stereoregular, regio- and stereo-selective polymers.²⁵⁰ We expect that the stereochemically controlled polymer systems will be useful in investigating important receptor-ligand interactions and defining their biological mechanisms more accurately.

III. 2. Synthesis of fertilin β mimic, cyritestin mimic, and mutant polymers

Various lengths of ECD polymers were synthesized by ROMP using fully protected peptide **9** and (H₂IMes)(PCy₃)Cl₂Ru=CHPh, catalyst **2**, or (H₂IMes)(3-Br-

pyr)₂Cl₂Ru=CHPh, catalyst **3** in dichloromethane/methanol(3/1) with 3M LiCl. For more accurate interpretation of our biological assays, we needed to prepare better-defined polymers. In order to find the best conditions for the living polymerization with bioactive oligopeptides monomers, various reaction conditions were tested with the ECD polymers.

First, polymers were synthesized with catalyst **2**. However, catalyst **2** generally provides polymers with uncontrollable molecular weights and broad polydispersities.^{228, 251} The ROMP reactions at 55 °C with catalyst **2** produce relatively narrowly distributed polymers.^{163, 244} These polymers barely have high molecular weight shoulders, which indicated that intermolecular chain transfer reactions had decreased. Therefore, our second attempt to optimize the polymerization condition was to increase the reaction temperature to 55 °C.

Third, we examined the ROMP reaction conditions by using catalyst **3** as well. This new class of ruthenium catalysts is coordinated with pyridines.^{230, 231, 233, 252} Especially 3-bromo-pyridine substituted catalyst **3** was reported as the most rapid initiator among them. Of the pyridine-coordinated catalysts, catalyst **3** displayed exceptional reaction activities and exhibited fast initiation kinetics in a large number of ROMP reactions.

Based on the analytical data for polymerizations and the significant control obtaining, catalyst **3** was used. This data is discussed in the next section. As control, mutant ESA polymers were synthesized by ROMP using fully protected peptide **13** and catalyst **3** to obtain **13_n'-[3]**. QCD polymers and the corresponding mutant ASD polymer were prepared by ROMP using fully protected peptides **18** and **21** respectively. QCD

polymers, **18_n'-[3]** and ASD polymer, **21₁₀'-[3]**, as well as a series of block copolymers of fertilin β and cyritestin mimic, and mutant.

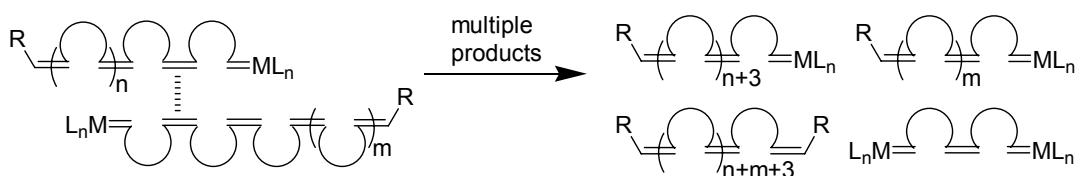
III. 3. Analysis of fertilin β mimic, cyritestin mimic, and mutant polymers.

Side-chain protection-intact fertilin β and cyritestin mimic, and mutant homo and block copolymers were characterized by NMR spectroscopy, GPC utilizing a UV visible detector, or a differential refractometer, and a multiangle light scattering detector.

The molecular weights of the fertilin β mimic, ECD polymers prepared with catalyst **2** at 25 °C did not match with the expected theoretical M_n . Although the molecular weight distributions were monomodal for all of the polymers, **9₃'-[2]**, **9₁₀'-[2]**, **9₅₀'-[2]**, and **9₁₀₀'-[2]**, the polydispersities were broad. The M_n of short polymer, **9₃'-[2]** was 6 000, which was 2-fold greater than the desired polymer. When longer polymers were prepared, the M_n s were progressively worse. The M_n s of longer ECD polymers prepared with catalyst **2** at 25 °C did not correspond to the originally intended polymer sizes. For example, the actual average length of **9₁₀'-[2]** was 100-mer monomer units, which was 10-fold longer than we expected. Although the ratio of the peptide monomer to catalyst **2** was increased, the molecular weights of **9₁₀'-[2]**, **9₅₀'-[2]**, and **9₁₀₀'-[2]** barely increased (M_n of 82 100, 120 300, and 130 700, respectively). Using ROMP with catalyst **2** at 25 °C, we were not able to control the polymerization or prepare our desired polymers. These observations of ROMP with catalyst **2** agree with the results Grubbs and coworkers reported, that generally, catalyst **2** produces polymers with uncontrolled

molecular weights and broad polydispersities, due to the slow initiation rates and the high propagation rates,^{251, 253} and competing chain-transfer reactions (Figure 2-3).^{218, 228, 254}

Intermolecular Chain Transfer:



Intramolecular Chain Transfer:

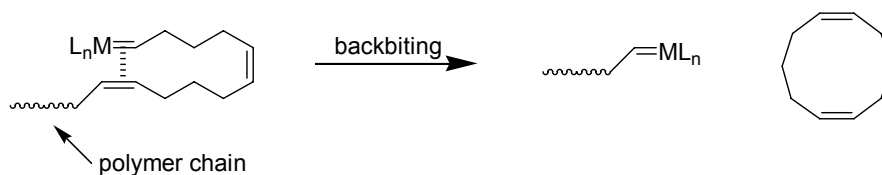


Figure 2-3. Examples of secondary metathesis reactions in ROMP.

Intermolecular chain transfer produces multiple products with varying molecular weights, which broadens the polydispersity.¹⁸³ In the case of intramolecular chain transfer, active polymer chains of reduced molecular weights and cyclic species are produced.

Because ROMP was not initiated efficiently with catalyst **2** and monomer **9** at 25 °C, the polymers had relatively high PDIs. Catalysts of the type $[L_2X_2Ru=CHR]$ initiate by dissociating one L-type ligand;^{251, 253} in catalyst **2**, L is a phosphine (PR_3), and the catalytic initiation depends on its rate of dissociation and rebinding of L.^{251, 255, 256} The initiation rates of catalyst **2** are fast and rebinding of the phosphine is not slow enough at 25 °C, which decreases the catalytic activity. However, chain transfer was minimal at 55 °C.²⁴⁴ So, we tested the polymerization at high temperature, 55 °C, in order to increase

the initiation rate of the polymerization and to minimize chain transfer. ROMP with catalyst **2** in dichloromethane /methanol (2/1) at 55 °C yielded **9₁₀'-[2]-a** with nearly the desired M_n . Catalyst **2** initiated rapidly with the first monomer, and the metallocyclobutane intermediate propagated efficiently with the remaining monomers at 55 °C. So, serious intermolecular chain transfer yielding polymers of high molecular weights did not occur. The M_n was smaller than that of **9₁₀'-[3]**, however, its polydispersity (PDI of 1.37) was still broad. Besides yielding a high PDI, the polymerization with catalyst **2** at 55 °C in dichloromethane/methanol was synthetically difficult. Because dichloromethane boils at 41 °C and evaporates at 55 °C, the reaction must be performed in sealed vials. However, even in a sealed vial, the reaction concentration is not controlled.

In an attempt to increase initiation rate, 3-bromo-pyridine substituted catalyst **3** was synthesized from catalyst **2**. Because the electron-deficient 3-bromo-pyridine ligand is dissociated rapidly and rebinding of the ligand is slow, catalyst **3** initiates the reaction at least six orders of magnitude faster than catalyst **2**.²³¹⁻²³³ The fertilin β mimic polymer, **9₁₀'-[3]** synthesized with catalyst **3** at 25 °C was obtained as the desired polymer with a low PDI of 1.15. In order to obtain more narrowly distributed polymers, the solution was cooled below 0 °C before addition of catalyst **3**. Due to fully pre-mixed reaction solution, catalyst **3** was initiated at once as the reaction temperature was raised. PDIs were slightly lower than when the catalyst was added to the reaction at 25 °C. Owing to the significantly increased initiation rates, catalyst **3** catalyzed the controlled living polymerization of norbornenyl oligopeptides, similar to the polymerization of norbornene and oxo-norbornene derivatives with catalyst **3**.²⁵⁷

Polymers containing a simple *N*-hydroxysuccinimide ester, **22₁₀-[2]-a**, **22₁₀-[2]-b**, and **22₁₀-[3]-c** were synthesized and characterized to compare the polymerization phenomena with fertilin β mimic oligopeptide polymers. The molecular weights of **22₁₀-[2]-a** with catalyst **2** at 25 °C were 169 800 (M_n) and 248 400 (M_w), which were at least 70-fold greater than the theoretical value. Due to the inefficient initiation and the chain transfer of the polymerization with catalyst **2** at 25 °C, the chain length of **22₁₀-[2]-a** was broadly distributed with a PDI of 1.48. **22₁₀-[2]-b** with catalyst **2** at 55 °C had an M_n of 4 600 with a high PDI value (1.58), which indicated that intermolecular chain transfer was dramatically reduced, while an M_n of **22₁₀-[3]-c** with catalyst **3** at 25 °C was 2 400. The molecular weight distribution pattern for **22₁₀-[2]-a**, **22₁₀-[2]-b**, and **22₁₀-[3]-c** was the same as that of **9₁₀-[2]-a**, **9₁₀-[2]-b**, and **9₁₀-[3]-c**. This pattern suggests that the increased initiation rate of ROMP is essential to obtain the desired polymers containing bioactive oligopeptides as well as simple pendant esters.

Since ROMP with catalyst **3** initiated exceptionally fast and was living at 25 °C, we synthesized the polymers with catalyst **3** for the biological assays. After catalyst **3** was added to the reaction at 0 °C, polymerization was completed at 25 °C within 1 h. The polymerization was terminated by adding ethylvinyl ether. First, a series of fertilin β mimic polymers were prepared. The desired homopolymers of various lengths, **9₃'-[3]**, **9₆'-[3]**, **9₁₀'-[3]**, and **9₁₀₀'-[3]**, and a series of block copolymers, **9₂'-13₉'-[3]**, **9₂'-13₇'-9₂'-[3]**, and **9₂'-13₉₆'-9₂'-[3]** were produced by ROMP with low PDIs.

The norbornenyl polymers containing various oligopeptides such as QCD, ESA and ASD sequences were synthesized and characterized as well. For the polymerization of cyritestin mimic polymers, catalyst **3** was initiated with NB-Q(Trt)C(Trt)D(OtBu)-

trityl groups on the glutamate might hinder the coordination of the catalyst with the norbornenyl cyritestin monomer **18**. Even after the fast initiation with catalyst **3**, the metallocyclobutane intermediate did not propagate efficiently with the remaining QCD monomers, while the intermolecular chain transfer occurred to yield polymers of high molecular weights. The decreased reactivity for the QCD monomer caused the formation of a broadly distributed polymer, especially for the longer polymer **18**₁₀₀'-[**3**]. It suggests that more chain transfer reactions occur when the chain length of polymers is increased with the norbornenyl cyritestin monomer, **18**. However, the M_n s of **18**₁₀'-[**3**] and **18**₁₀₀'-[**3**] were as we intended.

The fertilin β and cyritestin mixed block copolymers, **9**₂'-**18**₇'-**9**₂'-[**3**], **18**₂'-**9**₇'-**18**₂'-[**3**], **9**₂'-**13**₇'-**18**₂'-[**3**], and **9**₂'-**13**₉₆'-**18**₂'-[**3**] were synthesized with catalyst **3** as narrowly distributed monomodal polymers as well. As control mutated polymers, **13**₁₀'-[**3**], and **13**₁₀₀'-[**3**] were prepared with catalyst **3**, and these polymers had the expected molecular weights.

IV. Summary

Synthetic multivalent polymers which mimic binding elements of sperm proteins have been synthesized to identify the receptors as well as the mechanism of sperm-oocyte binding events. For designing more precise and efficient inhibitors of fertilization, the ruthenium-based ROMP was applied to make our biologically active, oligopeptide polymers. Because ruthenium catalyst **2** was not initiated efficiently with norbornenyl

monomers bearing oligopeptides at 25 °C, polymers had uncontrolled molecular weights with relatively broad polydispersities (PDIs of around 1.5). In order to increase the initiation rate of the polymerization and make chain transfer minimal, we catalyzed the ROMP with catalyst **2** at 55 °C. Although the higher temperature promoted the controlled living polymerization, it still produced broadly distributed polymers.

3-Bromo-pyridine substituted catalyst **3** initiates more rapidly than catalyst **2**. Therefore, the controlled living ROMP of norbornenyl polymers was achieved. We have demonstrated that catalyst **3** enhanced the initiation process and reactivity for the polymerization of norbornenyl oligopeptides. Hence, we obtained the narrowly distributed fertilin β and cyritestin mimic polymers, and their mutated polymers.

Chapter 3

Mixed Fertilin β and Cyritestin Mimic Polymers Interrogate Sperm-Oocyte Binding Mechanisms

I. Introduction

II. Results

III. Discussion

IV. Summary

I. Introduction

Mammalian fertilization is a multi-step process whereby two gametes (oocyte and sperm) bind and fuse together to form a zygote. The oocyte activates the sperm metabolism, and the sperm reciprocates by activation of the oocyte metabolism to initiate fertilization.¹ The ovulated oocyte is surrounded by the cumulus layer and the zona pellucida. A capacitated and acrosome-intact sperm can pass through the cumulus complex and bind to the zona pellucida. The acrosome reaction results in the release of the contents of the acrosomal vesicle including proteolytic enzymes, and allows the sperm to penetrate the zona pellucida. Finally, the sperm adheres to and fuses with the oocyte plasma membrane, at which point oocyte activation is triggered. However, the precise mechanisms of sperm binding and fusion are not yet understood. Therefore, an understanding of the molecular interaction between sperm and oocyte proteins is essential for the study of infertility and the development of new contraception strategies.

We undertook a chemical biology approach to elucidate the molecular mechanism of sperm-oocyte binding. The ADAM family of proteins³⁵⁻³⁸ is widely expressed with a large subset present in mouse testis.^{35, 68} About half of ADAMs found in testis including fertilin β and cyritestin are exclusively or predominantly expressed there.^{49, 68} These testis specific proteins, fertilin β and cyritestin, have roles in sperm-oocyte adhesion, and their disintegrin domains are the primary binding domains.^{90, 91}

ADAM2, fertilin β and ADAM3, cyritestin are located in the equatorial region of the sperm head, and during sperm maturation, their disintegrin domains are exposed on the sperm head.^{3, 39, 92-94, 103, 104} ADAM2 forms a heterodimer with both ADAM1a and ADAM1b.¹⁰⁷ However, only the ADAM1b/ADAM2 complex is present on the sperm

surface.⁶¹ Elucidation of their respective roles in fertilization is complicated by the interdependence of testicular ADAM protein expression and maturation.⁴⁸ For example, ADAM1a plays an intracellular chaperone role for the transport of sperm proteins from the endoplasmic reticulum of testicular germ cells onto the sperm surface.⁶⁰ ADAM1a $-/-$ sperm are impaired in their ability to migrate into the oviduct. This phenotype is due to the loss of other sperm surface proteins including ADAM3.⁶⁰ In contrast, ADAM1b $-/-$ sperm migrate normally and have normal levels of ADAM3 on the sperm surface.^{61, 62} We sought an alternative approach to elucidate the ADAM2 and ADAM3 functions without disrupting protein expression in sperm.

The short peptide sequence glutamic acid-cysteine-aspartic acid (ECD) and glutamine-cysteine-aspartic acid (QCD) are highly conserved in the fertilin β and cyritestin disintegrin loops, respectively.¹⁰³ These tripeptides, ECD^{78, 95, 101, 105} and QCD^{96, 101} are the minimal recognition element necessary for binding to the oocyte.

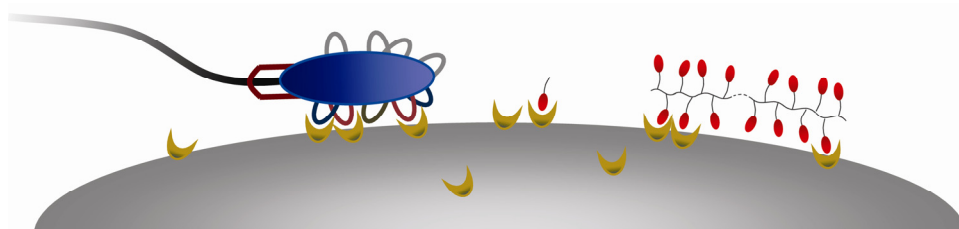
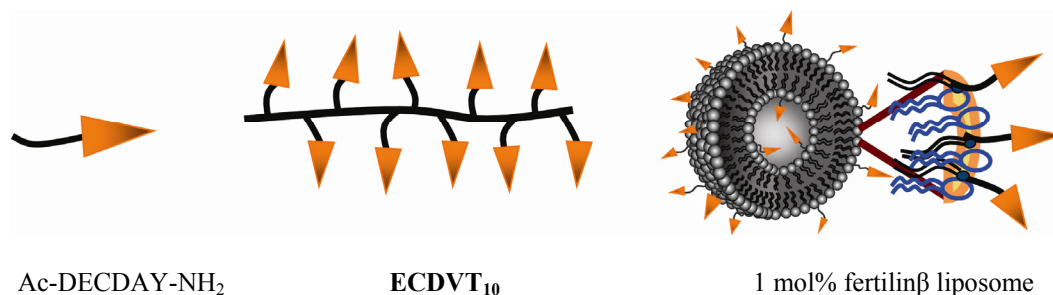


Figure 3-1. Schematic representation of competition between sperm and mimics for binding to the oocyte plasma membrane.

Short peptides incorporating the ECD or QCD sequence inhibit sperm binding at high micromolar concentrations. To improve the binding affinity of monomeric peptide

ligands for the oocyte surface, we developed synthetic multivalent polymers to mimic the multivalent display of fertilin β on the sperm surface (Figure 3-1).^{153, 165, 239, 258}



Mimic	IC ₅₀ [μ M peptide] by F.I.	IC ₅₀ [μ M peptide] by F.R.	Maximal inhibition observed [%]	IC ₅₀ [complexes/mL] by F.R.
Ac-DECDAY-NH ₂ ¹⁰¹	360 \pm 30	306 \pm 10	79 \pm 3	n.a. ^a
ECDVT ₁₀	5.1 \pm 1.4	5.8 \pm 0.3	72 \pm 6	3 \times 10 ¹⁴
CTEVD ₁₀	n.i. ^b	n.i. ^b	n.i. ^b	n.i. ^b
1 mol% fertilin β liposome	2.4 \pm 1.9	2.5 \pm 0.3	97 \pm 2	1 \times 10 ¹³

Table 3-1. Inhibition of fertilization by fertilin β mimics.²³⁹ ^an.i.: not applicable. ^bn.i.: no inhibition; tested at 400 μ M.

Inhibition of fertilization by liposomes presented 1% ECD was increased 100-fold more than the monomeric ECD tripeptide.^{101, 153, 258} To define the optimal ECD presentation system for inhibition of fertilization, we needed to simplify the multivalent system for further ligand-receptor binding studies. Therefore, we employed ruthenium-catalyzed ring opening metathesis polymerization (ROMP) with (PCy₃)₂Cl₂Ru=CHPh, catalyst **1** to mimic the multivalent display of sperm protein fertilin β . A linear 10-mer

unit long polymer containing oligopeptides of Glu-Cys-Asp-Val-Tyr, **ECDVT₁₀** had a significantly better inhibition than its monomeric counterpart, and its IC₅₀ was 50 to 70-fold improved.²³⁹

The interrelationship between fertilin β and cyritestin is unclear. We raised the following questions about the contribution of these proteins in binding to the oocyte surface membrane. First, we synthesized ECD and QCD polymers, and tested the inhibition of fertilization with these polymers individually to determine if their structure activity profiles are identical or not. Here, we present the synthesis and testing of a series of linear ECD and QCD polymers and we compare their inhibition potencies and patterns. Owing to increased initiation rates with catalyst **3**, we obtained much narrower molecular weight distributions for these polymers than in previous work. Therefore, we resynthesized the ECD polymers to compare their potencies to the newly synthesized QCD polymers. We found that longer polymers were better inhibitors.

Then, the interdependence of these two polymers was tested. Inhibition by a copolymer of ECD and QCD was compared to inhibition by individual polymers. Lastly, we examined the importance of β_1 integrin for inhibition by both binding sequences. ECD and QCD polymers both inhibit fertilization through the β_1 integrin receptor.

II. Results

II-1. Synthesis of oligopeptides polymers

The norbornenyl tripeptide monomers, fertilin β peptide, **9**, cyritestin peptide, **18**, and mutant peptides, **13** and **21** were synthesized by Fmoc, Cbz α -amino protection in solution phase. The side-chains on monomers were protected with *tert*-butyl and trityl groups. Polymers were produced by ROMP using the fully protected monomers in dichloromethane/methanol (3/1) with 3M LiCl.¹⁶⁴ The polymerization of the norbornenyl monomers was catalyzed with (H₂IMes)(PCy₃)₂Cl₂Ru=CHPh, catalyst **2** or (H₂IMes)(3-Br-pyr)₂Cl₂Ru=CHPh, catalyst **3** to form homopolymers, and the polymerizations were terminated by adding ethylvinyl ether.

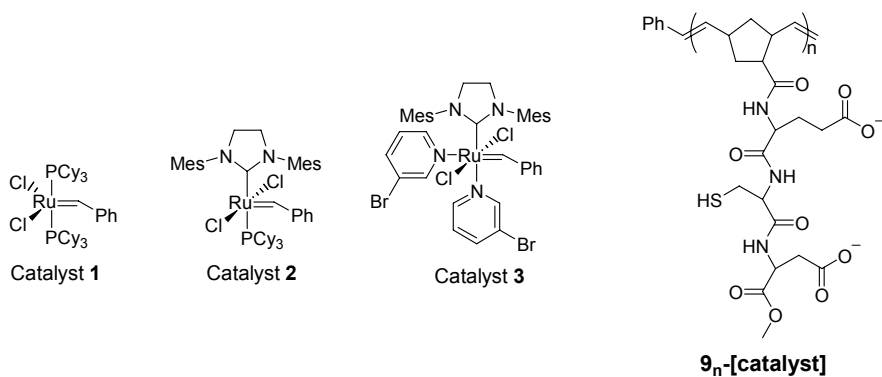


Figure 3-2. Ru catalysts **1**, **2** and **3**, and fertilin β mimic polymers, **9_n-[catalyst]**. Ru catalyst **2** and **3** were initiated with monomer **9** to be fertilin β mimic polymers. After deprotection of *tert*-butyl/trityl groups on side-chains, fertilin β mimics, **9_n-[catalyst]** were tested for inhibition of fertilization.; *n* represents the length of polymers; [catalyst] represents the catalyst used for the polymerization.

The polymers were treated with a TFA/H₂O/TIPS cocktail mixture to deprotect the side-chains and were precipitated with diethyl ether. Polymers were reduced with tris(2-carboxyethyl)phosphine, were precipitated with dilute acid, 1N HCl, and were resuspended in aqueous ammonium hydroxide to a final pH of 7 before use in assays. Isolated yields were 67-90%. Polymers were characterized by NMR spectroscopy, gel permeation chromatography (GPC), and laser light scattering. ¹H NMR spectra confirmed that no monomer was retained in the polymer precipitation. The integration of the phenyl end group against the ligand side-chains in the ¹H NMR spectra agreed with the expected degree of polymerization. The number-average molecular weights (*M_n*), the weight-average molecular weights (*M_w*), and the polydispersity index (PDI) were determined for the protected polymers by gel permeation chromatography utilizing a differential refractometer and a multiangle light scattering detector. The size distribution profiles of deprotected polymers in the assay buffer were monitored by dynamic light scattering to determine whether aggregates of polymers formed under the assay conditions.

Fertilinβ mimic polymers, **9₁₀-[2]**, **9₁₀₀-[2]**, **9₃-[3]**, **9₆-[3]**, **9₁₀-[3]**, and **9₁₀₀-[3]** were synthesized with catalyst **2** and **3**. Cyritestin mimic polymers, **18₁-[3]**, **18₂-[3]**, **18₃-[3]**, **18₆-[3]**, **18₁₀-[3]**, and **18₁₀₀-[3]**, and mutant polymers, **13₁₀-[3]**, **13₁₀₀-[3]**, and **21₁₀-[3]** were prepared with catalyst **3** and monomers **18**, **13**, and **21** respectively, as described above. The ABA and ABC block copolymers **9₂-13₉₆-9₂-[3]**, **18₂-13₉₆-18₂-[3]**, and **9₂-13₉₆-18₂-[3]** were synthesized with monomers **9**, **18**, and **13** with catalyst **3**. Two ECD or QCD ligands were placed at each terminus of the bivalent block copolymers, **9₂-13₉₆-9₂-[3]**, **18₂-13₉₆-18₂-[3]**, and **9₂-13₉₆-18₂-[3]** polymers, so that statistically at least one ligand was present on both ends of the polymers. Block copolymers were produced by

sequential addition of monomers. After complete disappearance of the first norbornenyl monomer, the second monomer was added to the reaction followed by the third. The consumption of monomers was monitored by TLC before addition of the subsequent monomers. They were deprotected and purified as described for homopolymers.

II-2. Assay of polymers

In vitro fertilization assays were executed with zona pellucida-free mouse oocytes (Figure 3-3). Oocytes were preincubated in Hoechst 33442, and polymers were added prior to insemination with sperm.

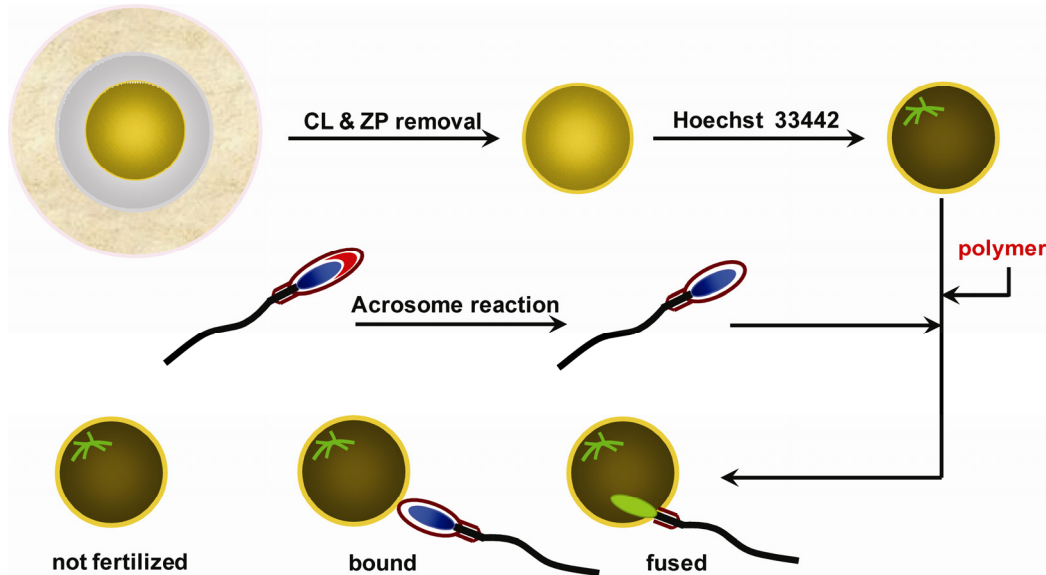


Figure 3-3. *In vitro* fertilization assay. The zona pellucida-free oocytes were incubated in polymers prior to adding sperms as inhibitors. Sperm fusion was used as an endpoint to measure inhibition of sperm binding.

Sperm fusion was used as an endpoint to measure inhibition of sperm binding. Sperm were scored as fused if their chromatin stained with Hoechst 33442 that was loaded into oocytes. Fertilization was scored two ways.²⁵⁹ The fertilization rate, F.R., reports the ratio of fertilized oocytes to the total number of oocytes. The fertilization index, F.I., reports the total number of sperm fused sperms divided by the total number of oocytes. The concentrations of inhibitors are reported for both peptide ligand and polymer. For example, a 1 μM solution of a 10-mer cyritestin mimic polymer, **18₁₀-[3]** contains 10 μM QCD ligand. The concentrations of cyritestin mimic homopolymers used covered at least a 1000-fold range to determine their $\text{IC}_{50\text{S}}$ by both F.R. and F.I. For other polymers, comparisons of inhibition were performed at fixed concentrations of polymer.

II-2-1. Assay of homopolymers

Previously in the Sampson laboratory, the multivalent fertilin β mimic polymer, **ECDVT₁₀-[1]** designed to display 10 copies of the ECDVT peptide was synthesized with catalyst **1** and tested for inhibition of fertilization. The linear fertilin β mimic showed significantly improved inhibition of fertilization compared to its monomer. So we resynthesized linear fertilin β mimic polymers, **9₁₀-[2]** and **9₇₀-[2]** with catalyst **2**, and tested their biological activities (Table 3-2). **9₁₀-[2]** had an IC_{50} of 0.34 μM by F.I. and of 0.32 μM by F.R., the biological activities of which were more than 100-fold improved compared to the monomer, Ac-ECD-OMe, **8**. The longer polymer, **9₇₀-[2]** had an IC_{50} of 34 μM by F.I. and at 1.4 μM by F.R. Inhibition was slightly worse than from the shorter

polymer, **9**₁₀-[2]. The mutant ESA polymers, **13**₁₀-[2] and **13**₇₀-[2] did not show any significant inhibition at 500 μ M in peptide concentration.

Polymer	IC ₅₀ [μ M] in peptide by F.I.	IC ₅₀ [μ M] in peptide by F.R.	IC ₅₀ [μ M] in polymer by F.I.	IC ₅₀ [μ M] in polymer by F.R.
8 (monomer)	>500 ^a	>500 ^a	n.a. ^b	n.a. ^b
ECDVT ₁₀ -[1] ²³⁹	5.1 \pm 1.4	5.8 \pm 0.3	0.51 \pm 0.14	0.58 \pm 0.03
9 ₁₀ -[2]	3.4 \pm 0.3	3.2 \pm 0.2	0.34 \pm 0.03	0.32 \pm 0.02
9 ₇₀ -[2]	68 \pm 11.1	99 \pm 31	0.97 \pm 0.16	1.4 \pm 0.44
13 ₁₀ -[2]	n.i. ^c	n.i. ^c	n.i. ^c	n.i. ^c
13 ₇₀ -[2]	n.i. ^c	n.i. ^c	n.i. ^c	n.i. ^c

Table 3-2. Inhibition of fertilization by fertilin β mimic and mutant polymers synthesized with catalyst **2**.¹⁶⁵ F.I. (fertilization index) is the average number of fused sperm per oocyte. The F.I. values of the control were between 1 and 2. F.R. (fertilization rate) is the percent of oocytes fertilized. The F.R. values of the control were greater than 70%. 200-300 oocytes were assayed for each polymer in 8-10 independent experiments. IC₅₀'s were calculated by a 3 parameter fit (GRAFIT software) using the equation: percent fertilization = (100-b)/{1+([I]/IC₅₀)^s. Where b is the remaining percent fertilization after saturation with inhibitor, and s is the slope of the fit. Errors are reported as s.e.m. ^aAt 500 μ M, monomer **8** (Ac-ECD-OMe), 29% (F.I.) and 32% (F.R.) was observed. ^bn.a.: not applicable. ^cn.i.: no inhibition. Negative control polymers **13**₁₀-[2] and **13**₇₀-[2] did not inhibit fertilization at 500 μ M (peptide).

Fertilin β mimic heteropolymer **9**₈/**13**₇₂-[3], and homopolymers **9**₃-[3], **9**₆-[3], **9**₁₀-[3], **13**₁₀-[3], and **13**₁₀₀-[3] also tested for inhibition of fertilization, and their biological activities compared with polymers synthesized with catalyst **2** (Table 3-3). The heteropolymer **9**₈/**13**₇₂-[3] was an 80-mer monomer unit polymer, but ECD ligands were randomly presented only at 10%, the rest of the peptides presented were ESA mutant

sequence. The IC₅₀s were at 0.34 μM by F.I. and at 0.32 μM by F.R., which were less effective than **9**₁₀-[**2**]. At 500 μM in peptide concentration, the inhibition of **9**₃-[**3**] was 66% by F.I., and 58% by F.R., and that of **9**₆-[**3**] was 57% by F.I., and 52% by F.R. The inhibition behaviors of **9**₃-[**3**] and **9**₆-[**3**] were analogous to monomer **8**. Moreover, 10-mer ECD polymer, **9**₁₀-[**3**] was a poor inhibitor, in contrast to **9**₁₀-[**2**]. Control polymers **13**₁₀-[**3**] and **13**₁₀₀-[**3**] inhibited less than 15% at 500 μM in peptide concentration.

Polymer	IC ₅₀ [μM] in peptide by F.I.	IC ₅₀ [μM] in peptide by F.R.	IC ₅₀ [μM] in polymer by F.I.	IC ₅₀ [μM] in polymer by F.R.
9 ₃ -[3]	~ 500	~ 500	~ 167	~ 167
9 ₆ -[3]	~ 500	~ 500	~ 83	~ 83
9 ₁₀ -[3]	191 ± 130	245 ± 190	19.1 ± 13	24.5 ± 19
9 ₈ / 13 ₇₂ -[3]	23 ± 5	80 ± 24	2.9 ± 0.7	10 ± 4
13 ₁₀ -[3]	n.i. ^a	n.i. ^a	n.i. ^a	n.i. ^a
13 ₁₀₀ -[3]	n.i. ^a	n.i. ^a	n.i. ^a	n.i. ^a

Table 3-3. Inhibition of fertilization by fertilinβ mimic and mutant polymers synthesized with catalyst **3**. 200-300 oocytes were assayed for each polymer in 8-10 independent experiments. Errors are reported as s.e.m. ^an.i.: no inhibition. Negative control polymers **13**₁₀-[**3**] and **13**₁₀₀-[**3**] did not inhibit fertilization at 500 μM in peptide concentration.

Inhibition of fertilization by **9**₁₀-[**2**], **9**₁₀-[**3**] and **9**₁₀₀-[**3**] was tested (Figure 3-4). Polymers **9**₁₀-[**2**] and **9**₁₀₀-[**3**] were nearly equipotent and inhibited fertilization more than 50% at 0.5 μM in polymer concentration. **9**₁₀-[**3**] was a poor inhibitor and its potency was 10-fold lower than that of **9**₁₀-[**2**] and **9**₁₀₀-[**3**].

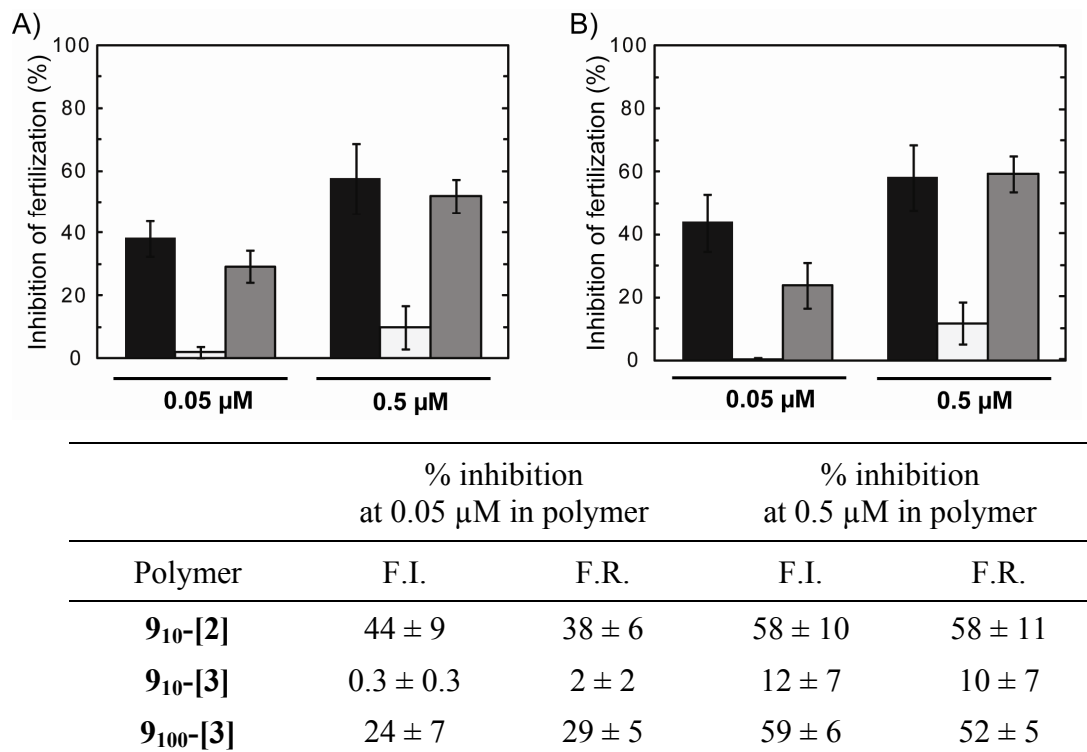


Figure 3-4. Inhibition of fertilization by fertilin β mimic polymers at 0.05 μ M and 0.5 μ M in polymer concentration. Black bars: **9₁₀-[2]**; White bars: **9₁₀-[3]**; Grey bars: **9₁₀₀-[3]** A) Fertilization inhibition (%) by F.R. B) Fertilization inhibition (%) by F.I. At least five independent experiments with 100-120 oocytes were assayed for each concentration. In the untreated controls, 79 \pm 3% oocytes were fertilized. The average number of sperm fused per oocyte was 1.5 \pm 0.1. Errors are reported as s.e.m.

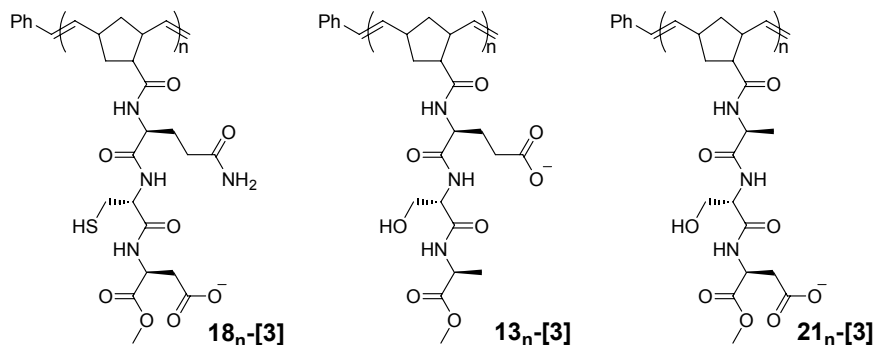


Figure 3-5. Cyritestin mimic polymers, **18_n-[3]**, and mutant polymers, **13_n-[3]** and **21_n-[3]**. After deprotection of trityl/*tert*-butyl groups on side-chains, **18_n-[3]**, **13_n-[3]** and **21_n-[3]** were tested for the inhibition of fertilization; n represents the length of polymers; [3] represents catalyst **3** used for the polymer.

Next, the inhibition potencies of cyritestin polymers **18₁-[3]**, **18₂-[3]**, **18₃-[3]**, **18₆-[3]**, **18₁₀-[3]**, and **18₁₀₀-[3]**, and their mutant polymer, **21₁₀-[3]** were measured (Table 3-4). Monomer **17** and polymer **18₁-[3]**, a one-mer, did not inhibit consistently at 500 μ M. **18₂-[3]**, isolated as a side product from the preparation of **18₁-[3]**, inhibited fertilization 50% at 500 μ M in polymer concentration. **18₁₀₀-[3]** was 100 times more potent with an IC₅₀ of 5.7 μ M by FR. The IC₅₀ of **18₁₀-[3]** was similar to that of **18₁₀₀-[3]** but the reproducibility was not as robust. On the other hand, **21₁₀-[3]** mutated to the ASD sequence inhibited 50% at 500 μ M in peptide concentration.

Polymer ^a	IC ₅₀ [μ M] in peptide		IC ₅₀ [μ M] in polymer	
	by F.I.	by F.R.	by F.I.	by F.R.
18₂-[3]	938 \pm 58	984 \pm 130	469 \pm 29	492 \pm 65
18₃-[3]	33.6 \pm 14.1	77.4 \pm 55.5	11.2 \pm 4.7	25.8 \pm 18.5
18₆-[3]	170 \pm 104	146 \pm 34	28.3 \pm 17.3	24.4 \pm 5.7
18₁₀-[3]	30 \pm 15	147 \pm 88	3.0 \pm 1.5	14.7 \pm 8.8
18₁₀₀-[3]	410 \pm 90	570 \pm 250	4.1 \pm 0.9	5.7 \pm 2.5
21₁₀-[3]	\sim 500 ^b	\sim 500 ^b	\sim 50	\sim 50

Table 3-4. Inhibition of fertilization by cyritestin mimic and mutant polymers. ^aSubscript represents monomer/catalyst ratio. ^bNegative control polymers, **21₁₀-[3]** inhibited fertilization at 500 μ M in peptide concentration, there are 57 \pm 14% by F.I. and 46 \pm 14% by F.R. inhibitions observed. At least 10-15 independent experiments with 250-350 oocytes were performed at each concentration. In the untreated controls, 71 \pm 2% oocytes were fertilized. The average number of sperm fused per oocyte was 1.3 \pm 0.2. Errors are the s.e.m.

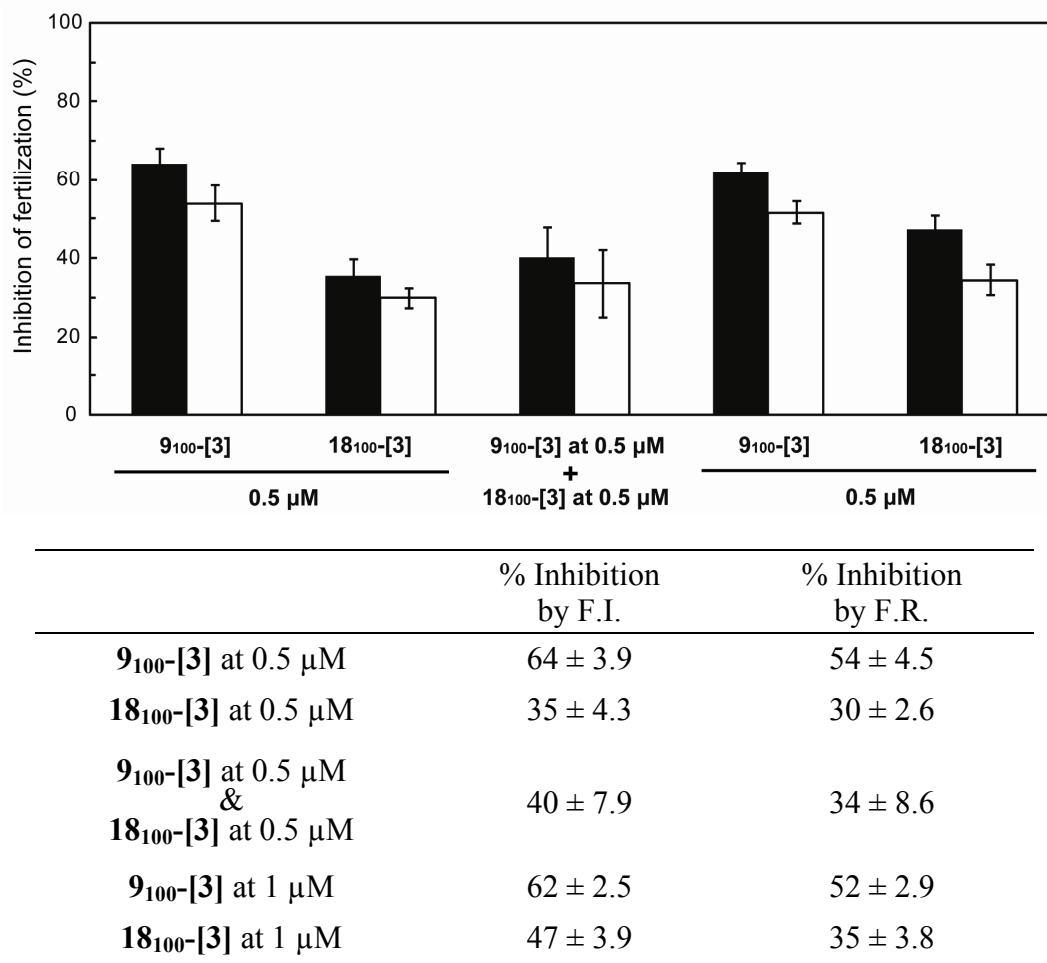
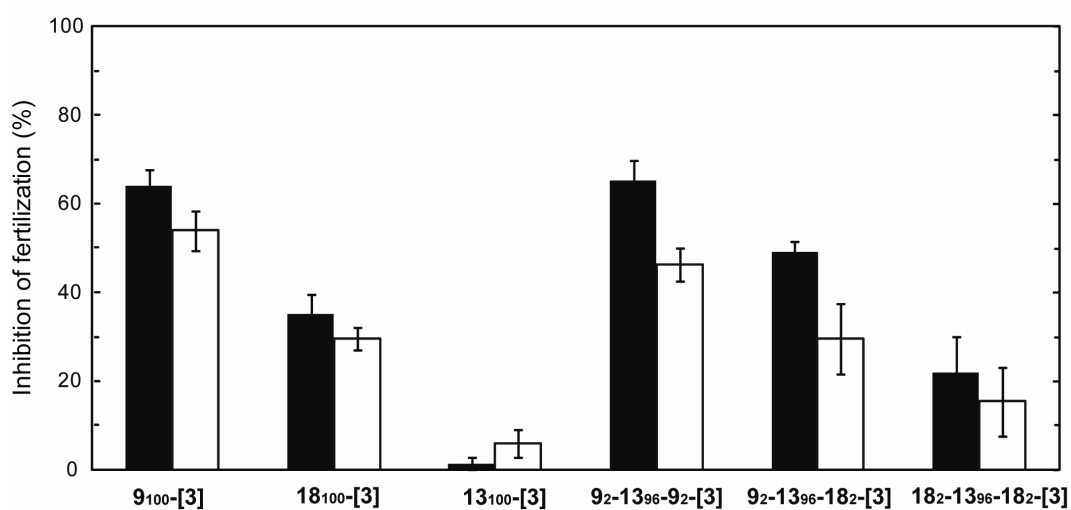


Figure 3-6. Inhibition of fertilization by a mixture of polymers **9₁₀₀-[3]** at 0.5 μM and **18₁₀₀-[3]** at 0.5 μM in polymer concentration. Black bars: Fertilization inhibition by F.R.; White bars: Fertilization inhibition by F.I. At least six independent experiments with 90-120 oocytes were assayed for single homopolymers. Three independent experiments with 60-70 oocytes were assayed for mixture homopolymers. In the untreated controls, 66 ± 8% oocytes were fertilized. The average number of sperm fused per oocyte was 1.5 ± 0.1. Errors are reported as s.e.m.

The codependency of inhibition of fertilization was investigated with a mixture of fertilinβ polymer **9₁₀₀-[3]** and cyritestin polymer **18₁₀₀-[3]** (Figure 3-6). These positive controls were tested at two independent polymer concentrations, 0.5 μM and 1 μM. The mixture of **9₁₀₀-[3]** at 0.5 μM and **18₁₀₀-[3]** at 0.5 μM in polymer concentration inhibited

34% of oocyte fertilization, whereas 9_{100} -[3] alone at 0.5 μ M in polymer concentration inhibited 54% of oocyte fertilization. This difference was not statistically significant.

II-2-2. Assay of bivalent copolymers

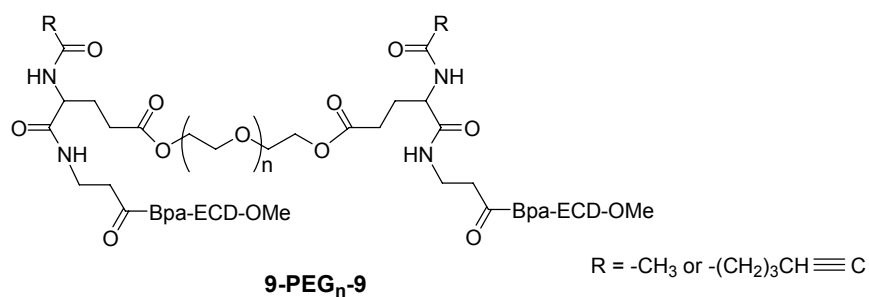


Polymer	% Inhibition at 0.5 μ M in polymer	
	by F.I.	by F.R.
9_{10} -[3]	64 ± 3.9	54 ± 4.5
18_{10} -[3]	35 ± 4.3	30 ± 2.6
13_{10} -[3]	1.5 ± 1.5	6.0 ± 3.0
9_2 - 13_{96} - 9_2 -[3]	65 ± 4.7	46 ± 3.8
9_2 - 13_{96} - 18_2 -[3]	49 ± 2.2	30 ± 8.0
18_2 - 13_{96} - 18_2 -[3]	22 ± 8.3	15 ± 7.8

Figure 3-7. Inhibition of fertilization by homopolymers and bivalent block copolymers at 0.5 μ M in polymer concentration. Black bars: F.I.; White bars: F.R. At least three independent experiments with 60-120 oocytes were assayed for each concentration. In the untreated controls, 65 ± 3% oocytes were fertilized. The average number of sperm fused per oocyte was 1.4 ± 0.2. Errors are reported as s.e.m.

Inhibition of fertilization by bivalent fertilin β mimic block copolymer **9₂-13₉₆-9₂-[3]** at 0.5 μ M in polymer concentration was 46% by F.R (Figure 3-7). This inhibition was equipotent to homopolymer **9₁₀₀-[3]**. Likewise, bivalent cyritestin mimic block copolymer **18₂-13₉₆-18₂-[3]** was nearly equipotent to homopolymer, **18₁₀₀-[3]** at 0.5 μ M in polymer concentration with 15% inhibition of oocyte fertilization.

Polymer **9₂-13₉₆-18₂-[3]**, the hetero bivalent, tri-block copolymer containing both ECD and QCD ligands with a 96 monomer spacer was tested. The inhibition potency of polymer **9₂-13₉₆-18₂-[3]** was lower than fertilin β mimic polymers, but better than cyritestin mimic polymers. It inhibited fertilization 30% by F.R. at 0.5 μ M in polymer concentration.



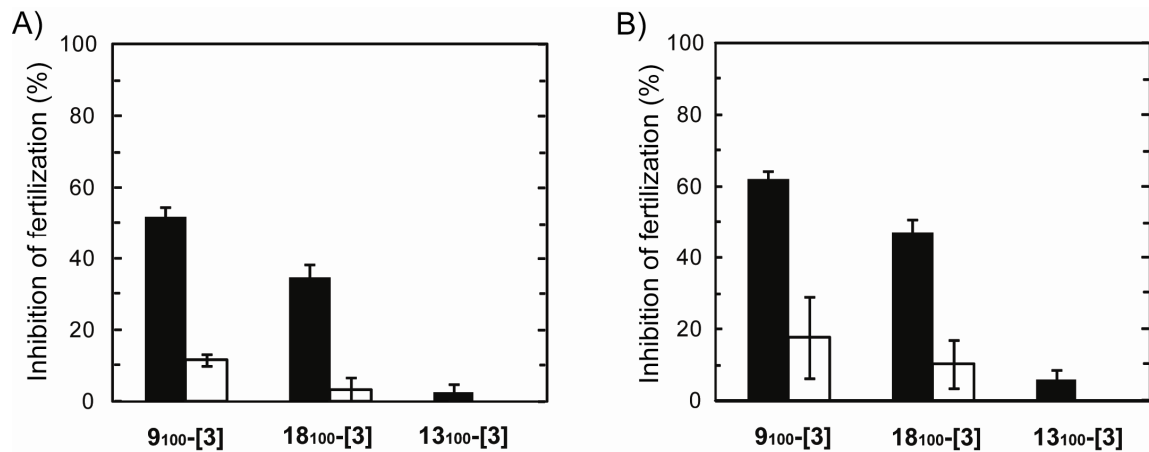
	Length of spacer	IC ₅₀ by F.I.	IC ₅₀ by F.R.
9-PEG₁₂-9	~5 nm	>250 μ M	>250 μ M
9-PEG₆₇-9	~25 nm	~50 μ M	~250 μ M
9-PEG₁₇₈-9	~70 nm	>250 μ M	>250 μ M

Figure 3-8. Inhibition of fertilization by PEGylated ECD polymers. At least three independent experiments with 60-80 oocytes were assayed for each polymer.

The biological results of bivalent block copolymers led us to design synthetically more accurate bivalent systems, PEGylated polymers. Since PEG (polyethylene glycol) is a flexible, water soluble, and narrowly distributed polymer (PDI < 1.06), each ECD ligand was placed at both end of the polymers to prepare **9-PEG_n-9**. The molecular weights were measured by mass spectroscopy. None of the **9-PEG_n-9** bivalent mimics inhibited fertilization equipotently to **9₂-13₉₆-9₂-[3]**.

II-2-3. Assay of KO oocytes

The inhibition potencies of **9₁₀₀-[3]** and **18₁₀₀-[3]** were tested with β_1 integrin knockout oocytes (Figure 3-9). Oocytes homozygous for the β_1 integrin knockout allele (Cre⁺ β_1 f/f, KO) and wild-type (Cre⁻ β_1 +/+, WT) oocytes were obtained as previously described.¹²⁵ Immuno-fluorescence microscopy with anti- β_1 and anti- α_6 integrin antibodies confirmed that the β_1 integrin knockout oocytes had no β_1 integrin or α_6 integrin on the plasma membrane.²⁶⁰ **9₁₀₀-[3]** inhibited fertilization of 12% by F.R. at 1 μ M in polymer concentration, as compared to 52% in WT oocytes. **18₁₀₀-[3]** also inhibited oocyte fertilization around 10%, as compared to 35% in WT oocytes.



% inhibition at 1 μ M in polymer				
Polymer	WT mice		KO mice	
	F.I.	F.R.	F.I.	F.R.
9₁₀₀-[3]	62 \pm 2.5	52 \pm 2.9	18 \pm 12	11 \pm 6.7
18₁₀₀-[3]	47 \pm 3.9	35 \pm 3.8	12 \pm 1.5	3.3 \pm 3.3
13₁₀₀-[3]	5.7 \pm 3.0	2.3 \pm 2.3	-	-

Figure 3-9. Inhibition of β_1 integrin knockout oocyte fertilization by homopolymers at 1 μ M in polymer concentration. A) Fertilization inhibition by F.R. B) Fertilization inhibition by F.I. Black bars: wild-type (WT) oocytes. At least six independent experiments with 100-120 oocytes were performed at each polymer concentration. In the untreated controls, 76 \pm 2% oocytes were fertilized. The average number of sperm fused per oocyte was 1.6 \pm 0.1. White bars: β_1 integrin KO oocytes. Two independent experiments with 25 oocytes for **9₁₀₀-[3]**, and three independent experiments with 39 oocytes for **18₁₀₀-[3]** were performed. In the untreated controls, 70 \pm 3% oocytes were fertilized. The average number of sperm fused per oocyte was 1.2 \pm 0.1. *P < 0.05 for WT vs. β_1 KO oocytes. Errors are the s.e.m.

III. Discussion

Testing the functions of molecules that have been implicated in mediating mammalian sperm-oocyte binding and fusion is the first step for understanding the molecular mechanisms of gamete interactions. For this type of discovery, it is critical to develop specific methods for exploring the mechanisms of binding. Probe-protein interaction studies are a valuable tool in many biological systems, but they have been applied in a limited fashion to fertilization because of the limited quantities of material available to study gametes in mammalian systems and the lack of cell culture models. Most experiments in the field of fertilization biology rely on genetic and immunohistochemical methods. Here, we employed chemical synthesis, ROMP, to produce multivalent mimics of fertilin β and cyritestin to imitate sperm complexes that bind the oocyte with optimal binding affinity.

III-1. Assay of homopolymers

Because the molecular weight analysis revealed that the most potent inhibitor, **9**₁₀-**[2]** was a 100-mer polymer, we tested **9**₁₀₀-**[3]** which also displays 100 copies of the ECD peptide, but is synthesized with catalyst **3** to compare their biological activities. Although their average molecular weights are the same, the ranges (dispersities) and backbone stereochemistry (cis/trans alkene ratio) were not identical. Inhibition by **9**₁₀₀-**[3]** was equipotent to that by **9**₁₀-**[2]** and was 100-fold more potent than the corresponding monomeric peptide. These results suggested that the 100-mer fertilin β mimic polymer bound multivalently to the oocyte surface.

Polymers mimicking sperm protein cyritestin were also prepared with catalyst **3**. These mimic polymers contained the conserved QCD tripeptide sequence thought to be required for fertilization. Their sizes ranged from 1 to 100 monomer units in length. **18**₁₀₀-**[3]** was more potent than the monomeric peptide or the shorter mimic polymers as an inhibitor of fertilization, but its inhibition potency (IC₅₀) was 4 times worse than the corresponding fertilin β mimics, **9**₁₀-**[2]** and **9**₁₀₀-**[3]**.

We also mutated the ECD and QCD sequences to ESA, glutamic acid-serine-alanine and ASD, alanine-serine-aspartic acid to synthesize control polymers **13**₁₀-**[3]**, **13**₁₀₀-**[3]**, and **21**₁₀-**[3]** with catalyst **3**. We chose to mutate ECD and QCD rather than scramble it, because two of the amino acids contained carboxylates.¹⁶⁵ ESA polymers, similar in length to the ECD and QCD polymers, were tested as inhibitors of fertilization and no inhibition was observed. Thus, the polymer backbone does not contribute to inhibition. However, another mutant, ASD (alanine-serine-aspartic acid) polymer, **21**₁₀-**[3]** inhibited fertilization similar to monomeric fertilin β mimic peptide, Ac-ECD-OMe, **8**. Because the aspartic acid residue is critical for binding,^{95, 105} **21**₁₀-**[3]** specifically bind to the oocyte plasma membrane with weak binding affinities.

III-2. Are the fertilin β and cyritestin receptors the same?

Based on the inhibition results, we explored the identity between fertilin β and cyritestin receptors. We expected two possibilities. In the first case, different receptors or protein complexes on the oocyte membrane might be targeted by either mimic. If so, their inhibitory behaviors should be independent, and the combination of two mimics

would inhibit more than each individual mimic. On the other hand, in a second scenario, fertilin β and cyritestin might bind the same receptors on the oocyte and no net increase in inhibition at a fixed concentration of polymer would be expected. Therefore a mixture of polymers **9₁₀₀-[3]** and **18₁₀₀-[3]** was tested.

Inhibition by the mixture of 0.5 μ M **9₁₀₀-[3]** and 0.5 μ M **18₁₀₀-[3]** was not dramatically increased relative to inhibition by 1 μ M of either homopolymer. Within experimental error, inhibition by a mixture of **9₁₀₀-[3]** and **18₁₀₀-[3]** was the same as by **18₁₀₀-[3]** alone. The combination of **9₁₀₀-[3]** and **18₁₀₀-[3]** decreased the potency of **9₁₀₀-[3]** 20%. Thus, these two mimic polymers **9₁₀₀-[3]** and **18₁₀₀-[3]** appear to compete for the same receptor rather than bind to independent receptors.

This comparison was further tested with a series of tri-block copolymers. First homobivalent polymers 100 units in length, **9₂-13₉₆-9₂-[3]** and **18₂-13₉₆-18₂-[3]** were synthesized. Two ECD or QCD ligands were at each terminus of the polymers to ensure that statistically at least one ligand would be present on the end of every polymer. The inactive ESA peptides were incorporated in the center of the tri-block copolymers as spacers. These polymers are the same average length as **9₁₀₀-[3]** and **18₁₀₀-[3]**, but they have a lower density of fertilin β and cyritestin peptides. Interestingly, they were only 10-15% less potent as inhibitors of fertilization compared to their corresponding homopolymers, **9₁₀₀-[3]** and **18₁₀₀-[3]**. This result suggested that of the 100 ligands present in the homopolymers only a small percentage are required for binding to the oocyte surface and that it is the overall size of the polymer that is most important for inhibition, rather than the ligand density.

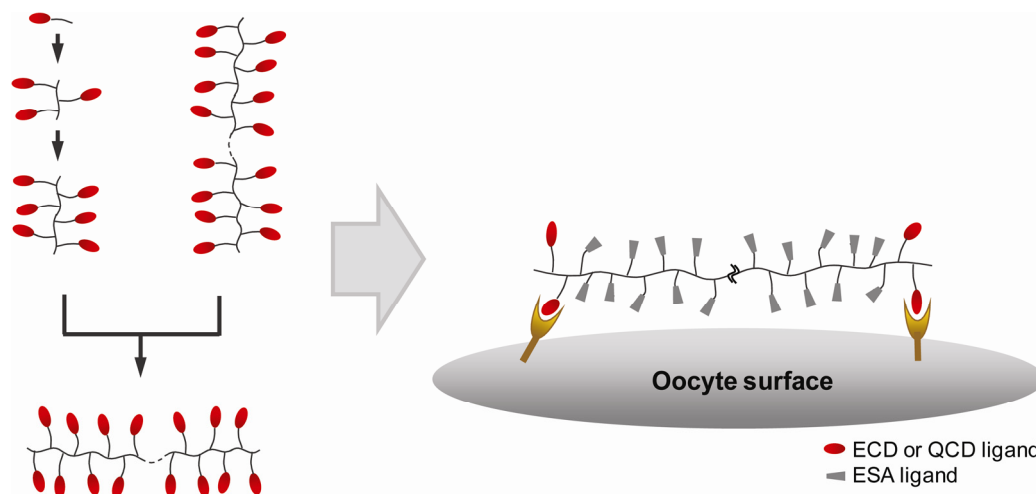


Figure 3-10. Proposed model for bivalent fertilin β or cyritestin receptors on polymer binding.¹⁵⁵ Testing a series of inhibitors of different lengths and valencies led to the design of the bivalent block copolymers. At both termini of polymer were contained fertilin β peptide, ECD or cyritestin peptide, QCD.

Because both the fertilin β and cyritestin bivalent mimics were effective inhibitors, we replaced the norbornenyl ESA spacer with a flexible linker, polyethylene glycol (PEG) between the ligands. PEG is resistant to the nonspecific adsorption of proteins,^{261, 262} and would be better suited for covalent cross-linking experiments to identify receptors and coreceptors. PEG linkers comprised of 12, 67, and 178 ethylene glycol units were introduced between ECD ligands. However, inhibition by all of three of the PEG-linked polymers was no more effective than with the monomeric peptides. The increased degrees of freedom in the PEG backbone compared to norbornyl polymers most likely diminished their binding affinities.¹⁵² Thus, the conformational constraints inherent to the norbornyl backbone dictate the shape of the polymers and consequently, make a positive contribution to the binding affinity.

Next, **9₂-13₉₆-18₂-[3]**, a heterobivalent tri-block copolymer containing both ECD and QCD ligands separated by a 96-monomer spacer was tested to explore the relationship and degree of identity between fertilin β and cyritestin receptors. The inhibition potency of polymer **9₂-13₉₆-18₂-[3]** was lower than fertilin β mimic polymers, **9₂-13₉₆-9₂-[3]** and **9₁₀₀-[3]**. However, its potency was better than cyritestin mimic polymers, **18₂-13₉₆-18₂-[3]** and **18₁₀₀-[3]**. Thus, synergy between fertilin β and cyritestin mimics was not observed. In agreement with the results of the mixed inhibition experiments, these data suggest that these two mimics engage the same oocyte surface receptors or protein complex and that the QCD ligand binds more weakly than the ECD ligand to the receptor.

Because, $\alpha_6\beta_1$ integrin on the mouse oocyte plasma membrane was identified as the ECD binding partner on the oocyte,^{94, 120, 122, 260} we tested whether **9₁₀₀-[3]** and **18₁₀₀-[3]** inhibit fertilization of β_1 integrin knockout oocytes (Figure 3). Polymer **9₁₀₀-[3]** did not significantly inhibit fertilization of β_1 integrin knockout oocytes as expected from earlier studies. Consistent with cyritestin binding to the same receptor, polymer **18₁₀₀-[3]** also did not inhibit fertilization of knockout oocytes.

IV. Summary

The molecular mechanisms whereby sperm bind to and fuse with the oocyte plasma membrane are still unclear. Even though fertilin β and cyritestin are well-characterized sperm proteins, their roles and their binding partners on the oocyte plasma

membrane are ambiguous. In this work, we synthetically mimic the ADAM proteins, fertilin β and cyritestin, to represent the sperm-oocyte binding events in vitro, to discover optimal inhibition models, and furthermore to explore the relationship and degree of identity between fertilin β and cyritestin receptors. A series of fertilin β and cyritestin mimic polymers were synthesized and their biological activities compared. In both the fertilin β and cyritestin polymer series, 100-mers were the most potent inhibitors. However, the potency of the cyritestin mimic was lower than that of the fertilin β mimic in both wild-type and β_1 integrin knockout oocytes. Block copolymers of the same length as their corresponding homopolymers, but with a low density of ligand peptides, were equipotent to their corresponding homopolymers. These data suggested that fertilin β and cyritestin mimic polymers bound to oocyte plasma membrane bivalently. However, synergistic inhibition was not observed with fertilin β and cyritestin mimics. The inhibition data of mixed homopolymers and bivalent heteropolymers suggest that fertilin β and cyritestin mimic polymers bind in the same complex of proteins and may bind to the same receptors. Moreover, we confirm that β_1 -related integrins are adhesion proteins for fertilin β and cyritestin mimic binding to oocytes.

Chapter 4

Identification of Fertilin β and Cyritestin Receptors on the Oocyte Surface
Membrane with “Clickable” Polymers

I. Introduction

II. Results

III. Discussion

IV. Summary

I. Introduction

Cell surface membranes contain various proteins such as receptor proteins, cell adhesion proteins, as well as other functional proteins. Especially understanding the pathway of receptor proteins is crucial to grasp a cell activity in its entirety. Although cell surface receptors vary the ways to carry the information into the cellular interior, universally the binding of substrate to receptor initiates a series of responsive incidents. These binding events on cell surface trigger molecular interactions, and then send signals to the cell nucleus. Through understanding cell surface and substrate interactions, elucidation of the receptor topology on a cell surface that initiates and antagonizes cellular signaling, and imaging of specific cell types *in vivo* is possible. Moreover, a practical application could be further developed such as biosensing pathogens and toxins, drug delivery to specific cell types, and tissue engineering.

ADAM proteins are also known to interact with transmembrane protein, integrins, combinations of α and β integrins in mammals. A monoclonal antibody to integrin α_6 (GoH3) inhibited sperm binding to mouse oocyte surface membrane.⁹⁹ Chen and Sampson showed that a photoaffinity tagged fertilin β peptide binds and labels the integrin $\alpha_6\beta_1$ on the mouse oocyte surface.¹²² Peptide competition and direct adhesion experiments have suggested that integrin $\alpha_9\beta_1$ binds fertilin β as well as cyritestin on epithelial cells.^{73, 84, 98} However, female mice with a conditional knockout of integrin β_1 in their oocytes are fertile *in vivo* and *in vitro*.¹²⁵ None of the known integrins present on the oocyte plasma membrane are necessary in sperm-oocyte binding and fusion,^{121, 125} which suggest that there might be the receptors other than integrin $\alpha_6\beta_1$ or $\alpha_9\beta_1$ for fertilin β and cyritestin on oocyte surface membrane.

Previously, Chen in the Sampson group synthesized ^{125}I -labeled fertilin β mimic oligopeptide containing a benzophenone photoaffinity probe (Bpa-RLAQDECDVTEYA-NH $_2$, I 125 -labeled on tyrosine).¹²² After the active peptide site binds to the receptors, 4-benzoyl phenylalanine (Bpa) in the peptide was cross-linked with oocyte plasma membrane under the long wave UV light. The peptide-integrin cluster was immunoprecipitated with anti- α_6 antibody (GoH3) and analyzed by SDS-PAGE gel (Figure 4-1). They confirmed that the fertilin β mimic peptide specifically binds to an integrin $\alpha_6\beta_1$ on the oocyte surface membrane. However, it was not clearly demonstrated whether integrin $\alpha_6\beta_1$ is the only binding partner of fertilin β mimic peptide or not.

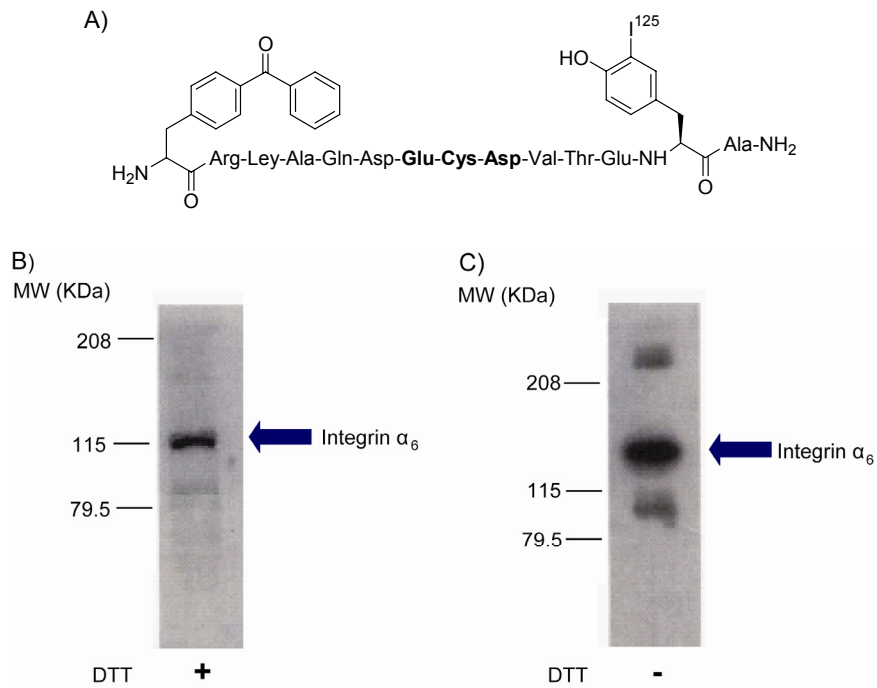


Figure 4-1. Autoradiograms of photoaffinity-labeled oocyte proteins.¹²² A) Structure of ^{125}I -labeled fertilin β mimic oligopeptide. B) A 6% reducing SDS PAGE gel of labeling reaction with DTT. C) A 6% non-reducing SDS PAGE gel of labeling reaction.

Hence, Jaechul Lee in the Sampson group prepared a 13-mer monomer unit long polymer, which was a fluorophore-linked fertilin β mimic block copolymer, and applied it in photoaffinity labeling to identify its binding partners on the oocyte plasma membrane. They employed a multivalent system to enhance the binding efficiency. Photoaffinity labeling was performed with Bpa in the mimic polymer under the long wave UV light. Although zona pellucida-free oocytes were labeled with the fertilin β mimic polymer, the identification of the labeled oocyte receptors was not achieved (Figure 4-2).

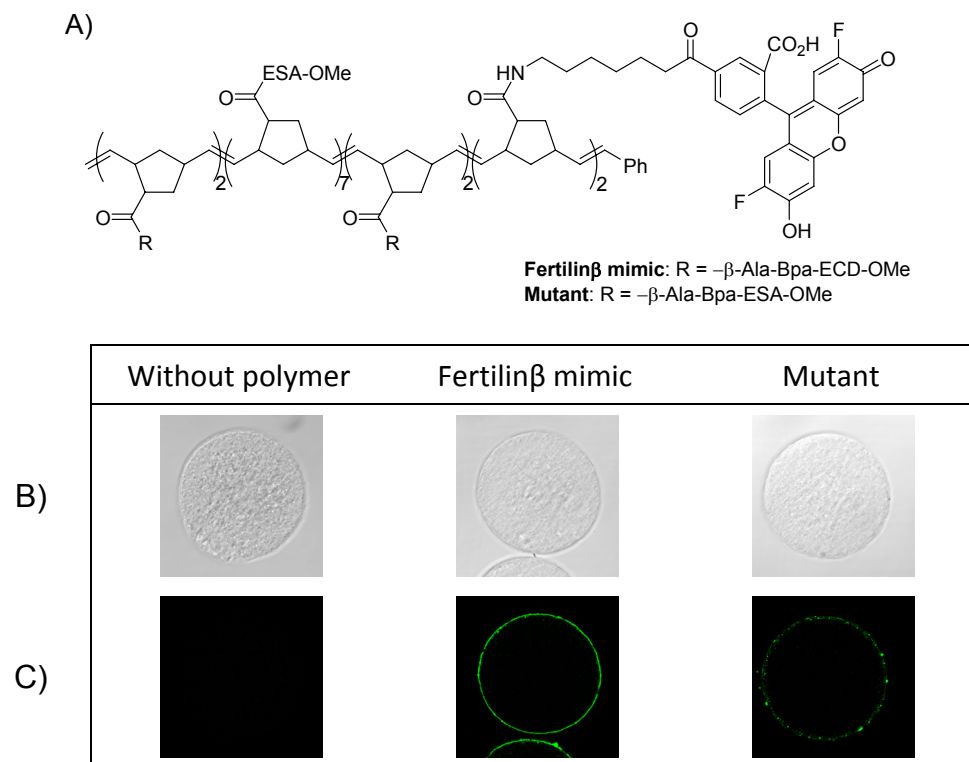
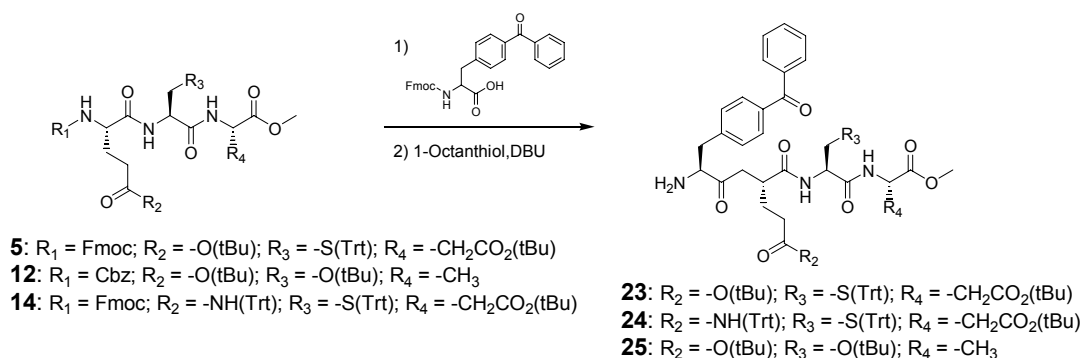


Figure 4-2. Photoaffinity labeling of zona pellucida-free oocytes performed by Jaechul Lee in the Sampson group.²⁶³ A) Fluorophore-linked polymers. B) DIC images by confocal microscopy. C) Fluorescence images by confocal microscopy.

There were two important features that we should consider to enhance the binding efficiency. First, the length of fertilin β mimic polymers was optimized. Because of different catalytic activities between catalyst **2** and catalyst **3**, we resynthesized mimic polymers based on results described in chapter 2. Second, we increased the detection efficiency of polymer-protein complexes by replacing an Oregon Green₄₈₈-antibody system with a stronger and more specific biotin-avidin system. Here, we introduce a more optimal bivalent mimic system, which might serve as a strategy for identifying receptors of fertilin β and cyritestin mimics.

II. Results

II-1. Synthesis of fertilin β mimic, cyritestin mimic, and mutant oligopeptides and polymers

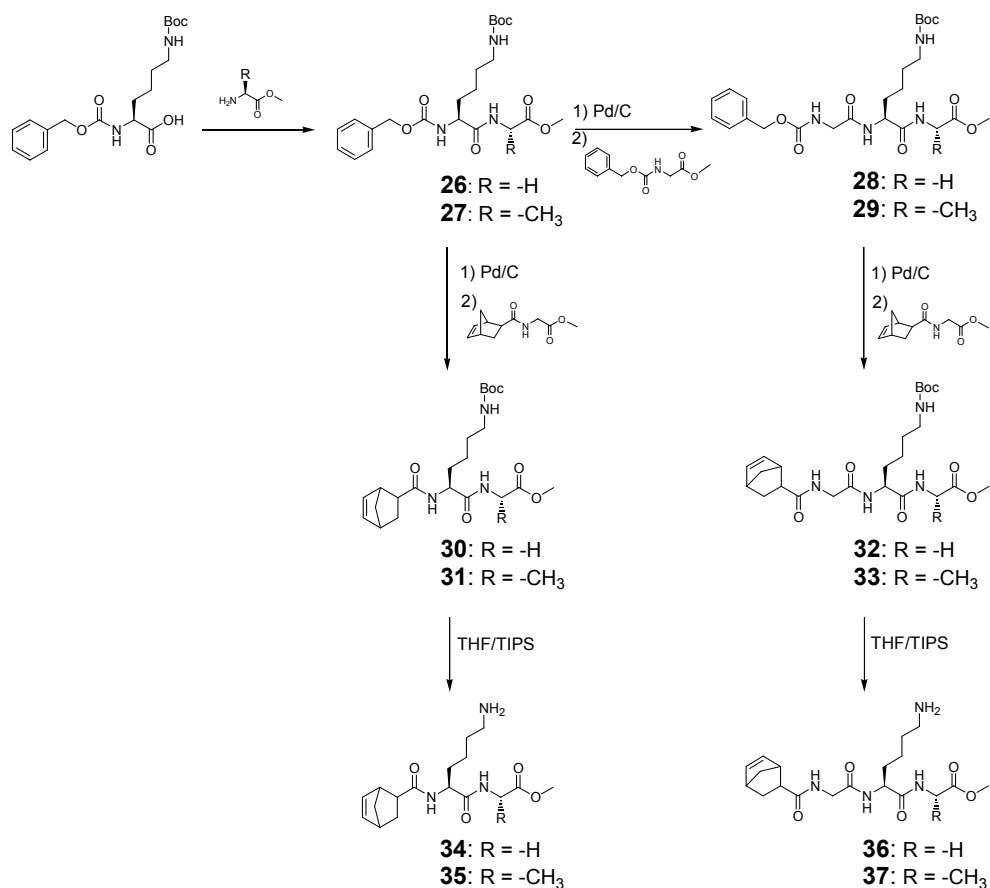


Scheme 4-1. Synthesis of fertilin β mimic, cyritestin mimic, and mutant oligopeptides containing Bpa.

Based on the inhibition data presented in chapter 3, we designed and synthesized new bivalent fertilin β and cyritestin mimic and mutant polymers. Monomeric

oligopeptides were synthesized first. After removing the Fmoc/Cbz groups in Fmoc-E(OtBu)C(Trt)-D(OtBu)-OMe, **5**, Fmoc-Q(Trt)C(Trt)D(OtBu)-OMe, **14**, and Cbz-E(OtBu)S(tBu)A-OMe, **12**, the Fmoc/Cbz groups deprotected oligopeptides were coupled with 4-benzoylphenylalanine (Bpa). The Fmoc groups were removed with 1-octanethiol and DBU to obtain **23**, **24**, and **25** respectively (Scheme 4-1).

In order to cleave oligopeptides selectively from polymer backbones by trypsin, we prepared four different oligopeptide candidates for trypsin digestion (Scheme 4-2).



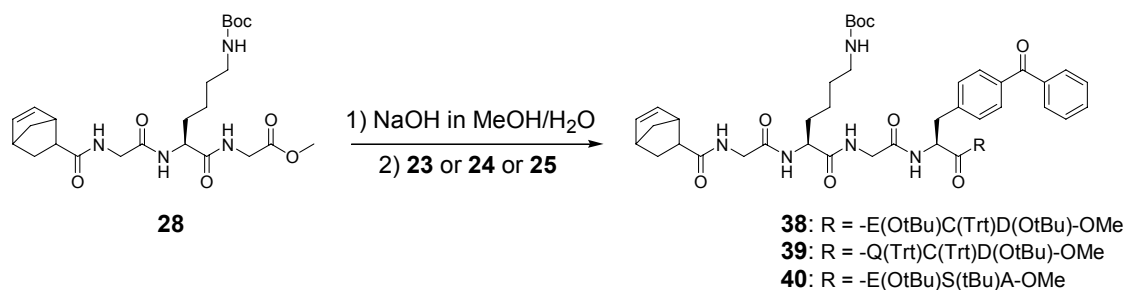
Scheme 4-2. A series of norbornenyl monomers containing trypsin cleavable oligopeptides.

Alanine or glycine was coupled at the C-terminus of Cbz-Lys-OH to prepare **26** and **27**. Half of **26** and **27** underwent Cbz group deprotection with Pd/C and H₂, followed by coupling with Cbz-Gly-OH to provide **28** and **29**. After removing Cbz groups in **26**, **27**, **28** and **29**, the oligopeptides were coupled with norbornenyl carboxylic acid. Boc groups in lysine were removed with TFA/TIPS in methylene chloride to prepare NB-KG-OMe, **34**, NB-KA-OMe **35**, NB-GKG-OMe, **36** and NB-GKA-OMe, **37**. These four oligopeptides were purified by reversed phase C₁₈ HPLC. 1 μL of diluted trypsin solution (0.15 μg/μL) was added to the peptide solutions that had been treated with DTT and iodoacetamide.

Trypsin digestion was performed at 36 °C for 16 h. As controls, norbornenyl peptides which were not treated with trypsin, were also incubated at 36 °C for 16 h. The degree of trypsin digestion was checked by ESI mass spectroscopy (Table 4-1). None of the control peptides without trypsin treatment were cleaved. Trypsin digestions with dipeptides, **34** and **35** were not complete, so original peptide still remained. However, tripeptides, **36** and **37** were completely cleaved at the C-terminus of lysine by trypsin.

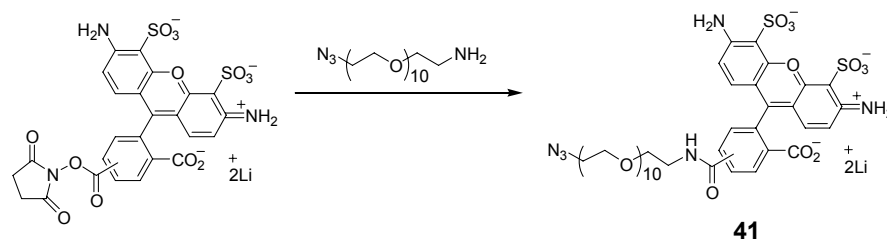
	34		35		36		37	
Trypsin	+	-	+	-	+	-	+	-
Digestion (%)	~40%	0%	~10%	0%	100%	0%	100%	0%

Table 4-1. Results of trypsin digestion.



Scheme 4-3. Synthesis of norbornenyl fertilin β and cyritestin mimic, and mutant monomers containing enzymatic cleavable peptide, Lys.

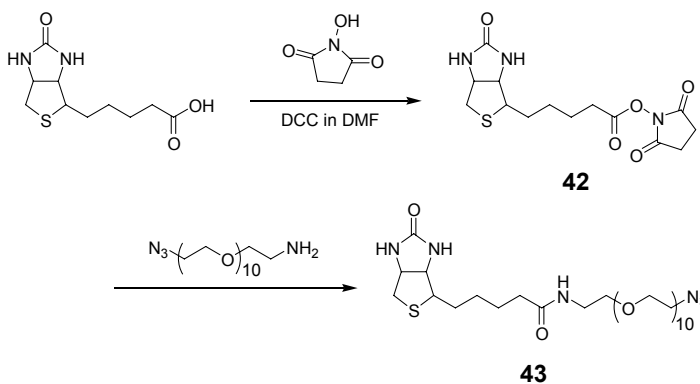
28 in which Lys was protected with a Boc group, was chosen for further coupling with mimic oligopeptides. After **28** was treated with sodium hydroxide in MeOH/H₂O, NB-GK(Boc)G-OH was coupled with the free α -amine of **23**, **24** and **25** to prepare norbornenyl peptides, **38**, **39** and **40** respectively, for polymerization (Scheme 4-3).



Scheme 4-4. Synthesis of Alexa₄₈₈-conjugated azido compound, **41**.

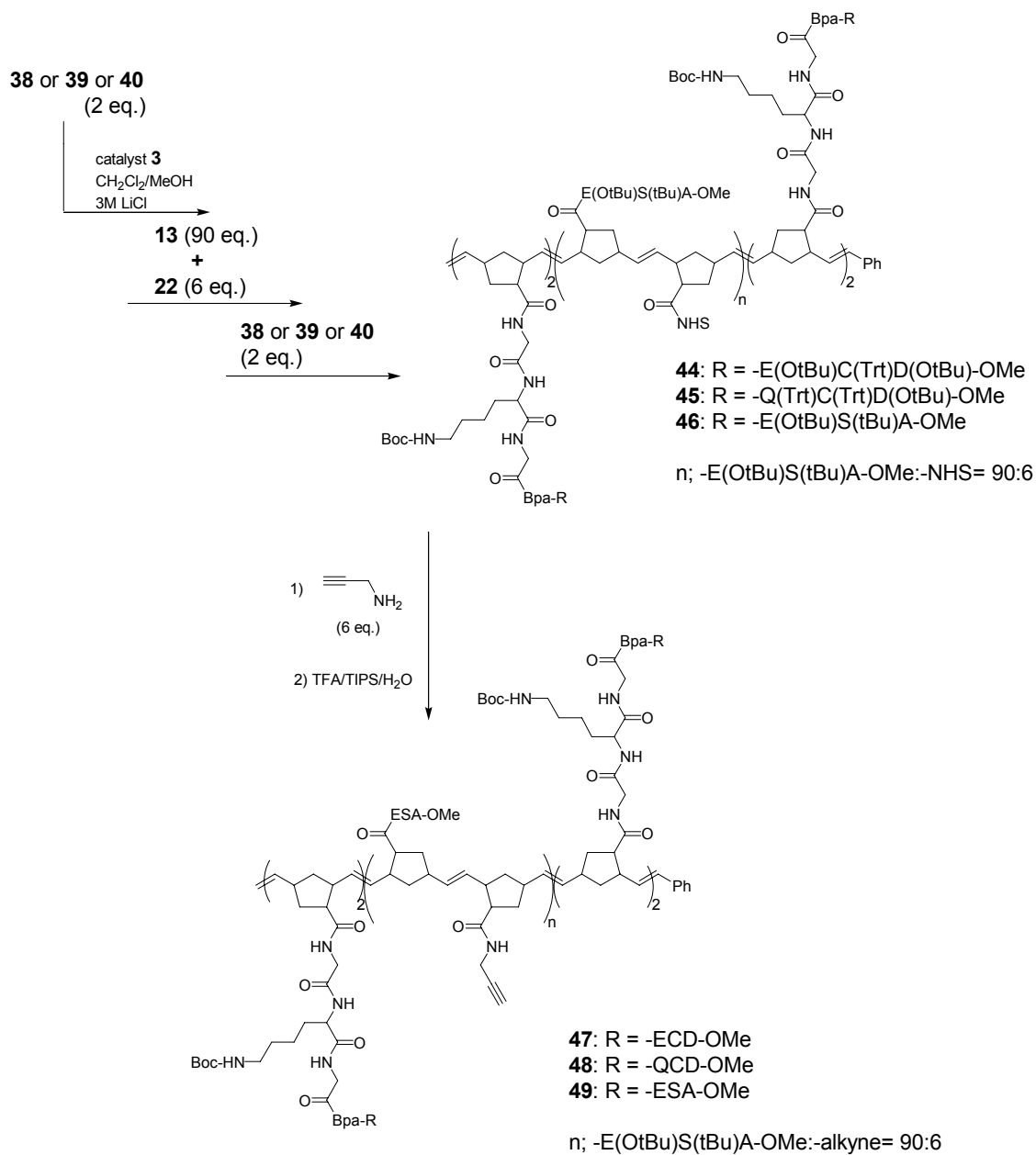
Fluorophore-conjugated azido compound **41** was prepared from Alexa fluor₄₈₈ dye and PEGylated azido compound, N₃-PEG₁₀-NH₂ in dimethyl formamide (Scheme 4-4). The reaction was performed with minimum exposure to light for 16 h, and the target compound was obtained by precipitation with diethyl ether. The formation of compound **41** was confirmed by ESI spectroscopy.

The carboxylic acid in biotin was activated as the *N*-hydroxysuccinimide (NHS) ester to obtain **42**. Then N₃-PEG₁₀-NH₂ was coupled with **42** for 16 h to yield biotin-tagged azido compound **43** (Scheme 4-5).



Scheme 4-5. Synthesis of biotin-tagged azido compound, **43**.

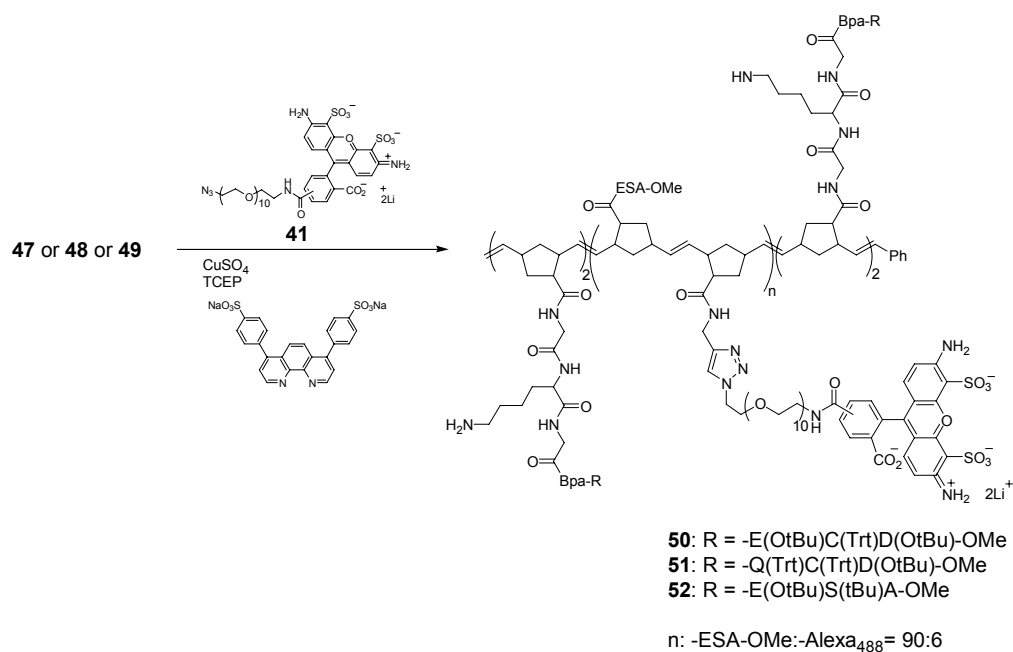
100-mer monomer unit bivalent polymers were synthesized by ROMP using fully protected peptides **38**, **39**, and **40** with catalyst **3** in chloroform/dichloromethane/methanol (1/2/1) with 3M LiCl to solubilize the polymers during the polymerization (Scheme 4-6). Synthetically two oligopeptides were placed at each terminus of the polymers, so that statistically at least one ligand was present on both ends of the polymers. As a spacer, 90 equivalents of biologically inactive norbornene ESA peptide **13** and 6 equivalents of norbornene carboxylic acid *N*-hydroxysuccinimide (NHS) ester **22** were inserted in the center of the tri-block copolymers, as a random mixture.



Scheme 4-6. Synthesis of alkyne-tagged bivalent polymers, **47**, **48**, and **49** synthesized by ROMP.

The polymerizations were terminated by adding ethylvinyl ether, and polymers **44**, **45**, and **46** were obtained by precipitation with diethyl ether. NHS activated carboxylic acids in **44**, **45**, and **46** were coupled with propynyl amine in dichloromethane to prepare

alkyne-tagged polymers. The side chain protecting groups were treated with a cocktail of TFA/TIPS/H₂O (95/2.5/2.5) for 6 h, and polymers **47**, **48**, and **49** were obtained.



Scheme 4-7. Synthesis of fluorophore-labeled bivalent polymers, **50**, **51**, and **52** synthesized by Huisgen 1,3-dipolar cycloaddition.

Fluorophore-labeled polymers with fertilin β and cyritestin peptides, **50** and **51** were prepared as well as a control polymer, **52** with a mutant sequence (Scheme 4-7). The Cu(I) mediated azide-alkyne Huisgen 1,3-dipolar cycloaddition (click chemistry) was performed with Alexa₄₈₈-PEG₁₀-azido compound **41** and alkyne-tagged polymers **47**, **48** and **49**. A water-soluble sulfonated bathophenanthroline ligand was used to improve the reaction efficiency. After reaction for 16 h, 1N HCl was added to precipitate polymers. These polymers were freshly reduced by TCEP before IVF assays.

II-2. Staining mouse oocyte with fluorophore-conjugated fertilin β mimic, cyritestin mimic, and mutant polymers

II-2-1. Binding experiment with wild- type oocytes

Zona pellucida-free oocytes were incubated with Alexa₄₈₈-conjugated polymers, **50**, **51**, and **52**. Zona pellucida-free oocytes were recovered for 2.5 h in 0.5% BSA/M16, and incubated in 20 μ M polymer using goat serum to block non-specific binding at 37 °C for 45 min. As a control, the oocytes were incubated in a drop of 10% goat serum, 0.5% BSA/M16 without polymers at 37 °C for 45 min as well. The oocytes were washed, were fixed with 4% paraformaldehyde, and were imaged using DIC and epi-fluorescence microscopy (Figure 4-3).

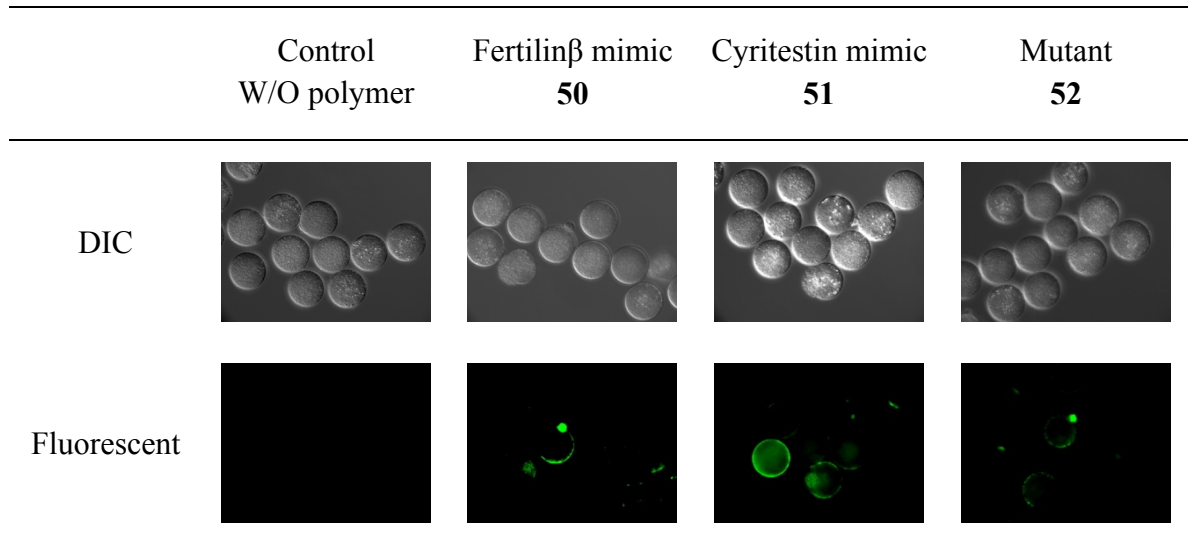


Figure 4-3. Binding of polymers with zona pellucida-free wild-type oocytes. About 20 oocytes were used in each experiment. DIC and epi-fluorescent images were taken with on a Zeiss Axiovert with a GFP/FITC filter and 0.55 NA, 20x objective.

In the control, none of the oocytes were fluorescently stained. The oolemma of oocytes incubated in fertilin β and cyritestin mimic polymers, **50** and **51** were faintly labeled, but the staining was not obvious. Mutant polymer **52** also labeled some oocytes weakly.

II-2-2. Labeling experiment with wild-type oocytes

Recovered zona pellucida-free oocytes were incubated in 20 μ M polymer drops (**50**, **51**, and **52**) with 1% polyvinylpyrrolidone (PVP) as a blocking agent at 37 °C for 45 min. In the control, the oocytes were incubated in 1% PVP/M16 without polymers at 37 °C for 45 min as well.

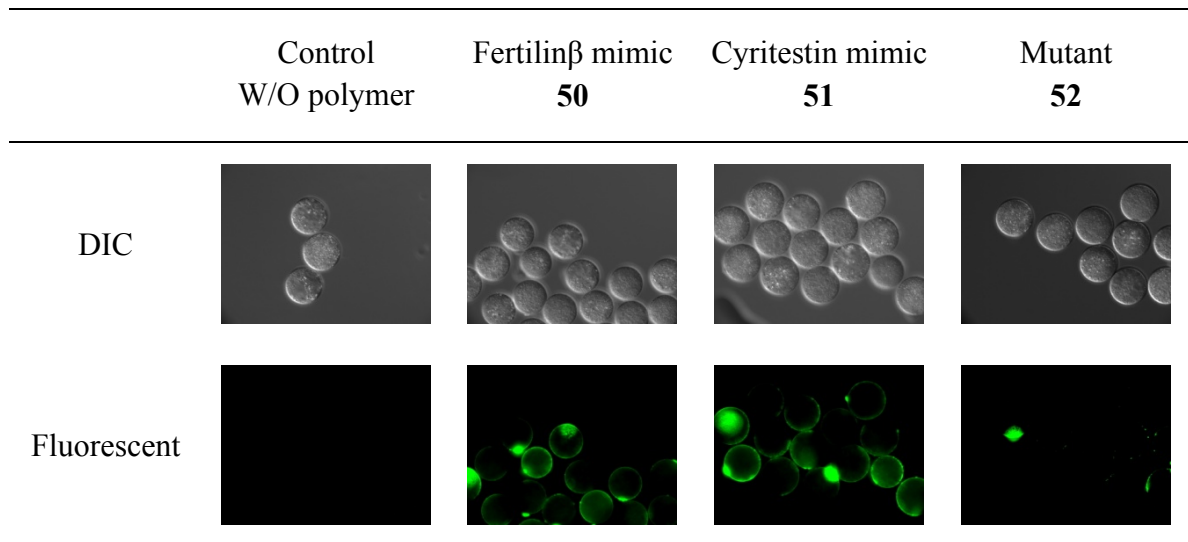


Figure 4-4. Labeling of polymers with zona pellucida-free wild-type oocytes. About 20 oocytes were used in each experiment. DIC and epi-fluorescent images were taken with on a Zeiss Axiovert with a GFP/FITC filter and 0.55 NA, 20x objective.

After incubation in polymer, the oocytes were irradiated with the long wave UV light (λ_{\max} = 350 nm, 15 cm) at 4 °C for 15 min. After washing, the oocytes were fixed with 4% paraformaldehyde and were mounted on a glass bottom dish. The images of photoaffinity labeled oocytes were acquired with DIC and epi-fluorescence microscopy (Figure 4-4). In the control, none of the oocytes were labeled. Mutant polymer **52** labeled the first polar body and the oolemma of some oocytes weakly. On the other hand, the oocytes incubated in fertilin β and cyritestin mimic polymers, **50** and **51** were labeled very clearly.

II-2-3. Labeling experiment with β_1 integrin knockout oocytes

β_1 integrin knockout oocytes were labeled with fluorophore-conjugated polymers, **50**, **51**, and **52** as described above. Zona pellucida-free oocytes were incubated in 20 μ M polymer with 1% PVP/M16 at 37 °C for 45 min. Oocytes were also incubated in 1% PVP/M16 without polymers at 37 °C for 45 min as a control. Then, the oocytes were irradiated with the long wave UV light (λ_{\max} = 350 nm) at 4 °C for 15 min. The UV light was 15 cm above the oocytes in the dish. After washing and fixing with 4% paraformaldehyde, the oocytes were washed and mounted on a glass bottom dish. The resulting images are shown in Figure 4-5. In the control, none of the oocytes were labeled, and mutant polymer **52** labeled the oolemma barely. Moreover, the oocytes incubated in fertilin β and cyritestin mimic polymers, **50** and **51** were labeled very weakly as well.

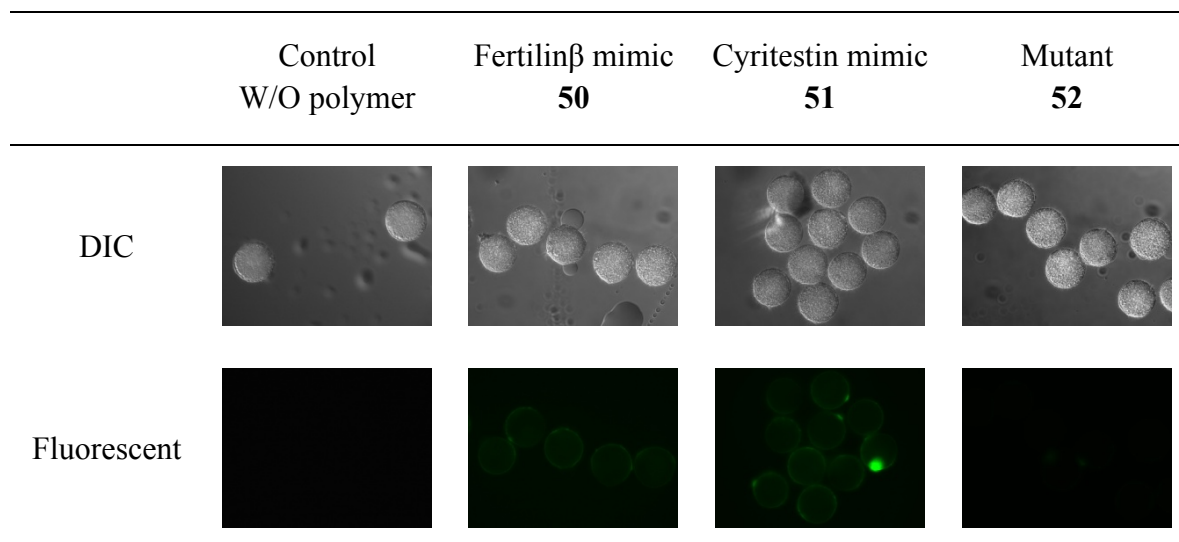


Figure 4-5. Labeling of polymers with zona pellucida-free β_1 integrin knockout oocytes. . About 20 oocytes were used in each experiment. DIC and epi-fluorescent images were taken with on a Zeiss Axiovert with a GFP/FITC filter and 0.55 NA, 20x objective.

II-3. Photoaffinity labeling mouse oocyte with fertilin β mimic polymer and mass analysis

About 10 000 wild-type mouse oocytes were cross-linked with fertilin β mimic polymer **47** with PVP as the blocking agent from 10 separate photoaffinity labeling reactions. For each assay, about 1 000 cumulus-intact oocytes were collected from 8 continuous dissections of 64 female mice in a day. The cumulus and the zona pellucida of the oocytes in 8 drops were removed continuously, and the zona pellucida-free oocytes were recovered in 8 separate drops for 1.5-3 h. After washing with 1% PVP/M16, the oocytes in 2 drops were combined. About 1 000 oocytes were incubated in 4 drops of 100 μ M polymer **47** in 1% PVP/M16 for 45 min. In order to remove the unreacted polymer, the oocytes were transferred to 4 drops of 1% PVP/M16. Then, the long wave UV light passed through the buffer to directly irradiate the oocytes at 4 $^{\circ}$ C for 15 min. The oocytes

were washed with 1% PVP/M16 and phosphate buffered saline (PBS), were combined, were lysed by RIPA lysis buffer, and were stored at – 80 °C.

After centrifuging, the combined lysates from about 10 000 oocytes labeled with polymer **47** were collected. The lysates were precleared with avidin beads. Then the Cu(I) mediated azide-alkyne Huisgen 1,3-dipolar cycloaddition was performed with the lysates and azido-PEG₁₀-biotin, **43**. The lysates contained proteins labeled with alkyne bearing polymer **47**. After 16 h cycloaddition reaction, the precipitant was washed with cold methanol, 1.2% sodium dodecyl sulfate (SDS)/PBS was added, and the mixture heated to 80-90 °C for 15 min. The solution was diluted to 0.2% SDS/PBS, and affinity purification was performed with avidin beads for 16 h. After washing, trypsin was added to the beads, and the reaction mixture was incubated at 37 °C for 16 h. The supernatant was desalted, and analyzed by LTQ Orbitrap XL ETD mass spectrometry. However, no peaks of transmembrane proteins were observed (Table 4-2). There were keratins and other proteins that were usually seen as contaminants. However, there were no transmembrane proteins on the beads. Actin was on the beads, however it was a common non-specific binder to beads. Then, we performed second affinity purification with avidin beads for 16 h. After enzyme digestion by trypsin and desalting, the sample was analyzed by MALDI-TOF mass spectrometry. However, no integrin peaks or oocyte transmembrane peaks were detected (Appendix A-2).

IPI	protein description	Total of ID
IPI00019359	KRT9 Keratin, type I cytoskeletal 9	69
IPI00220327	KRT1 Keratin, type II cytoskeletal 1	68
IPI00009865	KRT10 Keratin, type I cytoskeletal 10	62
IPI00021304	KRT2 Keratin, type II cytoskeletal 2 epidermal	51
IPI00217963	KRT16 Keratin, type I cytoskeletal 16	12
IPI00384444	KRT14 Keratin, type I cytoskeletal 14	7
IPI00397801	FLG2 Filaggrin-2	7
IPI00005859	KRT75 Keratin, type II cytoskeletal 75	6
IPI00009867	KRT5 Keratin, type II cytoskeletal 5	6
IPI00293665	KRT6B Keratin, type II cytoskeletal 6B	5
IPI00007047	S100A8 Protein S100-A8	3
IPI00025753	DSG1 Desmoglein-1	3
IPI00219217	LDHB L-lactate dehydrogenase B chain	3
IPI00465436	CAT Catalase	3
IPI00003269	ACTBL2 Beta-actin-like protein 2	2
IPI00027547	DCD Dermcidin UBC;UBB;RPS27A ubiquitin and ribosomal protein S27a	2
IPI00179330	Precursor	2
IPI00884222	Similar to Keratin, type I cytoskeletal 10	2
IPI00004550	KRT24 Keratin, type I cytoskeletal 24	1
IPI00008359	KRT76 Keratin, type II cytoskeletal 2 oral	1
IPI00290857	KRT3 Keratin, type II cytoskeletal 3	1

Table 4-2. List of proteins analyzed by LTQ Orbitrap XL ETD mass spectrometry. IPI represents international protein index, and the total of ID means the number of peptides identified.

III. Discussion

III-1. Synthesis of fertilin β mimic, cyritestin mimic, and mutant oligopeptides and polymers

In chapter 3, 100-mer monomer unit polymers were the best inhibitors of fertilization, whether fertilin β or cyritestin mimics. Their bivalent mimic systems inhibited oocyte fertilization similarly to homopolymers, within experimental error. The bivalent polymers contain the minimum of binding ligands, and improve inhibition of fertilization greatly compared to monovalent monomers. Based on the inhibition data of fertilin β and cyritestin mimic bivalent polymers, we redesigned and resynthesized bivalent polymer systems to label oocytes, and furthermore to identify a receptor on the oocyte plasma membrane.

There were two features we considered for designing fertilin β and cyritestin mimic and mutant monomers before polymerization for a labeling experiment. First, after binding, polymers should label the receptor proteins on the oocyte plasma membrane by photoaffinity cross-linking. A covalent bond between polymers and protein receptors would be created. Second, oligopeptide ligands in polymer-receptor complexes should be cleaved from polymer backbone for more accurate mass spectroscopy analysis. In addition to these two aspects, we also regarded a suitable way to improve the immunoprecipitation efficiency of the polymer-receptor complexes by introducing a biotin-avidin binding pair.

Benzophenone-based photoaffinity labeling has been used for probing the bimolecular interaction between ligand and receptor. Benzophenone is a photosensitizer which upon irradiated by the long wave ultraviolet (UV) light, forms a diradical (Figure

4-6). One radical on oxygen attacks a hydrogen donor from nearby protein to form a hydroxyl group and a new radical on the protein. The remaining radical on benzophenone reacts with the newly formed radical on protein to create a carbon-carbon covalent bond. Therefore benzophenone is cross-linked to the target protein. The benzophenone moiety has high cross-linking specificity and efficiency, and low reactivity with water. Hence, for oocytes photoaffinity labeling with fertilin β and cyritestin polymers, Bpa was positioned at the *N*-terminus adjacent to the ECD, QCD and ESA sequence to yield **23**, **24** and **25**.

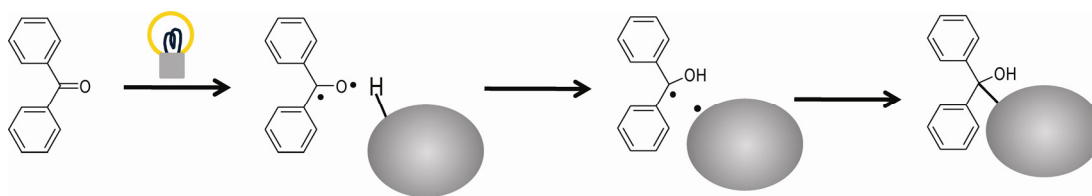


Figure 4-6. Photoaffinity cross-linking of benzophenone with a hydrogen donor compound.

For mass spectrometric analysis of polymer-receptor complexes, proteomic digestion was used. Trypsin is a commonly used enzyme to digest proteins into peptides, and preferentially cleaves after arginine and lysine. However, a bulky and high molecular weight polymer backbone would not be cleaved by trypsin. So, we placed lysine between norbornenyl and binding ligands (Figure 4-7). After trypsin digestion, the binding ligands might be cleaved from the polymer backbone. The fertilin β and cyritestin mimics, ECD- and QCD-labeled peptide residues in target proteins might be analyzed by mass

spectroscopy, and then the exact binding sites of ECD and QCD in target proteins would be determined.

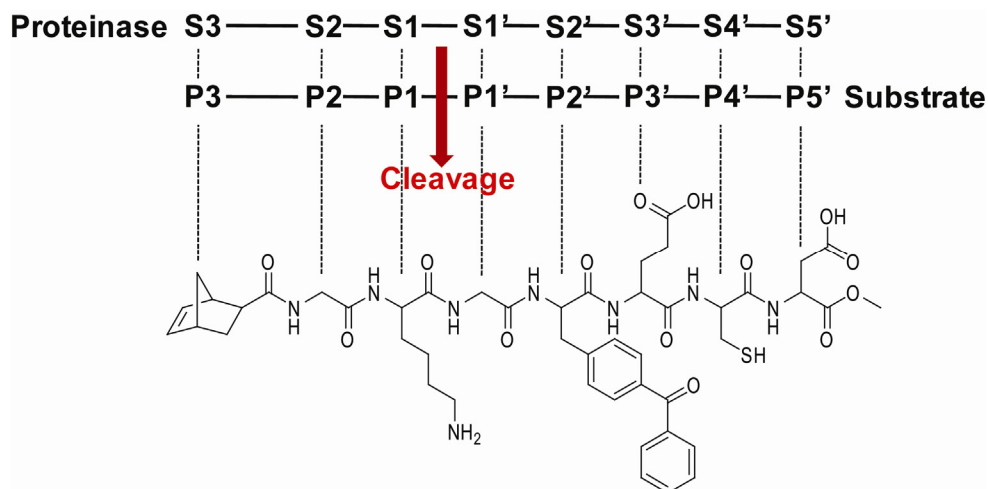


Figure 4-7. Schematic representation of enzyme-substrate (NB-GKG-Bpa-ECD-OMe) complex. The cleavage occurs at the bond between P1 and P1' in substrate.

To perform enzymatic cleavage with trypsin, we verified which combination of oligopeptides could be best for proper cleavage. We designed four norbornenyl oligopeptides containing lysine, and tested the degree of their enzyme digestion. Trypsin completely cleaved next to lysine in tripeptides, NB-GKG-OMe, **36** and NB-GKA-OMe, **37**, but not in dipeptides, NB-KG-OMe, **36** and NB-KA-OMe, **37**. At least one natural amino acid was needed between norbornene and lysine. There might be racemization during coupling of NB-GK(Boc)A-OH and fertilin β and cyritestin mimic and mutant ligands. Hence, we synthesized NB-GK(Boc)G-OMe, **32**, and coupled with binding ligands, **23**, **24** and **25** to prepare norbornenyl monomers, **38**, **39** and **40**.

To increase the immunoprecipitation rate, biotin would be more efficient than previously used Oregon green₄₈₈. Because biotin binds very tightly to the tetrameric protein, avidin, with a dissociation constant $K_d \approx 10^{-15}$ mol/L,²⁶⁴⁻²⁶⁶ biotin-tagged compounds are simply extracted with avidin beads. So we designed biotin-tagged mimic polymers. However, direct use of biotin-tagged fertilin β and cyritestin mimic polymers with the zona pellucida-free oocytes might cause nonspecific extraction of other biotin-binding proteins, thereby increasing the signal background. Therefore, biotin was incorporated after specific polymers-oocytes binding.

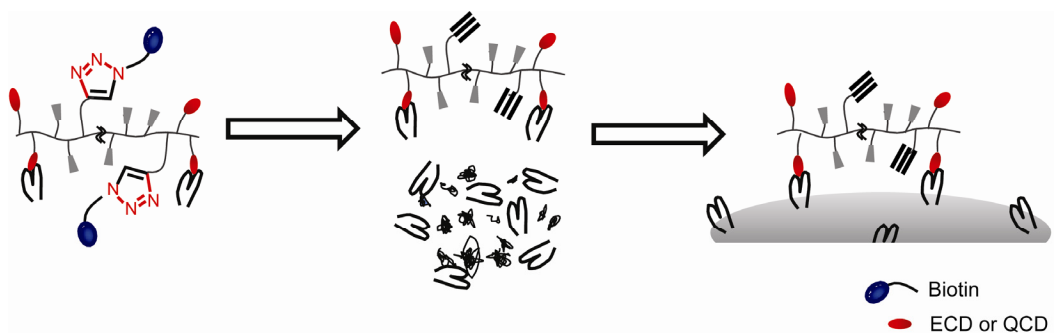


Figure 4-8. Representation of biotin-tagged polymer-protein receptor complex extraction strategy.

Cu(I) mediated azide-alkyne Huisgen 1,3-dipolar cycloaddition has emerged as an efficient method for simply connecting two molecules together. So, either an alkyne or an azide group should be attached to the polymers. However, the azide group is reactive under UV irradiation conditions required for photoaffinity labeling. Only the alkyne moiety could be incorporated into polymers. Because the triple bond might be initiated with Ru catalysts during ROMP, we could not directly use alkyne-tagged monomers for

ROMP. The active NHS ester served as a simple monomer for ROMP reaction, and as a molecular handle for further coupling of the alkyne moiety after polymerization. The alkyne-tagged polymers would cross-link to oocytes specifically, and then the alkyne groups in the polymers would be converted into the biotin-tagged azido moiety (Figure 4-8).

Based on these three considerations, ROMP reactions of fertilin β and cyritestin mimic and mutant polymers were performed. 2 equivalents of norbornenyl monomers, **38**, **39** and **40** were initiated with catalyst **3** respectively. As a spacer of bivalent polymers, 90 equivalents of NB-E(OtBu)S(tBu)A-OMe, **13** and 6 equivalents of NB-NHS, **22** were mixed and randomly incorporated into the middle of the polymer as shown in Scheme 4-6. Another 2 equivalents of norbornenyl monomers containing binding ligands were added to prepare bivalent polymers, **44**, **45** and **46**. Then we introduced the alkyne moiety into the spacer after polymerization. Propynyl amine was coupled to the NHS activated carboxylic esters in the polymer spacer.

Huisgen 1,3-dipolar cycloaddition, “click chemistry” of alkyne-tagged polymers with a fluorophore, **41** was performed to prepare fluorophore-conjugated polymers **50**, **51** and **52** in over 95% isolated yield.

III-2. Staining mouse oocyte with fluorophore-conjugated fertilin β mimic, cyritestin mimic and mutant polymers

The affinities of Alexa₄₈₈-conjugated polymers **50**, **51** and **52** were tested in an oocyte binding experiment. After incubation of zona pellucida-free wild-type oocytes

with polymers, the oocytes were washed without cross-linking or UV cross-linked without washing.

The oocytes that were washed without cross-linking were not obviously labeled with the polymers. The polymers dissociated from the oocytes during the washing step. However, after UV cross-linking without the washing step, most of oocytes were labeled with fertilin β mimic polymer **50**, and cyritestin mimic polymer **51**. The mutant polymer **52** did not label the oolemma of the oocytes. The polymer-conjugated fluorophore, Alexa₄₈₈ allowed us to confirm direct binding between polymers and the oocyte surface membrane. Fertilin β and cyritestin mimic polymers directly bind to the oocyte surface, and inhibit sperm binding to the oocytes. Cross-linking oocytes with polymers appears to be highly specific. This result also supports that the mutant polymer **52** does not bind to the oocytes, correlating with its inability to inhibit sperm binding to the oocytes.

Alexa₄₈₈-conjugated polymers **50**, **51** and **52** were also tested in a β_1 knockout oocyte labeling experiment. After incubation of zona pellucida-free KO oocytes in polymer, polymers were irradiated under the long wave UV to cross-link to the oocytes. No distinct labeling of the oolemma by the polymers was observed. This result confirmed that fertilin β and cyritestin mimic polymers predominantly bind to the β_1 -related receptors on the oocyte plasma membrane.

III-3. Photoaffinity labeling mouse oocyte with fertilin β mimic polymer and mass analysis

Based on the result of oocyte staining microscopy, we performed photoaffinity cross-linking with the alkyne-tagged fertilin β mimic polymer, **47** of about 10 000 oocytes

for identifying the fertilin β receptors on the oocyte plasma membrane. The proposed scheme for the process of the photoaffinity labeling and the identification of the fertilin β mimic-labeled receptors on the oocyte plasma membrane is shown in Figure 4-9.

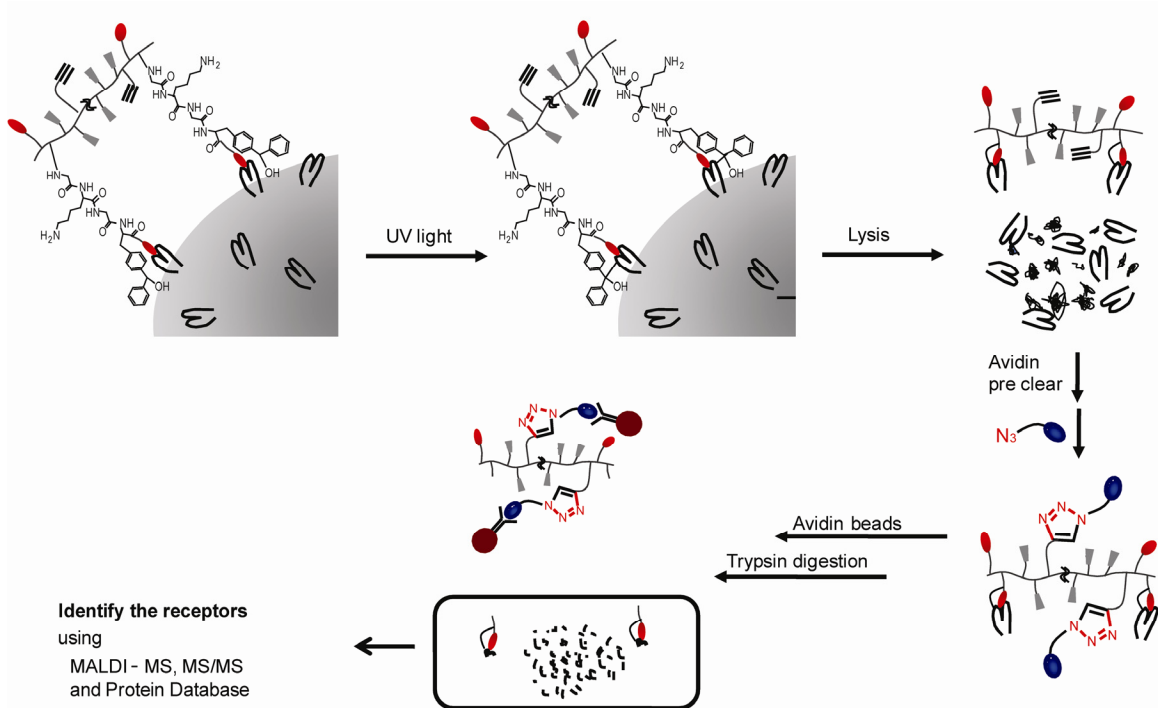


Figure 4-9. Schematic representation of the photoaffinity labeling and identification of the receptors.

Fertilin β mimic ligand was bound to the receptors on the oocyte plasma membrane. Then, in the polymer, oocyte solution was irradiated with the long wave UV light to create a covalent bond to the receptors. After oocyte lysis, the biotin moiety was introduced into the polymer in the lysates. Then, we isolated biotin-tagged polymer-receptor complexes with avidin beads. Enzyme digestion with trypsin was performed on

the bead state, and the supernatant was analyzed by LTQ Orbitrap XL ETD mass spectroscopy. However, no peak of oocyte transmembrane proteins was detected from the sample. There were keratins and other proteins such as ribosomal-like or actin-like protein that are usually seen as contaminants or non-specific binders to the beads. Because keratin peaks normally show up if there is nothing detectable, the level of transmembrane proteins from oocytes was not enough, but not in keratins. No oocyte transmembrane peaks were detected.

Because the mass detection of LTQ Orbitrap XL ETD mass spectrometry might be less sensitive than that of MALDI-TOF mass spectrometry, we performed second affinity purification. Although there were peaks observed, no oocyte transmembrane peaks were detected. Most of polymer-oocyte receptor complexes might be isolated by first affinity purification and analyzed by less sensitive LTQ Orbitrap XL ETD mass spectrometry.

We increased the labeling efficiency through the following ways. First, appropriate bivalent polymers increased polymer-receptor binding affinities. Second, in order to improve the efficiency of immunoprecipitation, high affinity of biotin-avidin pair was introduced. Also, increasing the number of oocyte provided more proteins. Still the binding efficiency was not enhanced sufficiently. We already verified that the bivalent fertilin β mimic polymer binds and cross-links directly to the oocytes. Moreover introducing an azido-tagged target moiety such as Alexa₄₈₈ and biotin, to the bivalent polymer by “click chemistry” was successfully achieved. So, we should fix the conditions for each step more carefully to improve the labeling efficiency. Especially, the suitable sample and reagent concentrations should be determined.

IV. Summary

ADAM proteins are known to interact with integrins, combinations of α and β integrins in mammals. Especially, integrin $\alpha_6\beta_1$, and $\alpha_9\beta_1$ are known as the binding partners of sperm protein fertilin β and cyritestin. Moreover, we already confirmed β_1 -related integrins are the predominant proteins for binding of fertilin β and cyritestin mimic polymers by inhibition data of wild type and β_1 integrin knockout mouse fertilization. Here, we developed a more optimal bivalent mimic system for labeling oocytes. Photoaffinity cross-linkable peptide, Bpa and trypsin digestive peptide, lysine were placed next to fertilin β and cyritestin mimic and mutant oligopeptides. Also alkyne moiety was inserted in the middle of polymer backbone to introduce a fluorophore and a biotin by “click chemistry”. Alex₄₈₈-tagged fertilin β and cyritestin mimic bivalent polymers labeled the oolemma of the wild-type mouse oocytes, but not β_1 integrin knockout mouse oocytes. This result also supported that β_1 -related integrins are the predominant proteins for binding of fertilin β and cyritestin mimic polymers. However, identifying the receptors of the fertilin β mimic by a biotin-tagged bivalent polymer were not achieved. Hence, more optimal conditions for each labeling step should be determined to improve the labeling efficiency.

Chapter 5

Experimental Methods

- I. Synthesis and Preparation of Compounds
- II. *In vitro* Fertilization Assay
- III. Fluorescence Staining Protocol
- IV. Photoaffinity Labeling Protocol

I. Synthesis and Preparation of Compounds

Materials. Amino acids and coupling agents used were purchased from Advanced Chem Tech. (Louisville, KY) or Novabiochem (Gibbstown, NJ). Solvents and chemical reagents were obtained from Fisher Scientific, Inc. (Springfield, NJ) or Sigma-Aldrich (Milwaukee, WI). $(\text{H}_2\text{IMes})(\text{PCy})_2\text{Cl}_2\text{Ru}=\text{CHPh}$ was purchased from Sigma-Aldrich (Milwaukee, WI). $(\text{H}_2\text{IMes})(3\text{-Br-pyr})_2\text{Cl}_2\text{Ru}=\text{CHPh}$ was prepared according to the literature.²³¹ CH_2Cl_2 , CH_3OH and Et_2O were dried and purified by pushstill (SG Water USA LLC, Nashua, NH). LiCl was oven dried and stored over P_2O_5 before use. All reactions were carried out under an Ar atmosphere in oven-dried glassware unless otherwise specified. Moisture and oxygen-sensitive reagents were handled in an N_2 -filled drybox. 5-Norbornene-exo-carboxylic acid was synthesized according to the literature.²⁶⁷

General Methods. Analytical thin layer chromatography (TLC) was performed on precoated silica gel plates (60F₂₅₄) and flash chromatography on silica gel-60 (230–400 mesh). TLC spots were detected by UV light and by staining with 10% phosphomolybdic acid (PMA) in ethanol. Peptides were purified by flash column chromatography on silica gel-60. The purities of all peptide monomers were assessed by RP-HPLC on a Vydac C₁₈ column. Gradient elution was performed at 1 mL/min with CH_3CN and H_2O (both containing TFA, 0.1%). The molecular weight of the polymers was assessed by gel permeation chromatography (Phenogel 5 μ Linear (2), Phenomenex) eluting with 10% CH_3OH in CH_2Cl_2 or THF. Inova400, Inova500, and Inova600 MHz NMR spectrometers were used to perform NMR analysis, and spectra were recorded in CDCl_3 unless otherwise noted. ^1H -NMR spectra are reported as chemical shift in parts per million (multiplicity, coupling constant in Hz, integration). ^1H -NMR data are assumed to be first

order. Copies of spectra are available in the appendix. The usual workup for peptide coupling reactions was three washes of the CH₂Cl₂ solution with 5% NaHCO₃, followed by three washes with 1 N HCl, and drying of the CH₂Cl₂ over Na₂SO₄. After evaporation of solvent, the peptide product was purified by flash silica chromatography.

I-1. Peptide synthesis.

Fmoc-Cys(Trt)Asp(OtBu)-OMe, **4**.¹⁶⁵ H-Asp(OtBu)-OMe·HCl (16.69 mmol, 4.00 g), Fmoc-Cys(Trt)-OH (18.36 mmol, 10.75 g), EDC·HCl (20.03 mmol, 3.83 g), and HOBt·hydrate (20.03 mmol, 3.07 g) were dissolved in 40 mL dry CH₂Cl₂ and cooled to 0 °C. DIEA (18.36 mmol, 3.25 mL) was added to the mixture, and the reaction was stirred for 4 h at rt. The usual workup and chromatography (acetone:CH₂Cl₂/1:20) yielded Fmoc-Cys(Trt)Asp(OtBu)-OMe (12.7 g, 98%) as a white powder. ¹H-NMR (400 MHz) δ 7.74 (t, *J*= 7.6 Hz, 2), 7.57 (d, *J*= 4.8 Hz, 2H), 7.31 (m, 19H), 6.78 (d, *J*= 7.6 Hz, 1H), 5.01 (d, *J*= 6.8 Hz, 1H), 4.71 (m, 1H), 4.34 (m, 2H), 4.19 (t, *J*= 7.0 Hz, 1H), 3.76 (dd, *J*= 6.8, 6.8 Hz, 1H), 3.66 (s, 3H), 2.89 (dd, *J*= 17.0, 4.6 Hz, 1H), 2.73 (m, 1H), 2.65 (m, 2H), 1.38 (s, 9H).

Fmoc-Glu(OtBu)Cys(Trt)Asp(OtBu)-OMe, **5**.¹⁶⁵ Fmoc-Cys(Trt)Asp(OtBu)-OMe (5.19 mmol, 4.00 g) was dissolved in 10 mL dry CH₂Cl₂. 1-Octanethiol (51.9 mmol, 9.04 mL) and DBU (0.52 mmol, 78 μL) were added, and the reaction was stirred for 15 h at rt under Ar. After evaporation of the solvent, the resulting product was purified by flash chromatography eluting with a step gradient ranging from 2% to 50% EtOAc/CH₂Cl₂. H-Cys(Trt)Asp(OtBu)-OMe (2.09 g, 73%) was obtained as a fine white powder. H-

Cys(Trt)Asp(OtBu)-OMe, (3.65 mmol, 2.00 g), Fmoc-Glu(OtBu)-OH (4.02 mmol, 1.71 g), EDC·HCl (4.38 mmol, 0.84 g), and HOBt-hydrate (4.38 mmol, 0.67 g) were dissolved in 10 ml dry CH₂Cl₂ and were cooled to 0 °C. DIEA (4.02 mmol, 0.71 mL) was added to the mixture, and the reaction was stirred for 5 h at rt. The usual workup and chromatography (acetone:CH₂Cl₂/1:20) yielded Fmoc-Glu(OtBu)Cys(Trt)Asp(OtBu)-OMe (3.04 g, 87%) as a white powder. ¹H-NMR (400 MHz) δ 7.76 (d, *J*= 7.6 Hz, 2H) 7.56 (t, *J*= 7.2 Hz, 2H), 7.40 (m, 8H), 7.28 (m, 8H), 7.18 (m, 3H), 6.90 (d, *J*= 8.4 Hz, 1H), 6.61(d, *J*= 7.6 Hz, 1H), 5.84 (d, *J*= 6.4 Hz, 1H), 4.72 (m, 2H), 4.35 (d, *J*= 7.2 Hz, 2H), 4.15 (m, 2H), 4.04 (m, 1H), 3.67 (s, 3H), 2.82 (m, 2H), 2.67 (dd, *J*= 17.0 and 4.8 Hz, 1H), 2.57 (dd, *J*= 13.2 and 5.2 Hz, 1H), 2.40 (m, 1H), 2.30 (m, 1H), 2.03 (m, 1H), 1.88 (m, 1H), 1.44 (s, 9H), 1.40 (s, 9H).

Ac-Glu(OtBu)Cys(Trt)Asp(OtBu)-OMe, 7.¹⁶⁵ Fmoc-Glu(OtBu)Cys(Trt)Asp(OtBu)-OMe (0.31 mmol, 300 mg) was dissolved in 1 mL dry CH₂Cl₂. 1-Octanethiol (3.14 mmol, 546 μL) and DBU (0.031 mmol, 30 μL) were added, and the reaction was stirred for 16 h at rt. The resulting product was purified by flash chromatography eluting with a step gradient ranging from 2% to 50% EtOAc/CH₂Cl₂. H-Glu(OtBu)Cys(Trt)Asp(OtBu)-OMe (163 mg, 72%) was obtained as a fine white powder. H-Glu(OtBu)Cys(Trt)Asp(OtBu)-OMe (0.27 mmol, 198 mg) was dissolved in 3 mL dry CH₂Cl₂. Acetic anhydride (2.70 mol, 257 μL) was added to the reaction followed by DIEA (0.82 mmol, 114 μL), and the reaction was stirred for 1 h at rt under Ar. The usual workup and recrystallization of the crude product from CH₂Cl₂ yielded Ac-Glu(OtBu)Cys(Trt)Asp(OtBu)-OMe (163 mg, 78%) as a white powder. ¹H-NMR (400 MHz) δ 7.42 (m, 6H) 7.30 (m, 6H), 7.21 (m, 3H), 6.86 (d, *J*= 8.4 Hz, 1H), 6.70 (d, *J*= 7.6

Hz, 1H), 5.53 (d, $J= 6.8$ Hz, 1H), 4.70 (m, 1H), 4.33 (m, 1H), 4.01 (m, 1H), 3.67 (s, 3H), 2.84 (dd, $J= 16.8$ and 5.2 Hz, 1H), 2.77 (dd, $J= 13.2$ and 8.0 Hz, 1H), 2.67 (dd, $J= 16.8$ and 4.8 Hz, 1H), 2.58 (dd, $J= 12.8$ and 5.2 Hz, 1H), 2.40 (m, 1H), 2.28 (m, 1H), 2.03 (m, 1H), 1.97 (s, 3H), 1.88 (m, 1H) 1.43 (s, 9H), 1.40 (s, 9H). ESI mass spectrum: Calcd (MNa⁺) 798.35, Found 798.52.

Ac-GluCysAsp-OMe, **8**.¹⁶⁵ Ac-Glu(OtBu)Cys(Trt)Asp(OtBu)-OMe was deprotected in a cocktail of H₂O, TIPS, and TFA (2.5:2.5:95) for 5 h. The reaction mixture was concentrated with N₂ and precipitated with cold Et₂O. The precipitate was dissolved in 10% CH₃CN in H₂O, and it was reduced with DTT (10 mM) for 1 h with stirring at 37 °C. Pure deprotected product was isolated as a white solid by reversed-phase C₁₈ HPLC (1 cm × 30 cm, 5 μ) by using 0.1% TFA/H₂O and a linear gradient of CH₃CN. ESI mass spectrum: Calcd (MH⁺) 420.12, Found 420.16.

NB-Glu(OtBu)Cys(Trt)Asp(OtBu)-OMe, **9**.¹⁶⁵ H-Glu(OtBu)Cys(Trt)Asp(OtBu)-OMe (0.22 mmol, 163 mg), 5-norbornene-exo-carboxylic acid (0.24 mmol, 34 mg), TBTU (0.24 mmol, 78 mg), and HOBt·hydrate (0.08 mmol, 13 mg) were dissolved in 2 mL dry CH₂Cl₂. DIEA (0.24 mmol, 43 μL) was added to the mixture, and the reaction was stirred for 1 h at rt. The usual workup and chromatography (acetone:CH₂Cl₂/1:20) yielded **9** (144 mg, 76%) as a white powder. ¹H-NMR (400 MHz) δ 7.41 (m, 6H) 7.29 (m, 6H), 7.21 (m, 3H), 6.94 (d, $J= 8.4$ Hz, 1H), 6.73 (m, 1H), 6.67 (m, 1H), 6.11 (m, 1H), 6.02 (m, 1H), 4.72 (m, 1H), 4.29 (m, 1H), 4.04 (m, 1H), 3.67 (s, 3H), 2.92 (m, 1H), 2.83 (m, 3H), 2.70 (m, 1H), 2.48 (m, 2H), 2.29 (m, 1H), 2.02 (m, 2H), 1.88 (m, 4H), 1.64 (d, $J= 7.2$ Hz, 1H), 1.44 (d, $J= 5.6$ Hz, 9H), 1.41 (s, 9H), 1.27 (m, 2H).; ¹³C-NMR (400

MHz) δ 27.15, 27.21, 28.23, 28.28, 30.72, 30.77, 32.19, 32.24, 33.70, 33.77, 37.48, 41.78, 41.81, 44.77, 46.57, 46.63, 47.24, 47.39, 49.10, 52.39, 52.44, 52.69, 53.54, 53.64, 67.40, 81.43, 81.76, 127.11, 128.28, 128.29, 129.79, 136.08, 136.24, 138.34, 138.47, 144.58, 169.67, 169.94, 171.05, 171.36, 171.37, 173.68, 173.69, 176.58.

Cbz-Ser(tBu)Ala-OMe, 11.¹⁶⁵ H-Ala-OMe·HCl (27.20 mmol, 3.80 g), Cbz-Ser(tBu)-OH (29.91 mmol, 8.84 g), EDC·HCl (32.64 mmol, 6.26 g), and HOBt·hydrate (32.64 mmol, 5.00 g) were dissolved in 25 mL dry CH₂Cl₂ and were cooled to 0 °C. DIEA (29.91 mmol, 5.30 mL) was added to the mixture, and the reaction was stirred for 12 h at rt. The usual workup and chromatography (acetone:CH₂Cl₂/1:20) yielded Cbz-Ser(tBu)Ala-OMe (7.81 g, 76%) as a white powder. ¹H-NMR (400 MHz) δ 7.34 (m, 5H), 5.73 (m, 1H), 5.12 (m, 2H), 4.57 (m, 1H), 4.23 (m, 1H), 3.81 (m, 1H), 3.74 (s, 3H), 3.38 (t, J = 8.4 Hz, 1H), 1.40 (d, J = 7.2 Hz, 3H), 1.21 (s, 9H).

Cbz-Glu(OtBu)Ser(tBu)Ala-OMe, 12.¹⁶⁵ Cbz-Ser(tBu)Ala-OMe (1.62 mmol, 616 mg) was dissolved in 3 mL CH₃OH. 10% Pd/C (0.16 mmol, 17 mg) was added, and the reaction was stirred for 3 h at rt under H₂. After filtration of the catalyst with celite, the resulting amine product was used without further purification. H-Ser(tBu)Ala-OMe (1.62 mmol, 400 mg), Cbz-Glu(OtBu)-OH (1.79 mmol, 604 mg), TBTU (1.34 mmol, 430 mg), and HOBt·hydrate (0.45 mmol, 69 mg) were dissolved in 3 mL dry CH₂Cl₂. DIEA (2.60 mmol, 460 μ L) was added to the mixture, and the reaction was stirred for 12 h at rt. The usual workup and chromatography (acetone:CH₂Cl₂/1:20) yielded Cbz-Glu(OtBu)Ser(tBu)Ala-OMe (627 mg, 68%) as a white powder. ¹H-NMR (400 MHz) δ 7.33 (m, 6H) 7.01 (d, J = 6.8, 1H), 5.72 (d, J = 6.4 Hz, 1H), 5.10 (m, 2H), 4.56 (q, 1H),

4.43 (m, 1H), 4.23 (m, 1H), 3.81 (m, 1H), 3.73 (s, 3H), 3.36 (t, $J=7.6$ Hz, 1H), 2.38 (m, 2H), 2.12 (m, 1H), 1.95 (m, 1H), 1.43 (s, 9H), 1.39 (d, $J=7.2$ Hz, 3H), 1.21 (s, 9H).

***NB-Glu(OtBu)Ser(tBu)Ala-OMe*, 13.**¹⁶⁵ Cbz-Glu(OtBu)Ser(tBu)Ala-OMe (0.53 mmol, 300 mg) was dissolved in 3 mL CH₃OH. 10% Pd/C (0.053 mmol, 6 mg) was added, and the reaction was stirred for 2 h at rt under H₂. After filtration of the catalyst with celite, the resulting amine product was used without further purification. H-Glu(OtBu)Ser(tBu)Ala-OMe (0.51 mmol, 220 g), 5-norbornene-exo-carboxylic acid (0.56 mmol, 78 mg), TBTU (0.56 mmol, 180 mg), and HOBt·hydrate (0.19 mmol, 29 mg) were dissolved in 3 mL dry CH₂Cl₂. DIEA (0.61 mmol, 108 μ L) was added to the mixture, and the reaction was stirred for 3 h at rt. The usual workup and chromatography (acetone:CH₂Cl₂/2:10) yielded NB-Glu(OtBu)Ser(tBu)Ala-OMe (226 mg, 74%) as a white powder. ¹H-NMR (400 MHz) δ 7.38 (t, $J=8.0$ Hz, 1H) 7.02 (t, $J=7.4$ Hz, 1H), 6.82 (d, $J=5.6$ Hz, 1H), 6.12 (m, 2H), 4.56 (q, 1H), 4.44 (m, 1H), 4.38 (m, 1H), 3.86 (m, 1H), 3.73 (s, 3H), 3.37 (m, 1H), 2.96 (m, 1H), 2.91 (m, 1H), 2.47 (m, 1H), 2.37 (m, 1H), 2.13 (m, 1H), 2.07 (m, 1H), 2.00 (m, 1H), 1.90 (m, 1H), 1.65 (m, 1H), 1.45 (d, $J=4.0$ Hz, 9H), 1.41 (dd, $J=7.2$ and 0.8 Hz, 3H), 1.35 (m, 2H), 1.19 (d, $J=4.8$ Hz, 9H).; ¹³C-NMR (400 MHz) δ 18.30, 27.47, 27.52, 28.23, 30.62, 30.79, 32.25, 41.74, 41.76, 44.62, 44.67, 46.51, 46.57, 47.22, 47.37, 48.38, 48.41, 52.45, 52.47, 53.24, 53.87, 53.89, 61.48, 74.13, 74.18, 81.32, 81.33, 136.12, 138.40, 169.86, 169.88, 171.35, 171.38, 173.07, 173.62, 176.54, 176.55.

***Fmoc-Gln(Trt)Cys(Trt)Asp(OtBu)-OMe*, 14.**²⁶⁸ Fmoc-Cys(Trt)Asp(OtBu)-OMe, (5.19 mmol, 4.00 g) was dissolved in 10 mL dry CH₂Cl₂. 1-Octanethiol (51.9 mmol, 9.04 mL) and DBU (0.52 mmol, 78 μ L) were added, and the reaction was stirred for 15 h at rt

under Ar. After evaporation of the solvent, the resulting product was purified by flash chromatography eluting with a step gradient ranging from 2% to 50% EtOAc/CH₂Cl₂. H-Cys(Trt)Asp(OtBu)-OMe (2.09 g, 73%) was obtained as a fine white powder. H-Cys(Trt)Asp(OtBu)-OMe, (3.47 mmol, 1.90 g), Fmoc-Gln(Trt)-OH (3.82 mmol, 2.33 g), EDC·HCl (4.16 mmol, 0.79 g), and HOBt·hydrate (4.16 mmol, 0.64 g) were dissolved in 13 mL dry CH₂Cl₂ and cooled to 0 °C. DIEA (3.82 mmol, 0.49 mL) was added to the mixture, and the reaction was stirred for 5 h at rt under Ar. The usual workup and chromatography (acetone: CH₂Cl₂/1:20) yielded Fmoc-Gln(Trt)Cys(Trt)Asp(OtBu)-OMe (3.44 g, 87%) as a white powder. ¹H-NMR (400 MHz, CDCl₃) δ 7.75 (d, *J*= 7.6 Hz, 2H) 7.55 (d, *J*= 8.0 Hz, 2H), 7.38 (m, 8H), 7.21 (m, 26H), 6.87 (d, *J*= 8.0 Hz, 1H), 6.61(d, *J*= 6.8 Hz, 1H), 5.91 (d, *J*= 5.6 Hz, 1H), 4.62 (m, 1H), 4.33 (d, *J*= 7.6 Hz, 2H), 4.16 (t, d = 7.2, 1H), 4.00 (m, 1H), 3.93 (m, 1H), 3.60 (s, 3H), 2.70 (m, 2H), 2.57 (m, 2H), 2.45 (m, 1H), 2.40 (m, 1H), 2.02 (m, 1H), 1.92 (m, 1H), 1.38 (s, 9H).

Ac-Gln(Trt)Cys(Trt)Asp(OtBu)-OMe, **16**. Fmoc-Cys(Trt)Asp(OtBu)-OMe, (5.19 mmol, 4.00 g) was dissolved in 10 mL dry CH₂Cl₂. 1-Octanethiol (51.9 mmol, 9.04 mL), and DBU (0.52 mmol, 78 μL) were added, and stirred for 15 h at rt under Ar. After evaporation of the solvent, the resulting product was purified by flash chromatography eluting with a step gradient ranging from 2% to 50% EtOAc/CH₂Cl₂. H-Cys(Trt)Asp(OtBu)-OMe (2.09 g, 73%) was obtained as a fine white powder. H-Cys(Trt)Asp(OtBu)-OMe, (0.64 mmol, 0.35 g), Ac-Gln(Trt)-OH (0.70 mmol, 0.30 g), EDC·HCl (0.77 mmol, 0.15 g), and HOBt·hydrate (0.77 mmol, 0.10 g) were dissolved in 3 mL of dry CH₂Cl₂ and cooled to 0 °C. DIEA (0.77 mmol, 0.14 mL) was added to the mixture, and the reaction was stirred for 2 h at rt under argon. The usual workup and

chromatography (acetone:CH₂Cl₂/1:20) yielded Ac-Gln(Trt)Cys(Trt)Asp(OtBu)-OMe (403 mg, 66%) as a white powder. ESI mass spectrum: calcd (MNa⁺) 983.41, found 983.54.

***NB-Gln(Trt)Cys(Trt)Asp(OtBu)-OMe*, 18.**²⁶⁸ H-Gln(Trt)Cys(Trt)Asp(OtBu)-OMe (0.33 mmol, 300 mg), 5-norbornene-*exo*-carboxylic acid (0.36 mmol, 50 mg), EDC (0.40 mmol, 76 mg), and HOBt·hydrate (0.40 mmol, 61 mg) were dissolved in 2 mL dry CH₂Cl₂. DIEA (0.40 mmol, 70 μL) was added to the mixture, and the reaction was stirred for 1 h at rt under Ar. The usual workup and chromatography (acetone:CH₂Cl₂/1:20) yielded NB-Gln(Trt)Cys(Trt)Asp(OtBu)-OMe (220 mg, 64%) as a white powder. ¹H-NMR (400 MHz) δ 7.41 (m, 6H) 7.29 (m, 6H), 7.21 (m, 3H), 6.94 (d, *J*= 8.4 Hz, 1H), 6.73 (m, 1H), 6.67 (m, 1H), 6.11 (m, 1H), 6.02 (m, 1H), 4.72 (m, 1H), 4.29 (m, 1H), 4.04 (m, 1H), 3.67 (s, 3H), 2.92 (m, 1H), 2.83 (m, 3H), 2.70 (m, 1H), 2.48 (m, 2H), 2.29 (m, 1H), 2.02 (m, 2H), 1.88 (m, 4H), 1.64 (d, *J*= 7.2 Hz, 1H), 1.44 (d, *J*= 5.6 Hz, 9H), 1.41 (s, 9H), 1.27 (m, 2H); ¹³C-NMR (400 MHz) δ 26.92, 27.31, 28.24, 28.28, 30.61, 30.88, 33.72, 37.50, 41.79, 44.42, 46.51, 46.71, 46.96, 47.53, 49.22, 52.49, 52.59, 52.61, 54.21, 54.52, 67.39, 67.42, 70.90, 81.60, 127.12, 127.27, 128.16, 128.31, 128.94, 129.78, 136.24, 136.39, 138.06, 138.21, 144.55, 144.69, 144.72, 169.71, 169.87, 171.14, 171.43, 172.73, 172.82, 177.03, 177.14.

***Cbz-Ser(tBu)Asp(OtBu)-OMe*, 19.** H-Asp(OtBu)-OMe·HCl (4.17 mmol, 1.0 g), Cbz-Ser(tBu)-OH (4.59 mmol, 1.36 g), EDC·HCl (5.00 mmol, 959 mg), and HOBt·hydrate (5.00 mmol, 766 mg) were dissolved in 10 mL dry CH₂Cl₂ and were cooled to 0 °C. DIEA (5.00 mmol, 885 μL) was added to the mixture, and the reaction was stirred for 4 h at rt. The usual workup and chromatography (acetone:CH₂Cl₂/1:20)

yielded Cbz-Ser(tBu)Asp(OtBu)-OMe (1.87 g, 90%) as a white powder. ¹H-NMR (500 MHz) δ 7.72 (d, J= 5.9 Hz, 1H), 7.35 (m, 5H), 5.75 (d, J= 3.5 Hz, 1H), 5.14 (m, 2H), 4.83 (m, 1H), 4.27 (m, 1H), 3.83 (m, 1H), 3.76 (s, 3H), 3.44 (t, d= 8.3 Hz, 1H), 2.94 (dd, J= 16.8, 4.4 Hz, 1H), 2.73 (dd, J= 17.0, 4.0 Hz, 1H), 1.44 (s, 9H), 1.24 (s, 9H).

Cbz-AlaSer(tBu)Asp(OtBu)-OMe, 20. Cbz-Ser(tBu)Asp(OtBu)-OMe (3.73 mmol, 1.79 g) was dissolved in 8 mL CH₃OH. 10% Pd/C (0.75 mmol, 80 mg) was added, and the reaction was stirred for 1 h at rt under H₂. After filtration of the catalyst with celite, the resulting amine product was used without further purification. H-Ser(tBu)Asp(OtBu)-OMe (3.73 mmol, 1.29 g), Cbz-Ala-OH (4.10 mmol, 915 mg), EDC·HCl (4.48 mmol, 859 mg), and HOBt·hydrate (4.48 mmol, 686 mg) were dissolved in 10 mL dry CH₂Cl₂. DIEA (4.48 mmol, 579 μL) was added to the mixture, and the reaction was stirred for 5 h at rt. The usual workup and chromatography (CH₃OH:CH₂Cl₂/1:50) yielded Cbz-AlaSer(tBu)Asp(OtBu)-OMe (1.51 g, 74%) as a white powder. ¹H-NMR (500 MHz) δ 7.74 (d, J= 7.8 Hz, 1H), 7.34 (m, 5H), 6.82 (d, J= 4.6 Hz, 1H), 5.39 (d, H= 3.7 Hz, 1H), 5.13 (q, J=12.2 Hz, 2H), 4.83 (m, 1H), 4.43 (m, 1H), 4.30 (m, 1H), 3.81 (m, 1H), 3.76 (s, 3H), 3.38 (m, 1H), 2.93 (dd, J= 16.8, 4.6 Hz, 1H), 2.73 (dd, J= 16.8, 4.7 Hz, 1H), 1.44 (m, 12H), 1.25 (s, 9H).

NB-AlaSer(tBu)Asp(OtBu)-OMe, 21. Cbz-AlaSer(tBu)Asp(OtBu)-OMe (2.72 mmol, 1.5 g) was dissolved in 8 mL CH₃OH. 10% Pd/C (0.54 mmol, 60 mg) was added, and the reaction was stirred for 2 h at rt under H₂. After filtration of the catalyst with celite, the resulting amine product was used without further purification. H-AlaSer(tBu)Asp(OtBu)-OMe (2.72 mmol), 5-norbornene-exo-carboxylic acid (2.99 mmol, 413 mg), EDC·HCl (3.26 mmol, 625 mg), and HOBt·hydrate (3.26 mmol, 450 mg)

were dissolved in 12 mL dry CH₂Cl₂. DIEA (3.26 mmol, 578 μL) was added to the mixture, and the reaction was stirred for 5 h at rt. The usual workup and chromatography (acetone:CH₂Cl₂/1:11) yielded NB-AlaSer(tBu)Asp(OtBu)-OMe (1.29 g, 88%) as a white powder. ¹H NMR (500 MHz) δ 7.70 (d, *J*= 8.0, 1H), 6.82 (t, *J*= 7.1, 1H), 6.21 (d, *J*= 6.2, 1H), 6.15 (d, *J*= 2.8, 1H), 6.11 (m, 1H), 4.82 (m, 1H), 4.53 (dt, *J*= 12.9, 6.4, 1H), 4.44 (ddd, *J*= 10.8, 6.9, 3.5, 1H), 3.81 (dd, *J*= 8.6, 4.5, 1H), 3.75 (s, 3H), 3.40 (td, *J*= 8.3, 3.2, 1H), 2.93 (m, 3H), 2.73 (dd, *J*= 16.8, 4.8, 1H), 2.06 (dd, *J*= 7.2, 3.2, 1H), 1.92 (ddd, *J*= 11.1, 7.4, 3.4, 1H), 1.70 (d, *J*= 8.3, 1H), 1.44 (m, 12H), 1.35 (m, 2H), 1.24 (s, 9H).

NB-NHS, 22. *N*-hydroxysuccinimide (4.0 mmol, 463 mg), 5-norbornene-exo-carboxylic acid (4.0 mmol, 552 mg), and EDC·HCl (3.62 mmol, 694 mg) were dissolved in 5 mL dry CH₂Cl₂. DIEA (4.0 mmol, 709 μL) was added to the mixture, and the reaction was stirred for 5 h at rt. The usual workup and chromatography (acetone:CH₂Cl₂/2:10) yielded NB-NHS (672 mg, 79%) as a white powder. ¹H-NMR (500 MHz) δ 6.21 (dd, *J*= 5.5, 3.0 Hz, 1H), 3.28 (s, 1H), 3.01 (s, 1H), 2.84 (m, 4H), 2.51 (dd, *J*= 9.5, 5.0 Hz, 1H), 2.06 (dt, *J*=12.0, 4.0 Hz, 1H), 1.5 (m, 3H).

Fmoc-BpaGlu(OtBu)Cys(Trt)Asp(OtBu)-OMe, 23'. Fmoc-Glu(OtBu)Cys(Trt)-Asp(OtBu)-OMe, (3.14 mmol, 3.00 g) was dissolved in 10 mL dry CH₂Cl₂. 1-Octanethiol (31.4 mmol, 5.45 mL), and DBU (0.63 mmol, 95 μL) were added, and stirred the reaction for 15 h at rt under Ar. After evaporation of the solvent, the resulting product was purified by flash chromatography eluting with a step gradient ranging from 2% to 50% EtOAc/CH₂Cl₂. H-Glu(OtBu)Cys(Trt)Asp(OtBu)-OMe (2.2 g, impure, 96%) was obtained as a fine white powder. H-Glu(OtBu)Cys(Trt)Asp(OtBu)-OMe, (3.00 mmol, 2.2 g), Fmoc-Bpa-OH (3.3 mmol, 1.62 g), EDC·HCl (3.6 mmol, 0.69 g), and

HOBt-hydrate (3.6 mmol, 0.55 g) were dissolved in 10 mL dry CH₂Cl₂ and cooled to 0 °C. DIEA (3.6 mmol, 0.64 mL) was added to the mixture, and the reaction was stirred for 16 h at rt. The usual workup and chromatography (acetone:CH₂Cl₂/1:20) yielded Fmoc-BpaGlu(OtBu)Cys(Trt)Asp(OtBu)-OMe (1.3 g, 30%) as a white powder. ¹H-NMR (400 MHz) δ 7.73 (m, 6H) 7.56 (d, *J*= 7.2 Hz, 3H), 7.47-7.35 (m, 11H), 7.29-7.16 (m, 12H), 6.94 (d, NH), 6.85 (br d, NH), 6.29(br s, NH), 5.59 (br s, NH), 4.74 (m, 1H), 4.63 (m, 1H), 4.30 (m, 3H), 4.13 (m, 2H), 3.66 (s, 3H), 3.39 (br s, 2H), 3.20 (dd, *J*= 14.0 and 5.6 Hz, 1H), 3.06 (dd, *J*= 14.0 and 8.4 Hz, 1H), 2.82 (m, 2H), 2.71 (dd, *J*= 16.4 and 5.2 Hz, 1H), 2.60 (dd, *J*= 13.2 and 5.2 Hz, 1H), 2.39 (m, 3H), 2.27 (m, 1H), 1.98 (m, 1H), 1.90 (m, 1H), 1.40 (s, 9H), 1.39 (s, 9H).

Fmoc-BpaGln(Trt)Cys(Trt)Asp(OtBu)-OMe, 24'. H-Gln(Trt)Cys(Trt)Asp(OtBu)-OMe, (0.91 mmol, 900 mg), Fmoc-Bpa-OH (1.0 mmol, 492 mg), EDC·HCl (1.09 mmol, 209 mg), and HOBt-hydrate (1.09 mmol, 147 mg) were dissolved in 7 mL dry CH₂Cl₂ and cooled to 0 °C. DIEA (1.09 mmol, 193 μL) was added to the mixture, and the reaction was stirred for 16 h at rt. The usual workup and chromatography (acetone:CH₂Cl₂/1:10) yielded Fmoc-BpaGln(Trt)Cys(Trt)Asp(OtBu)-OMe (800 mg, 63%) as a white powder. ¹H NMR (500 MHz) δ 7.87 (d, *J*= 3.8 Hz, 1H), 7.74 (m, 7H), 7.59 (t, *J*= 7.4, 1H), 7.48 (dt, *J*= 21.9, 7.6, 5H), 7.38 (d, *J*= 7.6, 9H), 7.32 (dd, *J*= 7.2, 4.9, 2H), 7.22 (m, 37H), 7.00 (s, 1H), 6.95 (d, *J*= 8.1, 1H), 6.74 (d, *J*= 7.7, 1H), 5.37 (s, 1H), 4.70 (s, 1H), 4.36 (s, 2H), 4.19 (s, 2H), 4.12 (d, *J*= 7.0, 1H), 4.05 (s, 1H), 3.64 (s, 3H), 3.13 (s, 1H), 2.91 (s, 1H), 2.78 (dd, *J*= 16.4, 5.9, 2H), 2.70 (s, 1H), 2.59 (s, 2H), 2.45 (s, 1H), 2.03 (m, 2H), 1.39 (m, 9H).

Fmoc-BpaGlu(OtBu)Ser(tBu)Ala-OMe, 25'. H-Glu(OtBu)Ser(tBu)Ala-OMe, (1.45 mmol, 625 mg), Fmoc-Bpa-OH (1.60 mmol, 786 mg), EDC·HCl (1.74 mmol, 334 mg), and HOBt-hydrate (1.74 mmol, 235 mg) were dissolved in 10 mL dry CH₂Cl₂ and cooled to 0 °C. DIEA (1.74 mmol, 308 μL) was added to the mixture, and the reaction was stirred for 16 h at rt. The usual workup and chromatography (acetone:CH₂Cl₂/1:10) yielded Fmoc-BpaGlu(OtBu)Ser(tBu)Ala-OMe (1.1 g, 84%) as a white powder. ¹H NMR (500 MHz) δ 7.76 (m, 6H), 7.58 (m, 3H), 7.47 (t, *J*= 7.6, 2H), 7.39 (dd, *J*= 17.2, 9.7, 3H), 7.31 (m, 1H), 7.15 (m, 1H), 7.09 (d, *J*= 5.8, 1H), 5.36 (d, *J*= 5.4, 1H), 4.58 (m, 2H), 4.47 (d, *J*= 20.5, 3H), 4.35 (m, 1H), 4.20 (t, *J*= 6.7, 1H), 3.77 (m, 1H), 3.75 (s, 3H), 3.42 (m, 1H), 3.20 (m, 2H), 2.43 (m, 1H), 2.35 (m, 1H), 2.10 (m, 1H), 1.95 (m, 1H), 1.42 (m, 12H), 1.21 (s, 9H).

Cbz-Lys(Boc)Gly-OMe, 26. H-Gly-OMe·HCl (3.18 mmol, 400 mg), Cbz-Lys(Boc)-OH (3.5 mmol, 1.332 g), EDC·HCl (3.82 mmol, 732 mg), and HOBT (3.82 mmol, 516 mg) were dissolved in 17 mL dry CH₂Cl₂. DIEA (3.82 mmol, 676 μL) was added to the mixture, and the reaction was stirred for 16 h at rt. The usual workup and chromatography (acetone:CH₂Cl₂/7:100) yielded Cbz-Lys(Boc)Gly-OMe (1.37 g, 95%) as a white powder. ¹H NMR (500 MHz) δ 7.35 (s, 5H), 6.75 (br s, 1H), 5.59 (br s, 1H), 5.11 (s, 2H), 4.69 (br s, 1H), 4.22 (br s, 1H), 4.02 (m, 2H), 3.75 (s, 3H), 3.10 (br s, 2H), 1.87 (m, 1H), 1.70 (m, 1H), 1.49 (m, 3H), 1.43 (m, 12H).

Cbz-GlyLys(Boc)Gly-OMe, 28. Cbz-Lys(Boc)Gly-OMe (2.33 mmol, 1.05 g) was dissolved in 8 mL CH₂Cl₂/CH₃OH (1:1). 10% Pd/C (0.47 mmol, 49 mg) was added, and the reaction was stirred for 1 h at rt under H₂. After filtration of the catalyst with celite, the resulting amine product was used without further purification. H-Lys(Boc)Gly-OMe

(0.78 mmol, 248 mg), Cbz-Gly-OH (0.86 mmol, 180 mg), EDC·HCl (0.94 mmol, 180 mg), and HOBt·hydrate (0.94 mmol, 127 mg) were dissolved in 5 mL dry CH₂Cl₂. DIEA (0.94 mmol, 122 μL) was added to the mixture, and the reaction was stirred for 16 h at rt. The usual workup and chromatography (acetone:CH₂Cl₂/2:10) yielded Cbz-GlyLys(Boc)Gly-OMe (380 mg, 89%) as a white powder. ¹H NMR (500 MHz) δ 7.34 (m, 5H), 7.09 (br s, 1H), 6.94 (br s, 1H), 5.76 (br s, 1H), 5.13 (s, 2H), 4.81 (br s, 1H), 4.53 (m, 1H), 4.00 (d, *J*= 4.8, 2H), 3.90 (d, *J*= 4.6, 2H), 3.74 (s, 3H), 3.09 (m, 2H), 1.88 (m, 2H), 1.68 (m, 1H), 1.48 (m, 1H), 1.44 (s, 9H), 1.37 (m, 2H).

NB-Lys(Boc)Gly-OMe, 30. Cbz-Lys(Boc)Gly-OMe (2.33 mmol, 1.05 g) was dissolved in 8 mL CH₂Cl₂/CH₃OH (1:1). 10% Pd/C (0.47 mmol, 49 mg) was added, and the reaction was stirred for 1 h at rt under H₂. After filtration of the catalyst with celite, the resulting amine product was used without further purification. H-Lys(Boc)Gly-OMe (94.5 μmol, 30 mg), 5-norbornene-exo-carboxylic acid (104 μmol, 14 mg), EDC·HCl (113.4 μmol, 22 mg), and HOBt·hydrate (113.4 μmol, 15 mg) were dissolved in 1 mL dry CH₂Cl₂. DIEA (113.4 μmol, 20 μL) was added to the mixture, and the reaction was stirred for 16 h at rt. The usual workup yielded NB-Lys(Boc)Gly-OMe as a white powder. ESI mass spectrum: calcd (MH⁺) 337.2, found 338.3.

NB-Lys(Boc)Ala-OMe, 31. Cbz-Lys(Boc)Ala-OMe (2.26 mmol, 1.05 g) was dissolved in 10 mL CH₂Cl₂/CH₃OH (1:1). 10% Pd/C (0.45 mmol, 48 mg) was added, and the reaction was stirred for 2 h at rt under H₂. After filtration of the catalyst with celite, the resulting amine product was used without further purification. H-Lys(Boc)Gly-OMe (90.5 μmol, 30 mg), 5-norbornene-exo-carboxylic acid (99.6 μmol, 14 mg), EDC·HCl (108.6 μmol, 21 mg), and HOBt·hydrate (108.6 μmol, 15 mg) were dissolved in 1 mL

dry CH₂Cl₂. DIEA (108.6 μmol, 19 μL) was added to the mixture, and the reaction was stirred for 16 h at rt. The usual workup yielded NB-Lys(Boc)Ala-OMe as a white powder. ESI mass spectrum: calcd (MH⁺) 351.2, found 352.3.

NB-GlyLys(Boc)Gly-OMe, 32. Cbz-GlyLys(Boc)Gly-OMe (98.3 μmol, 50 mg) was dissolved in 2 mL CH₂Cl₂/CH₃OH (1:1). 10% Pd/C (19.7 μmol, 2 mg) was added, and the reaction was stirred for 3 h at rt under H₂. After filtration of the catalyst with celite, the resulting amine product was used without further purification. H-GlyLys(Boc)Gly-OMe (98.3 μmol), 5-norbornene-exo-carboxylic acid (108.2 μmol, 15 mg), EDC·HCl (118 μmol, 23 mg), and HOBt-hydrate (118 μmol, 16 mg) were dissolved in 1 mL dry CH₂Cl₂. DIEA (118 μmol, 21 μL) was added to the mixture, and the reaction was stirred for 16 h at rt. The usual workup and chromatography (acetone:CH₂Cl₂/1:10) yielded NB-GlyLys(Boc)Gly-OMe as a white powder. ¹H NMR (500 MHz) δ 7.47 (d, *J*= 6.0, 1H), 7.37 (t, *J*= 8.3, 1H), 6.99 (br s, 1H), 6.13 (m, 1H), 6.13 (m, 1H), 4.91 (br s, 1H), 4.57 (m, 1H), 4.00 (m, 3H), 3.73 (s, 3H), 3.09 (br s, 2H), 2.92 (d, *J*= 15.5, 2H), 2.15 (m, 1H), 1.88 (m, 2H), 1.68 (m, 2H), 1.49 (m, 2H), 1.43 (s, 9H), 1.34 (m, 4H).; ESI mass spectrum: calcd (MH⁺) 494.30, found 495.3.

NB-GlyLys(Boc)Ala-OMe, 33. Cbz-GlyLys(Boc)Ala-OMe (95.7 μmol, 50 mg) was dissolved in 3 mL CH₂Cl₂/CH₃OH (1:1). 10% Pd/C (19 μmol, 2 mg) was added, and the reaction was stirred for 3 h at rt under H₂. After filtration of the catalyst with celite, the resulting amine product was used without further purification. H-GlyLys(Boc)Gly-OMe (95.7 μmol), 5-norbornene-exo-carboxylic acid (105.3 μmol, 14 mg), EDC·HCl (115 μmol, 22 mg), and HOBt-hydrate (115 μmol, 16 mg) were dissolved in 1 mL dry CH₂Cl₂. DIEA (115 μmol, 20 μL) was added to the mixture, and the reaction was stirred

for 16 h at rt. The usual workup yielded NB-GlyLys(Boc)Ala-OMe as a white powder. ESI mass spectrum: calcd (MH⁺) 408.2, found 409.3.

NB-LysGly-OMe, **34**. NB-Lys(Boc)Gly-OMe (45.7 μmol, 20 mg) was deprotected in 50% TFA/CH₂Cl₂ for 5 h. The reaction mixture was concentrated with N₂ and precipitated with cold Et₂O. The precipitate was dissolved in 10% CH₃CN in H₂O, and pure deprotected product was isolated as a white solid by reversed-phase C₁₈ HPLC. ESI mass spectrum: calcd (MH⁺) 337.20, found 338.2.

NB-LysAla-OMe, **35**. NB-Lys(Boc)Ala-OMe (44.3 μmol, 20 mg) was deprotected in 50% TFA/CH₂Cl₂ for 5 h. The reaction mixture was concentrated with N₂ and precipitated with cold Et₂O. The precipitate was dissolved in 10% CH₃CN in H₂O, and pure deprotected product was isolated as a white solid by reversed-phase C₁₈ HPLC. ESI mass spectrum: calcd (MH⁺) 351.22, found 352.2.

NB-GlyLysGly-OMe, **36**. NB-GlyLys(Boc)Gly-OMe (40.4 μmol, 20 mg) was deprotected in 50% TFA/CH₂Cl₂ for 5 h. The reaction mixture was concentrated with N₂ and precipitated with cold Et₂O. The precipitate was dissolved in 10% CH₃CN in H₂O, and pure deprotected product was isolated as a white solid by reversed-phase C₁₈ HPLC. ESI mass spectrum: calcd (MH⁺) 394.22, found 395.2.

NB-GlyLysAla-OMe, **37**. NB-GlyLys(Boc)Ala-OMe (39.4 μmol, 20 mg) was deprotected in 50% TFA/CH₂Cl₂ for 5 h. The reaction mixture was concentrated with N₂ and precipitated with cold Et₂O. The precipitate was dissolved in 10% CH₃CN in H₂O, and pure deprotected product was isolated as a white solid by reversed-phase C₁₈ HPLC. ESI mass spectrum: calcd (MH⁺) 408.24, found 409.2.

***NB-GlyLys(Boc)Gly-Bpa-Glu(OtBu)Cys(Trt)Asp(OtBu)-OMe*, 38.** NB-GlyLys(Boc)Gly-OMe (0.81 mmol, 570 mg) was dissolved in 25 mL CH₃OH. NaOH (8.09 mmol, 323 mg) dissolved in 25 mL H₂O was added to the reaction mixture at 0 °C, and the reaction was stirred for 2 h at rt. 10 N HCl was added to the reaction at 0 °C. After extraction with CH₂Cl₂, the resulting acid product (410 mg, 98%) was used without further purification. ESI mass spectrum: calcd (MH⁺) 480.22, found 481.2. H-Bpa-Glu(OtBu)Cys(Trt)Asp(OtBu)-OMe (0.18 mmol, 180 mg), NB-GlyLys(Boc)Gly-OH (0.22 mmol, 106 mg), EDC·HCl (0.22 mmol, 42 mg), and HOBt·hydrate (0.22 mmol, 30 mg) were dissolved in 5 mL dry CH₂Cl₂. DIEA (0.22 mmol, 39 μL) was added to the mixture, and the reaction was stirred for 16 h at rt. The usual workup and chromatography (CH₃OH:CH₃Cl/1:10) yielded NB-GlyLys(Boc)Gly-Bpa-Glu(OtBu)-Cys(Trt)Asp(OtBu)-OMe as a white powder. ESI mass spectrum: calcd (MH⁺) 1446.68, found 1447.7.

***NB-GlyLys(Boc)Gly-Bpa-Gln(Trt)Cys(Trt)Asp(OtBu)-OMe*, 39.** H-Bpa-Gln(Trt)Cys(Trt)Asp(OtBu)-OMe (0.182 mmol, 140 mg), NB-GlyLys(Boc)Gly-OH (0.14 mmol, 69 mg), EDC·HCl (0.14 mmol, 28 mg), and HOBt·hydrate (0.14 mmol, 20 mg) were dissolved in 5 mL dry CH₂Cl₂. DIEA (0.14 mmol, 26 μL) was added to the mixture, and the reaction was stirred for 16 h at rt. The usual workup and chromatography (CH₃OH:CH₃Cl/1:10) yielded NB-GlyLys(Boc)Gly-Bpa-Gln(Trt)Cys(Trt)Asp(OtBu)-OMe as a white powder.

***NB-GlyLys(Boc)Gly-Bpa-Glu(OtBu)Ser(tBu)Ala-OMe*, 40.** H-Bpa-Glu(OtBu)-Ser(tBu)Ala-OMe (0.19 mmol, 130 mg), NB-GlyLys(Boc)Gly-OH (0.23 mmol, 111 mg), EDC·HCl (0.23 mmol, 44 mg), and HOBt·hydrate (0.23 mmol, 31 mg) were dissolved in

5 mL dry CH₂Cl₂. DIEA (0.23 mmol, 41 μL) was added to the mixture, and the reaction was stirred for 16 h at rt. The usual workup and chromatography (CH₃OH:CH₂Cl₂/1:10) yielded NB-GlyLys(Boc)Gly-Bpa-Glu(OtBu)Ser(tBu)Ala-OMe as a white powder. ESI mass spectrum: calcd (MH⁺) 1144.61, found 1145.6.

Biotin-NHS, 42. *N*-hydroxysuccinimide (1.02 μmol, 117 mg), biotin (1.02 μmol, 250 mg) and DCC (1.02 μmol, 211 mg) were dissolved in 7 mL dry DMF, and the reaction was stirred for 16 h at rt. After filtration and evaporation of solvent, the product was precipitated with Et₂O, and was washed with a mixture of cold Et₂O/2-propanol (1:1). The precipitation yielded biotin-NHS (230 mg, 66%). ESI mass spectrum: calcd (MH⁺) 341.1, found 342.1.

Biotin-PEG₁₀-N₃, 43. Biotin-NHS (0.31 mmol, 107 mg) and *O*-(2-Aminoethyl)-*O'*-(2-azidoethyl)nonaethylene glycol (0.21 mmol, 110 mg) were dissolved in 1 mL dry DMF. DIEA (0.31 mmol, 56 μL) was added to the mixture, and the reaction was stirred for 16 h at rt. and the reaction was stirred for 16 h at rt. After evaporation of solvent, the product was precipitated with Et₂O. The chromatography (CH₃OH:EtOAc/1:1) yielded Bio-PEG₁₀-N₃. ¹H NMR (500 MHz, DMSO) δ 7.81 (t, *J*= 5.5, 1H), 6.40 (br s, 1H), 6.34 (br s, 1H), 4.30 (m, 1H), 4.12 (m, 1H), 3.60 (m, 2H), 3.53 (m, 38H), 3.39 (t, *J*= 5.1, 4H), 3.18 (q, *J*= 5.8, 2H), 3.09 (dd, *J*= 11.7, 7.3, 1H), 2.82 (dd, *J*= 12.4, 5.1, 1H), 2.58 (d, *J*= 12.4, 1H), 2.06 (t, *J*= 7.4, 2H), 1.62 (dd, *J*= 21.4, 7.9, 1H), 1.50 (dt, *J*= 14.4, 7.5, 3H), 1.30 (m, 2H).; ESI mass spectrum: calcd (MH⁺) 752.4, found 753.4.

I-2. Ring opening metathesis polymerization.

ROMP. The procedure detailed below for polymer **9₁₀-[2]** is representative of the procedure followed for synthesis of all of the homopolymers and the random copolymer. Scale, yield, and spectra are presented for each of the individual polymers. The number of ligands (n) is based on the monomer:catalyst ratio used in the synthesis.

9₁₀-[2]. NB-Glu(OtBu)Cys(Trt)Asp(OtBu)-OMe **9** (117 μ mol, 100 mg) was dissolved in 1 mL CH₂Cl₂/CH₃OH (3/1). To the reaction was added oven-dried LiCl (2.4 mmol, 102 mg), (H₂IMes)(PCy₃)Cl₂Ru=CHPh (11.7 μ mol, 10 mg) dissolved in 500 μ L CH₂Cl₂/CH₃OH (3/1), and an additional 200 μ L CH₂Cl₂/CH₃OH (3/1) at 0 °C under Ar. The reaction was stirred for 1 h at rt under Ar. Ethylvinyl ether (1 mL) was added to quench the reaction, and the mixture was stirred for an additional 40 min. After removing the solvent, the residue was dissolved in CH₂Cl₂. The solution was washed three times with H₂O, dried with Na₂SO₄, concentrated by rotary evaporation, and precipitated with cold Et₂O. The product was isolated by centrifugation and dried. Crude protected polymer was deprotected with TFA/TIPS/H₂O (95/2.5/2.5) for 5 h. The reaction mixture was concentrated with N₂ and was precipitated with cold Et₂O. The precipitate was collected by centrifugation. Polymer was dissolved in H₂O (1 mL) at pH 6 and reduced with 10~20 mM tris(2-carboxyethyl)phosphine (TCEP) for 2 h at 37°C. Reduced polymer was isolated by precipitation with 1 N HCl (200 μ L). Residual TCEP was removed by repeated washing of the precipitate with H₂O (3 \times 1 mL). **9₁₀-[2]**, a yellowish-white solid, was collected (40 mg, 67%), dried, and stored at -20 °C. ¹H-NMR (500 MHz, D₂O) δ 7.32 (m) 5.39 (m), 4.56–3.93 (with max at 4.68, 4.42, 4.25), 3.66 (br s), 3.02–2.40 (with max at 2.87, 2.63, 2.48), 2.34–1.44 (with max at 2.19, 1.95, 1.83, 1.60), 1.24 (br s).

9₃'-[2]. NB-Glu(OtBu)Cys(Trt)Asp(OtBu)-OMe **9** (117 μmol, 100 mg) and (H₂IMes)(Py₃)Cl₂Ru=CHPh (39 μmol, 33 mg) in a total volume of 1.5 mL CH₂Cl₂/CH₃OH (3/1) at 25 °C yielded **9₃'-[2]** as a brownish-white solid of protected polymer (84 mg, 84%). ¹H-NMR (500 MHz, CDCl₃) δ 7.30 (m) 5.18 (m), 4.85–4.29 (with max at 4.69, 4.41), 3.63(br s), 3.21–2.51 (with max at 2.83, 2.69, 2.57), 2.42–1.70 (with max at 2.30, 1.99, 1.87), 1.41 (br s).

9₁₀'-[2]-a. NB-Glu(OtBu)Cys(Trt)Asp(OtBu)-OMe **9** (46.8 μmol, 40 mg) and (H₂IMes)(Py₃)Cl₂Ru=CHPh (4.68 μmol, 4 mg) in a total volume of 1 mL CH₂Cl₂/CH₃OH (2/1) at 55 °C yielded **9₁₀'-[2]-a** as a brownish-white solid of protected polymer (33 mg, 84%). ¹H-NMR (500 MHz, CDCl₃) δ 7.66-7.08 with max at 7.40, 7.27, 7.19) 5.14 (m), 4.84–4.22 (with max at 4.64, 4.39), 3.62 (br s), 3.20–2.46 (with max at 2.81, 2.68), 2.46–1.49 (with max at 2.25, 1.94, 1.76), 1.40 (br s).

9₁₀₀'-[2]. NB-Glu(OtBu)Cys(Trt)Asp(OtBu)-OMe **9** (58.5 μmol, 50 mg) and (H₂IMes)(Py₃)Cl₂Ru=CHPh (0.58 μmol, 0.5 mg) in a total volume of 1 mL CH₂Cl₂/CH₃OH (3/1) yielded **9₁₀₀'-[2]** as a yellowish-white solid of protected polymer (44 mg, 87%). ¹H-NMR (500 MHz, CDCl₃) δ 7.29 (m) 5.20 (m), 4.59–4.18 (with max at 4.41), 3.63 (br s), 3.18–2.48 (with max at 2.82, 2.68), 2.49–1.51 (with max at 2.25, 1.92, 1.70), 1.40 (br s).

9₃-[3]. NB-Glu(OtBu)Cys(Trt)Asp(OtBu)-OMe **9** (82 μmol, 70 mg) and (H₂IMes)(3-Br-pyr)₂Cl₂Ru=CHPh (27 μmol, 24 mg) in a total volume of 400 μL CH₂Cl₂/CH₃OH (3/1) yielded **9₃-[3]** as a brownish-white solid (30 mg, 82%). ¹H-NMR

(500 MHz, D₂O) δ 7.26 (m) 5.35 (m), 4.65–4.01 (with max at 4.55, 4.26, 4.04), 3.24 (br s), 2.90–2.29 (with max at 2.81, 2.51), 2.22–1.45 (with max at 2.12, 1.93, 1.78), 1.19 (m).

9₆-[3]. NB-Glu(OtBu)Cys(Trt)Asp(OtBu)-OMe **9** (82 μ mol, 70 mg) and (H₂IMes)(3-Br-pyr)₂Cl₂Ru=CHPh (14 μ mol, 12 mg) in a total volume of 400 μ L CH₂Cl₂/CH₃OH (3/1) yielded **9₆-[3]** as a brownish-white solid (45 mg, 95%). ¹H-NMR (500 MHz, D₂O) δ 7.26 (m) 5.45–5.10 (with max at 5.36, 5.29, 5.26), 4.65–4.05 (with max at 4.59, 4.45, 4.27), 3.64 (br s), 2.90–2.45 (with max at 2.83, 2.63), 2.22–1.45 (with max at 2.21, 1.94, 1.84, 1.61), 1.21 (m).

9₁₀-[3]. NB-Glu(OtBu)Cys(Trt)Asp(OtBu)-OMe **9** (117 μ mol, 100 mg) and (H₂IMes)(3-Br-pyr)₂Cl₂Ru=CHPh (11.7 μ mol, 1.0 mg) in a total volume of 1.5 mL CH₂Cl₂/CH₃OH (3/1) yielded a yellowish-white solid (45 mg, 78%). ¹H-NMR (500 MHz, D₂O) δ 7.31 (m) 5.36 (m), 4.63–4.04 (with max at 4.45, 4.31), 3.64 (br s), 3.09–2.36 (with max at 2.83, 2.65), 2.33–1.39 (with max at 2.22, 1.93, 1.85, 1.63), 1.20 (br s), 0.93 (br s).

9₁₀₀-[3]. NB-Glu(OtBu)Cys(Trt)Asp(OtBu)-OMe **9** (117 μ mol, 100 mg) and (H₂IMes)(3-Br-pyr)₂Cl₂Ru=CHPh (1.17 μ mol, 1.0 mg) in a total volume of 1.5 mL CH₂Cl₂/CH₃OH (3/1) yielded a yellowish-white solid (47 mg, 80%). ¹H-NMR (500 MHz, D₂O) δ 7.34 (m) 5.34 (m), 4.65–4.14 (with max at 4.64, 4.39), 3.67 (br s), 3.15–2.44 (with max at 2.86, 2.74), 2.43–1.41 (with max at 2.34, 1.99, 1.87), 1.22 (br s), 0.95 (br s).

13₁₀-[3]. NB-Glu(OtBu)Ser(tBu)Ala-OMe **13** (38 μ mol, 21 mg) and (H₂IMes)(3-Br-pyr)₂Cl₂Ru=CHPh (13.8 μ mol, 3.3 mg) in a total volume of 200 μ L CH₂Cl₂/CH₃OH (3/1) yielded **13₁₀-[3]** as a brownish-white solid (10 mg, 67%). ¹H-NMR

(500 MHz, D₂O) δ 7.29 (m) 5.36 (m), 4.56-3.96 (with max at 4.34, 4.07), 3.77 (br s), 3.65 (br s), 3.07-2.34 (with max at 2.90, 2.51), 2.36-1.50 (with max at 2.20, 1.95, 1.86, 1.62), 1.44-1.12 (with max at 1.34, 1.27).

13₁₀₀-[3]. NB-Glu(OtBu)Ser(tBu)Ala-OMe **13** (225 μ mol, 124 mg) and (H₂IMes)(3-Br-pyr)₂Cl₂Ru=CHPh (2.25 μ mol, 2.0 mg) in a total volume of 2 mL CH₂Cl₂/CH₃OH (3/1) yielded **13₁₀₀-[3]** as a brownish-white solid (89 mg, 90%). ¹H-NMR (500 MHz, D₂O) δ 7.30 (m) 5.38 (m), 4.44-3.93 (with max at 4.35, 4.07), 3.77 (br s), 3.65 (br s), 3.10-2.30 (with max at 2.91, 2.51), 2.32-1.47 (with max at 2.15, 1.93, 1.82, 1.61), 1.43-1.03 (with max at 1.34, 1.25), 0.95 (br s).

18₁-[3] and **18₂-[3]**. NB-Gln(Trt)Cys(Trt)Asp(OtBu)-OMe **18** (96.9 μ mol, 100 mg) and (H₂IMes)(3-Br-pyr)₂Cl₂Ru=CHPh (101.7 μ mol, 90 mg) in a total volume of 2 mL CH₂Cl₂/CH₃OH (3/1) yielded **18₁-[3]** and **18₂-[3]** as a brownish white solid (62 mg, 56%). And the polymer was purified by RP-HPLC with prep C₁₈ column. MALDI mass spectrum; **18₁-[3]**; calcd.: (MNa⁺) 625.23, found: 625.20; **18₂-[3]**; calcd.: (MNa⁺) 1123.41, found: 1123.59.

18₃-[3]. NB-Gln(Trt)Cys(Trt)Asp(OtBu)-OMe **18** (145.3 μ mol, 150 mg) and (H₂IMes)(3-Br-pyr)₂Cl₂Ru=CHPh (48.4 μ mol, 43 mg) in a total volume of 2 mL CH₂Cl₂/CH₃OH (3/1) yielded **18₃-[3]** as a brownish white solid (68 mg, 84%). ¹H-NMR (500 MHz, D₂O) δ 7.28 (m) 5.33 (m), 4.65-4.01 (with max at 4.18), 3.63 (br s), 3.29-2.40 (with max at 3.13, 2.59), 2.35-1.80 (with max at 2.21, 2.00), 1.21 (m), 0.93 (br s).

18₆-[3]. NB-Gln(Trt)Cys(Trt)Asp(OtBu)-OMe **18** (145.3 μ mol, 150 mg) and (H₂IMes)(3-Br-pyr)₂Cl₂Ru=CHPh (24.22 μ mol, 22 mg) in a total volume of 2 mL

CH₂Cl₂/CH₃OH (3/1) yielded **18₆-[3]** as a brownish white solid (65 mg, 81%). ¹H-NMR (500 MHz, D₂O) δ 7.28 (m) 5.36 (m, br), 4.54-4.13 (with max at 4.44, 4.33), 3.63 (br s), 3.30-2.40 (with max at 2.84, 2.65, 2.59), 2.38-1.43 (with max at 2.23, 1.98, 1.86), 1.21 (m), 0.93 (br s).

18₁₀-[3]. NB-Gln(Trt)Cys(Trt)Asp(OtBu)-OMe **18** (145.3 μmol, 150 mg) and (H₂IMes)(3-Br-pyr)₂Cl₂Ru=CHPh (14.53 μmol, 12.9 mg) in a total volume of 2 mL CH₂Cl₂/CH₃OH (3/1) yielded **18₁₀-[3]** as a brownish white solid (58.9 mg, 79%). ¹H-NMR (500 MHz, D₂O) δ 7.28 (m) 5.35 (m), 4.58-4.13 (with max at 4.47, 4.33), 3.65 (br s), 3.10-2.42 (with max at 2.85, 2.74), 2.41-1.41 (with max at 2.25, 1.99, 1.88, 1.62), 1.21 (m), 0.93 (br s).

18₁₀₀-[3]. NB-Gln(Trt)Cys(Trt)Asp(OtBu)-OMe **18** (112.7 μmol, 117 mg) and (H₂IMes)(3-Br-pyr)₂Cl₂Ru=CHPh (1.13 μmol, 1.0 mg) in a total volume of 2 mL CH₂Cl₂/CH₃OH (3/1) yielded a yellowish white solid (44.5 mg, 79%). ¹H-NMR (500 MHz, D₂O) δ 7.26 (m) 5.36 (m), 4.56-4.09 (with max at 4.48, 4.33), 3.64 (br s), 3.04-2.38 (with max at 2.85, 2.66, 2.61), 2.38-1.32 (with max at 2.24, 1.98, 1.88, 1.60), 1.21 (m), 0.93 (br s).

21₁₀-[3]. NB-AlaSer(tBu)Asp(OtBu)-OMe **21** (223 μmol, 120 mg) and (H₂IMes)(3-Br-pyr)₂Cl₂Ru=CHPh (22.3 μmol, 19.8 mg) in a total volume of 1.5 mL CH₂Cl₂/CH₃OH (3/1) yielded **21₁₀-[3]** as a brownish-white solid (63 mg, 72%). ¹H-NMR (500 MHz, D₂O) δ 7.25 (m) 5.35 (m), 4.48-4.14 (with max at 4.36, 4.30), 3.78 (br s), 3.64 (br s), 3.08-2.36 (with max at 2.87, 2.65, 2.56, 2.47), 2.31-2.14 (with max at 2.25, 2.21), 2.08-1.41 (with max at 1.88, 1.60), 1.28(m), 0.94 (br s).

22₁₀-[2]-a. NB-NHS **22** (85 μmol , 20 mg) and $(\text{H}_2\text{IMes})(\text{Py}_3)\text{Cl}_2\text{Ru}=\text{CHPh}$ (8.5 μmol , 7 mg) in a total volume of 1 mL $\text{CH}_2\text{Cl}_2/\text{CH}_3\text{OH}$ (2/1) at 25 °C yielded **22₁₀-[2]-a** as a yellowish-white solid (19 mg, 95%). $^1\text{H-NMR}$ (500 MHz, CDCl_3) δ 5.56 (br s), 5.39 (m), 5.29 (m), 3.34 (br s), 3.09 (br s), 2.81 (br s), 2.39 –1.93 (with max at 2.25, 2.03), 1.92–1.32 (with max at 1.78, 1.61), 1.17 (br s).

22₁₀-[2]-b. NB-NHS **22** (85 μmol , 20 mg) and $(\text{H}_2\text{IMes})(\text{Py}_3)\text{Cl}_2\text{Ru}=\text{CHPh}$ (8.5 μmol , 7 mg) in a total volume of 1 mL $\text{CH}_2\text{Cl}_2/\text{CH}_3\text{OH}$ (2/1) at 55 °C yielded **22₁₀-[2]-b** as a yellowish-white solid (20 mg, 99%). $^1\text{H-NMR}$ (500 MHz, CDCl_3) δ 7.33 (m) 5.56 (br s), 5.39 (m), 5.28 (m), 3.31 (br s), 3.08 (br s), 2.81 (br s), 2.48 –1.94 (with max at 2.25, 2.03), 1.92–1.50 (with max at 1.78, 1.61), 1.22 (m).

22₁₀-[3]-c. NB-NHS **22** (85 μmol , 20 mg) and $(\text{H}_2\text{IMes})(3\text{-Br-pyr})_2\text{Cl}_2\text{Ru}=\text{CHPh}$ (8.5 μmol , 7.6 mg) in a total volume of 1 mL $\text{CH}_2\text{Cl}_2/\text{CH}_3\text{OH}$ (2/1) at 25 °C yielded **22₁₀-[2]-c** as a yellowish-white solid (18 mg, 88%). $^1\text{H-NMR}$ (500 MHz, CDCl_3) δ 7.34 (m) 5.56 (br s), 5.39 (m), 5.29 (m), 3.34 (br s), 3.13 (br s), 2.82 (br s), 2.49 –1.92 (with max at 2.26, 2.03), 1.90–1.47 (with max at 1.76, 1.58), 1.22 (m).

9₂-13₉₆-9₂-[3]. NB-Glu(OtBu)Cys(Trt)Asp(OtBu)-OMe **9** (4.5 μmol , 3.9 mg) was dissolved in 300 μL $\text{CH}_2\text{Cl}_2/\text{CH}_3\text{OH}$ (3/1). To the reaction was added oven-dried LiCl (1.2 mmol, 51 mg) and $(\text{H}_2\text{IMes})(3\text{-Br-pyr})_2\text{Cl}_2\text{Ru}=\text{CHPh}$ (2.25 μmol , 2.0 mg) dissolved in 100 μL $\text{CH}_2\text{Cl}_2/\text{CH}_3\text{OH}$ (3/1) and an additional 100 μL $\text{CH}_2\text{Cl}_2/\text{CH}_3\text{OH}$ (3/1) at 0 °C under Ar. The reaction was stirred for 20 min at rt under Ar. NB-Glu(OtBu)Ser(tBu)Ala-OMe **13** (216.3 μmol , 119.3 mg) dissolved in 500 μL $\text{CH}_2\text{Cl}_2/\text{CH}_3\text{OH}$ (3/1) was added to the reaction at 0 °C under Ar. The reaction was stirred for 1 h at rt under Ar. NB-

Glu(OtBu)Cys(Trt)Asp(OtBu)-OMe **9** (4.5 μ mol, 3.9 mg) was dissolved in 300 μ L CH₂Cl₂/CH₃OH (3/1) was added to the reaction at 0 °C under Ar. The reaction was stirred for 1 h at rt under Ar. After quenching the reaction, crude polymer was precipitated, and deprotected to yield **9₂-13₉₆-9₂-[3]** as a yellowish-white solid (77 mg, 77%). ¹H-NMR (500 MHz, D₂O) δ 7.24 (m), 5.37 (m), 4.53-3.97 (with max at 4.33, 4.07), 3.77 (br s), 3.65 (br s), 3.14-2.34 (with max at 2.90, 2.50), 2.35-1.45 (with max at 2.19, 1.94, 1.85, 1.61), 1.33 (br s), 1.27-0.90 (with max at 1.15, 0.95).

18₂-13₉₆-18₂-[3]. NB-Gln(Trt)Cys(Trt)Asp(OtBu)-OMe **18** (4.5 μ mol, 4.7 mg) was dissolved in 300 μ L CH₂Cl₂/CH₃OH (3/1). To the reaction was added oven-dried LiCl (1.2 mmol, 51 mg) and (H₂IMes)(3-Br-pyr)₂Cl₂Ru=CHPh (2.25 μ mol, 2.0 mg) dissolved in 100 μ L CH₂Cl₂/CH₃OH (3/1) and an additional 100 μ L CH₂Cl₂/CH₃OH (3/1) at 0 °C under Ar. The reaction was stirred for 20 min at rt under Ar. NB-Glu(OtBu)Ser(tBu)Ala-OMe **13** (216.3 μ mol, 119.3 mg) dissolved in 500 μ L CH₂Cl₂/CH₃OH (3/1) was added to the reaction at 0 °C under Ar. The reaction was stirred for 4 h at rt under Ar. NB-Gln(Trt)Cys(Trt)Asp(OtBu)-OMe **18** (4.5 μ mol, 4.7 mg) was dissolved in 300 μ L CH₂Cl₂/CH₃OH (3/1) and was added to the reaction at 0 °C under Ar. The reaction was stirred for 5 h at rt under Ar. After quenching the reaction, crude polymer was precipitated, and deprotected to yield **18₂-13₉₆-18₂-[3]** as a yellowish-white solid (82 mg, 82%). ¹H-NMR (500 MHz, D₂O) δ 7.36 (m), 5.37 (m), 4.52-3.94 (with max at 4.34, 4.07), 3.77 (br s), 3.65 (br s), 3.16-2.31 (with max at 2.90, 2.49), 2.34-1.50 (with max at 2.16, 1.93, 1.84, 1.60), 1.34 (br s), 1.29-1.04 (with max at 1.25, 1.14).

9₂-13₉₆-18₂-[3]. NB-Glu(OtBu)Cys(Trt)Asp(OtBu)-OMe **9** (4.5 μ mol, 3.9 mg) was dissolved in 300 μ L CH₂Cl₂/CH₃OH (3/1). To the reaction was added oven-dried

LiCl (1.2 mmol, 51 mg) and (H₂IMes)(3-Br-pyr)₂Cl₂Ru=CHPh (2.25 μmol, 2.0 mg) dissolved in 100 μL CH₂Cl₂/CH₃OH (3/1) and an additional 100 μL CH₂Cl₂/CH₃OH (3/1) at 0 °C under Ar. The reaction was stirred for 20 min at rt under Ar. NB-Glu(OtBu)Ser(tBu)Ala-OMe **13** (216.3 μmol, 119.3 mg) dissolved in 500 μL CH₂Cl₂/CH₃OH (3/1) was added to the reaction at 0 °C under Ar. The reaction was stirred for 4 h at rt under Ar. NB-Gln(Trt)Cys(Trt)Asp(OtBu)-OMe **18** (4.5 μmol, 4.7 mg) was dissolved in 300 μL CH₂Cl₂/CH₃OH (3/1) and was added to the reaction at 0 °C under Ar. The reaction was stirred for 5 h at rt under Ar. After quenching the reaction, crude polymer was precipitated, and deprotected to yield **9₂-13₉₆-18₂-[3]** as a yellowish-white solid (73 mg, 73%). ¹H-NMR (500 MHz, D₂O) δ 7.32 (m), 5.38 (m), 4.45-3.96 (with max at 4.36, 4.07), 3.77 (br s), 3.18-2.31 (with max at 2.90, 2.50), 2.32-1.42 (with max at 2.14, 1.93, 1.78, 1.60), 1.25 (br s), 1.12 (m).

47. NB-GlyLys(Boc)Gly-Bpa-Glu(OtBu)Cys(Trt)Asp(OtBu)-OMe **38** (4.5 μmol, 6.5 mg) was dissolved in 500 μL CH₂Cl₂/CH₃Cl/CH₃OH (2/1/1). To the reaction was added oven-dried LiCl (1.2 mmol, 51 mg) and (H₂IMes)(3-Br-pyr)₂Cl₂Ru=CHPh (2.25 μmol, 2.0 mg) dissolved in 100 μL CH₂Cl₂/CH₃Cl/CH₃OH (2/1/1) and an additional 100 μL CH₂Cl₂/CH₃Cl/CH₃OH (2/1/1) at 0 °C under Ar. The reaction was stirred for 30 min at rt under Ar. NB-Glu(OtBu)Ser(tBu)Ala-OMe **13** (202.8 μmol, 112 mg) and NB-NHS **22** (13.5 μmol, 3 mg) dissolved in 500 μL CH₂Cl₂/CH₃Cl/CH₃OH (2/1/1) was added to the reaction at 0 °C under Ar. The reaction was stirred for 1 h at rt under Ar. NB-GlyLys(Boc)Gly-Bpa-Glu(OtBu)Cys(Trt)Asp(OtBu)-OMe **38** (4.5 μmol, 6.5 mg) was dissolved in 300 μL CH₂Cl₂/CH₃Cl/CH₃OH (2/1/1) was added to the reaction at 0 °C under Ar. The reaction was stirred for 1 h at rt under Ar. After quenching the reaction,

crude polymer **44** was precipitated (132 mg, 95%). The polymer **44** (1.79 μmol , 107 mg) and propynyl amine (21.49 μmol , 1.2 mg) was dissolved in 2 mL CH_2Cl_2 . DIEA (21.49 μmol , 4 μL) was added to the mixture, and the reaction was stirred for 16 h at rt. After evaporating solvent, crude polymer was precipitated with Et_2O (105 mg, 99%). A portion of the precipitated polymer (20 mg) was deprotected to yield **47** as a yellowish-white solid (15 mg, 97%). $^1\text{H-NMR}$ (500 MHz, D_2O) δ 7.53 (m), 5.37 (m), 4.47-4.10 (with max at 4.34), 3.77 (br s), 3.72 (br s), 3.15-2.33 (with max at 2.87, 2.56), 2.31-1.48 (with max at 2.17, 1.92, 1.84, 1.57), 1.34 (br s).

48. NB-GlyLys(Boc)Gly-Bpa-Gln(Trt)Cys(Trt)Asp(OtBu)-OMe **39** (4.5 μmol , 7.4 mg) was dissolved in 500 μL $\text{CH}_2\text{Cl}_2/\text{CH}_3\text{Cl}/\text{CH}_3\text{OH}$ (2/1/1). To the reaction was added oven-dried LiCl (1.2 mmol, 51 mg) and $(\text{H}_2\text{IMes})(3\text{-Br-pyr})_2\text{Cl}_2\text{Ru}=\text{CHPh}$ (2.25 μmol , 2.0 mg) dissolved in 100 μL $\text{CH}_2\text{Cl}_2/\text{CH}_3\text{Cl}/\text{CH}_3\text{OH}$ (2/1/1) and an additional 100 μL $\text{CH}_2\text{Cl}_2/\text{CH}_3\text{Cl}/\text{CH}_3\text{OH}$ (2/1/1) at 0 $^\circ\text{C}$ under Ar. The reaction was stirred for 30 min at rt under Ar. NB-Glu(OtBu)Ser(tBu)Ala-OMe **13** (202.8 μmol , 112 mg) and NB-NHS **22** (13.5 μmol , 3 mg) dissolved in 500 μL $\text{CH}_2\text{Cl}_2/\text{CH}_3\text{Cl}/\text{CH}_3\text{OH}$ (2/1/1) was added to the reaction at 0 $^\circ\text{C}$ under Ar. The reaction was stirred for 4 h at rt under Ar. NB-GlyLys(Boc)Gly-Bpa-Gln(Trt)Cys(Trt)Asp(OtBu)-OMe **39** (4.5 μmol , 7.4 mg) was dissolved in 300 μL $\text{CH}_2\text{Cl}_2/\text{CH}_3\text{Cl}/\text{CH}_3\text{OH}$ (2/1/1) was added to the reaction at 0 $^\circ\text{C}$ under Ar. The reaction was stirred for 5 h at rt under Ar. After quenching the reaction, crude polymer **45** was precipitated (125 mg, 96%). The polymer **45** (1.69 μmol , 103 mg) and propynyl amine (21.3 μmol , 1.1 mg) was dissolved in 2 mL CH_2Cl_2 . DIEA (20.31 μmol , 4 μL) was added to the mixture, and the reaction was stirred for 16 h at rt. After evaporating solvent, crude polymer was precipitated with Et_2O (102 mg, 99%). A portion

of precipitated polymer (20 mg) was deprotected to yield **48** as a yellowish-white solid (15 mg, 95%). $^1\text{H-NMR}$ (500 MHz, D_2O) δ 7.54 (m) 5.36 (m), 4.47-3.95 (with max at 4.34, 4.06), 3.78 (br s), 3.65 (br s), 3.14-2.32 (with max at 2.91, 2.564), 2.30-1.48 (with max at 2.16, 1.93, 1.87, 1.62), 1.34 (br s), 1.17 (m).

49. NB-GlyLys(Boc)Gly-Bpa-Glu(OtBu)Ser(tBu)Ala-OMe **40** (4.5 μmol , 5.2 mg) was dissolved in 500 μL $\text{CH}_2\text{Cl}_2/\text{CH}_3\text{Cl}/\text{CH}_3\text{OH}$ (2/1/1). To the reaction was added oven-dried LiCl (1.2 mmol, 51 mg) and $(\text{H}_2\text{IMes})(3\text{-Br-pyr})_2\text{Cl}_2\text{Ru}=\text{CHPh}$ (2.25 μmol , 2.0 mg) dissolved in 100 μL $\text{CH}_2\text{Cl}_2/\text{CH}_3\text{Cl}/\text{CH}_3\text{OH}$ (2/1/1) and an additional 100 μL $\text{CH}_2\text{Cl}_2/\text{CH}_3\text{Cl}/\text{CH}_3\text{OH}$ (2/1/1) at 0 $^\circ\text{C}$ under Ar. The reaction was stirred for 30 min at rt under Ar. NB-Glu(OtBu)Ser(tBu)Ala-OMe **13** (202.8 μmol , 112 mg) and NB-NHS **22** (13.5 μmol , 3 mg) dissolved in 500 μL $\text{CH}_2\text{Cl}_2/\text{CH}_3\text{Cl}/\text{CH}_3\text{OH}$ (2/1/1) was added to the reaction at 0 $^\circ\text{C}$ under Ar. The reaction was stirred for 4 h at rt under Ar. NB-GlyLys(Boc)Gly-Bpa-Glu(OtBu)Ser(tBu)Ala-OMe **40** (4.5 μmol , 5.2 mg) was dissolved in 300 μL $\text{CH}_2\text{Cl}_2/\text{CH}_3\text{Cl}/\text{CH}_3\text{OH}$ (2/1/1) was added to the reaction at 0 $^\circ\text{C}$ under Ar. The reaction was stirred for 5 h at rt under Ar. After quenching the reaction, crude polymer **46** was precipitated (125 mg, 99%). The polymer **46** (2.02 μmol , 117 mg) and propynyl amine (24.2 μmol , 1.3 mg) was dissolved in 2 mL CH_2Cl_2 . DIEA (204.2 μmol , 4 μL) was added to the mixture, and the reaction was stirred for 16 h at rt. After evaporating solvent, crude polymer was precipitated with Et_2O (115 mg, 92%). A portion of precipitated polymer (14 mg) was deprotected to yield **49** as a yellowish-white solid (15 mg, 92%). $^1\text{H-NMR}$ (500 MHz, D_2O) δ 7.58 (m) 5.31 (m), 4.50-4.00 (with max at 4.34, 4.07), 3.77 (br s), 3.65 (br s), 3.11-2.34 (with max at 2.90, 2.49), 2.29-1.45 (with max at 2.16, 1.93, 1.85, 1.61), 1.30 (br s), 1.17 (m).

II. *In vitro* Fertilization Assay

Materials and General Methods. 8- to 10-week-old virgin female mice (ICR or CD-1) were purchased from Taconic Inc., NJ or Charles River Laboratories, NY. 8-month-old ICR retired male breeders were purchased from Taconic, NJ. Mice containing the floxed β_1 integrin gene^{269, 270} were provided by Ruth Globus (NASA Ames Research Center) with permission from Reinhardt Fässler (MPI, Martinsried). Transgenic mice expressing the Cre recombinase under the control of the ZP3 promoter were obtained from Paul Primakoff (UC Davis) with permission from Jamie Marth (UC San Diego). Pregnant mare's serum gonadotropin (PMSG, #367222), hyaluronidase (#H3506), and Hoechst-33342, were purchased from Sigma-Aldrich, and human chorionic gonadotropin (hCG, #230734) was obtained through the National Hormone and Peptide Program, the National Institute of Diabetes and Digestive Kidney Diseases, and Dr. A.F. Parlow. Chemicals for assay buffers were purchased from Sigma-Aldrich and Fisher Scientific. PMSG and hCG were resuspended in sterile PBS to 7.5 IU/100 μ L. These solutions were stored at -20 °C. Hyaluronidase was resuspended in sterile water to a final concentration of 30 mg/ml and was stored at -20 °C. Tyrode's acid was prepared with 0.8 g NaCl, 0.02 g KCl, 0.02 g CaCl₂, 0.01 g Mg Cl₂, 0.005 g Na₂HPO₄, 0.1 g glucose, and 0.4 g polyvinylpyrrolidone dissolved in 100 mL sterile water. After filtration through a 0.2 μ m filter, 1 N HCl was added to adjust the pH to 2.0. Tyrode's acid was stored at -20 °C. Hoechst 33342 (2'-[4 ethoxyphenol]-5-[4-methyl-1-piperazinyl]-2,5'-bi-1H-benzimidazole trihydrochloride) was stored in the dark at 4 °C. All of the steps involving the use of Hoechst 33342 were performed with minimum exposure to light.

M16 assay buffer. M16 is a modified Krebs-Ringer bicarbonate medium containing the following: 94.6 mM NaCl, 4.8 mM KCl, 1.19 mM KH₂PO₄, 1.19 mM MgSO₄·7H₂O, 23.28 mM sodium lactate, 5.56 mM glucose, 0.0006% penicillin G potassium salt, 0.0005% streptomycin sulfate, 25.0 mM NaHCO₃, 0.33 mM sodium pyruvate, 1.95 mM CaCl₂·2H₂O (Table 5-1). All solutions were stored at 4 °C. Stock B and stock C must be changed every other week, and stock A and D can be stored up to 3 months.

Stock solutions	Component	Quantity (g)	Concentration in assay buffer
Stock A (50 mL) 10 × Conc	NaCl	2.767	94.6 mM
	KCl	0.178	4.8 mM
	KH ₂ PO ₄	0.081	1.2 mM
	MgSO ₄ ·7H ₂ O	0.1465	1.2 mM
	60% w/v sodium lactate	2.2715	23.3 mM
	glucose	0.5	5.6 mM
	penicillin K ⁺ salt	0.03	0.0006%
	streptomycin sulfate	0.025	0.0005%
Stock B (20 mL) 10 × Conc.	NaHCO ₃	0.402	25.0 mM
	Phenol red	0.002	
Stock C (20 mL) 100 × Conc.	Sodium pyruvate	0.072	0.33 mM
Stock D (20 mL) 100 × Conc.	CaCl ₂ ·2H ₂ O	0.572	2.0 mM

Table 5-1. Composition of M16 buffer.

Preparation of 0.5% BSA and 3% BSA/M16 buffer. M16 modified Krebs-Ringer medium (0.5% and 3% BSA/M16) were made up as follows: The stock mixture solution of 2 mL stock A, 2 mL stock B, 0.2 mL stock C and 0.2 mL stock D was diluted to 20 mL with ddH₂O. To the stock mixture solution, 100 mg BSA was added to make a final concentration of 0.5% BSA. To the stock mixture solution, 600 mg BSA was added to make a final concentration of 3% BSA. Both 0.5% and 3% BSA/M16 buffers were filtered through a 0.2 µm sterile filter and stored at 4 °C.

Generation of oocyte-specific β_1 integrin conditional knockout mice.²⁶⁰ Mice with the floxed β_1 integrin gene and mice with the Cre recombinase behind the ZP3 promoter were used to generate oocyte-specific β_1 integrin conditional knockout mice as previously described by He et al.¹²⁵ PCR was used to genotype progeny to identify the ZP3-Cre transgene and the presence of the floxed β_1 integrin gene. For ZP3 detection the following primers were used:

Cre12: GGA CAT GTT CAG GGA TCG CCA GGC G

Cre13: GCA TAA CCA GTG AAA CAG CAT TGC TG

To detect the presence of the floxed β_1 integrin gene the following primers were used:

T56: AGG TGC CCT TCC CTC TAG A

L1: GTG AAG TAG GTG AAA GGT AAC

L26: TAA AAA GAC AGA ATA AAA CGCAC

Isolation of oocytes and spermatozoa for IVF assay. All experiments performed with mice were in accordance with the National Institute of Health and United States Department of Agriculture guidelines, and the specific procedures performed were approved by the Stony Brook University IACUC (protocol #0616). Oocytes were collected from the oviducts of 8- to 10-week-old superovulated female ICR/CD-1 mice or C57 mutant progeny that were wild type ($Cre^- \beta_1 +/+$), heterozygous ($Cre^+ \beta_1 +/f$), or knockouts ($Cre^+ \beta_1 f/f$) for the β_1 allele. Mice were superovulated by injecting 7.5 IU PMSG, followed 48~52 h later by an injection of 7.5 IU hCG. 12-14 h after hCG injection, mice were sacrificed. All manipulations and incubations of oocytes were performed at 37 °C, 5% CO₂ unless otherwise noted. The oviducts were removed from euthanized mice and were incubated in prewarmed 0.5% BSA/M16. Cumulus-oocyte complexes were collected and transferred to 500 μ L drops of medium containing 30 μ g/mL hyaluronidase surrounded by mineral oil. After 10 min of incubation at 37°C, 5% CO₂, cumulus free metaphase II oocytes (oocytes with one polar body) were collected, transferred first to a 80 μ L drop of medium, and then washed through six 80 μ L drops of medium. Oocytes were recovered for 1 h before treating with Tyrode's acid. Zona pellucida of metaphase II oocytes were removed by treating oocytes with a 100 μ L Tyrode's acid drop for 1 min at room temperature. Zona pellucida free oocytes were washed six times with 0.5% BSA/M16 and were recovered for 2 h, then preloaded with Hoechst 33342 dye at 10 μ g/mL for 30 min at 37°C, 5% CO₂. Meanwhile, sperm for the in vitro adhesion and fusion assay were isolated from the cauda epididymis and vas deferens of 8-month-old ICR retired male breeders. Sperm were released from dissected cauda and vas deferens into 3% BSA/M16 modified Krebs-Ringer medium. Released

sperm were incubated at 37°C, 5% CO₂ for 2.5-3 h in the same medium to allow them to capacitate and acrosome react.

Inhibitor Assay. The polymers were dissolved in aqueous NH₄OH and fully reduced with 10 mM TCEP for 1–2 h. The pH of reducing solutions was between 6 and 7 in order not to form precipitates. The solutions were centrifuged at 16 000 g for 3min, and the supernatants were collected. The polymers were precipitated by adding 1 N HCl to the supernatants, centrifuged at 2 000 g for 3 min until the polymers formed a thin film on the eppendorf tubes, washed with water three times, and residual water was removed by lyophilization. Polymers of high molecular weight were handled carefully to prevent aggregate formation upon centrifugation. Polymers were redissolved in water adjusted to pH 7 with NH₄OH immediately before assays to a final concentration of 0.1 mM. Zona free oocytes that had been loaded with Hoechst 33342 were washed six times with 3% BSA/M16, and placed in 100-μL drops of polymer solution in 3% BSA/M16, and incubated with oocytes for 45 min prior to sperm addition. No more than 6 μL of stock solution was diluted into an oocyte drop. Capacitated and acrosome reacted sperm were added to oocytes at a final concentration of $1-5 \times 10^4$ sperm/mL. After 45 min at 37 °C, 5% CO₂, oocytes were gently washed through six 60-μL drops of 3% BSA/M16. Oocytes were mounted onto glass microscope slides, covered with glass cover slips, and sperm binding and fusion were scored by epi-fluorescence microscopy and DIC microscopy (NIKON Eclipse 400, 40×, 0.75 NA objective). Fusion was scored as the fluorescent labeling of sperm nuclei with Hoechst 33342 present in the preloaded oocytes. Two measures of fusion were used: fertilization index (FI, mean number of fused sperm per oocyte) and fertilization rate (FR, percentage of oocytes fused with at least one

sperm). IC_{50} s were calculated by a three parameter fit (GRAFIT software) by the equation:

$$y = (100-b) / \{1 + ((I)/ IC_{50})\}^s \quad (1)$$

where y is the percent FR or FI, b is the remaining percent fertilization after saturation with inhibitor, and s is the slope of the fit. Errors were reported as SEM.

III. Fluorescence Staining Protocol

Materials and General Methods. Chemicals for assay buffer were purchased from Sigma-Aldrich and Fisher Scientific. Alexa fluor₄₈₈ carboxylic acid succinimidyl ester was purchased from Invitogen Corporation (cat. # A20100). All of the steps involving the use of dye were performed with minimum exposure to light. 1% polyvinyl pyrrolidone (PVP)/M16 buffer was composed of 94.6 mM NaCl, 4.8 mM KCl, 1.19 mM KH_2PO_4 , 1.19 mM $MgSO_4 \cdot 7H_2O$, 23.28 mM sodium lactate, 5.56 mM glucose, 0.0006% penicillin G potassium salt, 0.0005% streptomycin sulfate, 25.0 mM $NaHCO_3$, 0.33 mM sodium pyruvate, 1.95 mM $CaCl_2 \cdot 2H_2O$ and 1% PVP. The composition of 0.5% BSA/M16 is the same as 1% PVP/M16, but only 1% PVP was added instead of 0.5% BSA. 4% Paraformaldehyde in phosphate buffered saline (PBS) was used as fixing solution. Goat serum was purchased from Sigma-Aldrich (cat. # G9023).

Polymer staining of zona pellucida free oocytes. Zona pellucida free oocytes were collected as described previously. After removing the zona pellucida, zona pellucida

free oocytes were washed with six 80 μ L drops of 0.5% BSA/M16, incubated in 0.5% BSA/M16 for 1.5–2 h. The recovered zona pellucida free oocytes were placed in a 100 μ L drop of an Alex₄₈₈-conjugated polymer solution in 0.5% BSA/M16 containing 10% goat serum, and incubated at 37 °C, 5% CO₂ for 45 min. The polymer solutions were prepared by diluting the stock polymer solutions with the buffer, and no more than 6 μ L of stock solution was diluted. The concentration of polymers in the 100- μ L drop was 20 μ M in polymer concentration and 80 μ M in effective peptide ligand concentration. And then oocytes were gently washed through a 300- μ L drop of 0.5% BSA/M16 by shaking at 50 rpm for 10 min, and a second washing was performed in the same manner. After fixing the oocytes with a 100- μ L drop of 4% paraformaldehyde in PBS at rt for 10 min, oocytes were washed through four 60- μ L drops of 0.5% BSA/M16, mounted onto glass bottom dishes (MatTek Corp.) and surrounded by mineral oil. Oocytes were imaged on a Zeiss Axiovert with a GFP/FITC filter and 0.55 NA, 20x.

Photoaffinity labeling of zona pellucida free oocytes. After removing the zona pellucida, zona pellucida free oocytes were washed with six 80- μ L drops of 0.5% BSA/M16, incubated in 0.5% BSA/M16 for 1.5–2 h. The recovered zona pellucida free oocytes were washed with four 60- μ L drops of 1% PVP/M16, placed in a 100- μ L drop of Alex₄₈₈-conjugated polymer solution in 1% PVP/M16, and incubated at 37 °C, 5% CO₂ for 45 min. The polymer solutions were prepared by diluting the stock polymer solutions with the buffer, and no more than 6 μ L of stock solution was diluted. The concentration of polymers in the 100- μ L drop was 20 μ M in polymer concentration and 80 μ M in effective peptide ligand concentration. And then oocytes were irradiated with UV light ($\lambda_{\text{max}} = 350$ nm, under 15 cm) at 4 °C for 15 min. The photoaffinity labeled oocytes were

gently washed twice through 300- μ L drops of 1% PVP/M16 by shaking at 50 rpm for 10 min. After fixing the oocytes with a 100- μ L drop of 4% paraformaldehyde in PBS at rt for 10 min, oocytes were washed through four 60 μ L drops of 0.5% BSA/M16, mounted onto mounted onto glass bottom dishes (MatTek Corp.), and surrounded by mineral oil. Oocytes were imaged on a Zeiss Axiovert with a GFP/FITC filter and 0.55 NA, 20x.

IV. Photoaffinity Labeling Protocol

Materials and General Methods. Chemicals for assay buffer were purchased from Sigma-Aldrich and Fisher Scientific. 1% PVP/M16 buffer was composed of 94.6 mM NaCl, 4.8 mM KCl, 1.19 mM KH_2PO_4 , 1.19 mM $\text{MgSO}_4 \cdot 7\text{H}_2\text{O}$, 23.28 mM sodium lactate, 5.56 mM glucose, 0.0006% penicillin G potassium salt, 0.0005% streptomycin sulfate, 25.0 mM NaHCO_3 , 0.33 mM sodium pyruvate, 1.95 mM $\text{CaCl}_2 \cdot 2\text{H}_2\text{O}$ and 1% PVP. RIPA buffer was composed of 50 mM Tris-HCl, pH 7.4, 150 mM NaCl, 1% Triton X-100, 1% sodium deoxycholate, 0.1% sodium dodecyl sulfate (SDS), 1 mM CaCl_2 , and 1 M MgCl_2 . Aprotinin, leupeptin, pepstatin, and phenylmethanesulphonylfluoride or phenylmethylsulphonyl fluoride (PMSF) were purchased from Sigma-Aldrich. Tris[(1-benzyl-1*H*-1,2,3-triazol-4-yl)methyl]amine was purchased from Sigma-Aldrich (cat.# 678973). Sequencing-grade modified trypsin and trypsin resuspension buffer were purchased from Promega (cat. # V5111). NeutrAvidin Agarose Resin was purchased from Pierce (cat. # 29200).

Photoaffinity labeling of zona pellucida free oocytes. On a single day, 64 female mice were sacrificed. The mice were dissected in 8 batches. Each batch yielded ~125 zona pellucida-free oocytes that were washed with six 80- μ L drops of 0.5% BSA/M16 and incubated in 0.5% BSA/M16 for 1.5–2 h. At the end of the incubation 2 batches were combined. Each of the four batches was washed with four 80- μ L drops of 1% PVP/M16 and transferred into a 100- μ L drop of polymer solution in 1% PVP/M16 (250 oocytes in each drop) in a 2.5 cm petri dish, and incubated at 37 °C, 5% CO₂ for 45 min. The concentration of polymers in the 100- μ L drop was 10 μ M in polymer concentration and 40 μ M in effective peptide ligand concentration. All four dishes of oocytes were irradiated with UV light ($\lambda_{\text{max}} = 350$ nm, under 15 cm) at 4 °C for 15 min.

The four batches of polymer labeled oocytes were combined into one 80- μ L drop of 1% PVP/M16 and washed through three 80- μ L drop of 1% PVP/M16 and two 80- μ L drops of sterile PBS. Around 1 000 labeled oocytes were suspended in 300 μ L RIPA buffer in an eppendorf tube with protease inhibitors, and incubated for 1 h at 4 °C with gentle rocking. Protease inhibitors, aprotinin (1 μ g/mL), leupeptin (1 μ g/mL), pepstatin (1 μ g/mL), and PMSF (50 μ g/mL) were added to the RIPA buffer right before the oocyte addition. The lysate was centrifuged at 16 000 g for 30 min. The supernatant was flash frozen with liquid N₂, and stored at - 80 °C.

Pre-clearing lysates. The lysates supernatants from 640 mice (1 000 oocytes \times 10 \times 300 μ L) were combined, and concentrated with an ultra YM-3 membrane (3 000 molecular weight limit, Millipore, cat.# 42403) to 1 mL. NeutrAvidin agarose resin (100 μ L) was added to a 1.5 mL eppendorf tube, washed with 1 mL of PBS, and centrifuged at 1 400 g for 3 min at 25 °C. The solvent from the resin was removed, and the washing

was repeated two more times. The lysates were added to the resin and incubated for 1 h at rt. After centrifuging at 1 400 g for 3 min, the supernatant was collected.

Huisgen 1, 3-dipolar cycloaddition, “Click Chemistry”.²⁷¹ Concentrations must be followed exactly to avoid precipitation.

1. 500 μL of the pre-cleared lysates was transferred to each of two eppendorf tubes.
2. To each eppendorf tube, 115.6 μL of biotin-PEG₁₀-N₃, **43** (5 mM stock in water) was added, and the mixture vortexed.
3. 11.6 μL of freshly prepared 50 mM TCEP in water (14.4 mg/mL) was added to each eppendorf tube, and the mixture vortexed.
4. 35 μL of 1.7 mM stock of Tris[(1-benzyl-1*H*-1,2,3-triazol-4-yl)methyl]amine in 1:4 DMSO/*tert*-butanol (0.9 mg/mL) was added, and the mixture vortexed.
5. 11.6 μL of 50 mM copper (II) sulfate in water (12.5 mg/mL) was added to each eppendorf tube, and the mixture vortexed.
6. The cycloaddition reactions were performed at rt for 16 h.
7. After the cycloaddition reactions, the reaction solutions were combined and centrifuged at 6 500 g for 4 min at 4 °C.
8. After removing the supernatant, 500 μL of cold methanol was added to the pellet, and the mixture sonicated for 5 sec.
9. The sample was rotated at 4 °C for 10 min and centrifuged at 6 500 g for 4 min at 4 °C.
10. The supernatant was removed, and the washing of pellet with 500 μL of cold methanol was repeated.

11. After removing the supernatant, 1 ml of 1.2% SDS/PBS was added to the pellet, the mixture was sonicated for 5 sec, and heated to 80–90 °C for 5 min.
12. The solution was transferred to a 15 mL conical tube and diluted to 0.2% SDS with 5 mL of PBS. This mixture is referred to as the sample solution.

Affinity purification.

1. NeutrAvidin agarose resin (100 μ L) was added to a 1.5 mL eppendorf tube, washed with 1 mL PBS, and centrifuged at 1 400 g for 3 min at 25 °C to remove the solvent. Washing steps were repeated two more times.
2. The sample solution was added to the resin and incubated for 16 h at rt and centrifuged at 1 400 g for 3 min at rt. The supernatant was removed.
3. The resin was washed with 1 mL 0.2% SDS/PBS by gentle rotation for 10 min, centrifuged at 1 400 g for 3 min, and the supernatant was removed.
4. 1 mL PBS was added to the resin, and the resin was rotated for 1 min, centrifuged at 1 400 g for 3 min.
5. The supernatant was removed, and the washing steps with 1 mL PBS (step 4) were repeated two more times.
6. After washing the resin with 1 mL water three times, the resin was transferred to another eppendorf tube using 1 mL of water, and centrifuged. The supernatant was removed by pipetting to yield the loaded beads.

On-bead trypsin digestion.

1. 50 μL of a 6 M urea/PBS solution and 2.5 μL of a 200 mM TCEP solution in water were added to the loaded beads.
2. The tube was placed in a 65 $^{\circ}\text{C}$ heat-block for 15 min, then cooled to 35 $^{\circ}\text{C}$.
3. 2.5 μL of a 400 mM iodoacetamide in water solution was added, and the mixture was incubated for 30 min at 35 $^{\circ}\text{C}$.
4. The reaction was diluted with 95 μL PBS, centrifuged at 1 400 g for 2 min and the supernatant was removed.
5. 200 μL of a 2 M urea/PBS solution, 2 μL of 100 mM calcium chloride in water, and 4 μL of a stock trypsin solution (20 μg reconstitute in 40 μL of the trypsin buffer) were added to the beads. The reaction was incubated for 16 h at 37 $^{\circ}\text{C}$. The mixture was centrifuged, and the supernatant collected.
6. 1 μL of glacial acetic acid was added to the supernatant. The solution was lyophilized.

Desalting. 10 μL of 0.1% TFA in H_2O was added to the lyophilized tryptic digest. A C_{18} zip-tip was washed with 0.1% TFA in $\text{CH}_3\text{CH}/\text{H}_2\text{O}(1:1)$ twice, and was washed with 0.1% TFA in H_2O ten times. The tryptic digestion solution was loaded on the zip-tip, and the solvent was expelled from the zip-tip. The sample loaded zip-tip was washed with 0.1% TFA in H_2O five times. The sample peptide in the zip-tip was eluted with 5 μL of 0.1% TFA in CH_3CN five times. The eluted solutions were combined and lyophilized.

Mass analysis. 1.5 μL of 0.1% TFA in $\text{CH}_3\text{CH}/\text{H}_2\text{O}(1:1)$ and 1.5 μL of saturated α -cyano-4-hydroxycinnamic acid solution were added to the lyophilized sample. The whole sample solution was loaded onto a target plate by loading 1 μL each for MALDI-TOF spectroscopic analysis.

Bibliography

1. Gilbert, S. F., *Developmental biology*. 7th ed.; Sinauer Associates: Sunderland, Mass., 2003; p 183-219.
2. Schultz, R. M.; Kopf, G. S., Molecular-basis of mammalian egg activation. *Curr. Top. Dev. Bio.* **1995**, 30, 21-62.
3. Yanagimachi, R., *The physiology of reproduction*. 2nd ed.; Raven Press: New York, 1994; p 189-317.
4. Evans, J. P.; Florman, H. M., The state of the union: the cell biology of fertilization. *Nat. Cell Biol.* **2002**, 4, S57-S63.
5. Visconti, P. E.; Galantino-Homer, H.; Moore, G. D.; Bailey, J. L.; Ning, X. P.; Fornes, M.; Kopf, G. S., The molecular basis of sperm capacitation. *J. Andrology* **1998**, 19, (2), 242-248.
6. Breitbart, H., Signaling pathways in sperm capacitation and acrosome reaction. *Cell. Mol. Biol.* **2003**, 49, (3), 321-327.
7. Florman, H. M.; Arnoult, C.; Kazam, I. G.; Li, C.; O'Toole, C. M. B., An intimate biochemistry: egg-regulated acrosome reactions of mammalian sperm. *Adv. Devel. Biochem.* **1999**, 5, 147-186.
8. Chen, Y. Q.; Cann, M. J.; Litvin, T. N.; Iourgenko, V.; Sinclair, M. L.; Levin, L. R.; Buck, J., Soluble adenylyl cyclase as an evolutionarily conserved bicarbonate sensor. *Science* **2000**, 289, (5479), 625-628.
9. Wiesner, B.; Weiner, J.; Middendorff, R.; Hagen, V.; Kaupp, U. B.; Weyand, I., Cyclic nucleotide-gated channels on the flagellum control Ca²⁺ entry into sperm. *J. Cell Biol.* **1998**, 142, (2), 473-484.
10. Arnoult, C.; Kazam, I. G.; Visconti, P. E.; Kopf, G. S.; Villaz, M.; Florman, H. M., Control of the low voltage-activated calcium channel of mouse sperm by egg ZP3 and by membrane hyperpolarization during capacitation. *Proc. Natl. Acad. Sci. U. S. A.* **1999**, 96, (12), 6757-6762.
11. Wassarman, P. M., Zona pellucida glycoproteins. *Annu. Rev. Biochem.* **1988**, 57, 415-442.

12. Schmell, E. D.; Gulyas, B. J., Ovoperoxidase activity in ionophore treated mouse Eggs. 2. Evidence for the enzymes role in hardening the zona pellucida. *Gamete Res.* **1980**, 3, (3), 279-290.
13. Moller, C. C.; Bleil, J. D.; Kinloch, R. A.; Wassarman, P. M., Structural and functional-relationships between mouse and hamster zona pellucida glycoproteins. *Dev. Biol.* **1990**, 137, (2), 276-286.
14. Bleil, J. D.; Wassarman, P. M., Autoradiographic visualization of the mouse eggs sperm receptor bound to sperm. *J. Cell Biol.* **1986**, 102, (4), 1363-1371.
15. Bleil, J. D.; Wassarman, P. M., Mammalian sperm-egg interaction - identification of a glycoprotein in mouse egg zonae pellucidae possessing receptor activity for sperm. *Cell* **1980**, 20, (3), 873-882.
16. Wassarman, P. M.; Jovine, L.; Litscher, E. S., A profile of fertilization in mammals. *Nat. Cell Biol.* **2001**, 3, E59-E64.
17. Florman, H. M.; Wassarman, P. M., O-Linked oligosaccharides of mouse egg ZP3 account for its sperm receptor activity. *Cell* **1985**, 41, (1), 313-324.
18. Yonezawa, N.; Fukui, N.; Kuno, M.; Shinoda, M.; Goko, S.; Mitsui, S.; Nakano, M., Molecular cloning of bovine zona pellucida glycoproteins ZPA and ZPB and analysis for sperm-binding component of the zona. *Eur. J. Biochem.* **2001**, 268, (12), 3587-3594.
19. Chen, J.; Litscher, E. S.; Wassarman, P. M., Inactivation of the mouse sperm receptor, mZP3, by site-directed mutagenesis of individual serine residues located at the combining site for sperm. *Proc. Natl. Acad. Sci. U. S. A.* **1998**, 95, (11), 6193-6197.
20. Kinloch, R. A.; Sakai, Y.; Wassarman, P. M., Mapping the mouse ZP3 combining site for sperm by exon swapping and site-directed mutagenesis. *Proc. Natl. Acad. Sci. U. S. A.* **1995**, 92, (1), 263-267.
21. Snell, W. J.; White, J. M., The molecules of mammalian fertilization. *Cell* **1996**, 85, 629-637.
22. Hardy, D. M.; Garbers, D. L., A sperm membrane-protein that binds in a species-specific manner to the egg extracellular-matrix is homologous to von-willebrand-factor. *J. Biol. Chem.* **1995**, 270, (44), 26025-26028.

23. Hardy, D. M.; Garbers, D. L., Species-specific binding of sperm proteins to the extracellular-matrix (zona-pellucida) of the egg. *J. Biol. Chem.* **1994**, 269, (29), 19000-19004.
24. Miller, D. J.; Macek, M. B.; Shur, B. D., Complementarity between sperm surface β -1,4-galactosyl-transferase and egg-coat ZP3 mediates sperm-egg binding. *Nature* **1992**, 357, 589-593.
25. Shur, B. D., Glycosyltransferases as cell adhesion molecules. *Curr. Opin. Cell Biol.* **1993**, 5, 854-863.
26. Arnoult, C.; Cardullo, R. A.; Lemos, J. R.; Florman, H. M., Activation of mouse sperm T-type Ca^{2+} channels by adhesion to the egg zona pellucida. *Proc. Natl. Acad. Sci. U. S. A.* **1996**, 93, (23), 13004-13009.
27. Ward, C. R.; Storey, B. T.; Kopf, G. S., Selective activation of G(I1), and G(I2), in mouse sperm by the zona-pellucida, the eggs extracellular-matrix. *J. Biol. Chem.* **1994**, 269, (18), 13254-13258.
28. Tomes, C. N.; McMaster, C. R.; Saling, P. M., Activation of mouse sperm phosphatidylinositol-4,5 biphosphate-phospholipase C by zona pellucida is modulated by tyrosine phosphorylation. *Mol. Reprod. Dev.* **1996**, 43, (2), 196-204.
29. Fukami, K.; Nakao, K.; Inoue, T.; Kataoka, Y.; Kurokawa, M.; Fissore, R. A.; Nakamura, K.; Katsuki, M.; Mikoshiba, K.; Yoshida, N.; Takenawa, T., Requirement of phospholipase C delta 4 for the zona pellucida-induced acrosome reaction. *Science* **2001**, 292, (5518), 920-923.
30. Roldan, E. R. S.; Murase, T.; Shi, Q. X., Exocytosis in spermatozoa in response to progesterone and zona-pellucida. *Science* **1994**, 266, (5190), 1578-1581.
31. Florman, H. M.; Tombes, R. M.; First, N. L.; Babcock, D. F., An adhesion-associated agonist from the zona pellucida activates G protein-promoted elevations of internal Ca^{2+} and Ph that mediate mammalian sperm acrosomal exocytosis. *Dev. Biol.* **1989**, 135, (1), 133-146.
32. Arnoult, C.; Zeng, Y.; Florman, H. M., ZP3-dependent activation of sperm cation channels regulates acrosomal secretion during mammalian fertilization. *J. Cell Biol.* **1996**, 134, (3), 637-645.
33. Florman, H. M., Sequential focal and global elevations of sperm intracellular Ca^{2+} are initiated by the zona-pellucida during acrosomal exocytosis. *Dev. Biol.* **1994**, 165, (1), 152-164.

34. Walensky, L. D.; Snyder, S. H., Inositol 1,4,5-trisphosphate receptors selectively localized to the acrosomes of mammalian sperm. *J. Cell Biol.* **1995**, 130, (4), 857-869.
35. Wolfsberg, T. G.; White, J. M., ADAMs in fertilization and development. *Dev. Biol.* **1996**, 180, (2), 389.
36. Wolfsberg, T. G.; Straight, P. D.; Gerena, R. L.; Huovila, A. P. J.; Primakoff, P.; Myles, D. G.; White, J. M., ADAM, a widely distributed and developmentally regulated gene family encoding membrane proteins with a disintegrin and metalloprotease domain. *Dev. Biol.* **1995**, 169, (1), 378-383.
37. Katagiri, T.; Harada, Y.; Emi, M.; Nakamura, Y., Human metalloprotease/disintegrin-like (MDC) gene: exon-intron organization and alternative splicing. *Cytogenet. Cell Genet.* **1995**, 68, (1-2), 39-44.
38. Perry, A. C. F.; Jones, R.; Barker, P. J.; Hall, L., A mammalian epididymal protein with remarkable sequence similarity to snake venom haemorrhagic peptides. *Biochem. J.* **1992**, 286, 671-675.
39. Yuan, R.; Primakoff, P.; Myles, D. G., A role for the disintegrin domain of cyritestin, a sperm surface protein belonging to the ADAM family, in mouse sperm-egg plasma membrane adhesion and fusion. *J. Cell Biol.* **1997**, 137, (1), 105-112.
40. Kasahara, M.; Gutknecht, J.; Brew, K.; Spurr, N.; Goodfellow, P. N., Cloning and mapping of a testis-specific gene with sequence similarity to a sperm-coating glycoprotein gene. *Genomics* **1989**, 5, (3), 527-534.
41. Okabe, M.; Yagasaki, M.; Oda, H.; Matzno, S.; Kohama, Y.; Mimura, T., Effect of a monoclonal anti-mouse sperm antibody (Obf 13) on the interaction of mouse sperm with zona-free mouse and hamster eggs. *J. Reprod. Immunol.* **1988**, 13, (3), 211-219.
42. Blobel, C. P.; Wolfsberg, T. G.; Turck, C. W.; Myles, D. G.; Primakoff, P.; White, J. M., A potential fusion peptide and an integrin ligand domain in a protein active in sperm-egg fusion. *Nature* **1992**, 356, 248-251.
43. Runft, L. L.; Jaffe, L. A.; Mehlmann, L. M., Egg activation at fertilization: where it all begins. *Dev. Biol.* **2002**, 245, (2), 237-54.
44. Stricker, S. A., Comparative biology of calcium signaling during fertilization and egg activation in animals. *Dev. Biol.* **1999**, 211, (2), 157-176.

45. Saunders, C. M.; Larman, M. G.; Parrington, J.; Cox, L. J.; Royse, J.; Blayney, L. M.; Swann, K.; Lai, F. A., PLC zeta: a sperm-specific trigger of Ca²⁺ oscillations in eggs and embryo development. *Development* **2002**, 129, (15), 3533-44.
46. Moller, C. C.; Wassarman, P. M., Characterization of a proteinase that cleaves zona pellucida glycoprotein-ZP2 following activation of mouse eggs. *Dev. Biol.* **1989**, 132, (1), 103-112.
47. Cho, C., *Mammalian ADAMs with testis-specific or -predominant expression*. Dordrecht, The Netherlands, Springer: 2005; Vol. 4.
48. Kim, T.; Oh, J.; Woo, J. M.; Choi, E.; Im, S. H.; Yoo, Y. J.; Kim, D. H.; Nishimura, H.; Cho, C. H., Expression and relationship of male reproductive ADAMs in mouse. *Biol. Reprod.* **2006**, 74, (4), 744-750.
49. Choi, I. C.; Oh, J. S.; Cho, B. N.; Ahn, J. H.; Jung, Y. K.; Kim, D. H.; Cho, C. H., Characterization and comparative genomic analysis of intronless Adams with testicular gene expression. *Genomics* **2004**, 83, (4), 636-646.
50. Cho, C. H.; Turner, L.; Primakoff, P.; Myles, D. G., Genomic organization of the mouse fertilin beta gene that encodes an ADAM family protein active in sperm-egg fusion. *Dev. Genet.* **1997**, 20, (4), 320-328.
51. Choi, I.; Woo, J. M.; Hong, S.; Jung, Y. K.; Kim, D. H.; Cho, C., Identification and characterization of ADAM32 with testis-predominant gene expression. *Gene* **2003**, 304, 151-162.
52. Oh, J.; Woo, J. M.; Choi, E. Y.; Kim, T.; Cho, B. N.; Park, Z. Y.; Kim, Y. C.; Kim, D. H.; Cho, C. H., Molecular, biochemical, and cellular characterization of epididymal ADAMs, ADAM7 and ADAM28. *Biochem. Biophys. Res. Commun.* **2005**, 331, (4), 1374-1383.
53. Linder, B.; Heinlein, U. A. O., Decreased in vitro fertilization efficiencies in the presence of specific cyritestin peptides. *Dev. Growth Differ.* **1997**, 39, (2), 243-247.
54. Linder, B.; Bammer, S.; Heinlein, U. A., Delayed translation and posttranslational processing of cyritestin, an integral transmembrane protein of the mouse acrosome. *Exp. Cell Res.* **1995**, 221, (1), 66-72.
55. Cho, C.; Bunch, D. O. D.; Faure, J.-E.; Goulding, E. H.; Eddy, E. M.; Primakoff, P.; Myles, D. G., Fertilization defects in sperm from mice lacking fertilin β . *Science* **1998**, 281, 1857-1859.

56. Cho, C.; Ge, H.; Myles, D. G., Analysis of mouse fertilin in wild-type and fertilin beta-/- sperm: Evidence for C-terminal modification, alpha/beta dimerization and lack of essential role of fertilin alpha in sperm-egg fusion. *Dev. Biol.* **2000**, *222*, (2), 289-295.
57. Chen, M. S.; Almeida, E. A. C.; Huovila, A.-P. J.; Takahashi, Y.; Shaw, L. M.; Mercurio, A. M.; White, J. M., Evidence that distinct states of the integrin $\alpha 6\beta 1$ interact with laminin and an ADAM. *J. Cell Biol.* **1999**, *144*, (3), 549-561.
58. Shamsadin, R.; Adham, I. M.; Nayernia, K.; Heinlein, U. A.; Oberwinkler, H.; Engel, W., Male mice deficient for germ-cell cyritestin are infertile. *Biol. Reprod.* **1999**, *61*, (6), 1445-51.
59. Howard, L.; Maciewicz, R. A.; Blobel, C. P., Cloning and characterization of ADAM28: evidence for autocatalytic pro-domain removal and for cell surface localization of mature ADAM28. *Biochem. J.* **2000**, *348*, 21-27.
60. Nishimura, H.; Kim, E.; Nakanishi, T.; Baba, T., Possible function of the ADAM1a/ADAM2 Fertilin complex in the appearance of ADAM3 on the sperm surface. *J. Biol. Chem.* **2004**, *279*, (33), 34957-62.
61. Kim, E.; Nishimura, H.; Baba, T., Differential localization of ADAM1a and ADAM1b in the endoplasmic reticulum of testicular germ cells and on the surface of epididymal sperm. *Biochem. Biophys. Res. Commun.* **2003**, *304*, (2), 313-319.
62. Kim, E.; Nishimura, H.; Iwase, S.; Yamagata, K.; Kashiwabara, S.; Baba, T., Synthesis, processing, and subcellular localization of mouse ADAM3 during spermatogenesis and epididymal sperm transport. *J. Reprod. Dev.* **2004**, *50*, (5), 571-578.
63. Stein, K. K.; Go, J. C.; Primakoff, P.; Myles, D. G., Defects in secretory pathway trafficking during sperm development in ADAM2 knockout mice. *Biol. Reprod.* **2005**, *73*, (5), 1032-1038.
64. Zhu, G. Z.; Myles, D. G.; Primakoff, P., Testase 1 (ADAM 24) a plasma membrane-anchored sperm protease implicated in sperm function during epididymal maturation or fertilization. *J. Cell Sci.* **2001**, *114*, (9), 1787-1794.
65. Primakoff, P.; Hyatt, H.; Tredick-Kline, J., Identification and purification of a sperm surface protein with a potential role in sperm-egg membrane fusion. *J. Cell Biol.* **1987**, *104*, 141-149.

66. Waters, S. J.; White, J. M., Biochemical and molecular characterization of bovine fertilin α and β (ADAM 1 and ADAM 2): A candidate sperm-egg binding/fusion complex. *Biol. Reprod.* **1997**, 56, 1245-1254.
67. Barker, H. L.; Perry, A. C. F.; Jones, R.; Hall, L., Sequence and expression of a monkey testicular transcript encoding tMDC I, a novel member of the metalloproteinase-like, disintegrin-like, cysteine-rich (MDC) protein family. *Biochim. Biophys. Acta* **1994**, 1218, 429-431.
68. Heinlein, U. A. O.; Wallat, S.; Senftleben, A.; Lemaire, L., Male germ cell expressed mouse gene TAZ83 encodes a putative, cysteine-rich transmembrane protein (cyritestin) sharing homologies with snake toxins and sperm-egg fusion proteins. *Dev. Growth Differ.* **1994**, 36, 49-58.
69. Gould, R. J.; Polokoff, M. A.; Friedman, P. A.; Huang, T. F.; Holt, J. C.; Cook, J. J.; Niewiarowski, S., Disintegrins - a Family of Integrin Inhibitory Proteins from Viper Venoms. *Proc. Soc. Exp. Biol. Med.* **1990**, 195, (2), 168-171.
70. McLane, M. A.; Marcinkiewicz, C.; Vijay-Kumar, S.; Wierzbicka-Patynowski, I.; Niewiarowski, S., Viper venom disintegrins and related molecules. *Proc. Soc. Exp. Biol. Med.* **1998**, 219, (2), 109-119.
71. Evans, J. P., Fertilin beta and other ADAMs as integrin ligands: insights into cell adhesion and fertilization. *Bioessays* **2001**, 23, (7), 628-39.
72. Nath, D.; Slocombe, P. M.; Stephens, P. E.; Warn, A.; Hutchinson, G. R.; Yamada, K. M.; Docherty, A. J. P.; Murphy, G., Interaction of metargidin (ADAM-15) with $\alpha(v)\beta(3)$ and $\alpha(5)\beta(1)$ integrins on different haemopoietic cells. *J. Cell Sci.* **1999**, 112, (4), 579-587.
73. Eto, K.; Huet, C.; Tarui, T.; Kupriyanov, S.; Liu, H.-Z.; Puzon-McLaughlin, W.; Zhang, X.-P.; Sheppard, D.; Engvall, E.; Takada, Y., Functional classification of ADAMs based on a conserved motif for binding to integrin $\alpha_9\beta_1$. *J. Biol. Chem.* **2002**, 277, 17804-17810.
74. Huovila, A. P. J.; Turner, A. J.; Pelto-Huikko, M.; Karkkainen, L.; Ortiz, R. M., Shedding light on ADAM metalloproteinases. *Trends Biochem. Sci.* **2005**, 30, (7), 413-422.
75. Novak, U., ADAM proteins in the brain. *J. Clin. Neurosci.* **2004**, 11, (3), 227-235.
76. White, J. M., ADAMs: modulators of cell-cell and cell-matrix interactions. *Curr. Opin. Cell Biol.* **2003**, 15, (5), 598-606.

77. Tomczuk, M.; Takahashi, Y.; Huang, J.; Murase, S.; Mistretta, M.; Klaffky, E.; Sutherland, A.; Bolling, L.; Coonrod, S.; Marcinkiewicz, C.; Sheppard, D.; Stepp, M. A.; White, J. M., Role of multiple beta1 integrins in cell adhesion to the disintegrin domains of ADAMs 2 and 3. *Exp. Cell Res.* **2003**, 290, (1), 68-81.
78. Bigler, D.; Takahashi, Y.; Chen, M. S.; Almeida, E. A.; Osbourne, L.; White, J. M., Sequence-specific interaction between the disintegrin domain of mouse ADAM 2 (fertilin beta) and murine eggs. Role of the alpha(6) integrin subunit. *J. Biol. Chem.* **2000**, 275, 11576-84.
79. Nath, D.; Slocombe, P. M.; Webster, A.; Stephens, P. E.; Docherty, A. J. P.; Murphy, G., Meltrin gamma (ADAM-9) mediates cellular adhesion through alpha6beta1 integrin, leading to a marked induction of fibroblast cell motility. *J. Cell Sci.* **2000**, 113, 2319.
80. Bridges, L. C.; Sheppard, D.; Bowditch, R. D., ADAM disintegrin-like domain recognition by the lymphocyte integrins alpha 4 beta 1 and alpha 4 beta 7. *Biochem. J.* **2005**, 387, 101-108.
81. Mahimkar, R. M.; Visaya, O.; Pollock, A. S.; Lovett, D. H., The disintegrin domain of ADAM9: a ligand for multiple beta 1 renal integrins. *Biochem. J.* **2005**, 385, 461-468.
82. Mazzocca, A.; Coppari, R.; De Franco, R.; Cho, J. Y.; Libermann, T. A.; Pinzani, M.; Toker, A., Secreted form of ADAM9 promotes carcinoma invasion through tumor-stromal interactions. *Cancer Res.* **2005**, 65, (11), 4728-4738.
83. Zhao, Z.; Gruszczynska-Biegala, J.; Chevront, T.; Yi, H.; von der Mark, H.; von der Mark, K.; Kaufman, S. J.; Zolkiewska, A., Interaction of the disintegrin and cysteine-rich domains of ADAM12 with integrin alpha7beta1. *Exp. Cell Res.* **2004**, 298, (1), 28-37.
84. Eto, K.; Puzon-McLaughlin, W.; Sheppard, D.; Sehara-Fujikisawa, A.; Zhang, X.-P.; Takada, Y., RGD-independent binding of integrin alpha9beta1 to the ADAM-12 and -15 disintegrin domains mediates cell-cell interaction. *J. Biol. Chem.* **2000**, 275, 34922-34930.
85. Lafuste, P.; Sonnet, C.; Chazaud, B.; Dreyfus, P. A.; Gherardi, R. K.; Wewer, U. M.; Authier, F. J., ADAM12 and alpha(9)beta(1) integrin are instrumental in human myogenic cell differentiation. *Mol. Biol. Cell* **2005**, 16, (2), 861-870.
86. Thodeti, C. K.; Frohlich, C.; Nielsen, C. K.; Takada, Y.; Fassler, R.; Albrechtsen, R.; Wewer, U. M., ADAM 12-mediated focal adhesion formation is differently regulated by beta 1 and beta 3 integrins. *Febs Lett.* **2005**, 579, (25), 5589-5595.

87. Horiuchi, K.; Weskamp, G.; Lum, L.; Hammes, H. P.; Cai, H.; Brodie, T. A.; Ludwig, T.; Chiusaroli, R.; Baron, R.; Preissner, K. T.; Manova, K.; Blobel, C. P., Potential role for ADAM15 in pathological neovascularization in mice. *Mol. Cell. Biol.* **2003**, 23, (16), 5614-5624.
88. Huang, J.; Bridges, L. C.; White, J. M., Selective modulation of integrin-mediated cell migration by distinct ADAM family members. *Mol. Biol. Cell* **2005**, 16, (10), 4982-4991.
89. Cal, S.; Freije, J. M. P.; Lopez, J. M.; Takada, Y.; Lopez-Otin, C., ADAM 23/MDC3, a human disintegrin that promotes cell adhesion via interaction with the alpha v beta 3 integrin through an RGD-independent mechanism. *Mol. Biol. Cell* **2000**, 11, (4), 1457-1469.
90. Evans, J. P., Sperm disintegrins, egg integrins, and other cell adhesion molecules of mammalian gamete plasma membrane interactions. *Front. Biosci.* **1999**, 4, D114-31.
91. Cuasnicu, P. S.; Ellerman, D. A.; Cohen, D. J.; Busso, D.; Morgenfeld, M. M.; Da Ros, V. G., Molecular mechanisms involved in mammalian gamete fusion. *Arch. Med. Res.* **2001**, 32, (6), 614-618.
92. Hardy, C. M.; Clarke, H. G.; Nixon, B.; Grigg, J. A.; Hinds, L. A.; Holland, M. K., Examination of the immunocontraceptive potential of recombinant rabbit fertilin subunits in rabbit. *Biol. Reprod.* **1997**, 57, (4), 879-886.
93. Evans, J. P.; Schultz, R. M.; Kopf, G. S., Characterization of the binding of recombinant mouse sperm fertilin α subunit to mouse eggs: evidence for function as a cell adhesion molecule in sperm-egg binding. *Dev. Biol.* **1997**, 187, (1), 94-106.
94. Evans, J. P.; Kopf, G. S.; Schultz, R. M., Characterization of the binding of recombinant mouse sperm fertilin β subunit to mouse eggs: evidence for adhesive activity via an egg β 1 integrin-mediated interaction. *Dev. Biol.* **1997**, 187, (1), 79-93.
95. Zhu, X.; Bansal, N. P.; Evans, J. P., Identification of key functional amino acids of the mouse fertilin beta (ADAM2) disintegrin loop for cell-cell adhesion during fertilization. *J. Biol. Chem.* **2000**, 275, 7677-83.
96. Takahashi, Y.; Bigler, D.; Ito, Y.; White, J. M., Sequence-specific interaction between the disintegrin domain of mouse ADAM 3 and murine eggs: role of beta1 Integrin-associated proteins CD9, CD81, and CD98. *Mol. Biol. Cell* **2001**, 12, 809-20.

97. Wong, G. E.; Zhu, X.; Prater, C. E.; Oh, E.; Evans, J. P., Analysis of fertilin {alpha} (ADAM1)-mediated sperm-egg cell adhesion during fertilization and identification of an adhesion-mediating sequence in the disintegrin-like domain. *J. Biol. Chem.* **2001**.
98. Zhu, X.; Evans, J. P., Analysis of the roles of RGD-binding integrins, alpha(4)/alpha(9) integrins, alpha(6) integrins, and CD9 in the interaction of the fertilin beta (ADAM2) disintegrin domain with the mouse egg membrane. *Biol. Reprod.* **2002**, 66, 1193-1202.
99. Almeida, E. A. C.; Huovila, A. P. J.; Sutherland, A. E.; Stephens, L. E.; Calarco, P. G.; Shaw, L. M.; Mercurio, A. M.; Sonnenberg, A.; Primakoff, P.; Myles, D. G.; White, J. M., Mouse egg integrin $\alpha_6\beta_1$ functions as a sperm receptor. *Cell* **1995**, 81, (7), 1095-1104.
100. Evans, J. P.; Schultz, R. M.; Kopf, G. S., Mouse sperm-egg plasma membrane interactions: analysis of roles of egg integrins and the mouse sperm homologue of PH-30 (fertilin) β . *J. Cell Sci.* **1995**, 108, (10), 3267-3278.
101. Gupta, S.; Li, H.; Sampson, N. S., Characterization of fertilin β -disintegrin binding specificity in sperm-egg adhesion. *Bioorg. Med. Chem.* **2000**, 8, 723-729.
102. McLaughlin, E. A.; Frayne, J.; Bloomerg, G.; Hall, L., Do fertilin beta and cyritestin play a major role in mammalian sperm--oolemma interactions? A critical re-evaluation of the use of peptide mimics in identifying specific oocyte recognition proteins. *Mol. Hum. Reprod.* **2001**, 7, (4), 313-7.
103. McLaughlin, E. A.; Frayne, J.; Barker, H. L.; Jury, J. A.; Jones, R.; Ford, W. C. L.; Hall, L., Cloning and sequence analysis of rat fertilin α and β - developmental expression, processing and immunolocalization. *Mol. Hum. Reprod.* **1997**, 3, 801-809.
104. Phelps, B. M.; Koppel, D. E.; Primakoff, P.; Myles, D. G., Evidence that proteolysis of the surface is an initial step in the mechanism of formation of sperm cell-surface domains. *J. Cell Biol.* **1990**, 111, (5), 1839-1847.
105. Pyluck, A.; Yuan, R.; Galligan Jr., E.; Primakoff, P.; Myles, D. G.; Sampson, N. S., ECD peptides inhibit *in vitro* fertilization in mice. *Bioorg. Med. Chem. Lett.* **1997**, 7, 1053-1058.
106. Nishimura, H.; Cho, C.; Branciforte, D. R.; Myles, D. G.; Primakoff, P., Analysis of loss of adhesive function in sperm lacking cyritestin or fertilin β . *Dev. Biol.* **2001**, 233, 204-213.

107. Nishimura, H.; Myles, D. G.; Primakoff, P., Identification of an ADAM2-ADAM3 complex on the surface of mouse testicular germ cells and cauda epididymal sperm. *J. Biol. Chem.* **2007**, 282, (24), 17900-17907.
108. Kim, E.; Yamashita, M.; Nakanishi, T.; Park, K. E.; Kimura, M.; Kashiwabara, S.; Baba, T., Mouse sperm lacking ADAM1b/ADAM2 fertilin can fuse with the egg plasma membrane and effect fertilization. *J. Biol. Chem.* **2006**, 281, (9), 5634-5639.
109. Wolfsberg, T. G.; Primakoff, P.; Myles, D. G.; White, J. M., ADAM, a novel family of membrane proteins containing a disintegrin and metalloprotease domain: multipotential functions in cell-cell and cell-matrix interactions. *J. Cell Biol.* **1995**, 131, (2), 275-278.
110. Cameo, M. S.; Glaquier, J. A., Androgen-controlled specific proteins in rat epididymis. *J. Endocrinol.* **1976**, 69, (1), 47-55.
111. Foster, J. A.; Gerton, G. L., Autoantigen 1 of the guinea pig sperm acrosome is the homologue of mouse Tpx-1 and human TPX1 and is a member of the cysteine-rich secretory protein (CRISP) family. *Mol. Reprod. Dev.* **1996**, 44, (2), 221-229.
112. Mizuki, N.; Kasahara, M., Mouse submandibular glands express an androgen-regulated transcript encoding an acidic epididymal glycoprotein-like molecule. *Mol. Cell. Endocrinol.* **1992**, 89, (1-2), 25-32.
113. Haendler, B.; Kratzschmar, J.; Theuring, F.; Schleuning, W. D., Transcripts for cysteine-rich secretory protein-1 (Crisp-1, De/Aeg) and the novel related crisp-3 are expressed under androgen control in the mouse salivary-gland. *Endocrinology* **1993**, 133, (1), 192-198.
114. Cohen, D. J.; Ellerman, D. A.; Cuasnicu, P. S., Mammalian sperm-egg fusion: Evidence that epididymal protein DE plays a role in mouse gamete fusion. *Biol. Reprod.* **2000**, 63, (2), 462-468.
115. Rochwerger, L.; Cohen, D. J.; Cuasnicu, P. S., Mammalian sperm-egg fusion: the rat egg has complementary sites for a sperm protein that mediates gamete fusion. *Dev. Biol.* **1992**, 153, (1), 83-90.
116. Cuasnicu, P. S., Conesa, D. and Rochwerger, L., *Potential contraceptive use of an epididymal protein that participates in fertilization*. Wiley-Liss, New York, USA: 1990.

117. Okabe, M.; Adachi, T.; Takada, K.; Oda, H.; Yagasaki, M.; Kohama, Y.; Mimura, T., Capacitation-related changes in antigen distribution on mouse sperm heads and its relation to fertilization rate in vitro. *J. Reprod. Immunol.* **1987**, 11, (2), 91-100.
118. Xiong, J.; Stehle, T.; Diefenbach, B.; Zhang, R.; Dunker, R.; Scott, D.; Joachimiak, A.; Goodman, S.; Arnaout, M., Crystal structure of the extracellular segment of integrin α V β 3. *Science* **2001**, 294, 339-45.
119. Humphries, M. J.; McEwan, P. A.; Barton, S. J.; Buckley, P. A.; Bella, J.; Mould, A. P., Integrin structure: heady advances in ligand binding, but activation still makes the knees wobble. *Trends Biochem. Sci.* **2003**, 28, (6), 313-320.
120. Almeida, E. A.; Huovila, A. P.; Sutherland, A. E.; Stephens, L. E.; Calarco, P. G.; Shaw, L. M.; Mercurio, A. M.; Sonnenberg, A.; Primakoff, P.; Myles, D. G.; White, J. M., Mouse egg integrin α 6 β 1 functions as a sperm receptor. *Cell* **1995**, 81, (7), 1095-104.
121. Miller, B. J.; Georges-Labouesse, E.; Primakoff, P.; Myles, D. G., Normal fertilization occurs with eggs lacking the integrin α 6 β 1 and is CD9-dependent. *J. Cell Biol.* **2000**, 149, 1289-96.
122. Chen, H.; Sampson, N. S., Mediation of sperm-egg fusion: evidence that mouse egg α 6 β 1 integrin is the receptor for sperm fertilin β . *Chem. Biol.* **1999**, 6, 1-10.
123. Konkar, S., Understanding mammalian fertilization at the molecular level by investigating the proteins involved in sperm-egg plasma membrane interactions. Ph. D. Thesis, Stony Brook University, Stony Brook, 2003.
124. Stanton, J. L.; Green, D. P. L., A set of 840 mouse oocyte genes with well-matched human homologues. *Mol. Hum. Reprod.* **2001**, 7, (6), 521-543.
125. He, Z.-Y.; Brakebusch, C.; Fässler, R.; Kreidberg, J. A.; Primakoff, P.; Myles, D. G., None of the integrins known to be present on the mouse egg or to be ADAM receptors are essential for sperm-egg binding and fusion. *Dev. Biol.* **2003**, 254, 226-237.
126. Hemler, M. E., Tetraspanin functions and associated microdomains. *Nat. Rev. Mol. Cell Biol.* **2005**, 6, (10), 801-811.
127. Kitadokoro, K.; Bordo, D.; Galli, G.; Petracca, R.; Falugi, F.; Abrignani, S.; Grandi, G.; Bolognesi, M., CD81 extracellular domain 3D structure: insight into the tetraspanin superfamily structural motifs. *Embo J.* **2001**, 20, (1-2), 12-18.

128. Stipp, C. S.; Kolesnikova, T. V.; Hemler, M. E., Functional domains in tetraspanin proteins. *Trends Biochem. Sci.* **2003**, 28, (2), 106-112.
129. Boucheix, C.; Rubinstein, E., Tetraspanins. *Cell. Mol. Life Sci.* **2001**, 58, (9), 1189-1205.
130. Hemler, M., Specific tetraspanin functions. *J. Cell Biol.* **2001**, 155, (7), 1103-7.
131. Hemler, M. E., Tetraspanin proteins mediate cellular penetration, invasion, and fusion events and define a novel type of membrane microdomain. *Ann. Rev. Cell Dev. Biol.* **2003**, 19, 397-422.
132. Hemler, M. E., Integrin associated proteins. *Curr. Opin. Cell Biol.* **1998**, 10, (5), 578-585.
133. Berditchevski, F.; Odintsova, E., Characterization of integrin-tetraspanin adhesion complexes: Role of tetraspanins in integrin signaling. *J. Cell Biol.* **1999**, 146, (2), 477-492.
134. Woods, A.; Couchman, J. R., Integrin modulation by lateral association. *J. Biol. Chem.* **2000**, 275, (32), 24233-24236.
135. Kaji, K.; Oda, S.; Shikano, t.; Ohnuki, T.; Uematsu, Y.; Sakagami, J.; Tada, N.; Miyazaki, S.; Kudo, A., The gamete fusion process is defective in eggs of CD9-deficient mice. *Nat. Genet.* **2000**, 24, 279-282.
136. Le Naour, F.; Rubinstein, E.; Jasmin, C.; Prenant, M.; Boucheix, C., Severely reduced female fertility in CD9-deficient mice. *Science* **2000**, 287, 319-321.
137. Miyado, K.; Yamada, G.; Yamada, S.; Hasuwa, H.; Nakamura, Y.; Ryu, F.; Suzuki, K.; Kosai, K.; Inoue, K.; Ogura, A.; Okabe, M.; Mekada, E., Requirement of CD9 on the egg plasma membrane for fertilization. *Science* **2000**, 287, (321-324).
138. Chen, M. S.; Tunge, K. S. K.; Coonrod, S. A.; Takahashi, Y.; Bigler, D.; Change, A.; Yamashita, Y.; Kincade, P. W.; Herr, J. C.; White, J. M., Role of the integrin-associated protein CD9 in binding between sperm ADAM 2 and the egg integrin $\alpha_6\beta_1$: implications for murine fertilization. *Proc. Natl. Acad. Sci. U.S.A.* **1999**, 96, (21), 11830-11835.
139. Zhu, G. Z.; Miller, B. J.; Boucheix, C.; Rubinstein, E.; Liu, C. C.; Hynes, R. O.; Myles, D. G.; Primakoff, P., Residues SFQ (173-175) in the large extracellular loop of CD9 are required for gamete fusion. *Development* **2002**, 129, 1995-2002.

140. Vjugina, U.; Evans, J. P., New insights into the molecular basis of mammalian sperm-egg membrane interactions. *Front. Biosci.* **2008**, 13, 462-476.
141. Higginbottom, A.; Takahashi, Y.; Bolling, L.; Coonrod, S. A.; White, J. M.; Partridge, L. J.; Monk, P. N., Structural requirements for the inhibitory action of the CD9 large extracellular domain in sperm/oocyte binding and fusion. *Biochem. Biophys. Res. Commun.* **2003**, 311, (1), 208-214.
142. Lammerding, J.; Kazarov, A. R.; Huang, H.; Lee, R. T.; Hemler, M. E., Tetraspanin CD151 regulates alpha 6 beta 1 integrin adhesion strengthening. *Proc. Natl. Acad. Sci. U. S. A.* **2003**, 100, (13), 7616-7621.
143. Rubinstein, E.; Ziyat, A.; Prenant, M.; Wrobel, E.; Wolf, J. P.; Levy, S.; Le Naour, F.; Boucheix, C., Reduced fertility of female mice lacking CD81. *Dev. Biol.* **2006**, 290, (2), 351-358.
144. Kaji, K.; Oda, S.; Miyazaki, S.; Kudo, A., Infertility of CD9-deficient mouse eggs is reversed by mouse CD9, human CD9, or mouse CD81; polyadenylated mRNA injection developed for molecular analysis of sperm-egg fusion. *Dev. Biol.* **2002**, 247, (2), 327-334.
145. Tiede, A.; Nischan, C.; Schubert, J.; Schmidt, R. E., Characterisation of the enzymatic complex for the first step in glycosylphosphatidylinositol biosynthesis. *Int. J. Biochem. Cell Biol.* **2000**, 32, (3), 339-350.
146. Alfieri, J. A.; Martin, A. D.; Takeda, J.; Kondoh, G.; Myles, D. G.; Primakoff, P., Infertility in female mice with an oocyte-specific knockout of GPI-anchored proteins. *J. Cell Sci.* **2003**, 116, (Pt 11), 2149-55.
147. Coonrod, S. A.; Naaby-Hansen, S.; Shetty, J.; Shibahara, H.; Chen, M.; White, J. M.; Herr, J. C., Treatment of mouse oocytes with PI-PLC releases 70-kDa (pI 5) and 35- to 45-kDa (pI 5.5) protein clusters from the egg surface and inhibits sperm-oolemma binding and fusion. *Dev. Biol.* **1999**, 207, (2), 334-49.
148. Hooper, N. M., Glycosyl-phosphatidylinositol anchored membrane enzymes. *Clin. Chim. Acta* **1997**, 266, (1), 3-12.
149. Hooper, N. M., Determination of glycosyl-phosphatidylinositol membrane protein anchorage. *Proteomics* **2001**, 1, (6), 748-755.
150. Di Cecca, A.; Freire, J. J., Simulation of diffusion and relaxations of non-dilute star chains. *Polymer* **2003**, 44, (8), 2589-2597.

151. Schulte-Frohlinde, V.; Holovatch, Y.; von Ferber, C.; Blumen, A., Scaling of star polymers: high order results. *Phys. Lett. A* **2004**, 328, (4-5), 335-340.
152. Mammen, M.; Choi, S.-K.; Whitesides, G. M., Polyvalent interactions in biological systems: implications for design and use of multivalent ligands and inhibitors. *Angew. Chem. Int. Ed. Engl.* **1998**, 37, 2754-2794.
153. Konkar, S.; Gupta, S.; Sampson, N. S., Fertilin β liposomes inhibit in vitro fertilization by steric blockage. *Bioorg. Med. Chem. Lett.* **2004**, 14, 1381-1384.
154. Lee, C. C.; MacKay, J. A.; Frechet, J. M. J.; Szoka, F. C., Designing dendrimers for biological applications. *Nat. Biotechnol.* **2005**, 23, (12), 1517-1526.
155. Lee, Y.; Sampson, N. S., Romping the cellular landscape: linear scaffolds for molecular recognition. *Curr. Opin. Struct. Biol.* **2006**, 16, (4), 544-550.
156. Crommelin, D. J. A.; Storm, G., Liposomes: From the bench to the bed. *J. Liposome Res.* **2003**, 13, (1), 33-36.
157. Senaratne, W.; Andruzzi, L.; Ober, C. K., Self-assembled monolayers and polymer brushes in biotechnology: Current applications and future perspectives. *Biomacromolecules* **2005**, 6, (5), 2427-2448.
158. Heredia, K. L.; Bontempo, D.; Ly, T.; Byers, J. T.; Halstenberg, S.; Maynard, H. D., In situ preparation of protein - "Smart" polymer conjugates with retention of bioactivity. *J. Am. Chem. Soc.* **2005**, 127, (48), 16955-16960.
159. Bontempo, D.; Li, R. C.; Ly, T.; Brubaker, C. E.; Maynard, H. D., One-step synthesis of low polydispersity, biotinylated poly(N-isopropylacrylamide) by ATRP. *Chem. Comm.* **2005**, (37), 4702-4704.
160. Mortell, K. H.; Gingras, M.; Kiessling, L. L., Synthesis of cell agglutination inhibitors by ring-opening metathesis polymerization. *J. Am. Chem. Soc.* **1994**, 116, 7248-7255.
161. Kanai, M.; Mortell, K. H.; Kiessling, L. L., Varying the size of multivalent ligands: the dependence of concanavalin A binding on neoglycopolymer length. *J. Am. Chem. Soc.* **1997**, 119, 9931-9932.
162. Cairo, C. W.; Gestwicki, J. E.; Kanai, M.; Kiessling, L. L., Control of multivalent interactions by binding epitope density. *J. Am. Chem. Soc.* **2002**, 124, (8), 1615-1619.

163. Maynard, H. D.; Okada, S. Y.; Grubbs, R. H., Inhibition of cell adhesion to fibronectin by oligopeptide-substituted polynorbornenes. *J. Am. Chem. Soc.* **2001**, 123, 1275-1279.
164. Roberts, K. S.; Sampson, N. S., Increased polymer length of oligopeptide-substituted polynorbornenes using LiCl. *J. Org. Chem.* **2003**, 68, 2020-2023.
165. Baessler, K. A.; Lee, Y.; Roberts, K. S.; Facompre, N.; Sampson, N. S., Multivalent fertilin beta oligopeptides: The dependence of fertilization inhibition on length and density. *Chem. Biol.* **2006**, 13, (3), 251-259.
166. Handl, H. L.; Vagner, J.; Han, H.; Mash, E.; Hruby, V. J.; Gillies, R. J., Hitting multiple targets with multimeric ligands. *Expert Opin. Ther. Targets* **2004**, 8, (6), 565-86.
167. Krishnamurthy, V. M.; Semetey, V.; Bracher, P. J.; Shen, N.; Whitesides, G. M., Dependence of effective molarity on linker length for an intramolecular protein-ligand system. *J. Am. Chem. Soc.* **2007**, 129, (5), 1312-1320.
168. Fan, E. K.; Zhang, Z. S.; Minke, W. E.; Hou, Z.; Verlinde, C. L. M. J.; Hol, W. G. J., High-affinity pentavalent ligands of Escherichia coli heat-labile enterotoxin by modular structure-based design. *J. Am. Chem. Soc.* **2000**, 122, (11), 2663-2664.
169. Kramer, R. H.; Karpen, J. W., Spanning binding sites on allosteric proteins with polymer-linked ligand dimers. *Nature* **1998**, 395, (6703), 710-713.
170. Loidl, G.; Musiol, H. J.; Groll, M.; Huber, R.; Moroder, L., Synthesis of bivalent inhibitors of eucaryotic proteasomes. *J. Pept. Sci.* **2000**, 6, (1), 36-46.
171. Rao, J. H.; Lahiri, J.; Isaacs, L.; Weis, R. M.; Whitesides, G. M., A trivalent system from vancomycin center dot D-Ala-D-Ala with higher affinity than avidin center dot biotin. *Science* **1998**, 280, (5364), 708-711.
172. Kiessling, L. L.; Strong, L. E.; Gestwicki, J. E., Principles for multivalent ligand design. *Annu. Rep. Med. Chem.* **2000**, 35, 321-330.
173. Semetey, V.; Moustakas, D.; Whitesides, G. M., Synthesis and conformational study of water-soluble, rigid, rodlike oligopiperidines. *Angew. Chem. Int. Ed.* **2006**, 45, (4), 588-591.
174. Wang, J. S.; Matyjaszewski, K., Controlled living radical polymerization - atom-transfer radical polymerization in the presence of transition-metal complexes. *J. Am. Chem. Soc.* **1995**, 117, (20), 5614-5615.

175. Chen, Y. M.; Wulff, G., Synthesis of poly(styryl sugar)s by TEMPO mediated free radical polymerization. *Macromol. Chem. Phys.* **2001**, 202, (17), 3426-3431.
176. Yoon, K. R.; Ramaraj, B.; Lee, S. M.; Kim, D. P., Surface initiated-atom transfer radical polymerization of a sugar methacrylate on gold nanoparticles. *Surf. Interface Anal.* **2008**, 40, (8), 1139-1143.
177. Ladmiral, V.; Mantovani, G.; Clarkson, G. J.; Cauet, S.; Irwin, J. L.; Haddleton, D. M., Synthesis of neoglycopolymers by a combination of "click chemistry" and living radical polymerization. *J. Am. Chem. Soc.* **2006**, 128, (14), 4823-4830.
178. Sumerlin, B. S.; Tsarevsky, N. V.; Louche, G.; Lee, R. Y.; Matyjaszewski, K., Highly efficient "click" functionalization of poly(3-azidopropyl methacrylate) prepared by ATRP. *Macromolecules* **2005**, 38, (18), 7540-7545.
179. Tsarevsky, N. V.; Bencherif, S. A.; Matyjaszewski, K., Graft copolymers by a combination of ATRP and two different consecutive click reactions. *Macromolecules* **2007**, 40, (13), 4439-4445.
180. Wagener, K. B.; Boncella, J. M.; Nel, J. G., Acyclic diene metathesis (Admet) polymerization. *Macromolecules* **1991**, 24, (10), 2649-2657.
181. Baughman, T. W.; Wagener, K. B., *Recent advances in ADMET polymerization*. Springer: Dramstadt, 2005; p 1-42.
182. Herisson, J. L.; Chauvin, Y., Transformation catalysis of olefins by tungsten complexes .2. telomerization of cyclic olefins in presence of acyclic olefins. *Makromol. Chem.* **1971**, 141, (Feb9), 161-176.
183. Bielawski, C. W.; Grubbs, R. H., Living ring-opening metathesis polymerization. *Prog. Polym. Sci.* **2007**, 32, (1), 1-29.
184. Benson, S. W.; Cruickshank, D. F. R.; Golden, D. M.; Haugen, G. R.; Oneal, H. E.; Rodgers, A. S.; Shaw, R.; Walsh, R., Additivity rules for estimation of thermochemical properties. *Chem. Rev.* **1969**, 69, (3), 279-&.
185. Szwarc, M., Living polymers. *Nature* **1956**, 178, (4543), 1168-1169.
186. Darling, T. R.; Davis, T. P.; Fryd, M.; Gridnev, A. A.; Haddleton, D. M.; Ittel, S. D.; Matheson, R. R.; Moad, G.; Rizzardo, E., Living polymerization: Rationale for uniform terminology. *J. Polym. Sci. A: Polym. Chem.* **2000**, 38, (10), 1706-1708.

187. Flory, P. J., Molecular size distribution in ethylene oxide polymers. *J. Am. Chem. Soc.* **1940**, 62, 1561-1565.
188. Matyjaszewski, K., Ranking living systems. *Macromolecules* **1993**, 26, (7), 1787-1788.
189. Tebbe, F. N.; Parshall, G. W.; Ovenall, D. W., Titanium-catalyzed olefin metathesis. *J. Am. Chem. Soc.* **1979**, 101, (17), 5074-5075.
190. Tebbe, F. N.; Parshall, G. W.; Reddy, G. S., Olefin homologation with titanium methylene-compounds. *J. Am. Chem. Soc.* **1978**, 100, (11), 3611-3613.
191. Klabunde, U.; Tebbe, F. N.; Parshall, G. W.; Harlow, R. L., Methylene exchange-reactions catalyzed by alkylidene derivatives of titanium and phosphorus. *J. Mol. Catal.* **1980**, 8, (1-3), 37-51.
192. Schrock, R. R.; Fellmann, J. D., Multiple metal-carbon bonds. 8. Preparation, characterization, and mechanism of formation of tantalum and niobium neopentylidene complexes, $M(\text{CH}_2\text{CMe}_3)_3(\text{CHCMe}_3)$. *J. Am. Chem. Soc.* **1978**, 100, (11), 3359-3370.
193. Rupprecht, G. A.; Messerle, L. W.; Fellmann, J. D.; Schrock, R. R., Multiple metal-carbon bonds. 15. Octahedral alkylidene complexes of niobium and tantalum by ligand-promoted alpha-abstraction. *J. Am. Chem. Soc.* **1980**, 102, (20), 6236-6244.
194. Wallace, K. C.; Dewan, J. C.; Schrock, R. R., Multiple metal-carbon bonds. v44. Isolation and characterization of the 1st simple tantalacyclobutane complexes. *Organometallics* **1986**, 5, (10), 2162-2164.
195. Rocklage, S. M.; Fellmann, J. D.; Rupprecht, G. A.; Messerle, L. W.; Schrock, R. R., Multiple metal-carbon bonds. 19. How niobium and tantalum complexes of the type- $M(\text{CHCMe}_3)(\text{Pr}_3)_2\text{Cl}_3$ can be modified to give olefin metathesis catalysts. *J. Am. Chem. Soc.* **1981**, 103, (6), 1440-1447.
196. Kress, J.; Wesolek, M.; Osborn, J. A., Tungsten(IV) carbenes for the metathesis of olefins - direct observation and identification of the chain carrying carbene complexes in a highly-active catalyst system. *J. Chem. Soc. Chem. Commun.* **1982**, (9), 514-516.
197. Kress, J.; Osborn, J. A., Tungsten carbene complexes in olefin metathesis - a cationic and chiral active species. *J. Am. Chem. Soc.* **1983**, 105, (20), 6346-6347.

198. Kress, J.; Osborn, J. A., Stereochemically nonrigid tungsten alkylidene complexes - barriers to rotation about the tungsten to carbon double-bond. *J. Am. Chem. Soc.* **1987**, 109, (13), 3953-3960.
199. Schrock, R. R.; Murdzek, J. S.; Bazan, G. C.; Robbins, J.; DiMare, M.; O'Regan, M., Synthesis of molybdenum imido alkylidene complexes and some reactions involving acyclic olefins. *J. Am. Chem. Soc.* **1990**, 112, 3875-3886.
200. Nguyen, S. T.; Johnson, L. K.; Grubbs, R. H.; Ziller, J. W., Ring-opening metathesis polymerization (ROMP) of norbornene by a group-VIII carbene complex in protic media. *J. Am. Chem. Soc.* **1992**, 114, (10), 3974-3975.
201. Coles, M. P.; Gibson, V. C.; Mazzariol, L.; North, M.; Teasdale, W. G.; Williams, C. M.; Zamuner, D., Amino-acid derived homochiral polymers via ring-opening metathesis polymerization. *J. Chem. Soc. Chem. Commun.* **1994**, (21), 2505-2506.
202. Biagini, S. C. G.; Coles, M. P.; Gibson, V. C.; Giles, M. R.; Marshall, E. L.; North, M., Living ring-opening metathesis polymerisation of amino ester functionalised norbornenes. *Polymer* **1998**, 39, (5), 1007-1014.
203. Bazan, G. C.; Schrock, R. R., Synthesis of star block copolymers by controlled ring-opening metathesis polymerization. *Macromolecules* **1991**, 24, (4), 817-823.
204. Bazan, G.; Schrock, R. R.; Khosravi, E.; Feast, W. J.; Gibson, V. C., Living and highly stereoregular ring-opening polymerization of 5,6-difunctionalized norbornadienes by a well-characterized molybdenum catalyst. *Polym. Commun.* **1989**, 30, 258.
205. Bazan, G. C.; Khosravi, E.; Schrock, R. R.; Feast, W. J.; Gibson, V. C.; Oregan, M. B.; Thomas, J. K.; Davis, W. M., Living ring-opening metathesis polymerization of 2,3-difunctionalized norbornadienes by Mo(Ch-Tert-Bu)(N-2,6-C6h3-Iso-Pr2)(O-Tert-Bu)2. *J. Am. Chem. Soc.* **1990**, 112, (23), 8378-8387.
206. Feast, W. J.; Gibson, V. C.; Marshall, E. L., A remarkable ancillary ligand effect in living ring-opening metathesis polymerization. *J. Chem. Soc. Chem. Commun.* **1992**, (16), 1157-1158.
207. Mcconville, D. H.; Wolf, J. R.; Schrock, R. R., Synthesis of chiral molybdenum ROMP initiators and all-cis highly tactic poly(2,3-(R)2norbornadiene) (R = Cf3 or Co2me). *J. Am. Chem. Soc.* **1993**, 115, (10), 4413-4414.
208. Dallasta, G.; Mazzanti, G.; Natta, G.; Porri, L., Anionic-coordinated polymerization of cyclobutene. *Makromol. Chem.* **1962**, 56, 224-227.

209. Natta, G.; Dallasta, G.; Mazzanti, G.; Motroni, G., Stereospecific polymerization of cyclobutene. *Makromol. Chem.* **1963**, 69, 163-179.
210. Natta, G.; Dallasta, G.; Donegani, G.; Mazzanti, G., Stereospecific homopolymerization of cyclopentene. *Angew. Chem. Inter. Ed.* **1964**, 3, (11), 723-729.
211. Michelot, F.; Keaveney, W. P., Coordinated polymerization of bicyclo-[2.2.1]-heptene-2 ring system (Norbornene) in polar media. *J. Polym. Sci.* **1965**, 3, (3pa), 895-905.
212. Kroll, W. R.; Doyle, G., Carbene complexes of group-VI metals as olefin disproportionation catalysts. *J. Chem. Soc. D. Chem. Commun.* **1971**, (15), 839.
213. Pampus, G.; Lehnert, G., Cis-trans rearrangement of polypentenamer. *Makromol. Chem.* **1974**, 175, (9), 2605-2616.
214. Porri, L.; Rossi, R.; Diversi, P.; Lucherini, A., Ring-opening polymerization of cycloolefins with catalysts derived from ruthenium and iridium. *Makromol. Chem.* **1974**, 175, (11), 3097-3115.
215. Porri, L.; Diversi, P.; Lucherini, A.; Rossi, R., Catalysts derived from ruthenium and iridium for ring-opening polymerization of cycloolefins. *Makromol. Chem.* **1975**, 176, (10), 3121-3125.
216. Trnka, T. M.; Grubbs, R. H., The development of $L_2X_2Ru = CHR$ olefin metathesis catalysts: An organometallic success story. *Acc. Chem. Res.* **2001**, 34, (1), 18-29.
217. Novak, B. M.; Grubbs, R. H., The ring-opening metathesis polymerization of 7-oxabicyclo[2.2.1]hept-5-ene derivatives - a new acyclic polymeric ionophore. *J. Am. Chem. Soc.* **1988**, 110, (3), 960-961.
218. Bielawski, C. W.; Benitez, D.; Morita, T.; Grubbs, R. H., Synthesis of end-functionalized poly(norbornene)s via ring-opening metathesis polymerization. *Macromolecules* **2001**, 34, (25), 8610-8618.
219. Lynn, D. M.; Kanaoka, S.; Grubbs, R. H., Living ring-opening metathesis polymerization in aqueous media catalyzed by well-defined ruthenium carbene complexes. *J. Am. Chem. Soc.* **1996**, 118, 784-790.
220. Weck, M.; Schwab, P.; Grubbs, R. H., Synthesis of ABA triblock copolymers of norbornenes and 7-oxanorbornenes via living ring-opening metathesis

- polymerization using well-defined, bimetallic ruthenium catalysts. *Macromolecules* **1996**, 29, (5), 1789-1793.
221. Maughon, B. R.; Grubbs, R. H., Ruthenium alkylidene initiated living ring-opening metathesis polymerization (ROMP) of 3-substituted cyclobutenes. *Macromolecules* **1997**, 30, (12), 3459-3469.
222. Weck, M.; Mohr, B.; Maughon, B. R.; Grubbs, R. H., Synthesis of discotic columnar side-chain liquid crystalline polymers by ring-opening metathesis polymerization (ROMP). *Macromolecules* **1997**, 30, (21), 6430-6437.
223. Herrmann, W. A.; Kocher, C., N-heterocyclic carbenes. *Angew. Chem. Int. Ed. Engl.* **1997**, 36, (20), 2163-2187.
224. Weskamp, T.; Schattenmann, W. C.; Spiegler, M.; Herrmann, W. A., A novel class of ruthenium catalysts for olefin metathesis. *Angew. Chem. Int. Ed.* **1998**, 37, (18), 2490-2493.
225. Huang, J. K.; Schanz, H. J.; Stevens, E. D.; Nolan, S. P., Stereoelectronic effects characterizing nucleophilic carbene ligands bound to the Cp*RuCl (Cp* = eta(5)-C5Me5) moiety: A structural and thermochemical investigation. *Organometallics* **1999**, 18, (12), 2370-2375.
226. Arduengo, A. J., Looking for stable carbenes: The difficulty in starting anew. *Acc. Chem. Res.* **1999**, 32, (11), 913-921.
227. Bourissou, D.; Guerret, O.; Gabbai, F. P.; Bertrand, G., Stable carbenes. *Chem. Rev.* **2000**, 100, (1), 39-91.
228. Bielawski, C. W.; Grubbs, R. H., Highly efficient ring-opening metathesis polymerization (ROMP) using new ruthenium catalysts containing N-heterocyclic carbene ligands *Angew. Chem. Int. Ed. Engl.* **2000**, 39, (16), 2903-2906.
229. Sanford, M. S.; Love, J. A.; Grubbs, R. H., A versatile precursor for the synthesis of new ruthenium olefin metathesis catalysts. *Organometallics* **2001**, 20, (25), 5314-5318.
230. Love, J. A.; Sanford, M. S.; Day, M. W.; Grubbs, R. H., Synthesis, structure, and activity of enhanced initiators for olefin metathesis. *J. Am. Chem. Soc.* **2003**, 125, (33), 10103-10109.

231. Love, J. A.; Morgan, J. P.; Trnka, T. M.; Grubbs, R. H., A practical and highly active ruthenium-based catalyst that effects the cross metathesis of acrylonitrile. *Angew. Chem. Int. Ed. Engl.* **2002**, 41, (21), 4035-7.
232. Slugovc, C.; Demel, S.; Stelzer, F., Ring opening metathesis polymerisation in donor solvents. *Chem. Comm.* **2002**, (21), 2572-2573.
233. Frenzel, U.; Weskamp, T.; Kohl, F. J.; Schattenman, W. C.; Nuyken, O.; Herrmann, W. A., N-Heterocyclic carbenes: application of ruthenium-alkylidene complexes in ring-opening metathesis polymerization. *J. Organomet. Chem.* **1999**, 586, (2), 263-265.
234. Gestwicki, J. E.; Kiessling, L. L., Inter-receptor communication through arrays of bacterial chemoreceptors. *Nature* **2002**, 415, (6867), 81-84.
235. Siuzdak, G., *Mass spectrometry for biotechnology*. Academic Press, Inc.: San Diego, 1996.
236. Debye, P., Light scattering in solutions. *J. Appl. Phys.* **1944**, 15, (4), 338-342.
237. Zimm, B. H., The scattering of light and the radial distribution function of high polymer solutions. *J. Chem. Phys.* **1948**, 16, (12), 1093-1099.
238. Zimm, B. H., Molecular theory of the scattering of light in fluids. *J. Chem. Phys.* **1945**, 13, (4), 141-145.
239. Roberts, S. K.; Konkar, S.; Sampson, N. S., Comparison of fertilinbeta-peptide-substituted polymers and liposomes as inhibitors of in vitro fertilization. *ChemBioChem* **2003**, 4, (11), 1229-31.
240. Kiessling, L. L.; Pohl, N. L., Strength in numbers: Non-natural polyvalent carbohydrate derivatives. *Chem. Biol.* **1996**, 3, (2), 71-77.
241. Bertozzi, C. R.; Kiessling, L. L., Chemical glycobiology. *Science* **2001**, 291, (5512), 2357-2364.
242. Clemons, P. A., Design and discovery of protein dimerizers. *Curr. Opin. Chem. Biol.* **1999**, 3, (1), 112-115.
243. Scholl, M.; Ding, S.; Lee, C. W.; Grubbs, R. H., Synthesis and activity of a new generation of ruthenium-based olefin metathesis catalysts coordinated with 1,3-dimesityl-4,5-dihydroimidazol-2-ylidene ligands. *Org. Lett.* **1999**, 1, (6), 953-956.

244. Maynard, H. D.; Okada, S. Y.; Grubbs, R. H., Synthesis of norbornenyl polymers with bioactive oligopeptides by ring-opening metathesis polymerization. *Macromolecules* **2000**, *33*, 6239-6248.
245. Manning, D. D.; Strong, L. E.; Hu, X.; Beck, P. J.; Kiessling, L. L., Neoglycopolymer inhibitors of the selectins. *Tetrahedron* **1997**, *53*, 11937-11952.
246. Gestwicki, J. E.; Cairo, C. W.; Strong, L. E.; Oetjen, K. A.; Kiessling, L. L., Influencing receptor-ligand binding mechanisms with multivalent ligand architecture. *J. Am. Chem. Soc.* **2002**, *124*, (50), 14922-14933.
247. Lee, Y.; Baessler, K.; Sampson, N. S., ROMP of norbornyl oligopeptides: A versatile synthetic method for exploring receptor topology. In *Understanding Biology Using Peptides*, Blondelle, S., Ed. American Peptide Society: 2005.
248. Wu, Z.; Benedicto, A. D.; Grubbs, R. H., Living ring-opening metathesis polymerization of bicyclo[3.2.0]heptene catalyzed by a ruthenium alkylidene complex. *Macromolecules* **1993**, *26*, (18), 4975-4977.
249. Amir-Ebrahimi, V.; Corry, D. A.; Hamilton, J. G.; Thompson, J. M.; Rooney, J. J., Characteristics of RuCl₂(CHPh)(PCy₃)₂ as a catalyst for ring-opening metathesis polymerization. *Macromolecules* **2000**, *33*, (3), 717-724.
250. Lee, J. C.; Parker, K. A.; Sampson, N. S., Amino acid-bearing ROMP polymers with a stereoregular backbone. *J. Am. Chem. Soc.* **2006**, *128*, (14), 4578-4579.
251. Sanford, M. S.; Love, J. A.; Grubbs, R. H., Mechanism and activity of ruthenium olefin metathesis catalysts. *J. Am. Chem. Soc.* **2001**, *123*, (27), 6543-6554.
252. Sanford, M. S.; Valdez, M. R.; Grubbs, R. H., Reaction of Tp(PPh₃)Ru(h²-O₂CCHPh₂) with carbene and vinylidene precursors. *Organometallics* **2001**, *20*, (25), 5455-5463.
253. Sanford, M. S.; Ulman, M.; Grubbs, R. H., New insights into the mechanism of ruthenium-catalyzed olefin metathesis reactions. *J. Am. Chem. Soc.* **2001**, *123*, (4), 749-750.
254. Scherman, O. A.; Kim, H. M.; Grubbs, R. H., Synthesis of well-defined poly((vinyl alcohol)(2)-alt-methylene) via ring-opening metathesis polymerization. *Macromolecules* **2002**, *35*, (14), 5366-5371.
255. Wakamatsu, H.; Blechert, S., A highly active and air-stable ruthenium complex for olefin metathesis. *Angew. Chem. Int. Ed.* **2002**, *41*, (5), 794-+.

256. Wakamatsu, H.; Blechert, S., A new highly efficient ruthenium metathesis catalyst. *Angew. Chem. Int. Ed.* **2002**, 41, (13), 2403-2405.
257. Choi, T. L.; Grubbs, R. H., Controlled living ring-opening-metathesis polymerization by a fast-initiating ruthenium catalyst. *Angew. Chem. Int. Ed.* **2003**, 42, (15), 1743-1746.
258. Gupta, S.; Sampson, N. S., Dimyristoylated peptides incorporated into liposomes are polyvalent fertilin β mimics. *Org. Lett.* **2001**, 3, 3333-3335.
259. Myles, D. G.; Kimmel, L. H.; Blobel, C. P.; White, J. M.; Primakoff, P., Identification of a binding site in the disintegrin domain of fertilin required for sperm-egg fusion. *Proc. Natl. Acad. Sci. U. S. A.* **1994**, 91, (10), 4195-8.
260. Baessler, K. A.; Lee, Y.; Sampson, N. S., β_1 Integrin is an adhesion protein for sperm binding to eggs. *Submitted.* **2008**.
261. Prime, K. L.; Whitesides, G. M., Self-assembled organic monolayers - Model systems for studying adsorption of proteins at surfaces. *Science* **1991**, 252, (5009), 1164-1167.
262. Prime, K. L.; Whitesides, G. M., Adsorption of proteins onto surfaces containing end-attached oligo(ethylene oxide) - a model system using self-assembled monolayers. *J. Am. Chem. Soc.* **1993**, 115, (23), 10714-10721.
263. Lee, J., Probing ligand-receptor interactions in mammalian fertilization using ring opening metathesis polymerization. Ph. D. Thesis, Stony Brook University, Stony Brook, 2006.
264. Bonjour, J. P., Biotin in mans nutrition and therapy - Review. *Inter. J. Vit. Nutrit. Res.* **1977**, 47, (2), 107-118.
265. Green, N. M., Avidin .1. Use of [14 C]biotin for kinetic studies and for assay. *Biochem. J.* **1963**, 89, (3), 585-&.
266. Green, N. M., Avidin .3. Nature of biotin-binding site. *Biochem. J.* **1963**, 89, (3), 599-&.
267. Strong, L. E.; Kiessling, L. L., A general synthetic route to defined, biologically active multivalent arrays. *J. Am. Chem. Soc.* **1999**, 121, 6193-6196.

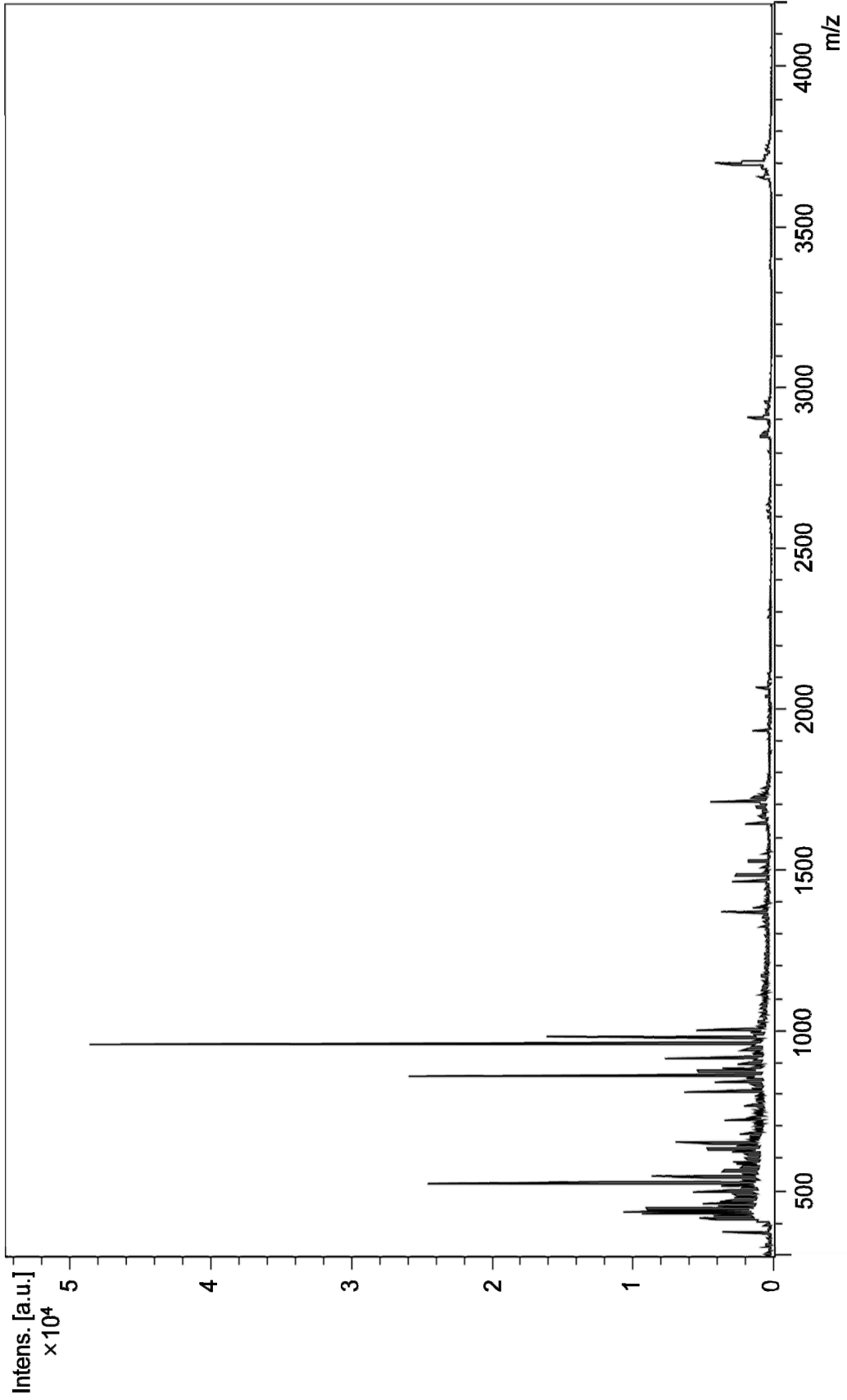
268. Lee, Y.; Sampson, N. S., Polymeric ADAM protein mimics interrogate mammalian sperm-egg binding. *Submitted*. **2008**.
269. Brakebusch, C.; Grose, R.; Quondamatteo, F.; Ramirez, A.; Jorcano, J. L.; Pirro, A.; Svensson, M.; Herken, R.; Sasaki, T.; Timpl, R.; Werner, S.; Fassler, R., Skin and hair follicle integrity is crucially dependent on beta 1 integrin expression on keratinocytes. *Embo J*. **2000**, 19, (15), 3990-4003.
270. Potocnik, A. J.; Brakebusch, C.; Fassler, R., Fetal and adult hematopoietic stem cells require beta 1 integrin function for colonizing fetal liver, spleen, and bone marrow. *Immunity* **2000**, 12, (6), 653-663.
271. Weerapana, E.; Speers, A. E.; Cravatt, B. F., Tandem orthogonal proteolysis-activity-based protein profiling (TOP-ABPP) - a general method for mapping sites of probe modification in proteomes. *Nature Prot*. **2007**, 2, (6), 1414-1425.

Appendix

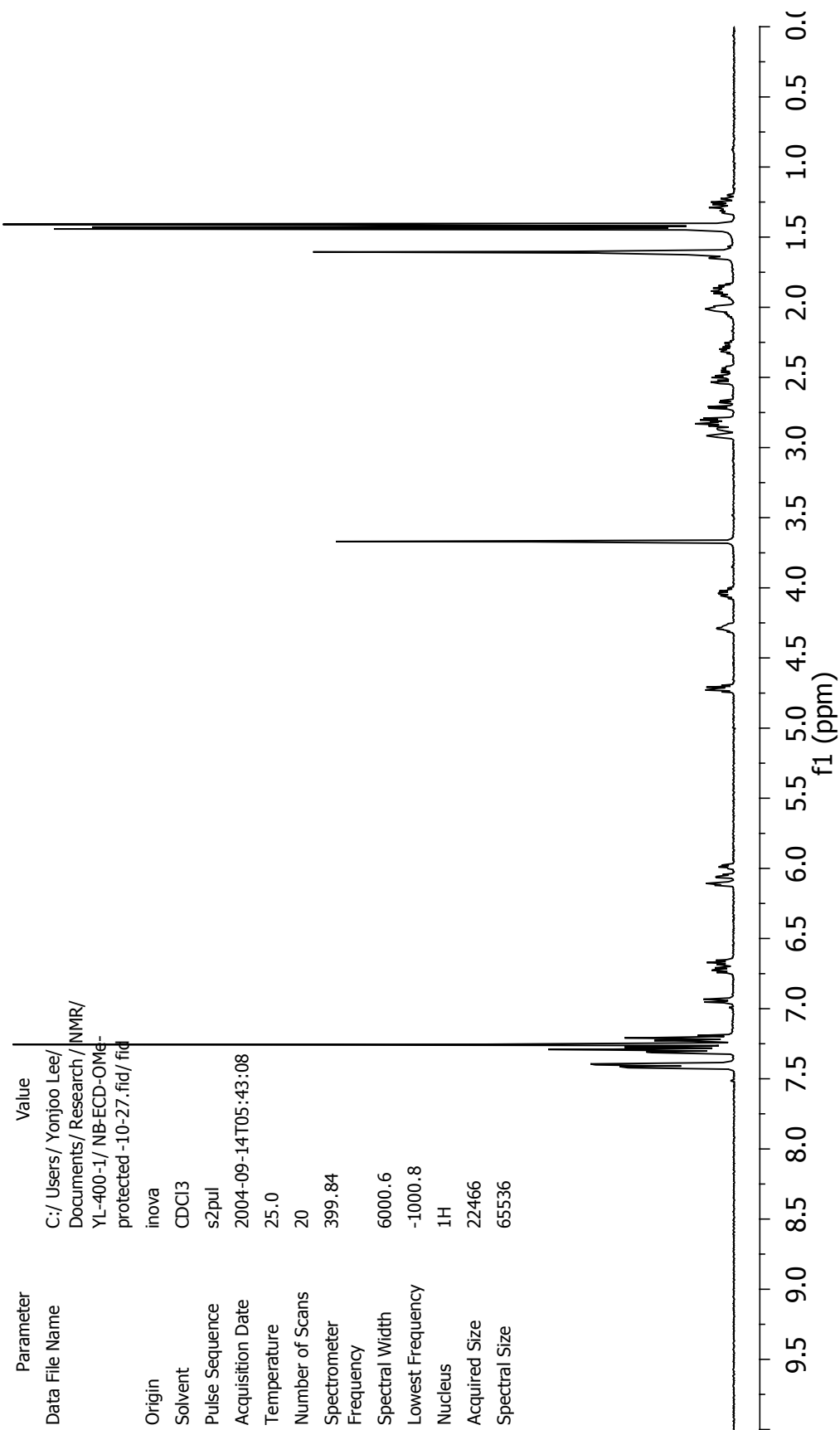
A-1: Checklist for compounds

Compound	Ref.	¹ H NMR	¹³ C NMR	Other
4	165	O		
5	165	O		
7	165	O		
8	165			ESI-MS
9	165	O	O	
11	165	O		
12	165	O		
13	165	O	O	
14	268	O		
16				ESI-MS
18	268	O	O	
19		O		
20		O		
21		O		
22		O		
23'		O		
24'		O		
25'		O		
26		O		
28		O		
30				ESI-MS
31				ESI-MS
33				ESI-MS
34				ESI-MS
35				ESI-MS
36				ESI-MS
37				ESI-MS
38				ESI-MS
39				ESI-MS

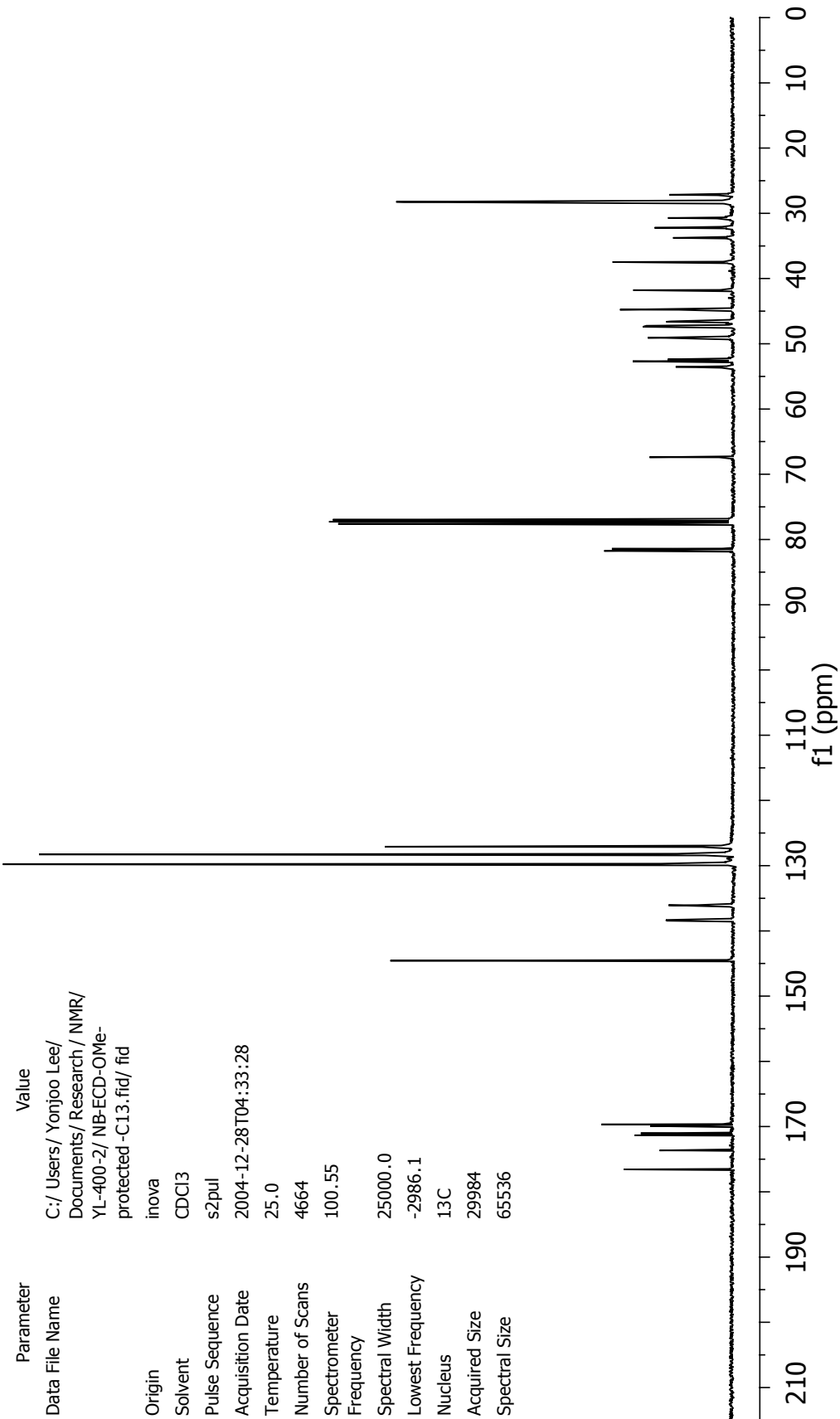
Compound	Ref.	¹ H NMR	¹³ C NMR	Other
40				ESI-MS
42				ESI-MS
43		O		ESI-MS
9₁₀-[2]	165	O		
9₃-[2]		O		
9₁₀'-[2]-a	268	O		
9₁₀₀'-[2]		O		
9₃-[3]	165	O		
9₆-[3]	165	O		
9₁₀-[3]	165	O		
9₁₀₀-[3]	268	O		
13₁₀-[3]	268	O		
13₁₀₀-[3]	268	O		
18₁-[3]				MALDI-TOF
18₂-[3]	268			MALDI-TOF
18₃-[3]	268	O		
18₆-[3]	268	O		
18₁₀-[3]	268	O		
18₁₀₀-[3]	268	O		
21₁₀-[3]		O		
22₁₀-[2]-a		O		
22₁₀-[2]-b		O		
22₁₀-[3]-c		O		
9₂-13₉₆-9₂-[3]	268	O		
18₂-13₉₆-18₂-[3]	268	O		
9₂-13₉₆-18₂-[3]	268	O		
47		O		
48		O		
49		O		



A-2: MALDI-TOF mass spectrum of photo-affinity labeling mouse oocyte with fertilin β mimic polymer after immunoprecipitation and trypsin digestion

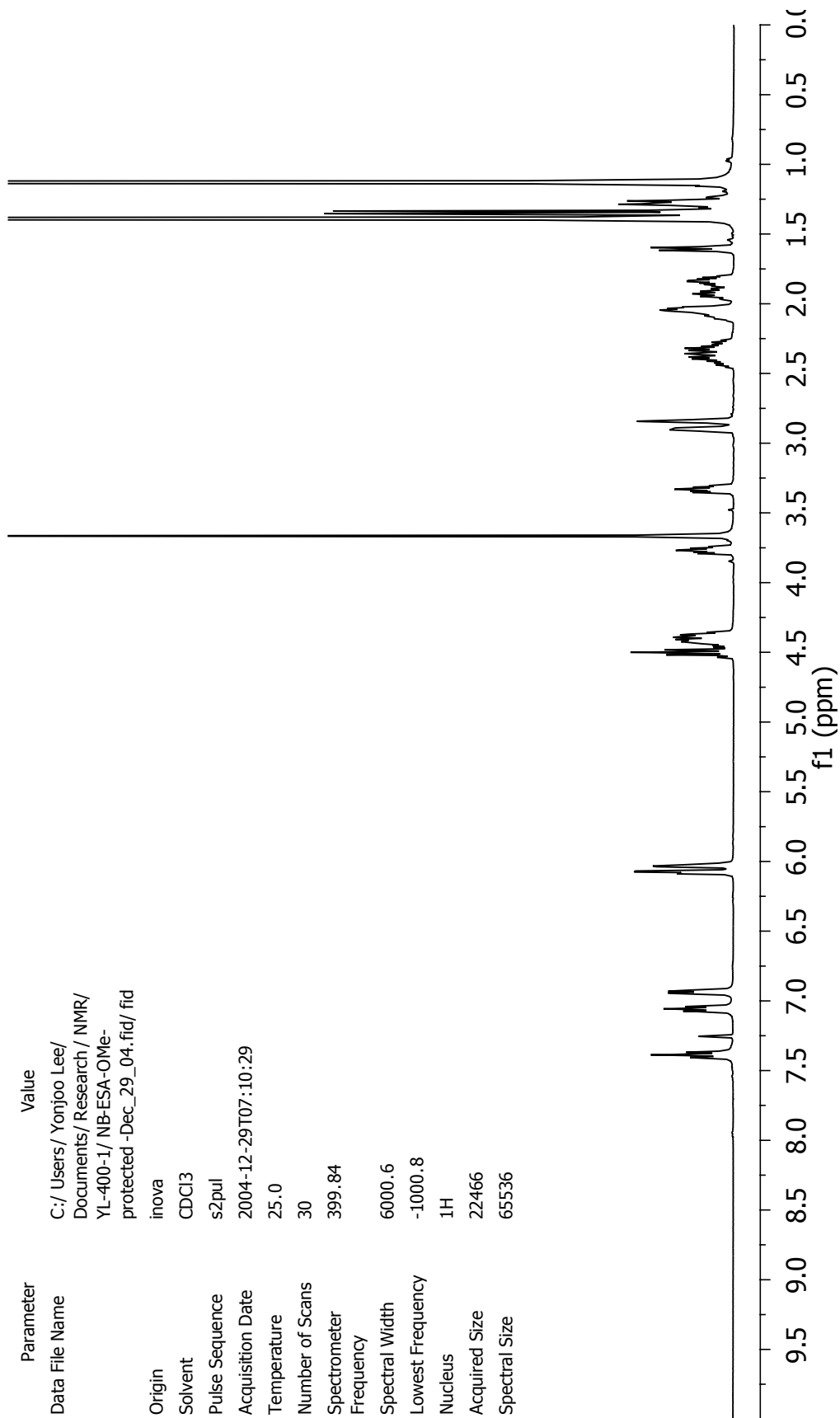


A-3: ¹H-NMR spectrum of NB-Glu(OtBu)Cys(Trt)Asp(OtBu)-OMe, 9

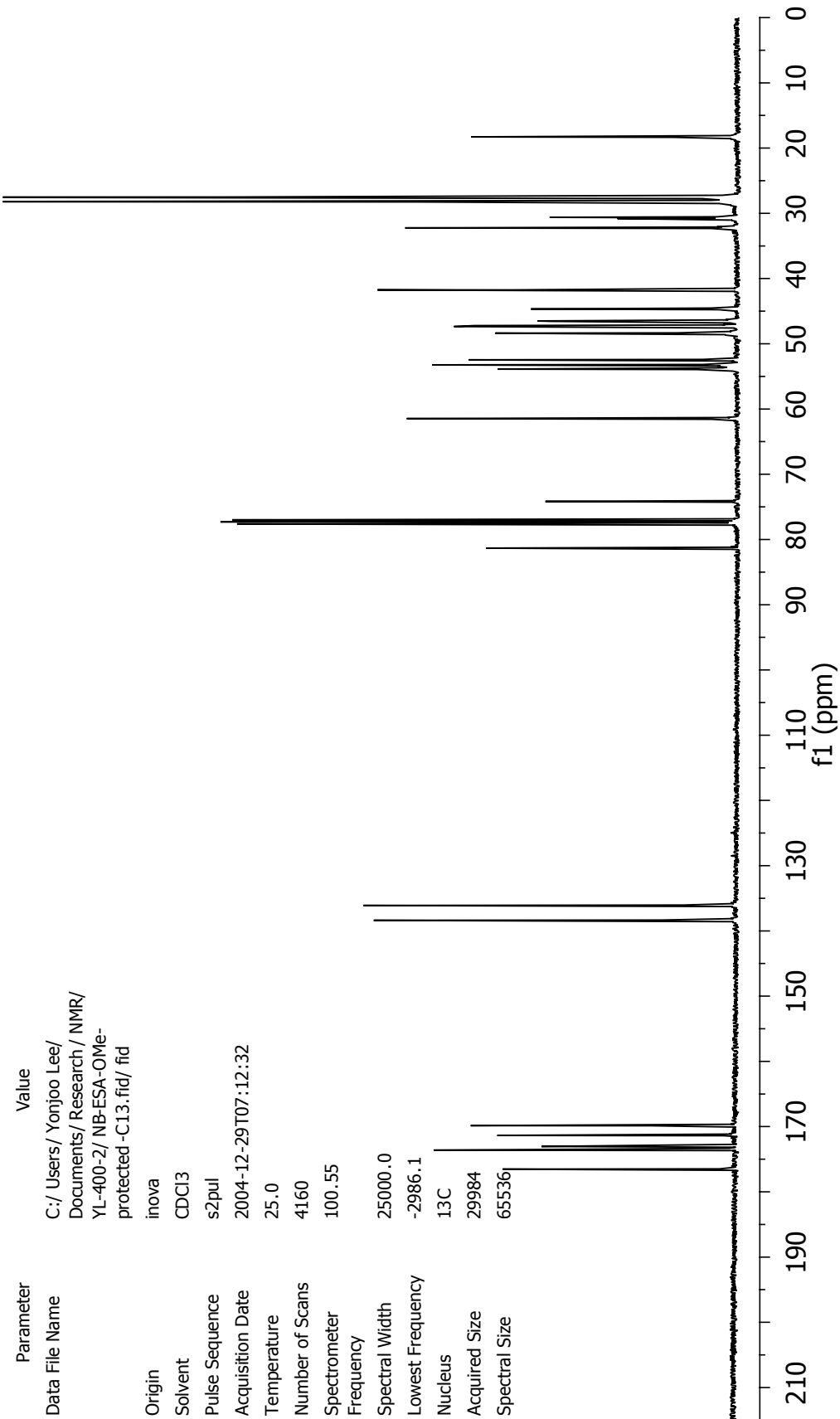


A-4: ^{13}C -NMR spectrum of NB-Glu(OtBu)Cys(Trt)Asp(OtBu)-OMe, 9

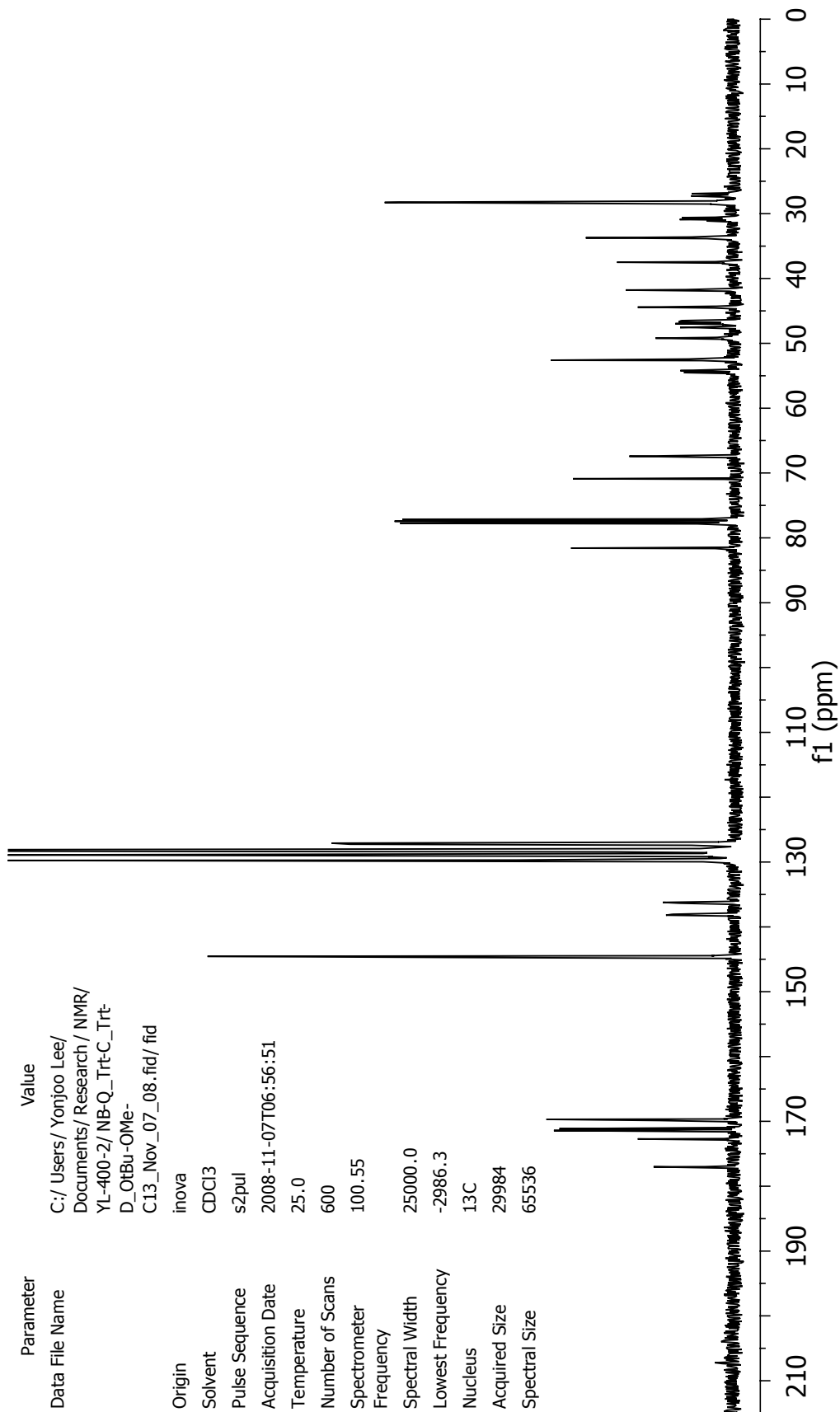
Parameter	Value
Data File Name	C:/Users/Yonjoo Lee/Documents/Research/NMR/YL-400-1/NB-ESA-OMe-protected-Dec_29_04.fid/ fid
Origin	inova
Solvent	CDCl3
Pulse Sequence	s2pul
Acquisition Date	2004-12-29T07:10:29
Temperature	25.0
Number of Scans	30
Spectrometer	399.84
Frequency	6000.6
Spectral Width	-1000.8
Lowest Frequency	1H
Nucleus	22466
Acquired Size	65536
Spectral Size	



A-5: ¹H-NMR spectrum of NB-Glu(OtBu)Ser(tBu)Ala-OMe, 13

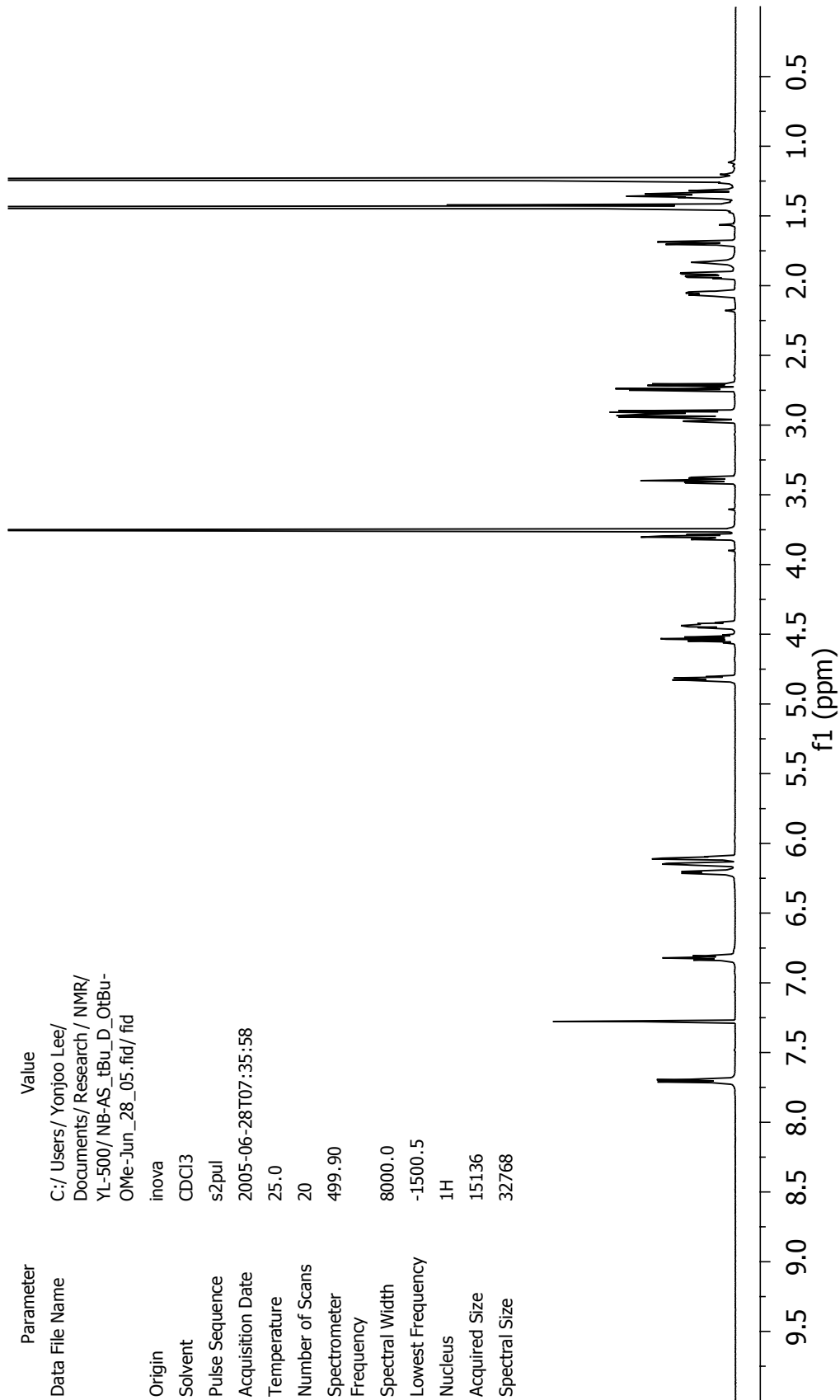


A-6: ^{13}C -NMR spectrum of NB-Glu(OtBu)Ser(tBu)Ala-OMe, 13



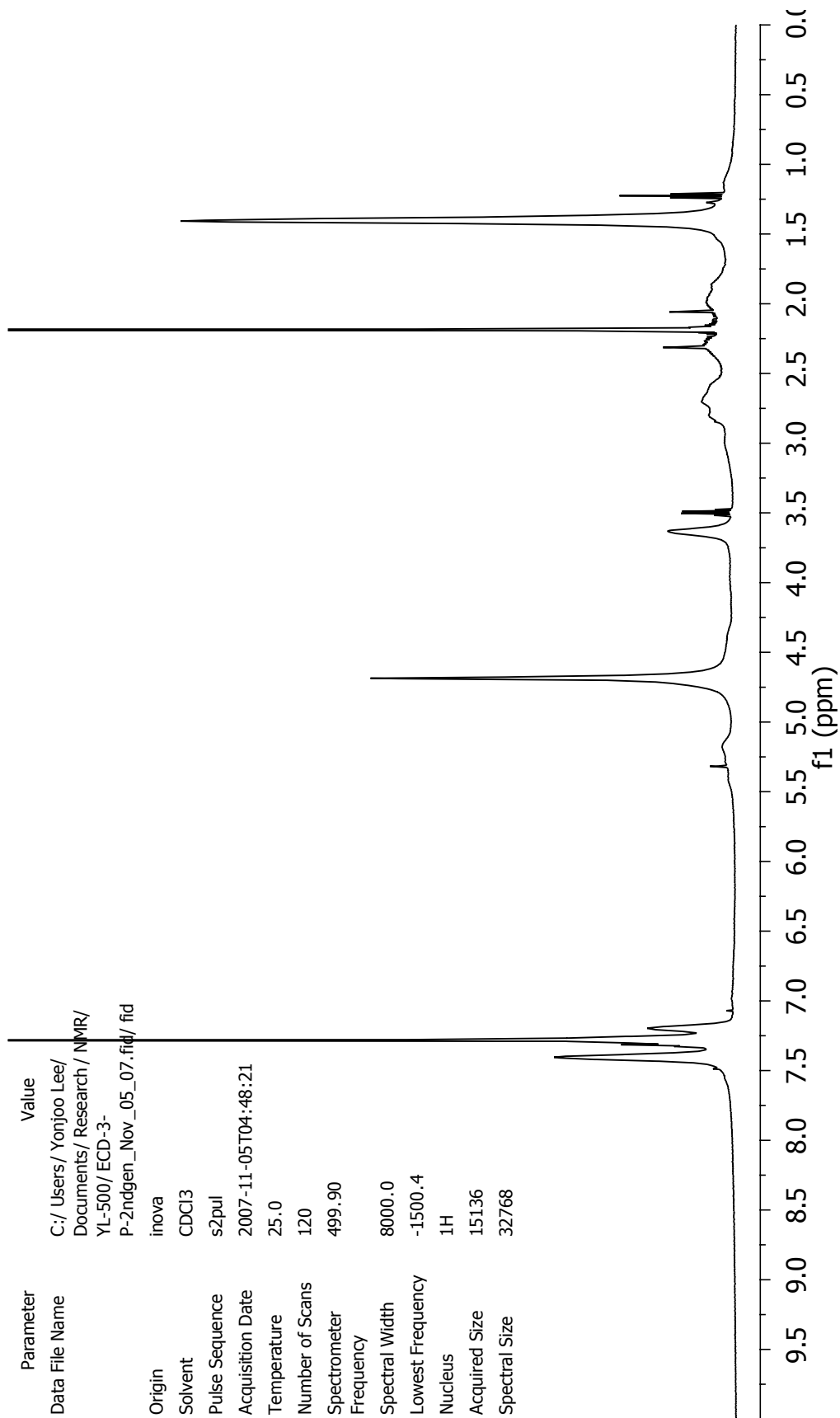
A-8: ¹³C-NMR spectrum of NB-Gln(Trt)Cys(Trt)Asp(OtBu)-OMe, 18

Parameter	Value
Data File Name	C:/Users/Yonjoo Lee/Documents/Research/NMR/YL-500/NB-AS_tBu_D_OtBu-OMe-Jun_28_05.fid/ fid
Origin	inova
Solvent	CDCl3
Pulse Sequence	s2pul
Acquisition Date	2005-06-28T07:35:58
Temperature	25.0
Number of Scans	20
Spectrometer	499.90
Frequency	8000.0
Spectral Width	-1500.5
Lowest Frequency	1H
Nucleus	15136
Acquired Size	32768
Spectral Size	



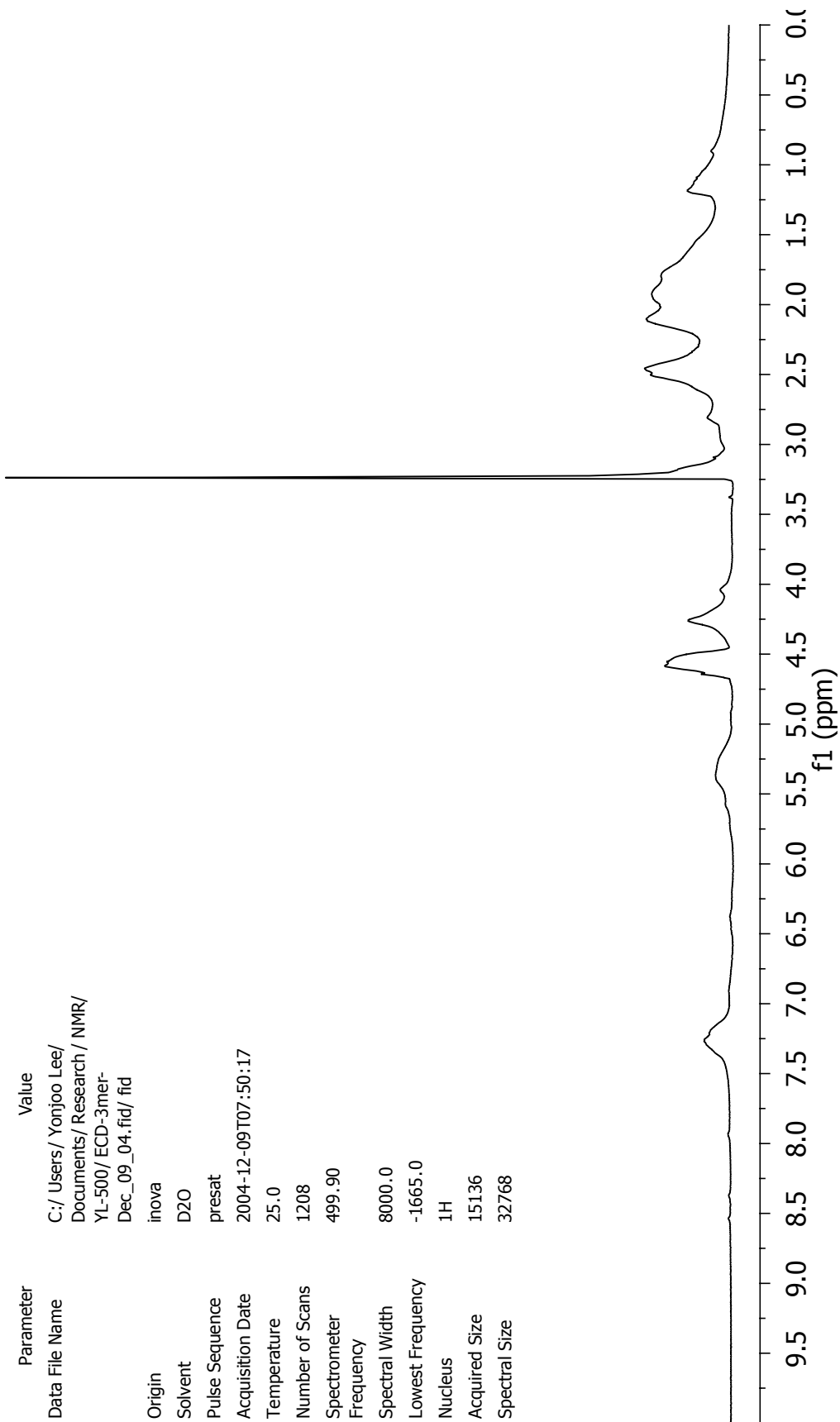
A-9: ¹H-NMR spectrum of NB-AlaSer(tBu)Asp(OtBu)-OMe, 21

Parameter	Value
Data File Name	C:/Users/Yonjoo Lee/Documents/Research/NMR/YL-500/ECD-3-P-2ndgen_Nov_05_07.fid/ fid
Origin	inova
Solvent	CDCl3
Pulse Sequence	s2pul
Acquisition Date	2007-11-05T04:48:21
Temperature	25.0
Number of Scans	120
Spectrometer Frequency	499.90
Spectral Width	8000.0
Lowest Frequency	-1500.4
Nucleus	1H
Acquired Size	15136
Spectral Size	32768



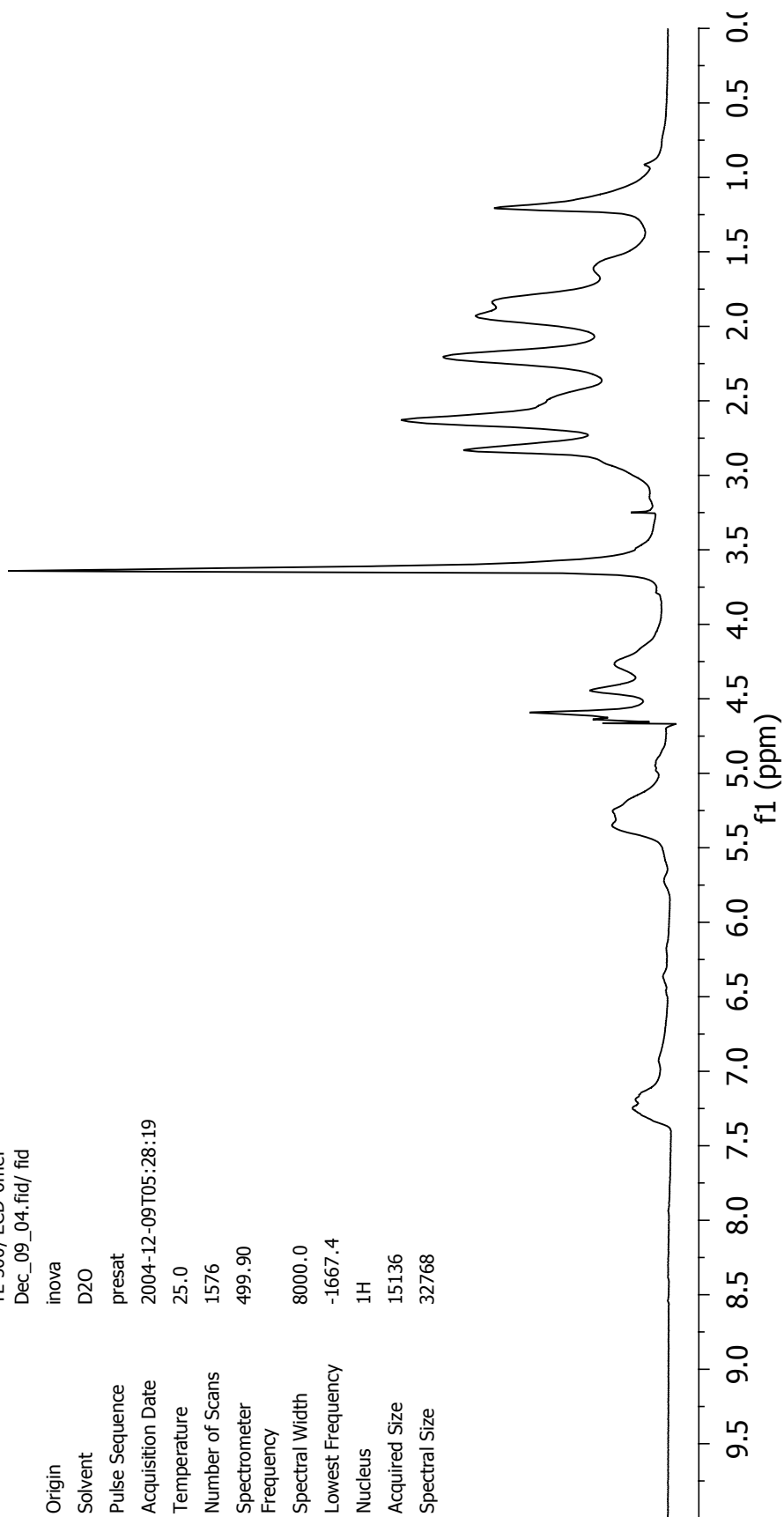
A-10: ¹H-NMR spectrum of polymer 9'3-[2]

Parameter	Value
Data File Name	C:/Users/Yonjoo Lee/Documents/Research/NMR/YL-500/ECD-3mer-Dec_09_04.fid/ fid
Origin	inova
Solvent	D2O
Pulse Sequence	presat
Acquisition Date	2004-12-09T07:50:17
Temperature	25.0
Number of Scans	1208
Spectrometer	499.90
Frequency	8000.0
Spectral Width	-1665.0
Lowest Frequency	1H
Nucleus	15136
Acquired Size	32768
Spectral Size	



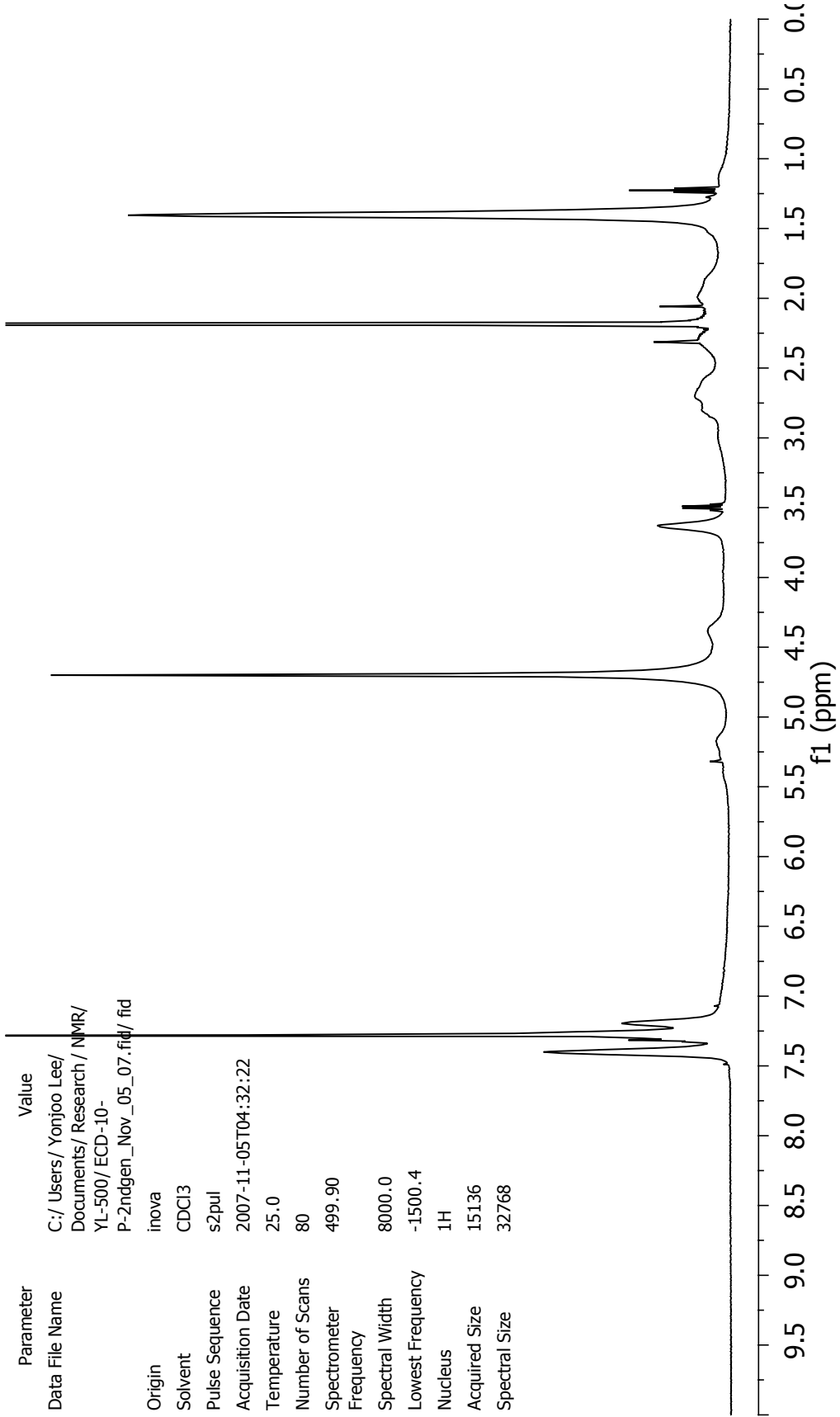
A-11: ¹H-NMR spectrum of polymer 9₃-[3]

Parameter	Value
Data File Name	C:/Users/Yonjoo Lee/Documents/Research/NMR/YL-500/ECD-6mer-Dec_09_04.fid/ fid
Origin	inova
Solvent	D2O
Pulse Sequence	presat
Acquisition Date	2004-12-09T05:28:19
Temperature	25.0
Number of Scans	1576
Spectrometer	499.90
Frequency	8000.0
Spectral Width	-1667.4
Lowest Frequency	1H
Nucleus	15136
Acquired Size	32768
Spectral Size	

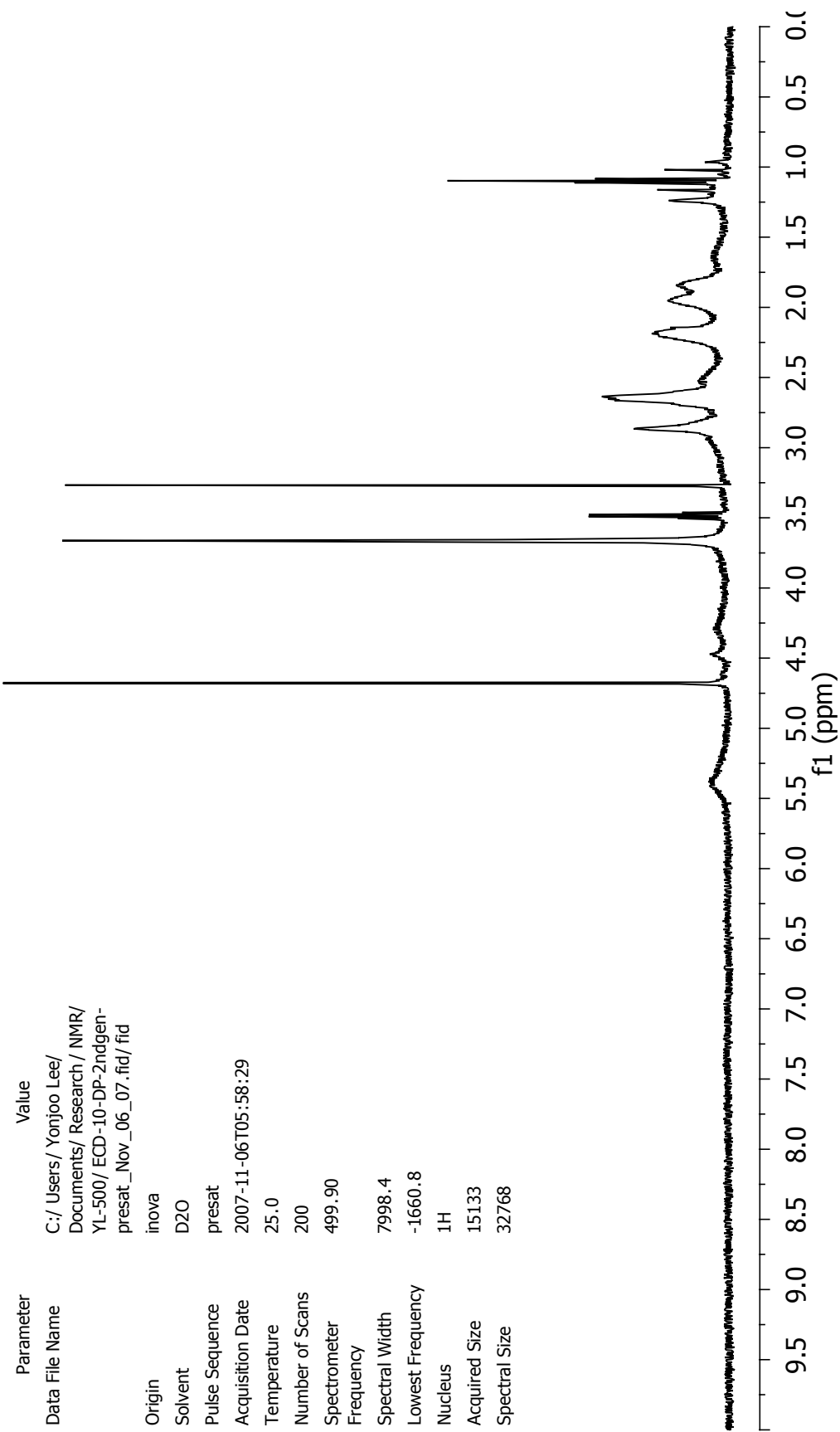


A-12: ¹H-NMR spectrum of polymer 9₆-[3]

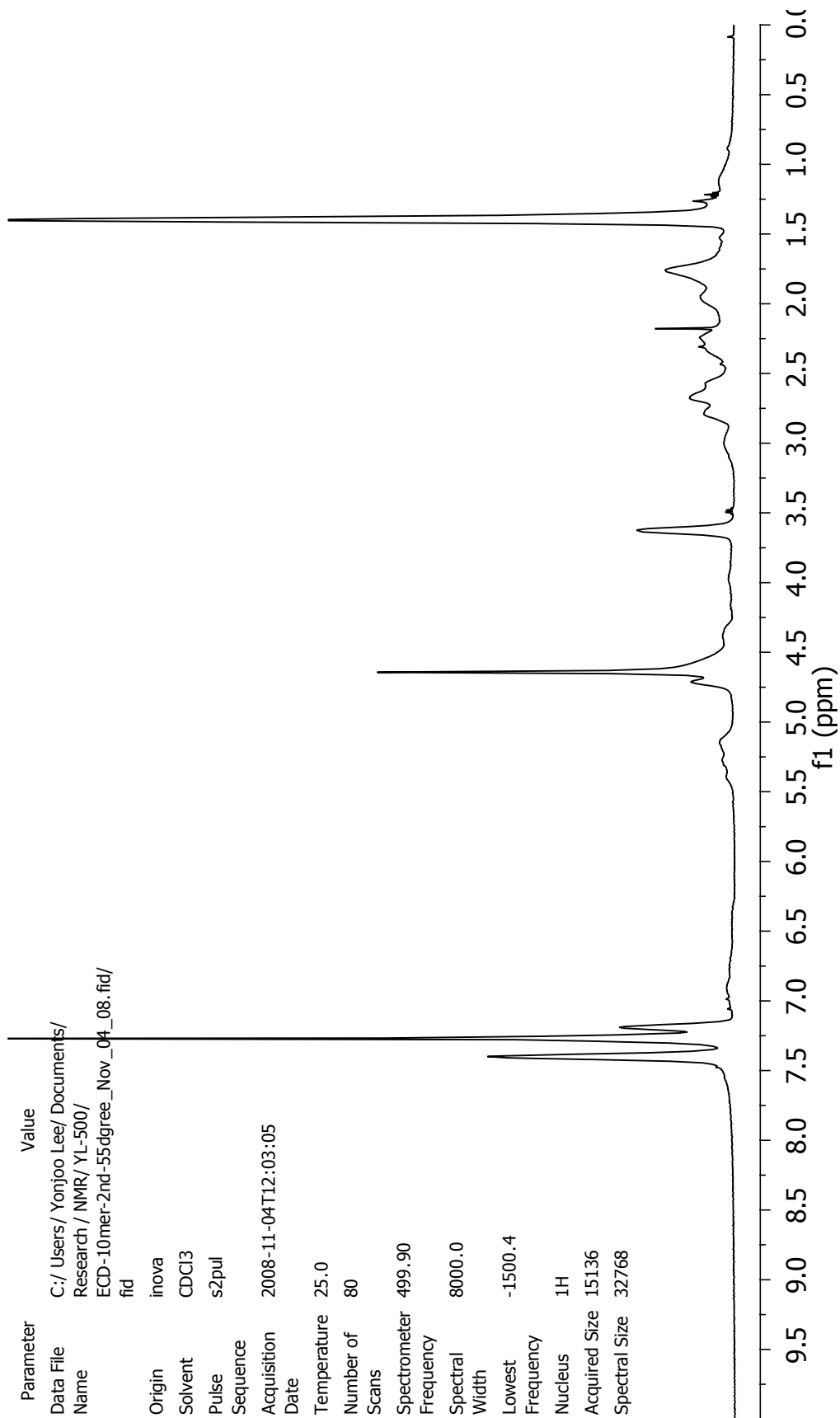
Parameter	Value
Data File Name	C:/Users/Yonjoo Lee/Documents/Research/NMR/YL-500/ECD-10-P-2ndgen_Nov_05_07.fid/ fid
Origin	inova
Solvent	CDCl3
Pulse Sequence	s2pul
Acquisition Date	2007-11-05T04:32:22
Temperature	25.0
Number of Scans	80
Spectrometer	499.90
Frequency	8000.0
Spectral Width	-1500.4
Lowest Frequency	1H
Nucleus	15136
Acquired Size	32768
Spectral Size	



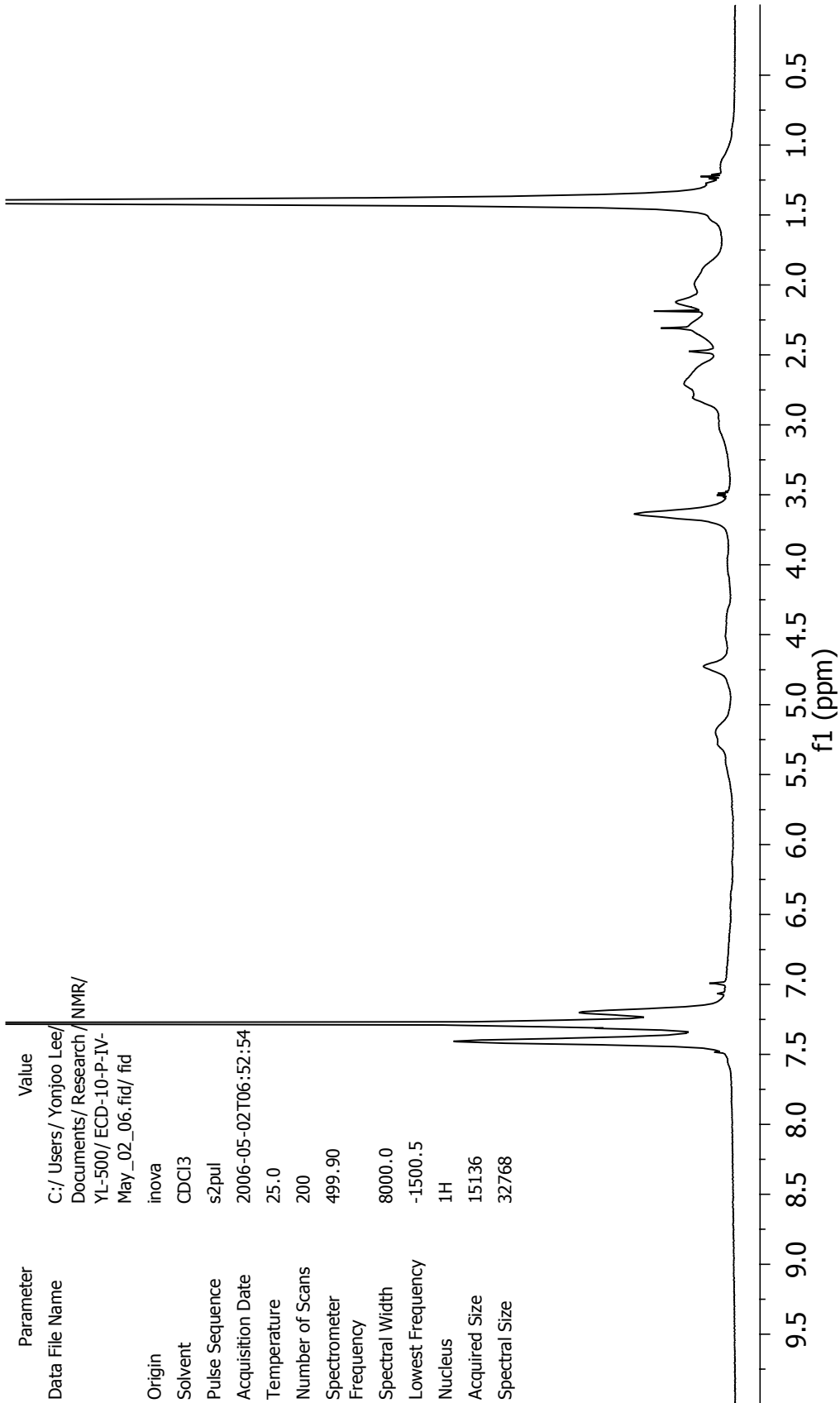
A-13: ¹H-NMR spectrum of polymer 9'10-[2]



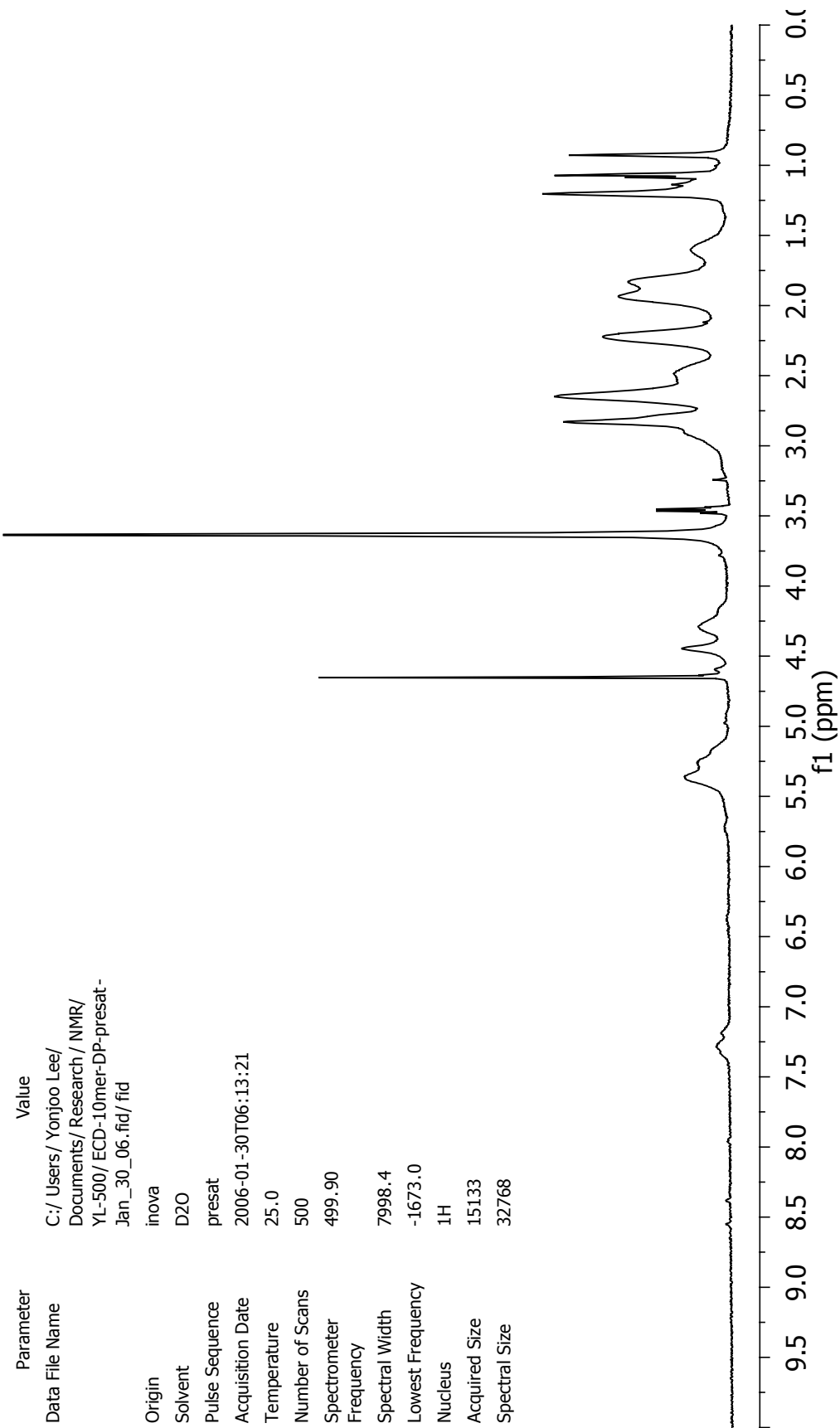
A-14: ¹H-NMR spectrum of polymer 9₁₀-[2]



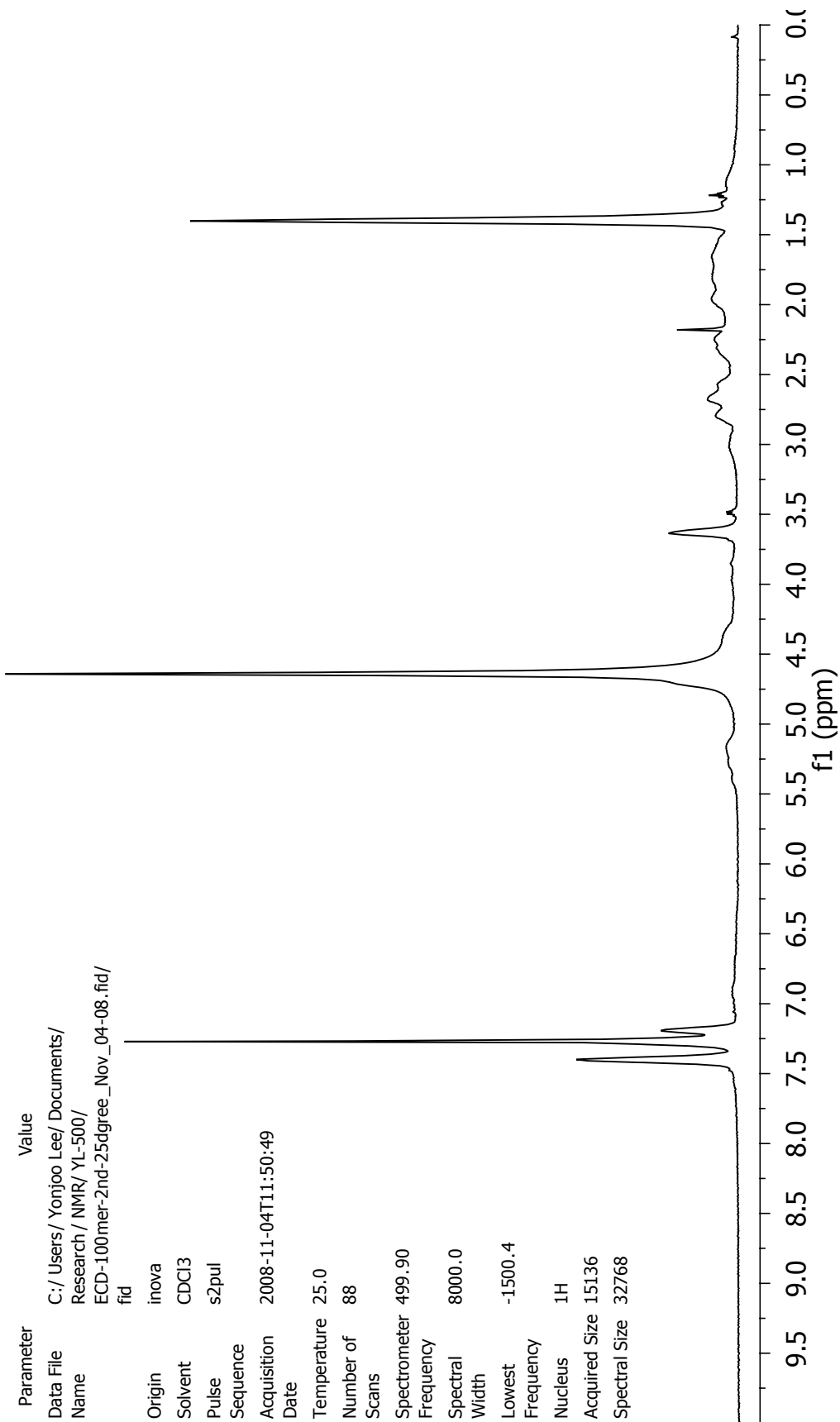
A-15: ¹H-NMR spectrum of polymer 9'10-[2]-a



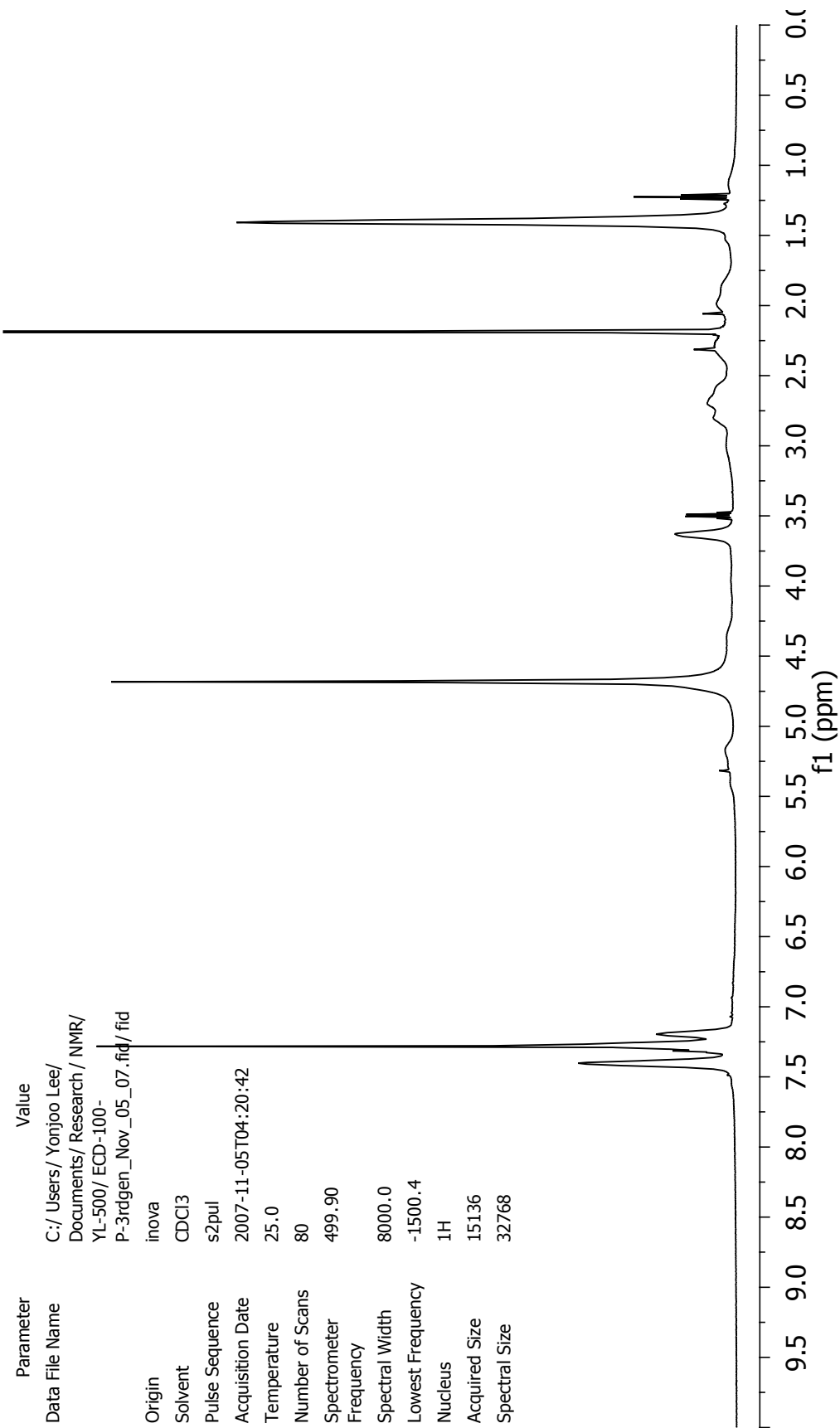
A-16: ¹H-NMR spectrum of polymer 9'10-[3]



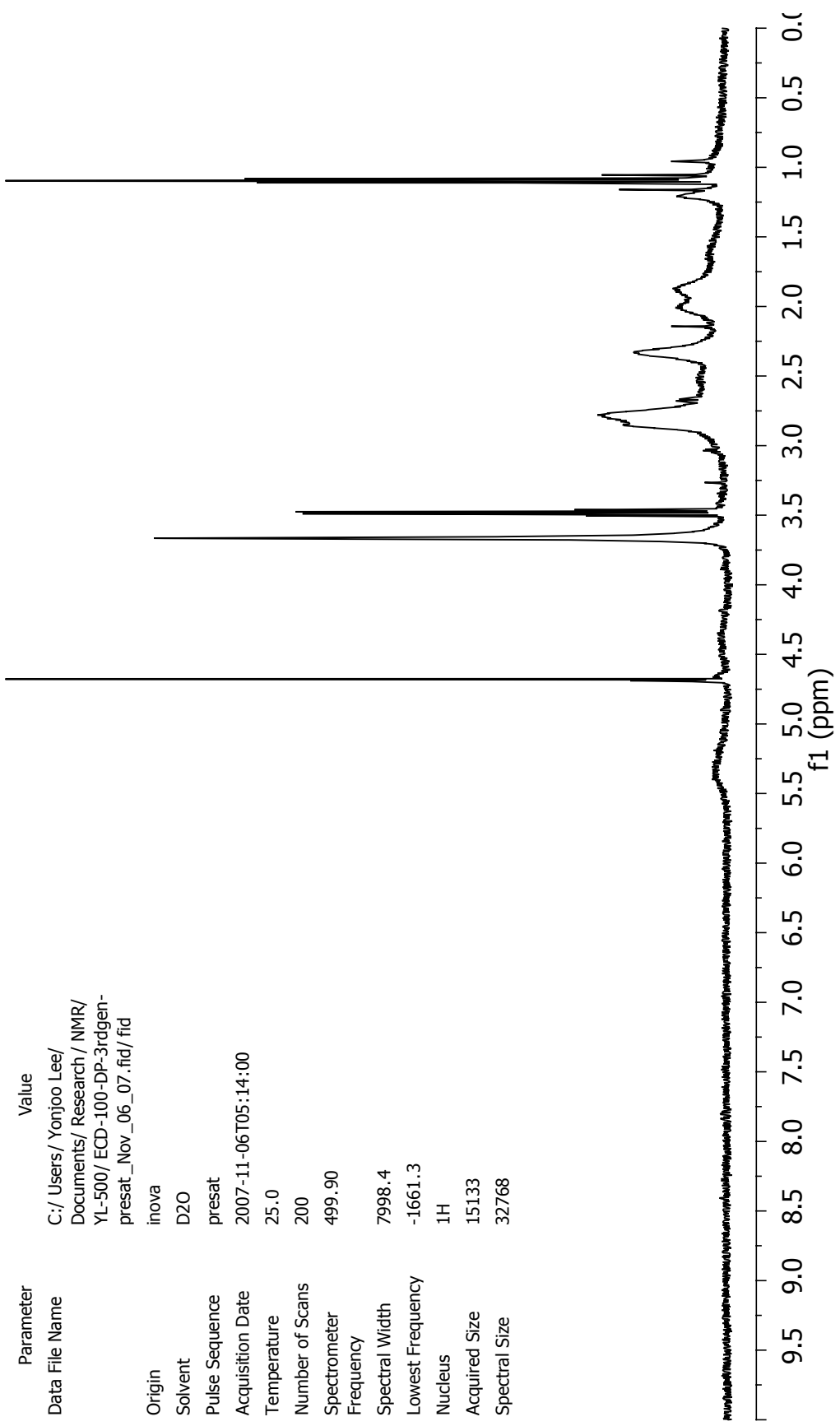
A-17: ¹H-NMR spectrum of polymer 9₁₀-[3]



A-18: ¹H-NMR spectrum of polymer 9'100-[2]



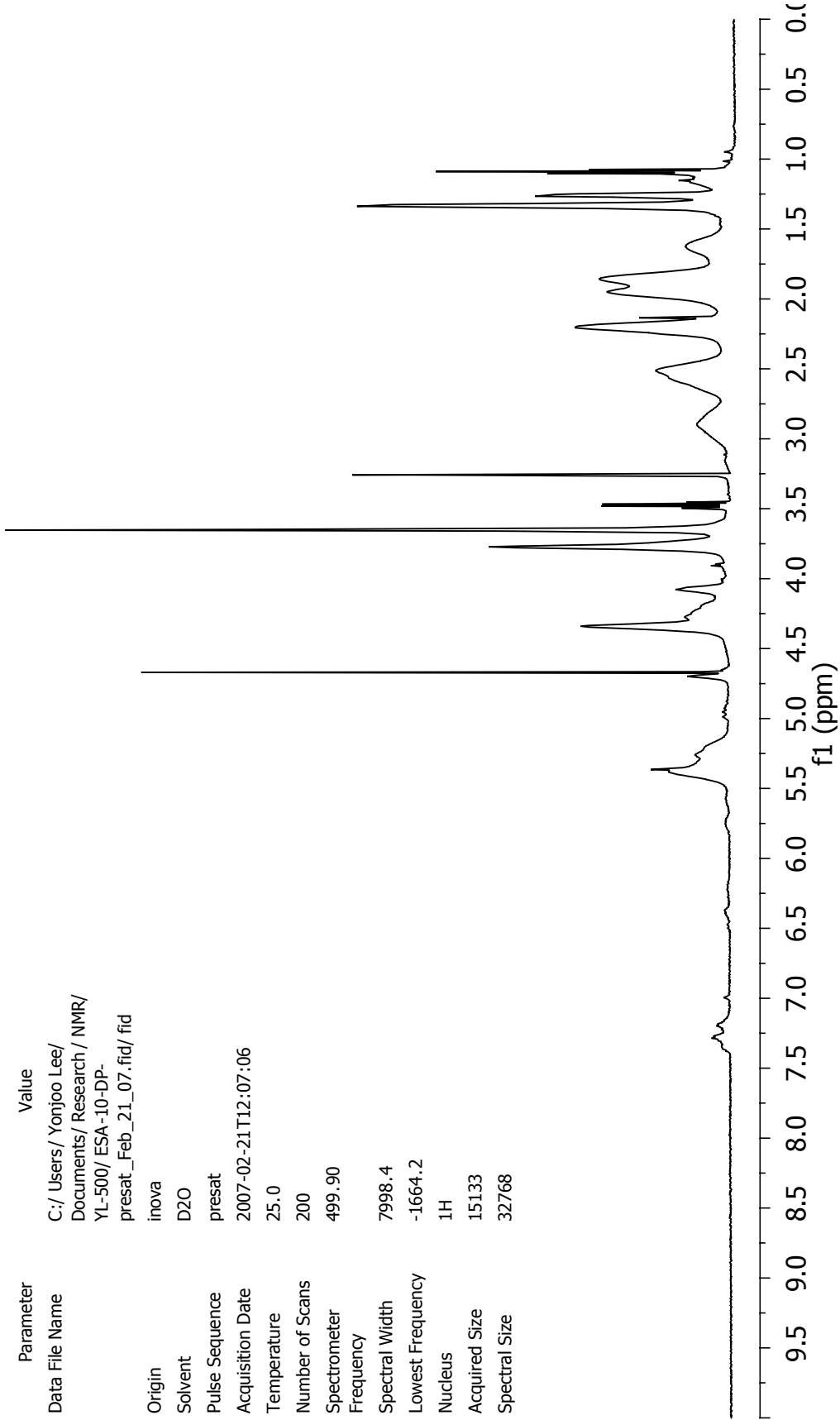
A-19: ¹H-NMR spectrum of polymer 9'100-[3]



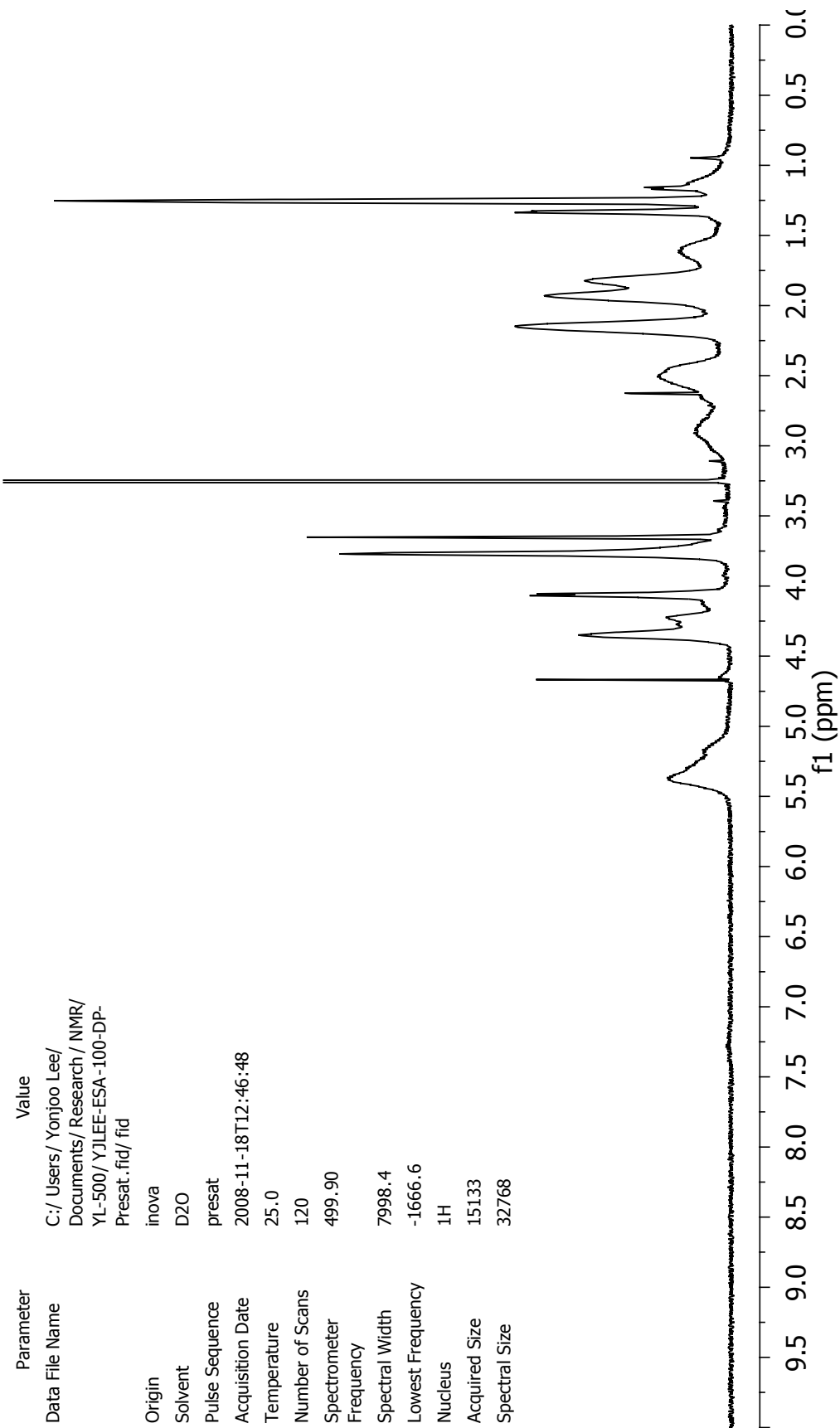
Parameter	Value
Data File Name	C:/Users/Yonjoo Lee/Documents/ Research / NMR/ YL-500/ ECD-100-DP-3rdgen-presat_Nov_06_07.fid/ fid
Origin	inova
Solvent	D2O
Pulse Sequence	presat
Acquisition Date	2007-11-06T05:14:00
Temperature	25.0
Number of Scans	200
Spectrometer	499.90
Frequency	7998.4
Spectral Width	-1661.3
Lowest Frequency	1H
Nucleus	15133
Acquired Size	32768
Spectral Size	

A-20: ¹H-NMR spectrum of polymer 9₁₀₀-[3]

Parameter	Value
Data File Name	C:/Users/Yonjoo Lee/Documents/Research/NMR/YL-500/ESA-10-DP-presat_Feb_21_07.fid/ fid
Origin	inova
Solvent	D2O
Pulse Sequence	presat
Acquisition Date	2007-02-21T12:07:06
Temperature	25.0
Number of Scans	200
Spectrometer	499.90
Frequency	7998.4
Spectral Width	-1664.2
Lowest Frequency	1H
Nucleus	15133
Acquired Size	32768
Spectral Size	

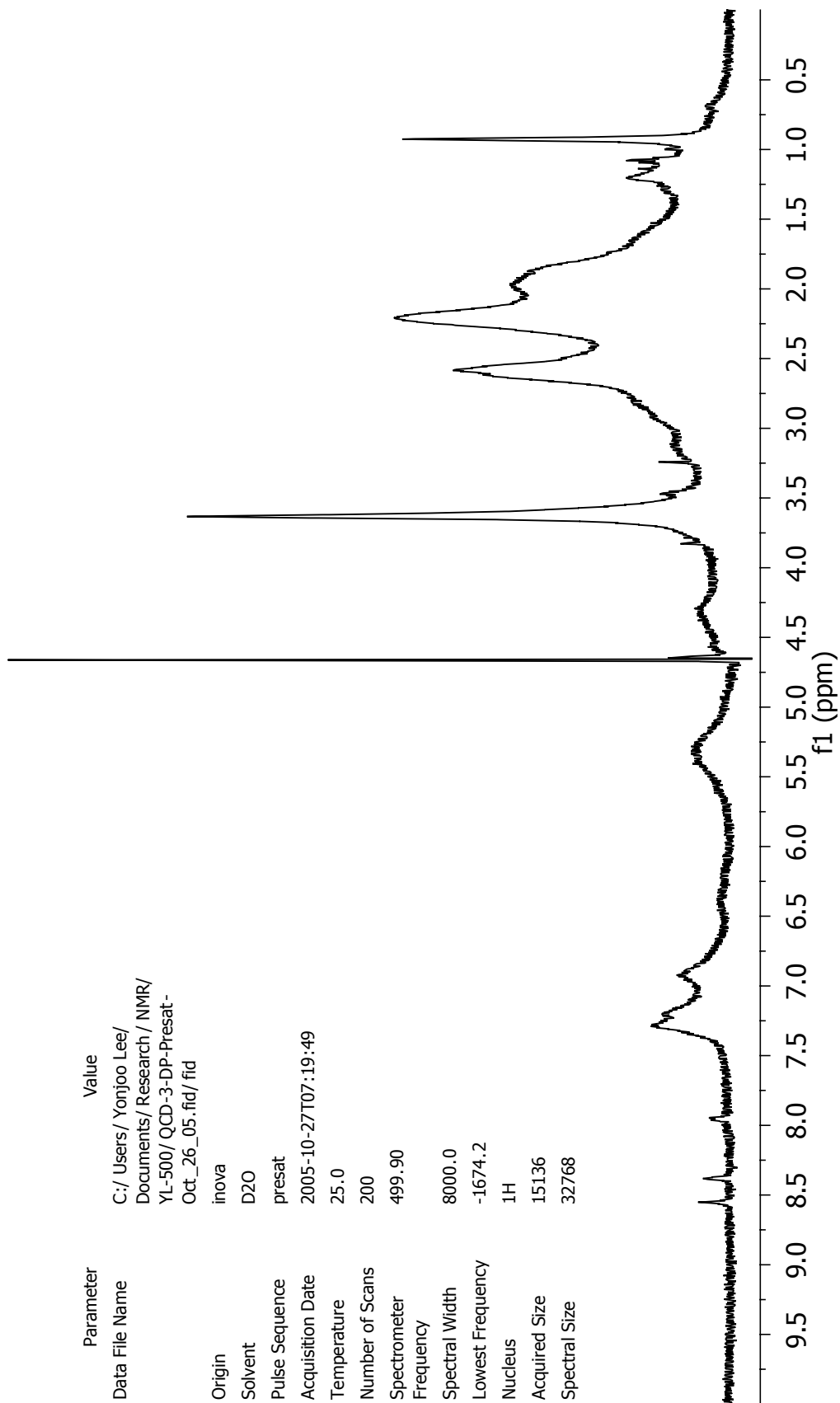


A-21: ¹H-NMR spectrum of polymer 13₁₀-[3]

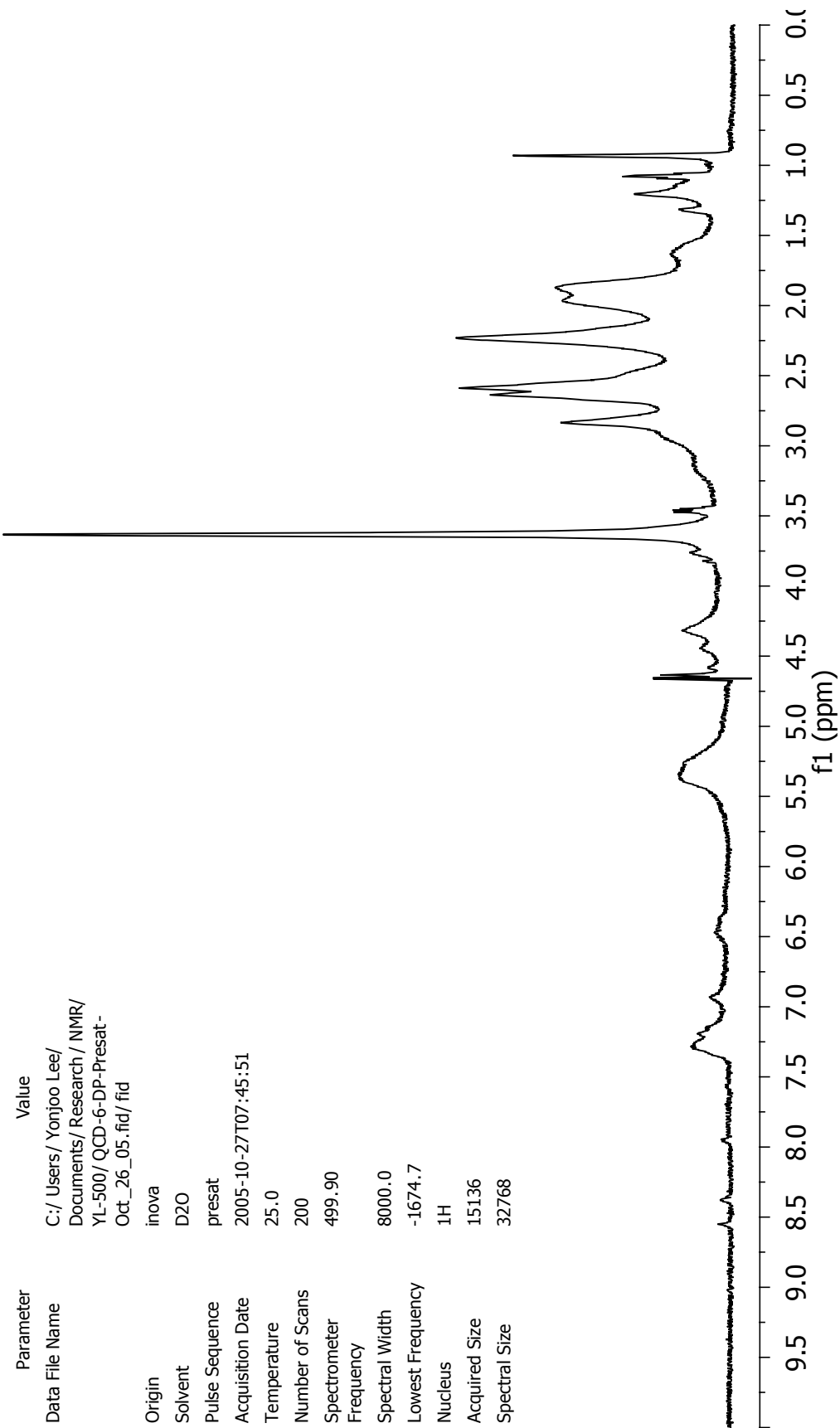


A-22: ¹H-NMR spectrum of polymer 13₁₀₀-[3]

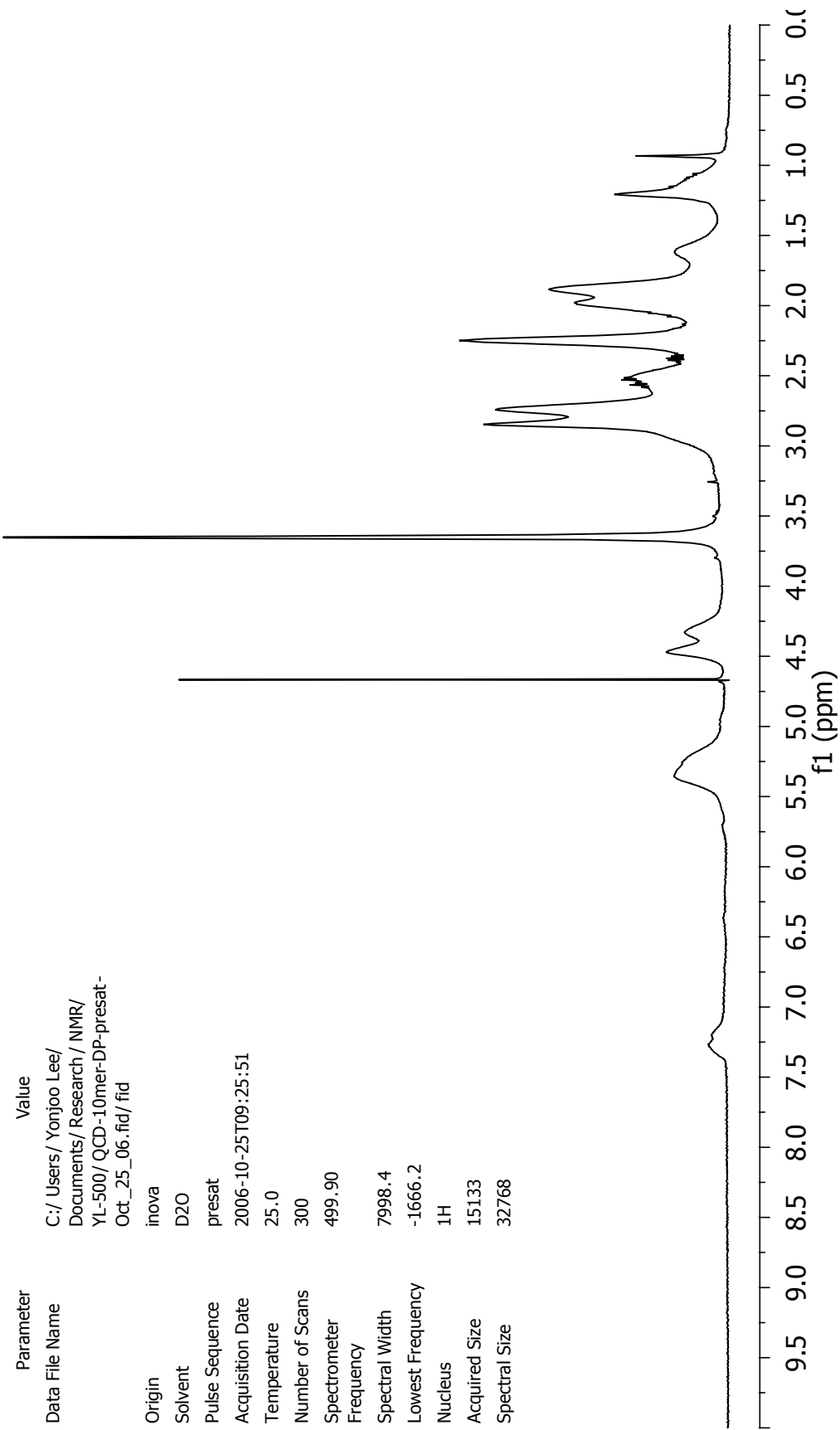
Parameter	Value
Data File Name	C:/Users/Yonjoo Lee/Documents/Research/NMR/YL-500/QCD-3-DP-Presat-Oct_26_05.fid/fid
Origin	inova
Solvent	D2O
Pulse Sequence	presat
Acquisition Date	2005-10-27T07:19:49
Temperature	25.0
Number of Scans	200
Spectrometer	499.90
Frequency	8000.0
Spectral Width	-1674.2
Lowest Frequency	1H
Nucleus	15136
Acquired Size	32768
Spectral Size	



A-23: ¹H-NMR spectrum of polymer 18₃-[3]

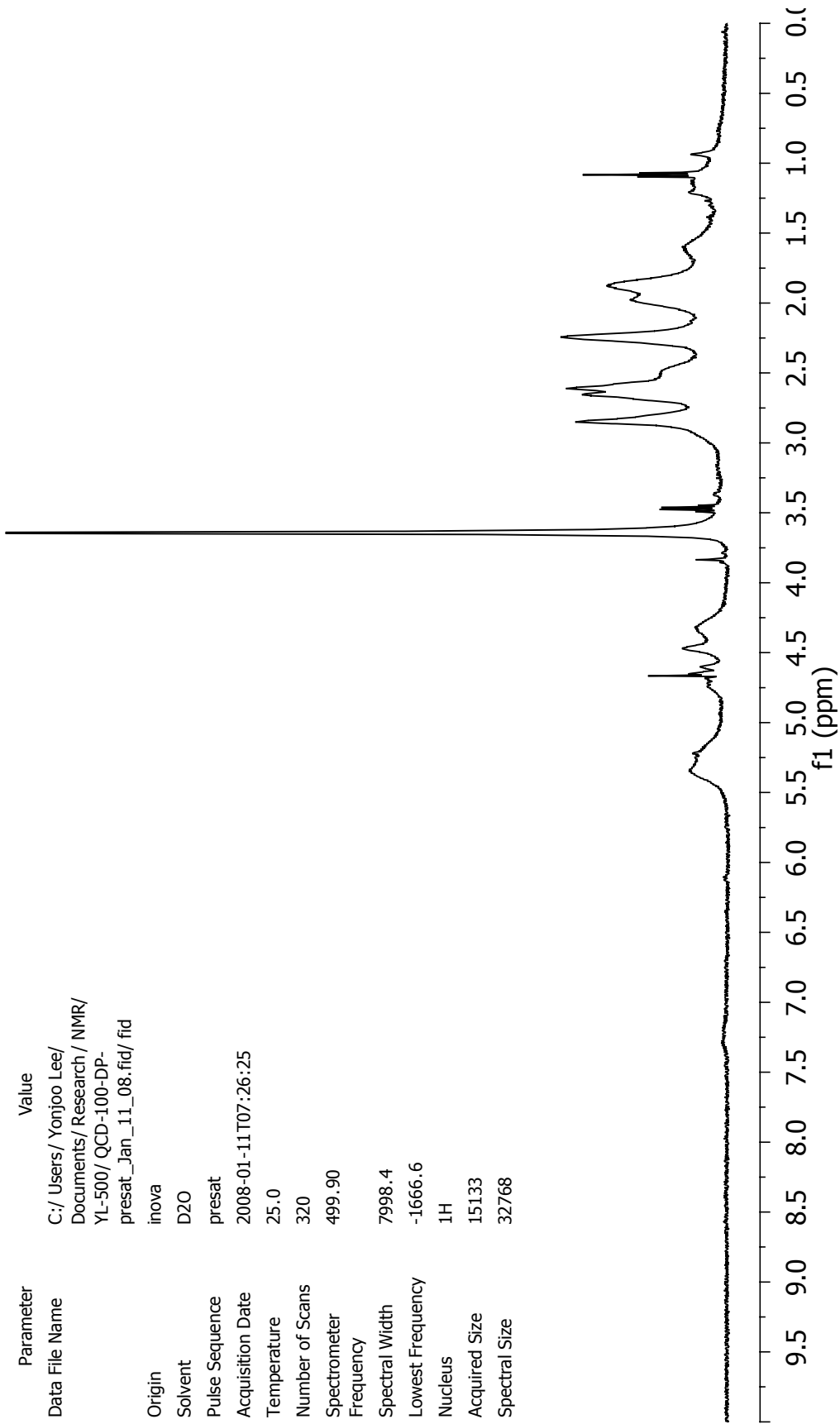


A-24: ¹H-NMR spectrum of polymer 18_c-[3]

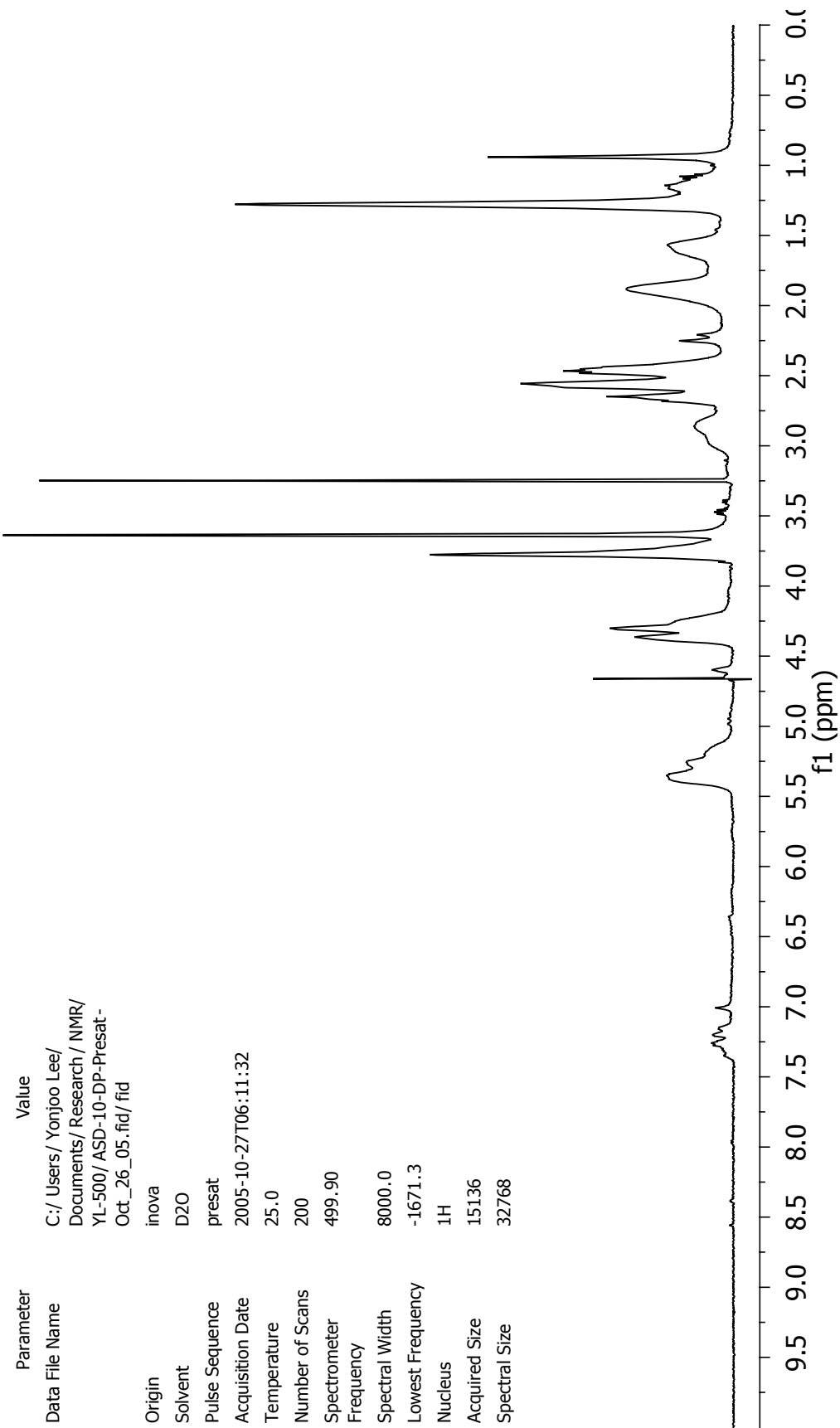


A-25: ¹H-NMR spectrum of polymer 18₁₀-[3]

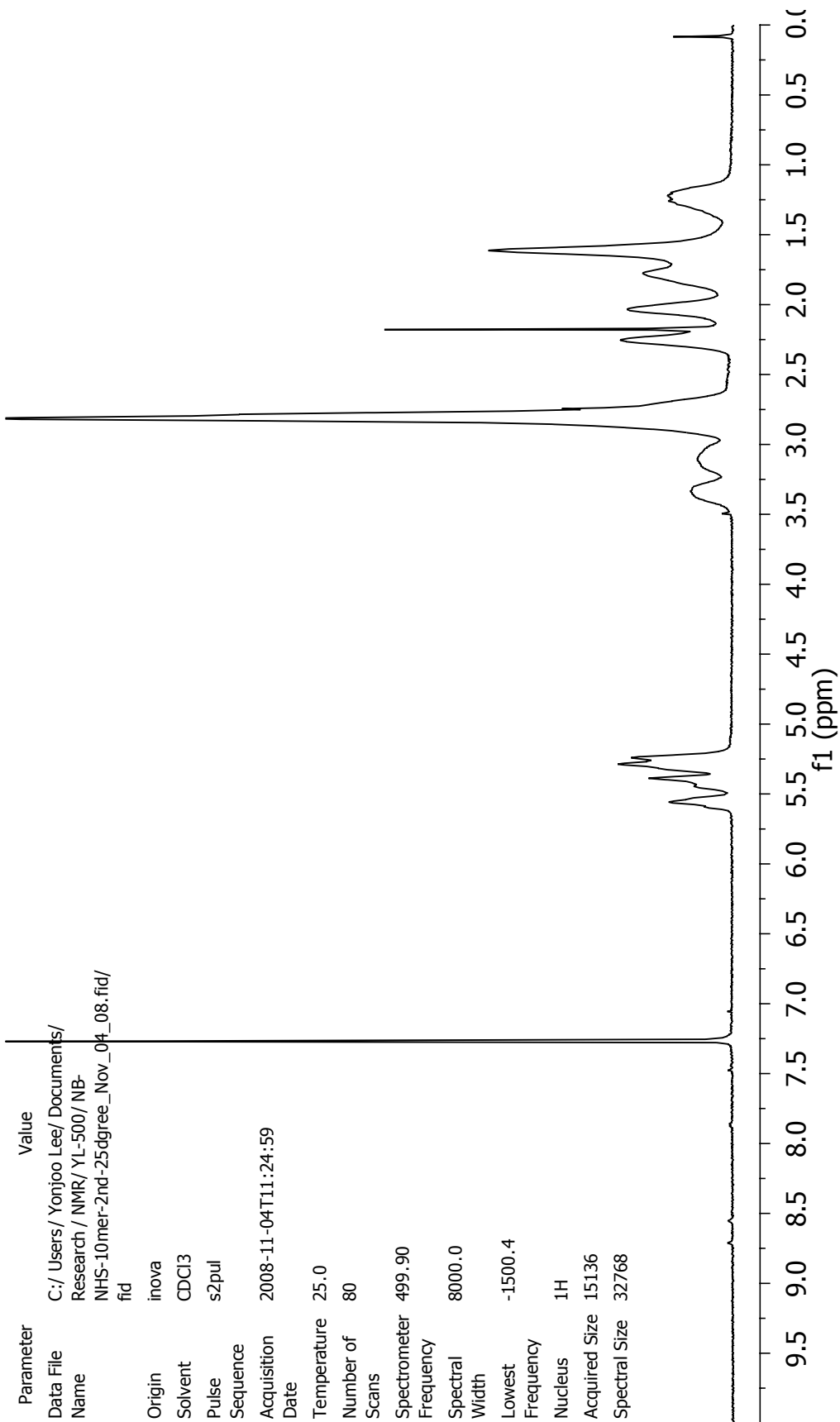
Parameter	Value
Data File Name	C:/Users/Yonjoo Lee/Documents/Research/NMR/YL-500/QCD-100-DP-presat_Jan_11_08.fid/ fid
Origin	inova
Solvent	D2O
Pulse Sequence	presat
Acquisition Date	2008-01-11T07:26:25
Temperature	25.0
Number of Scans	320
Spectrometer	499.90
Frequency	7998.4
Spectral Width	-1666.6
Lowest Frequency	1H
Nucleus	15133
Acquired Size	32768
Spectral Size	



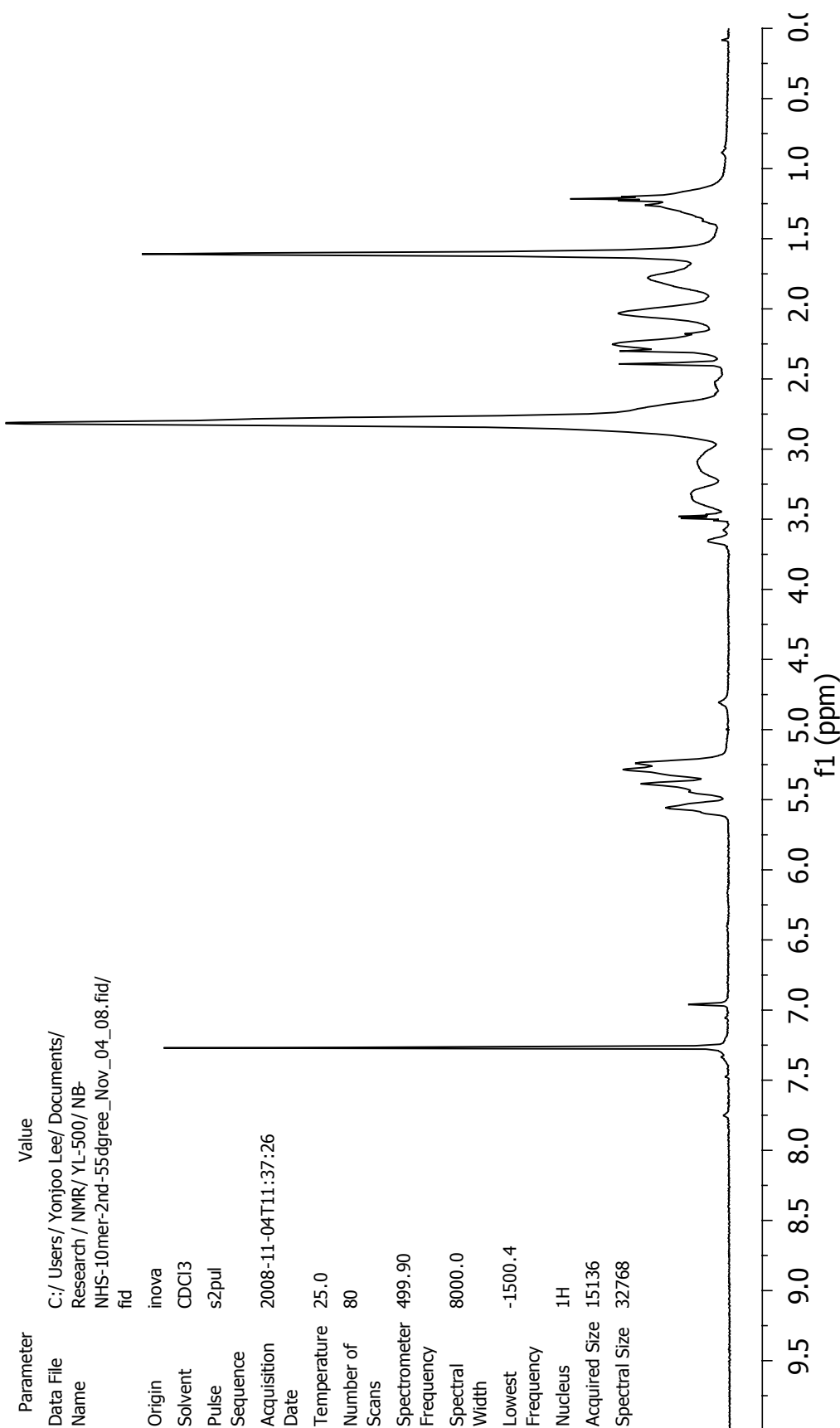
A-26: ¹H-NMR spectrum of polymer 18₁₀₀-[3]



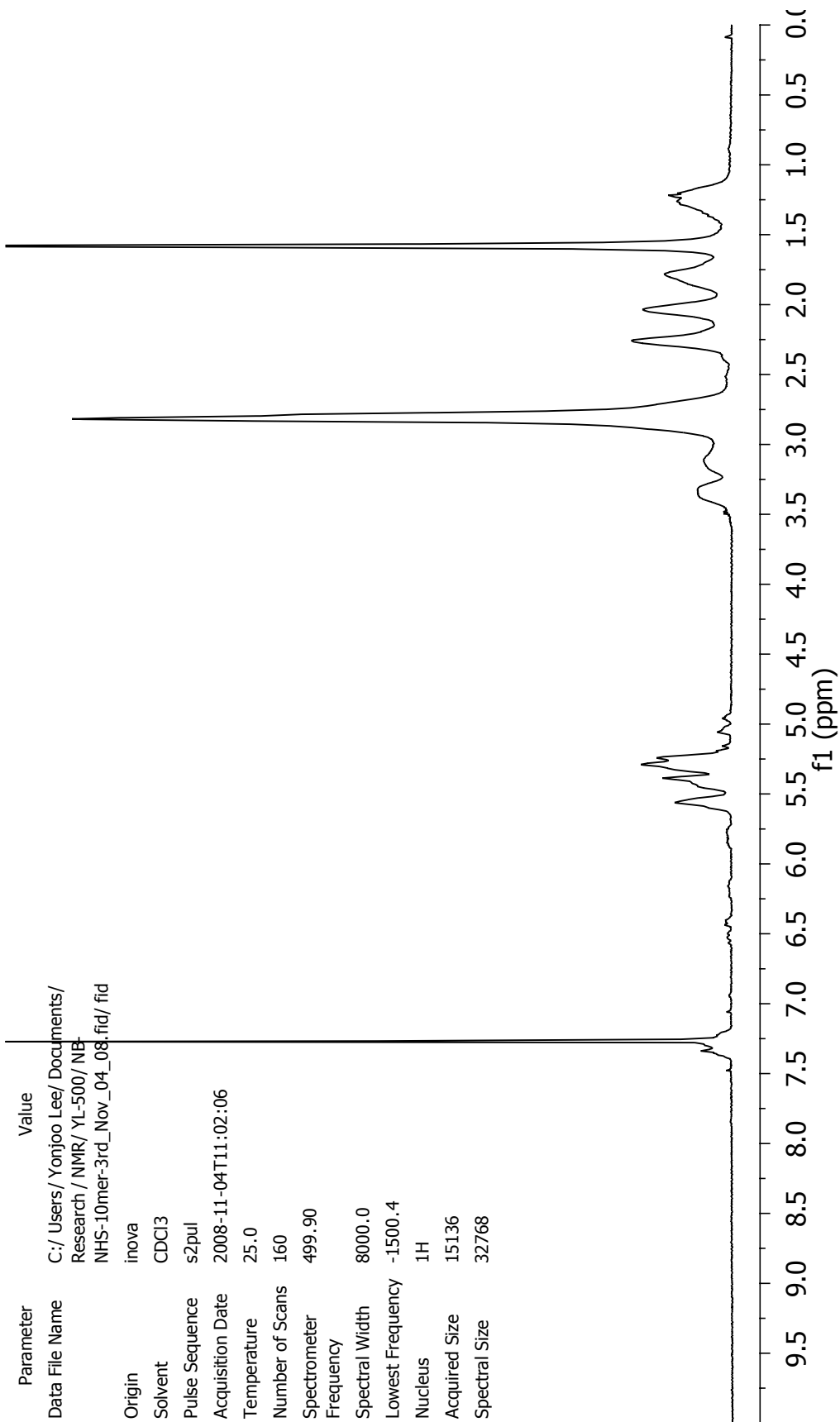
A-27: ¹H-NMR spectrum of polymer 21₁₀-[3]



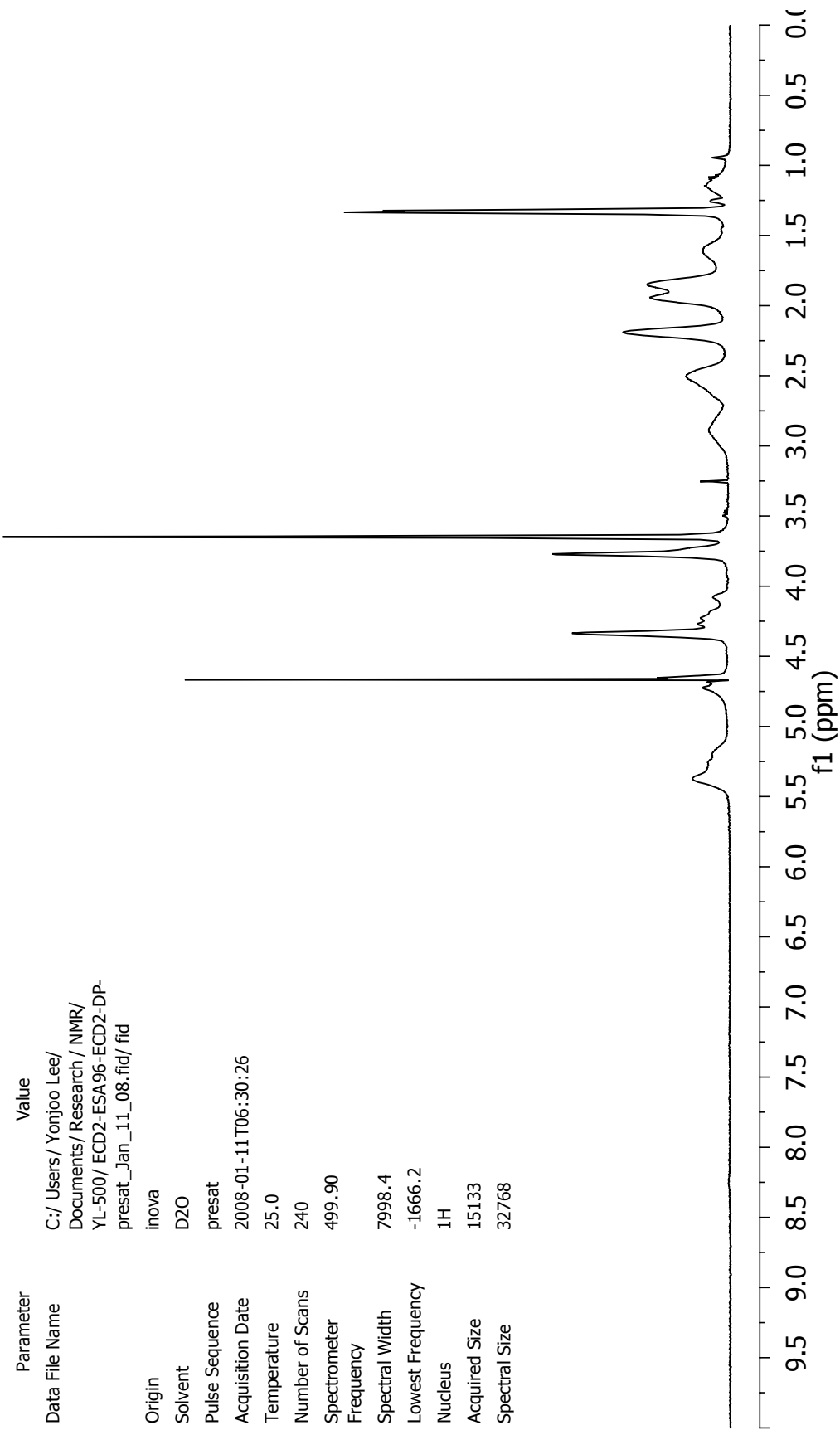
A-28: ¹H-NMR spectrum of polymer 22₁₀-[2]-a



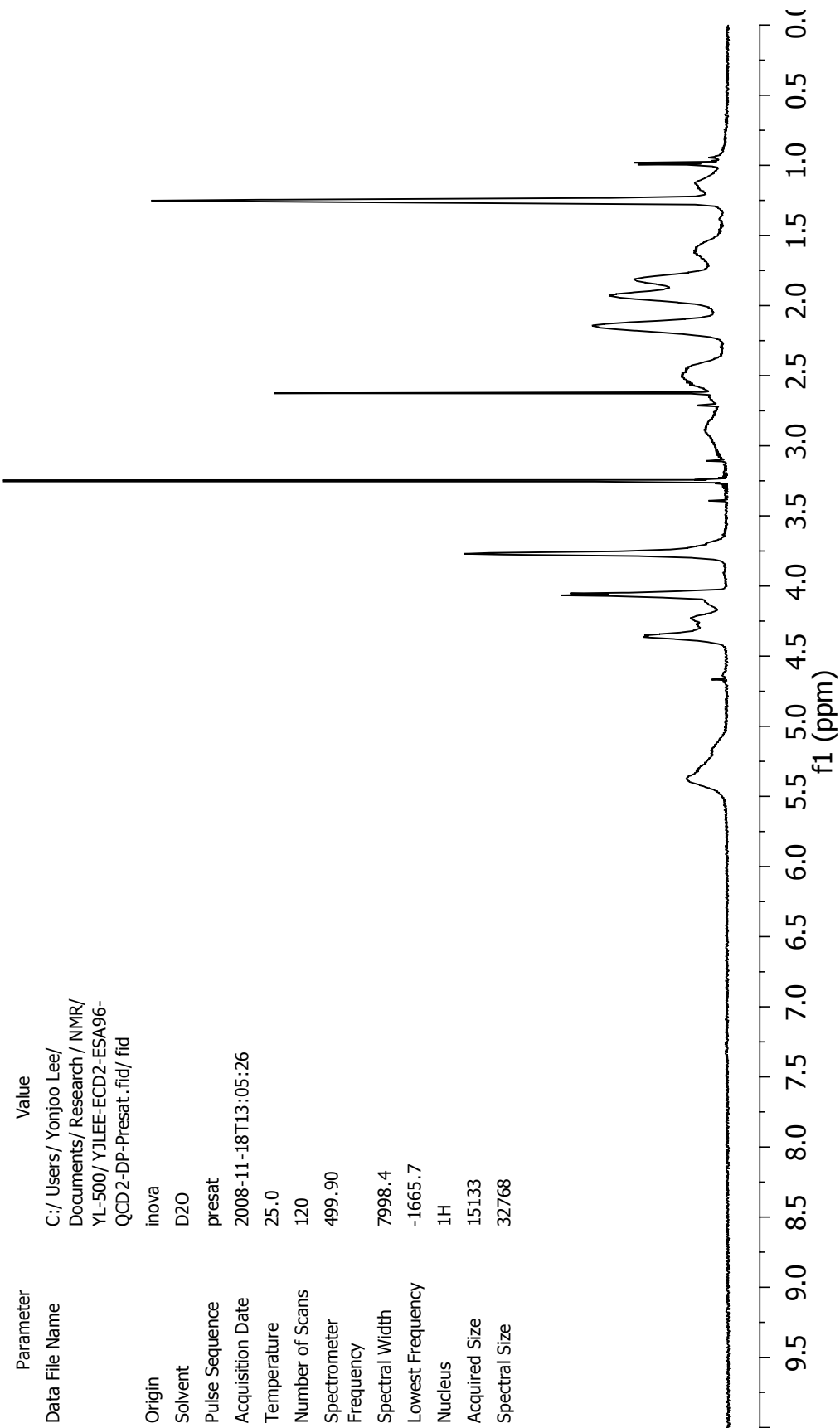
A-29: ¹H-NMR spectrum of polymer 22₁₀-[2]-b



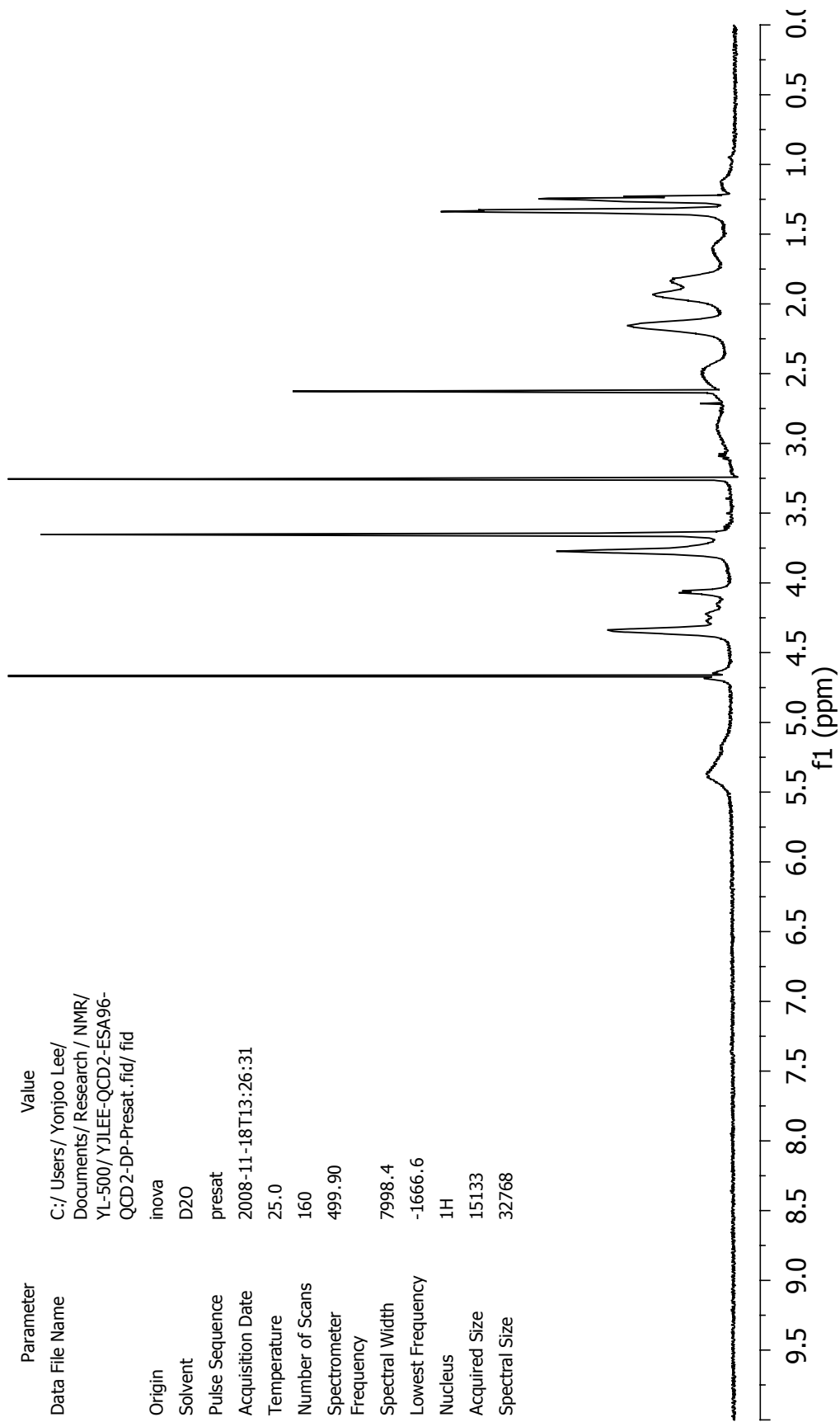
A-30: ¹H-NMR spectrum of polymer 22₁₀-[3]-c



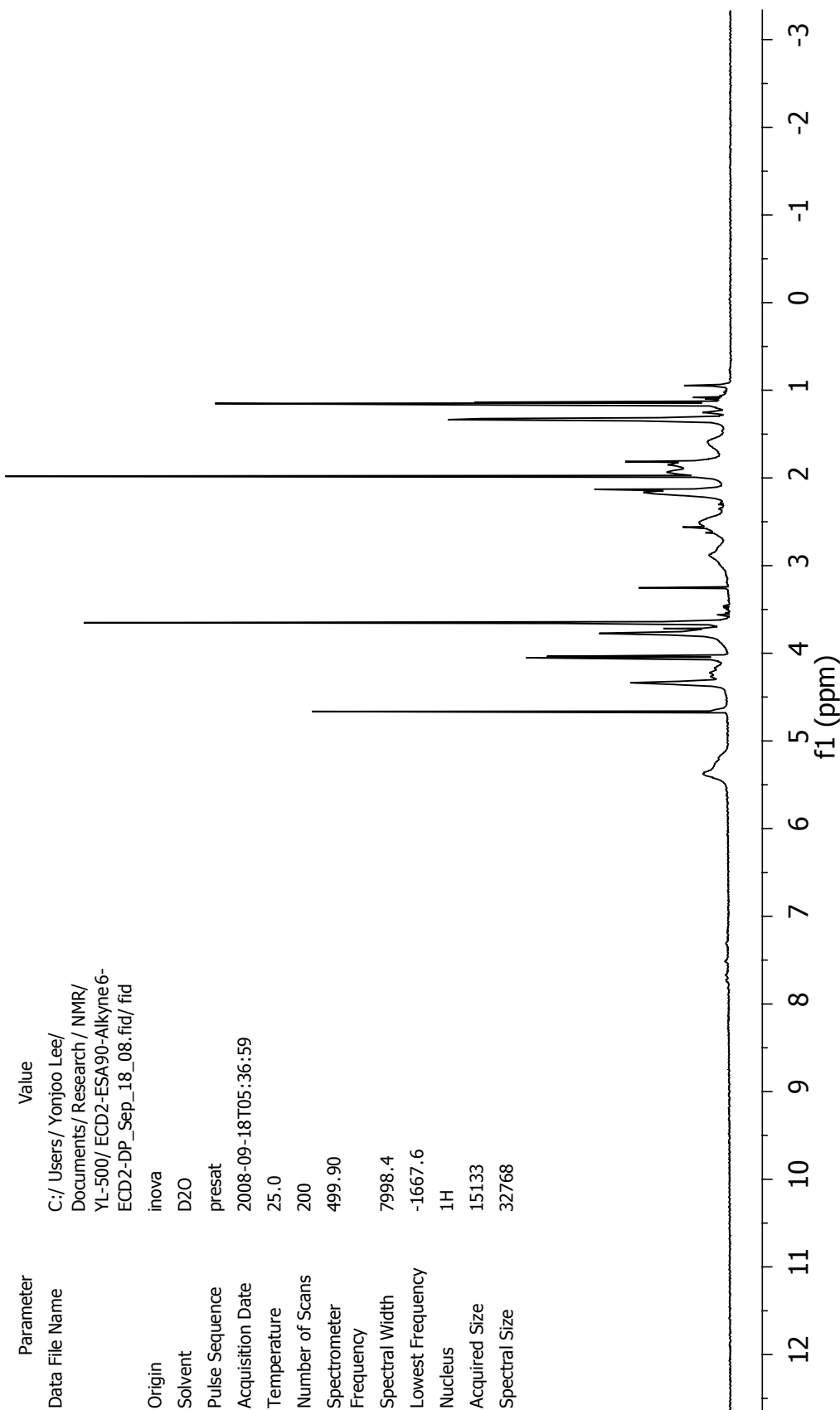
A-31: ¹H-NMR spectrum of polymer 9₂-13₉₆-9₂-[3]



A-32: ¹H-NMR spectrum of polymer 9₂-13₉₆-18₂-[3]

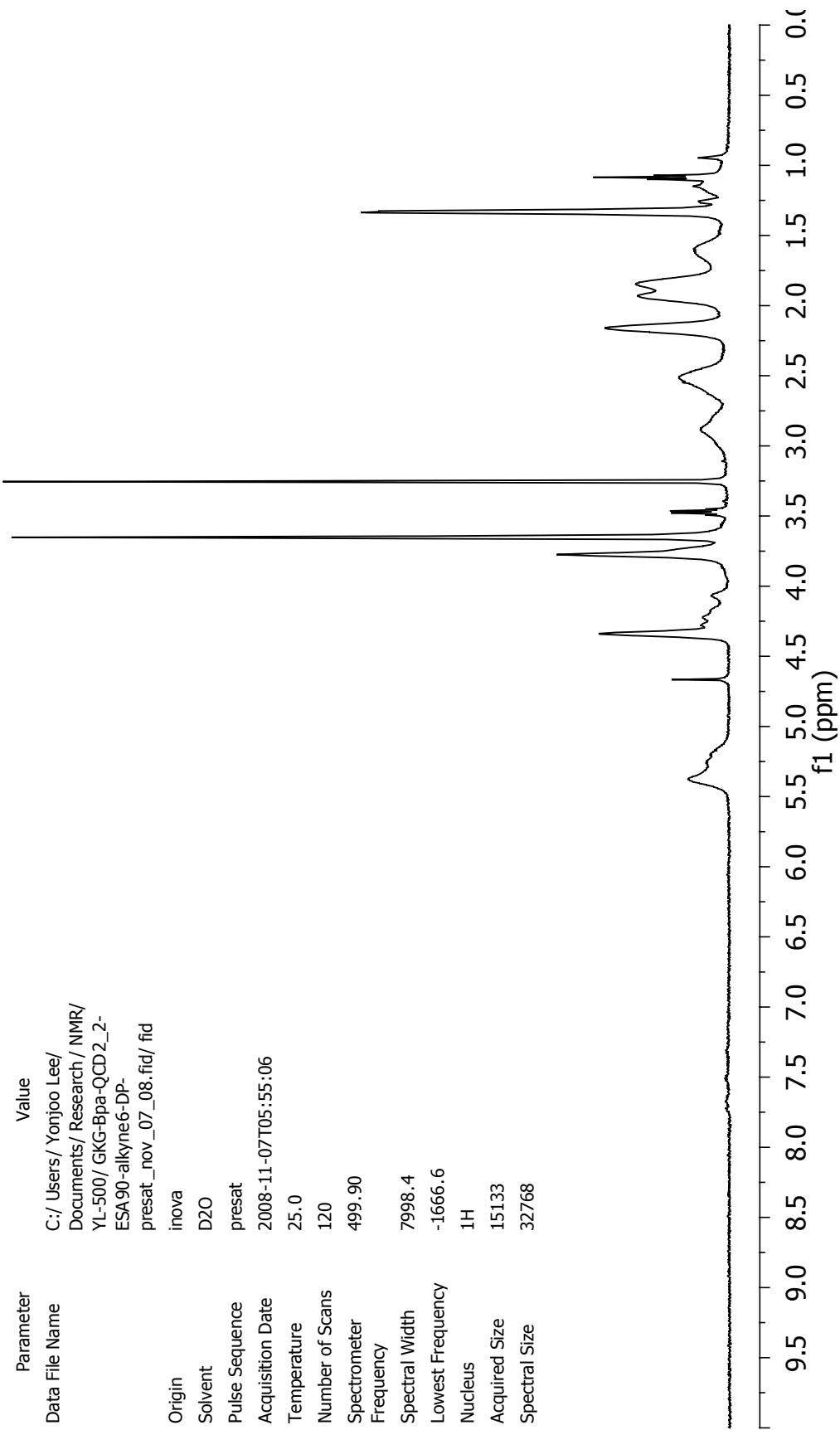


A-33: ¹H-NMR spectrum of polymer 18₂-13₉₆-18₂-[3]

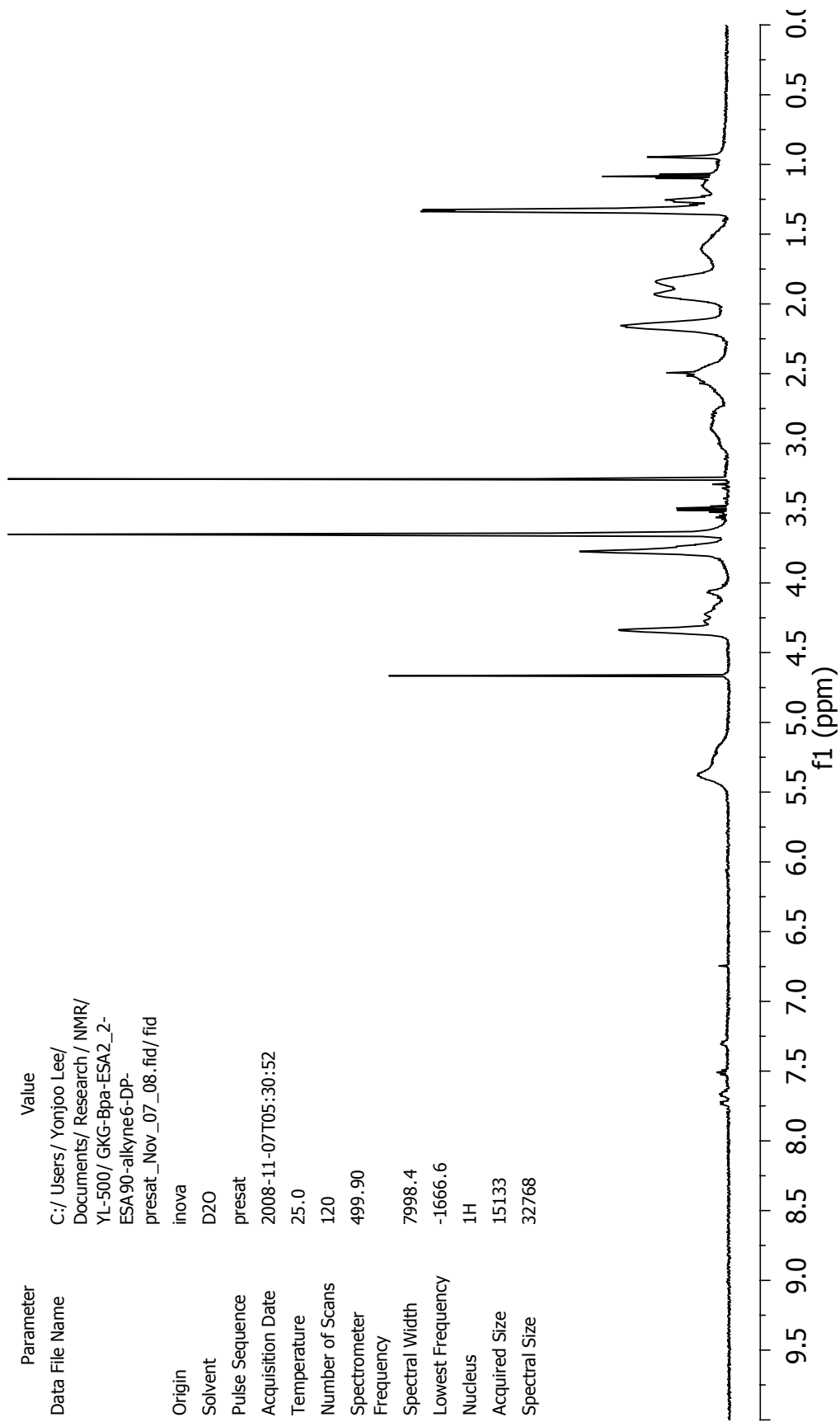


Parameter	Value
Data File Name	C:/Users/Yonjoo Lee/Documents/Research/NMR/YL-500/ECD2-ESA90-Alkyne 6-ECD2-DP_Sep_18_08.fid/ fid
Origin	inova
Solvent	D2O
Pulse Sequence	presat
Acquisition Date	2008-09-18T05:36:59
Temperature	25.0
Number of Scans	200
Spectrometer	499.90
Frequency	7998.4
Spectral Width	-1667.6
Lowest Frequency	1H
Nucleus	15133
Acquired Size	32768
Spectral Size	

A-34: ¹H-NMR spectrum of polymer 47



A-35: ¹H-NMR spectrum of polymer 48



A-36: ¹H-NMR spectrum of polymer 49